Cranfield Institute of Technology

College of Aeronautics

Department of Aerodynamics

Ph.D. Thesis

Academic Years 1987-1990

Hong-Chia Lin

Topics in Numerical Computation of Compressible Flow

Supervisor Professor P.L.Roe

July 1990

SUMMARY

This thesis aims to assist the development of a multiblock implicit Navier-Stokes code for hypersonic flow applications. There are mainly three topics, which concern the understanding of basic Riemann solvers, the implementing of implicit zonal method, and grid adaption for viscous flow.

Three problems of Riemann solvers are investigated. The post-shock oscillation problem of slowly moving shocks is examined, especially for Roe's Riemann solver, and possible cures are suggested for both first and second order schemes. The carbuncle phenomenon associated with blunt body calculation is cured by a formula based on pressure gradient, which will not degrade the solutions for viscous calculations too much. The grid-dependent characteristic of current upwind schemes is also demonstrated.

Several issues associated with implicit zonal methods are discussed. The effects of having different mesh sizes in different zones when shock present are examined with first order explicit scheme and such effects are shown to be unwanted therefore big mesh size change should be avoided. Several implicit schemes are tested for hypersonic flow. The conservative DDADI scheme is found to be the most robust one. A simple and robust implicit zonal method is demonstrated. A proper treatment of the diagonal Jacobian and choosing the updating method are found to be crucial.

The final topic concerns the calculation and grid adaption of viscous flow. We study the linear advection-diffusion equation thoroughly. The results are unfortunately not applicable to Navier-Stokes equations directly. Nevertheless a suggestion on the mesh size control for viscous flow is made and demonstrated.

An attempt to construct a cell-vertex TVD scheme is described in the appendix.

ACKNOWLEDGEMENT

First I would like to thank my parents for their encouragement and financial support, the British government for three years' ORS award, and the French company AMD-BA for one and half year of financial sponsorship.

Thanks to Dr. J.Periaux and Dr. Q.V.Dinh of AMD-BA for their hospitality during my stay in Paris.

Thanks to all my friends in Cranfield for their friendships ,especially Creigh McNeil and Sakher Hamwi, and to David Payne, Foley Lau, Cheng Gong, and Dr. Smadar Karni for their help I received during the last six months of this work.

Special thanks to Mr. Howard Jeffrey at Cranfield computer center for his help in accessing ULCC for me.

Finally I would like to express my appreciation to Professor P.L.Roe for supervision and to Professor J.F.Clarke for all his help at the last stage of my Ph.D. study, and to Mr. J. Pike for his useful comments on the thesis.

CONTENT

LIST OF FIGURES

Fig. 6.18 Streamlines for NACA 0012

Fig. 6.19 Density contours for NACA 0012

Fig. 6.20 Pressure contours for NACA 0012 with modified grid

CHAPTER 1 : INTRODUCTION

This work forms part of the French national project which aims to produce a multiblock implicit Navier-Stokes solver with real gas effects and a multiblock grid generator for hypersonic flow application (Mach number 4 to 20 steady state flow). Several organisations are involved while this work is part of the share of Dassault industries.

This thesis does not cover the real gas effects and grid generation. We are only concerned with the single- and multi-zone solver in two dimension.

1.1 General Theoretical Background

The steady state solution is obtained by pseudo-unsteady method. Start with fixed boundary conditions and an arbitrary initial condition we compute the unsteady solution until the solution state ceases to change. This final state is thus the steady state solution.

The equations governing the compressible inviscid and viscous flow are the Euler and Navier-Stokes equations respectively. For viscous flow we are more interested in high Reynolds number flow, which is convection dominated. The method used on such flow is mainly based on the method for Euler equations.

Before one can solve a partial differential equation numerically it is very important to understand the equation type. The unsteady Euler equations are hyperbolic in time. For the hyperbolic system the information is transferred with finite speed waves. The point at later time is only influenced by a limited domain in previous time. The hyperbolic system can

generate discontinuity solutions (shocks) even when the initial condition is smooth (Lax 1973).

Another property of Euler equations is that it satisfies conservation law. A conservation law can be expressed as

$$\frac{\partial}{\partial t}\iiint_V W dV + \oint_S \vec{F}\cdot d\vec{S} = 0$$

The first term is the time change of conservative variables W in the control volume V. The second term expressesthe net fluxes $\vec{F}(W)$ across the surface S of the control volume. The conservation law simply says nothing is generated inside the control volume. The Euler equations have mass, momentum, and energy as conservative variables. The differential form of the conservation law is

$$\frac{\partial W}{\partial t} + \nabla\cdot\vec{F} = 0$$

The differential equation does not allow solutions with shocks (weak solutions).

The Euler equations are thus a hyperbolic conservation system. The presence of shocks is probably the chief difficulty in solving a hyperbolic conservation system. A breakthrough was made by Lax (1954) who proved the limit solution of any finite-difference scheme in a conservative form can capture the discontinuities automatically. The idea of conservative scheme can be made clear by considering the one dimension case. Consider a scalar conservation law

$$\frac{\partial U}{\partial t} + \frac{\partial f}{\partial x} = 0$$

where the f is the flux function in x direction. With a central difference applied to the mesh of Fig. 1.1 we obtain a discretised equation at i:

$$\frac{\partial U_i}{\partial t} + \frac{f_{i+1/2} - f_{i-1/2}}{\Delta x} = 0$$

The same discretisation applied to point i+1 will give

$$\frac{\partial U_{i+1}}{\partial t} + \frac{f_{i+3/2} - f_{i+1/2}}{\Delta x} = 0$$

and for i-1

$$\frac{\partial U_{i-1}}{\partial t} + \frac{f_{i-1/2} - f_{i-3/2}}{\Delta x} = 0$$

The sum of these three equations is a consistent discretisation of the conservation law from x=i-2/3 to i+2/3 since the fluxes at internal points cancel each other. This concept is easy to generalise to multidimension.

To remain consistent with the conservation law the simplest way is to use finite-volume scheme. It approximates the integral form of conservation directly while the finite difference scheme uses the differential form. The FV approach guarantees conservation while the FD approach may not. Consider a grid with polygon cells one can write an integral form for each cell with area Aj

$$\frac{\partial}{\partial t}\iint_{A_j} W dA + \oint \vec{F}\cdot d\vec{\ell} = 0$$

The discretised equation associated with each cell is

$$\frac{\partial}{\partial t}(A_j W_j) + \sum_{sides}(\vec{F}\cdot d\vec{\ell}) = 0$$

where the sum of the flux terms are referred to all the external sides of the control cell Aj.

How to approximate the fluxes at the faces is not a simple problem. Although the shock capturing (conservative scheme) scheme can capture shocks it usually generates wiggles around discontinuities. The wiggles can either decrease accuracy or even cause the computer code to stop.

The classical shock capturing schemes use artificial dissipation to suppress the wiggles while the modern shock capturing schemes use a nonlinear filter to suppress the wiggles. The theory of producing monotone shocks is based on the nonlinear scalar equation (Godunov 1959, Van Leer 1973, Harten 1983)). To generalise it to a system it is through the use

of the Riemann solver, which solves the Riemann problem.

The Riemann problem is a classical initial value problem that can be posed for any hyperbolic system of equations. The initial data contains two constant states at the left and right sides of x=0. A Riemann problem and its solution for 1D Euler equation might look like Fig. 1.2. The solution is constant on each line (x/t)=constant, and consists of piecewise uniform regions separated by waves. A Riemann solver provides the waves information and therefore solution. The exact Riemann solver is usually computational expensive. Fortunately we do not need to use exact solution but a reasonable accurate solution is usually enough for numerical purposes. The nonexact Riemann solvers are often called approximate Riemann solvers (e.g. Roe 1981b, Osher 1982).

The Riemann solvers not only help one to generalise the schemes for scalar equation to systems but also make the schemes more physically based (Roe 1986a). In one dimension there are only two possible wave propagating directions. The 1D Riemann solver copes with this well. In two dimension the wave propagating directions are infinite. The two dimensional Riemann problem is too complicated to use numerically. The current solution is to consider the waves normal to the mesh boundaries only thus the 1D Riemann solver can be used on multidimension calculation. There are also more advanced approaches under development which find the main wave propagating directions instead of depending on the mesh orientation (Roe 1986b, Hirsch 1987).

In principal a finite volume scheme can be used on the grid consisted of any types of polygon. It is due to the accuracy and efficiency consideration that either quadrilateral or triangular grid are mainly used in two dimension.

It is easier and simpler to obtain accurate solutions on meshes with regular cells than on irregular cells. Another problem is that the cell relation needs to be established. If the cell relation can be fitted into a simple two dimension array we have structured grid. If it needs more complex ways of specifying cell relations it is called unstructured grid. Structured grid tends to be more efficient to compute but lacks the freedom of unstructured grid on complex domain. Triangular grid is often unstructured while the quadrilateral cell is often associated with structured grid.

For geometry complex problem, especially on three dimension, to generate a structured grid is sometimes impossible. A popular solution is to use zonal/multiblock grid generation. It first separates the computation domain to several nonoverlapped subdomains, then a structured grid is generated for each subdomain. A more flexible approach is to separate the original domain to several overlapped subdomain. For both approaches the global grid usually becomes unstructured. An advantage of using multiblock grid is that since each grid in the subdomain is generated independently one can use different mesh sizes in different subdomains to resolve fine flow feature locally. Another advantage is that different levels of governing equations can be used on different zones.

For the conservation problem one can consider the nonoverlapped zonal grid as a polygon grid on which the finite volume scheme keeps the conservation naturally. The overlapped grid is more flexible but to ensure a global conservation on such grid is quite difficult.

To simulate a realistic 3D configuration the memory required is very large for the mesh number is enormous big. It is currently impossible to put all the data in the primary memory in the CPU for full scale calculation. One has to swap the data between the primary and secondary memories constantly whether the multiblock or unstructured grid is used.

Once the grid is established it can be used to compute any flow condition in principle; however, the grid can not be optimum for every flow condition. For example one would like to have finer grid near the shock but the shock positions and numbers of shocks change for different Mach numbers. Even the grid is only used for one condition the grid can be too coarse or unnecessarily fine than it is actually required. Since the computer power is still far from sufficient one would like to make better use of computing resources. Grid adaption is a very effective solution to this problem. The original grid can be adjusted constantly during the calculation or the grid density can be increased/decreased locally to achieve uniform global accuracy.

1.2 Overview

The next five chapters are arranged in chronological order. There are mainly three topics covered in this thesis, which are either directly or indirectly related to the objective of producing a multiblock code for hypersonic flow.

The first topic contains three problems about Riemann solvers. The post-shock oscillation problem is discussed in chapter 2. The carbuncle phenomenon is examined at section 4.2 and section 6.7. The grid-dependent problem of current Riemann solver is demonstrated at section 6.8. The aim of these investigations is to improve the basic solver in single zone.

The second topic mainly concerns the zonal calculation. The effect of having different mesh sizes on different zones, especially with shocks present, is examined in chapter 3 with explicit schemes and a suggestion on mesh ratio between different zones is made. Chapter 4 discusses the implicit schemes for two dimensional steady state solutions. Various solvers are tried and special problems associated with hypersonic calculations are emphasized. The schemes tested are used in chapter 5. Chapter 5 concerns the implementation of implicit zonal method. A simple but robust treatment on the zonal boundary conditions is presented with results from different implicit solvers. The effect of shock present near the zonal boundary is also discussed.

The last topic which occupies most part of chapter 6 is about the calculation and grid adaption of viscous flow. A numerical study on Burgers equation and some suggestions on the mesh size control for grid adaption are presented.

An attempt to construct a cell-vertex TVD scheme is described in the appendix.

Since each chapter is quite independent the concluding remarks are given at the end of each chapters.

CHAPTER 2 : NUMERICAL STUDY OF RIEMANN SOLVERS ON SLOWLY MOVING SHOCKS

2.1 Introduction to Post-Shock Oscillation Problem

It has been observed for some time that when a shock is moving slowly some upwind schemes may produce wiggles at the higher density (post-shock) region, even when those schemes can not produce oscillations when used in the scalar equation. Note that this is not the same as the classical problem that some schemes produce wiggles around the discontinuities.

This problem only can happen in coupled systems, it does not occur in the scalar equation or in systems of equations that can be decouplable.

The non-monotone behaviour is certainly unwanted in unsteady flow calculations. Also it may cause convergence difficulty when one is using the time marching approach to find the steady state solution, which is the main reason that we want to investigate it.

We briefly review some Riemann solvers in section 2.2 and some previous works in section 2.3. In section 2.4 some results of extensive tests on Roe's scheme, which is known to have post-shock oscillations, are presented. We investigate the P variant of Osher's scheme and introduce Bell's method in section 2.5. In section 2.6 we show some results from Roe's scheme with dissipation. Section 2.7 shows how to reduce the post-shock oscillations of second order schemes. Concluding remarks are given in section 2.8.

2.2 Review of Riemann solvers

Here we only point out some important differences between various Riemann solvers. For more complete comparisons we recommend the paper by Van Leer (1984) for the scalar equation and the lecture notes by Pandolfi (1987) for nonlinear systems. The chapter 20 in the textbook by Hirsch (1990) also gave very good introductions.

We first start with the scalar equation

$$W_t + [f(W)]_x = 0$$

The 1st order conservative scheme can be written as, refer to Fig. 1.1,

$$W^{n+1} - W^n + \frac{\Delta t}{\Delta x}\left[H_{i+1/2}(W_i, W_{i+1}) - H_{i-1/2}(W_{i-1}, W_i)\right] = 0$$

For the Godunov's scheme (1959) $H^G(W_L, W_R)$, the interface flux, is equal to the exact flux value of the Riemann problem at $x=0.5(x_L+x_R)$ with W_L and W_R as left and right states. For Roe's scheme (1981a) we have

$$H^R(W_L, W_R) = \frac{1}{2}(f_R+f_L) - \frac{1}{2}\left|\frac{f(W_R)-f(W_L)}{W_R-W_L}\right|(W_R-W_L)$$

For Engquist-Osher's scheme (1980) we have

$$H^{EO}(W_L, W_R) = \frac{1}{2}(f_R+f_L) - \frac{1}{2}\int_{W_L}^{W_R}\left|\frac{df}{dW}\right| dW$$

For the case in which (W_L, W_R) does not contains the sonic point (where df/dw=0), these three fluxes are the same. However for the case where the interval contains the sonic point (now we only consider the sonic point in the compression wave) we have $H^G = H^R \neq H^{EO}$. Analytically H^{EO} is smooth but not H^G or H^R.

Take the inviscid Burgers' equation $w_t+(1/2w^2)_x=0$ for example. Using the Rankine-Hugoniot relation $f_R-f_L=w_s(w_R-w_L)$ we obtain the shock speed $w_s=1/2(w_L+w_R)$. The sonic point is $w=0$. Consider the right moving shock case, i.e. $w_L>w_s>0>w_R$. Both Godunov and Roe fluxes take the flux at $x=0$ therefore $H(w_L,w_R)=1/2w_L^2$, see Fig. 2.1a. E-O scheme considers the shock as an overturned centered compression wave (Van Leer 1984) and the interface flux is equal to the sum of three fluxes at $x=0$, thus $H^{EO}=1/2w_L^2+0+1/2w_R^2$, see Fig. 2.1b.

For the one dimension Euler equations

$$\frac{\partial W}{\partial t}+\frac{\partial F}{\partial x}=0$$

where

$$W=\begin{vmatrix}\rho\\ \rho u\\ e\end{vmatrix}, \qquad F=\begin{vmatrix}\rho u\\ \rho uu+p\\ u(e+p)\end{vmatrix}$$

the 1st order conservative scheme is again

$$W^{n+1}-W^n+\frac{\Delta t}{\Delta x}\left[H_{i+1/2}(W_i,W_{i+1})-H_{i-1/2}(W_{i-1},W_i)\right]=0$$

Godunov's scheme uses exact Riemann solution for $H_{i+1/2}$ which needs expensive iterations.

In the approximate Riemann solver of Roe three linearised waves replace two nonlinear waves and one linear wave, therefore the expansion wave is replace by a single wave. Roe defined a local matrix $A(W_L,W_R)$ whose eigenvector e_k and eigenvalues λ_k satisfy

$$W_R-W_L=\sum_{k=1}^{3}\alpha_k e_k$$

$$F_R-F_L=\sum_{k=1}^{3}\lambda_k\alpha_k e_k$$

where α_k is the wave strength. Roe's Riemann solver returns the exact solution whenever W_L and W_R lies on opposite sides of a shock or a contact discontinuity. The expression for λ_k,α_k, and e_k were given by Roe (1981b)

$$e_1=\begin{vmatrix}1\\ \tilde{u}-\tilde{a}\\ \tilde{h}-\tilde{u}\tilde{a}\end{vmatrix},\quad e_2=\begin{vmatrix}1\\ \tilde{u}\\ 1/2\tilde{u}^2\end{vmatrix},\quad e_3=\begin{vmatrix}1\\ \tilde{u}+\tilde{a}\\ \tilde{h}+\tilde{u}\tilde{a}\end{vmatrix}$$

$$\lambda_1=\tilde{u}-\tilde{a},\qquad \lambda_2=\tilde{u},\qquad \lambda_3=\tilde{u}+\tilde{a}$$

$$\alpha_1=\frac{1}{2\tilde{a}^2}\,[\Delta p-\tilde{\rho}\tilde{a}\Delta u],\qquad \alpha_2=\frac{1}{\tilde{a}^2}\,[\tilde{a}^2\Delta\rho-\Delta p],\qquad \alpha_3=\frac{1}{2\tilde{a}^2}\,[\Delta p+\tilde{\rho}\tilde{a}\Delta u]$$

where

$$\tilde{a}^2=(\gamma-1)[\tilde{h}-1/2\tilde{u}^2]$$

$$\tilde{\rho}^2=\rho_L\rho_R\qquad \tilde{u}=\frac{\rho_L^{1/2}u_L+\rho_R^{1/2}u_R}{\rho_L^{1/2}+\rho_R^{1/2}}\qquad \tilde{h}=\frac{\rho_L^{1/2}h_L+\rho_R^{1/2}h_R}{\rho_L^{1/2}+\rho_R^{1/2}}$$

For Osher's scheme (1982) three simple waves replace the real wave system, therefore shock wave is replaced by compression wave. On each simple wave the E-O method is applied. In the original Osher's paper (O variant) the left to right state is connected by u+a, u, and u-a waves in a physically reversed order. This can be considered as a solution of backward Riemann problem. Another possibility is to use P (physical) variant, see Fig. 2.2. The only difference to O variant is that the left to right state is connected by u-a, u, u+a simple waves in physically correct order. P variant has been used by Hemker (1986) for transonic calculation. The intermediate states separated by the simple waves can be found by using the Riemann invariants. Since there are two Riemann invariants along each simple wave in total six equations can be defined for the six unknowns in the two intermediate states $W_{1/3}$ and $W_{2/3}$. The possible sonic points, W_{s1} and W_{s2}, inside the u-a and u+a simple waves can also be found. Equipped with these data we can work out the interface flux. The O variant of Osher's solver is very expensive due to the evaluation of exponents and the logics involved. The P variant is cheaper to use (Hemker 1986) but the main problem with both variants is that they are very difficult to be used on real gas flow.

Fig. 2.3 gives a graphical picture of these Riemann solvers.

2.3 Previous Works

The first detailed account of this problem was given by Colella and Woodward (1984) in their paper about PPM method. They observed that low amplitude post-shock oscillations occurred when the characteristic speed associated with a strong shock, measured relative to the grid, vanished. And the dissipation introduced by Godunov's method vanished as the shock speed went to zero therefore dissipation presented in a slowly moving shock using Godunov's method was not sufficient to guarantee correct entropy production across the shock.

They showed an example for an extremely strong shock moving slowly from right to left (see Fig. 2.4). There were substantial oscillations on both entropy and the Riemann invariant $u-2a/(\gamma-1)$, but the quantity $u+2a/(\gamma-1)$ the Riemann invariant transported along the (u+a) characteristic was well behaved. Their explanation was that in (u+a) wave any errors generated in that variable were immediately driven back to the shock transition layer while in the u and u-a waves the errors were carried away from the shock (see Fig. 2.5), therefore post-shock oscillations only appeared in nonlinear system of equations. They proposed to add some dissipations to decrease the oscillations.

Roberts (1988) compared Godunov's, Roe's, and Osher's schemes on a Mach 3 shock which took 50 steps to cross a cell for Courant number 0.95. He showed Osher's scheme behaved quite well while Godunov's and Roe's schemes exhibited obvious post-shock oscillations not only for extremely strong shocks but

even for weak shocks. He also showed that the results from Roe's scheme with minmod limiter were worse than those from the first order Roe's scheme. The reason is because 2nd order scheme is less dissipative to suppress the oscillations. One more interesting result obtained from Osher's scheme with natural ordering of wave paths showed that it was not as good as the original scheme which used reversed ordering of wave paths. He also showed the oscillations would occur for schemes with flux functions that give "exact" shock resolution such as Godunov's and Roe's schemes.

2.4 Numerical Experiments and Results on Roe's Scheme

Our purposes in doing the numerical experiments are first to reproduce Roberts' results and then test the schemes more systematically to find the parameters associated with the post-shock phenomena.

The initial data for these tests are obtained by superimposing a velocity on a zero velocity shock, this velocity can be either positive or negative (see Fig. 2.6). The shock condition is labeled by 'Mach Number X'. Here the "Mach number X" shock means the shock data, such as pressure jump, are obtained from the steady normal shock relations for Mach number X and ratio of specific heats 1.4. The grid is uniform. The results shown later in some graphs are for the density, $u-2a/(\gamma-1)$, entropy, and $u+2a/(\gamma-1)$. The last three quantities are the Riemann invariants of u-a, u, and u+a waves, and they will be denoted as R1, R2, and R3 thereon. It should be noted that the scales change from graph to graph.

There are three main conclusions from this experiment.

Firstly, we stress again that the post-shock oscillation occur even when the shock strength is very weak. Fig. 2.7 is for Osher's and Roe's schemes with Mach no. 1.2 and SR -0.035 (SR to be defined later). The oscillations in density, R2, R3 are obvious while R1 behaves quite well. Because of the graph scale the oscillations seem quite large, actually they are very small. We can also observe from the pictures that Osher's scheme performs better than Roe's. Fig. 2.8 is for Osher's and Roe's schemes with Mach no. 20 for SR 0.035. The pictures speak for themselves for results from Osher's scheme, therefore we will concentrate on Roe's scheme.

Secondly, the Courant number is not important. In other words how many time steps the shock takes to cross a cell is not important. We have even tried with Courant no. 0.05.

Thirdly, the relative shock speed is important. If the shock moves slowly or fast enough then the oscillations are very small. The amplitude of oscillations first increases then decreases when the shock speed is increasing or decreasing from zero. The maximum amplitude of density oscillations for shocks moving from low density to high density region is bigger than for shocks moving in another direction, but for entropy oscillations the situation reverses. To nondimensionalise the shock velocity the shock speed is divided by the (u+a) of the right side state. The nondimensionalised shock speed is called SR. The reason to use (u+a) of right state instead of the associated characteristic speed is simply to avoid the SR value becoming too small; nevertheless, it seems to work well. Fig. 2.9 gives the maximum amplitude of density oscillation versus SR. The SR value which produces maximum oscillation is

around ±0.035. SR -0.035 with Courant number 0.95 is very close to Roberts' test. The peak error for downstream moving shock is higher than that of upwind moving shock in Fig. 2.9, which is simply due to the parameter we choose. If the SR is plotted with respect to entropy error the peak of the upstream moving shock will be bigger. The reason to use density is because the oscillation level is easier to measure than using other variables after the computer output is examined.

2.5 Results of P Variant and Bell's scheme

Although Roberts has pointed out that Osher's P variant does not produce as good results as O variant. We still try to look it again. From our experiment we confirm Roberts' results. We also observe one strange behaviour that when the Mach number is high and SR is more negative P variant tends to produce a very large overshoot, see Fig. 2.10. It will cause program to stop. The result seems to tell the E-O flux formulation is not the main or the only recipe for success. So the secret is not the smoothness of the flux function.

Nevertheless we try further to modify Roe's scheme with a view to obtaining properties closer to that of the E-O flux. Bell et al (1989) proposed an approximate Riemann solver to general systems of hyperbolic conservation laws. Their higher order scheme was basically a PPM approach. It has also been extended to problems that were not strictly hyperbolic and exhibited local linear degeneracies in the wave fields. However no result for Euler equations was given.

Here we give an outline of their first order scheme.

Their scheme can be thought as a simplification of Osher's scheme or an enhancement of Roe's scheme. Instead of evaluating the intermediate points $W_{i+1/3}$ and $W_{i+2/3}$, which separate different waves, and possible sonic points W_{s1} and W_{s2}, see Fig. 2.11, by equations of Riemann invariants in Osher's scheme, they are evaluated by eigenvector decomposition and interpolation, and natural ordering of wave paths is assumed. Or to start with Roe's linear wave decomposition, the u-a or u+a waves are not considered as a single wave each and then Engquist-Osher flux formula is used in stead of Roe flux formula.

Note that it is not possible to have O variant with this approach because unphysical intermediate states might occur.

Assume we have a subroutine of Osher's solver. That is, the flux $H_{i+1/2}$ will be computed from intermediate states $W_{i+1/3}$, $W_{i+2/3}$, and any sonic states that are met with. We only need to change few lines to become a subroutine of Bell's solver. First we replace the equations for $W_{i+1/3}$, and $W_{i+2/3}$ by

$$W_{i+1/3} = W_i + \alpha_1 e_1$$

$$W_{i+2/3} = W_{i+1/3} + \alpha_2 e_2$$

which involve no expensive exponent calculations. α_k and e_k are simply in term of $0.5(W_i + W_{i+1})$. Roe's averaging is not required. Since natural ordering of wave paths is used, the eigenvalue, λ_1 wave speed, associated with wave path 1 must be change back to u-a and u+a for wave path 3. Finally to replace the equations for sonic points, W_{s1} and W_{s2}, at wave paths 1 and 3, the wave speeds λ_1 and λ_3 are assumed to vary linearly from W_i to $W_{i+1/3}$ and from $W_{i+2/3}$ to W_{i+1}. For example, to find W_{s1}, we solve equations

$$C_1 (\lambda_1)_1 + C_2 = W_1$$

$$C_1 (\lambda_1)_{i+1/3} + C_2 = W_{i+1/3}$$

to obtain C_2 (C_1 and C_2 are vectors). And at sonic point λ_1 is zero, so $W_{s1} = C_2$. Again in evaluating the sonic points no exponent calculation is needed. Note that Bell used Hermite cubic interpolation. This approach is checked by using the Lax's shock tube problem, see Fig. 2.12.

In general the post shock oscillations are reduced but it does have another problem. For large Mach no. and negative SR it produces a very big overshoot similar to that by Osher's P variant, although it is not as large as Osher's P variant.

The results simply tell that incorporating a contribution from the sonic point within a shock is not the sole reason of the success of Osher's O variant.

2.6 Roe's Scheme with Harten's Dissipation

From the above results it is obvious that Osher's scheme is better than Roe's for solving slowly moving shocks. However Osher's scheme is quite expensive to compute and difficult to use on more complicated problems, such as real , reacting gas , etc because of the evaluation of the flux integral.

In contrast Roe's scheme is much cheaper to run and easier to use on complicated problems. Therefore we are trying to modify Roe's scheme to cure its post-shock oscillations. Following Colella and Woodward's approach we add some dissipations in Roe's scheme explicitly.

In Roe's approach, the interface flux is

$$H^R(W_L,W_R)=\frac{1}{2}(F_R+F_L)-\frac{1}{2}\sum_{k=1}^{3}|\lambda_k|\alpha_k e_k$$

In order to break the unphysical solution from this formula, Harten (1983a,1983b) used

$$H^H(W_L,W_R)=\frac{1}{2}(F_R+F_L)-\frac{1}{2}\sum_{k=1}^{3}Q_k\alpha_k e_k\frac{\Delta x}{\Delta t}$$

where

$$Q_k=\begin{cases}|\nu_k| & \text{if } |\nu_k|>\delta\\ \frac{1}{2}\left(\frac{\nu_k^2+\delta^2}{\delta}\right) & \text{if } |\nu_k|\le\delta\end{cases},\qquad \nu_k=\lambda_k\frac{\Delta t}{\Delta x}$$

at the expense of some deterioration in resolution, especially at the shock.

The post-shock oscillations can be suppressed by this dissipation with well-tuned δ and the solution can match that from Osher's scheme.

One main disadvantage is that δ needs to adjust for each case and it is CFL number dependent. We modify this formula by consider Q_k as function of ν_k, $\Delta\nu_k$ and Δt^{max}, where $\Delta\nu_k$ is the difference of Courant number in the same type of wave and Δt^{max} is the local maximum allowed time step , see Fig. 2.13. The modified Q_k is given by

$$Q_k=\frac{1}{2}\left(\frac{\nu_k^2+\delta_k^2}{\delta_k}\right),\qquad \delta_k=\frac{\Delta t}{\Delta t^{max}}\Delta\nu_k\bar{\delta}\ ,\qquad \Delta\nu_k=|(\nu_k)_R-(\nu_k)_L|$$

where $\bar{\delta}$ is taken as 0.5 from numerical experiments. This is only implemented in the interval which contains the shock point.

Fig. 2.14 shows side by side comparison of several schemes on the Mach 3 shock. Acceptable results are obtained with the modified dissipation.

2.7 Second Order Schemes

The first order schemes based on Riemann solvers can be extended to higher order schemes. Unfortunately the second or higher order schemes exhibits oscillations near discontinuity even for the linear scalar problems.

Since Godunov (1959) showed that all monotone linear schemes can be at most of first accuracy, the only way around the difficulty is to build in some nonlinearity, e.g. artificial dissipation and limiter. Limiters were first introduced by Van Leer (1973) and independently by Boris and Book (1973).

With the nonlinear limiter present the schemes defies the classic Fourier analysis. Fortunately stability can be guaranteed by using the TVD (total variation diminishing) condition (Harten 1983b).

The concept of bounded total variation is an important property of a scalar conservation law $u_t+f_x=0$ (Lax 1973). The total variation of any physically admissible solution

$$TV=\int\left|\frac{\partial u}{\partial x}\right|dx$$

does not increase in time. The discrete analogy is that the total variation in x of a discrete solution to a scalar conservation law is defined by

$$TV(u)\equiv\sum_i|u_{i+1}-u_i|$$

A numerical scheme is said to be total variation diminishing if

$$TV(u^{n+1})\leq TV(u^n)$$

Harten (1983b) proved that any TVD schemes do not produce oscillations and any TVD schemes are stable. However when it is generalized to nonlinear system as we have seen even for first order scheme it is not true.

Return to post-shock oscillation problem. Since second order scheme is less dissipative than the first order scheme, one can expect it will produce larger oscillations. Roberts gave a demonstration of 2nd order result with Roe's Riemann solver and minmod limiter. Here we attempt to decrease the oscillations from the second order or higher order schemes.

Lax-Wendroff scheme with TVD flux limiter is used, see Roe and Pike (1984). The interface flux between i and i+1 is

$$H_{i+1/2} = \text{1st order flux} + 0.5\sum_{k=1,3}^{k+}\beta^{k+}\phi(r^{k+}_{i+1/2})\,\Delta f^{k+}_{i+1/2} - 0.5\sum_{k=1,3}^{k-}\beta^{k-}\phi(r^{k-}_{i+1/2})\,\Delta f^{k-}_{i+1/2}$$

with

$$\Delta f^{k+}_{i+1/2} = \lambda_k \alpha_k e_k \text{ for } \lambda_k \geq 0$$

$$\Delta f^{k-}_{i+1/2} = \lambda_k \alpha_k e_k \text{ for } \lambda_k \leq 0$$

$$r^{k+}_{i+1/2} = \frac{\Delta f^{k+}_{i-1/2}}{\Delta f^{k+}_{i+1/2}}, \qquad r^{k-}_{i+1/2} = \frac{\Delta f^{k-}_{i+3/2}}{\Delta f^{k-}_{i+1/2}}, \qquad \beta^{k\pm} = 1 - \left|\nu^{k\pm}_{i+1/2}\right|$$

where ϕ is the limiter function. A detail account on the flux limiter can be found from Sweby (1983). Three popular limiters are

$$\text{minmod}: \phi(r) = \begin{cases} 0 & \text{if } r<0 \\ r & \text{if } 0\leq r\leq 1 \\ 1 & \text{if } r>1 \end{cases}$$

$$\text{van Albada}: \phi(r) = \frac{r+r^2}{1+r^2}$$

$$\text{superbee}: \phi(r) = \begin{cases} 0 & \text{if } r\leq 0 \\ 2r & \text{if } 0<r\leq 0.5 \\ 1 & \text{if } 0.5<r\leq 1 \\ r & \text{if } 1<r\leq 2 \\ 2 & \text{if } r>2 \end{cases}$$

To use Lax-Wendroff scheme we need to have the average wave speed for each wave family. Roe's scheme provides average

speeds but not Osher's. We can take the average wave speed as the average of the wave speeds at the start and end of each simple wave for Osher's scheme. This approach is verified by checking the Sod's shock tube problem, see Fig. 2.15. Note that Osher and Chakravarthy (1984) used entropy function to evaluate the limiter which is inferior to the current flux gradient approach especially on the contact and expansion waves, see Fig. 2.16 of Lax's shock tube problem.

The oscillations for the slow moving shock are obviously larger from second order schemes using Osher's scheme, see Fig. 2.17.

The cure we propose is to check if the interval between left and right states contains any sonic point then we switch off limiter. Therefore it reduces to first order scheme in the shock layer. This proves to work well. The global solution is not degraded and the postshock oscillations are decreased significantly. The method is especially easy to implement into Osher's solver. Note that in the sonic interval ϕ is not necessary zero because inside the shock layer the flow is smooth. It is only in the corner of the shock profile one can be sure that ϕ is zero.

Note that sonic points include not only the sonic point in the compression wave but also the sonic point in the expansion wave. It is well known that the numerical sonic flux for the expansion wave is not appropriate to simulate the physical expansion. Using limiter for the sonic flux will produce worse results. Therefore it is reasonable to switch off limiter when evaluating the sonic flux. For the 2nd scheme using Roe's solver same technique can be applied plus dissipation. The result is much improved. Fig. 2.17 give comparisons of results

from 2nd order schemes.

2.8 Concluding Remarks

We do not have real success in the quest of why Osher's O variant has the best performance on slow moving shocks. The dissipation approach for Roe's scheme is not a very good solution. Nevertheless some progress has been made to understand this problem. The theoretical analysis of discrete shock profile for scalar case was made by Jennings (1970) with very sophisticated mathematics. To perform similar analysis for system is nevertheless far beyond author's ability.

To switch off limiter inside the shock layer will reduce the noises generation for high order scheme. This should be quite useful for the unsteady calculations; however, as we find out later, this limiter-off approach is not suitable for implicit schemes on the steady state calculations because it introduces unsmoothness.

The dissipation approach is not implemented in later work for we understand later that for hypersonic calculation the problem to cure the carbuncle phenomenon (see chapter 4) outweighs the post shock oscillation problem.

CHAPTER 3 : EFFECTS OF MESH SIZE CHANGE ON SHOCKS

3.1 Introduction

For the zonal method, it allows local grid refinement to obtain better local flow resolution. Here we investigate two possible problems due to the mesh size change. The main purpose is to see the effects of mesh size change and to provide suggestions on choosing the mesh ratio. We try to explain the problems due to mesh size change but not to cure them.

Firstly, we apply 1st order flux difference splitting schemes (Roe's and Osher's) for the moving shock problem on nonuniform grid in one dimension. For simplicity, the grid consists of two nonoverlapped uniform zones with different mesh sizes.

The main purpose is to investigate how the mesh size change influences the solutions when shocks passing the zone boundary and hopefully to gain some insight for explaining similar problems on two dimensions.

Pike (1987) showed that 1st order schemes degraded to zero order schemes and 2nd order schemes became 1st order accurate on irregular grids. First and 2nd order schemes on irregular grids were developed, however no extension to multidimension was proposed. In this work, we only consider the original first order schemes.

Osher's scheme is used for most tests because it has least post-shock oscillations. If Roe scheme is used we might have difficulty to separate the post-shock oscillations and noises generated at zone boundary. We will also show that with

additional dissipations in Roe's scheme it will produce as good results as Osher's.

The other problem we investigate here is the case that the steady shock lies on two different uniform grids in two dimension. The motivation of this work is from Berger and Colella's paper (1989). They reported considerable degradation at interfaces where the shocks were not aligned with the mesh. Again first order scheme is used. To save the CPU time mainly Roe's scheme is used instead of Osher's since in the oblique shock case two schemes perform quite similarly due to the shock smearing.

In section 3.2 we discuss the test cases for the moving shock in one dimension. The results are discussed in section 3.3. Section 3.4 is for oblique shock results. Concluding remarks are given in Section 3.5.

3.2 Test Cases for the Moving Shock in One Dimension

By exchanging the mesh sizes of left and right zones and letting the shock move in either positive or negative directions four tests, A, B, C and D, can be done for a certain Mach number and shock speed (see Fig. 3.1).

In the graph for each test case, six shock positions, P1, P2, P3 ,P4 ,P5 and P6, are monitored, see Fig. 3.2. Because the initial data, which has no intermediate shock point, is not the form that a progressing wave would take in the numerical scheme, a starting error appears immediately after one time step. P1 is where the shock just travels across one cell. This is for seeing the starting error. P2 is where the shock position is just one or two cells from the zone boundary. It is for checking if the starting error has nearly vanished. In most

graphs, P3 is approximately where the noises generated by shock crossing zone boundary reaches its maximum and P4 is just little away from P3. P3 and P4 are for observing the mesh size change effect. P5 is where the shock position is a little away from the zone boundary and P6 is further away from the zone boundary. From P5 and P6 we can see how the noises are dissipated and propagated.

3.3 Results and Discussion of the Moving Shock

Fig. 3.3 is for Mach no. 20 shock and mesh ratio 5:1 with SR $\pm$0.035, and Fig. 3.4 is for SR=$\pm$0.28, for all four cases. We can observe that in cases A and D for which shocks move from coarse to fine zone bumps in density are created, and in case B and C for which shocks move from fine to coarse zone depressions in density are generated, especially for SR+0.28. It is also obvious that these noise magnitudes increase when SR increases which is different from the post shock oscillation problem. Some tests on intermediate SR values support this observation.

As we might expect the noises increase when the mesh size difference and Mach number increase.

Fig. 3.5a is for case A, Mach no. 20, SR 0.035 and mesh ratio 5:1 for Roe's scheme. The post-shock oscillation effect is mixed with the effect of noises induced by mesh size change. Fig. 3.5b is also for Roe's scheme but with Harten's dissipation. It is nearly as good as Fig. 3.3 since the post-shock oscillation is suppressed once the dissipation is added appropriately. Fig. 3.5c is for Roe's scheme with SR 0.28. The result is quite the same as Fig. 3.4 from Osher's scheme because the post-shock oscillation is nearly removed at such SR.

Now we present a explanation for some computed results. It is simply based on the shock resolution characteristics of 1st order FDS scheme.

The number of mesh points needed by FDS schemes to resolve shocks depends mainly on the shock speed. Therefore if the shock is resolved on coarse grid by N points it will also be resolved by N points on fine grid. But the shock transition lengths are different.

For shock move from zone 1 with mesh spacing DX1 to zone 2 with mesh spacing DX2, the shock transition length change is equal to N(DX1-DX2). The length change increases when DX1-DX2 or N increase. In other words, it increases when mesh ratio or shock speed increases (because 1st order FDS scheme is quite dissipative the N value increases with shock speed). This explain the results that relative noise magnitude increases when mesh ratio and shock speed increase.

Second order schemes will be less sensitive to shock speed change since they are less dissipative, but they will still suffer from mesh size change.

The bump or depression feature is not easy to explain. It is perhaps because in the case that shock moves from coarse to fine grid part of the shock profile is suddenly forced to steepen and in the case that shock moves from fine to coarse grid it is suddenly flattened.

3.4 Test Cases and Finite Volume Scheme for the Oblique Shock

The test case is a two dimensional steady oblique shock. One can imagine it is the flow past a wedge and the computational domain is rotated with respect to the free stream flow direction. Therefore we can have arbitrary shock to grid angle but keep the shock strength unchanged, see Fig. 3.6.

First order finite volume upwind scheme (not operator splitting) is used. The initial condition can be either the free stream or postshock condition. The initial shock will appear at the bottom/left boundary if the initial condition is the freestream/postshock condition then it will move to its steady state position. We choose the flow conditions and computational domain such that we have always supersonic flow boundaries. At inflow boundaries the exact boundaries are prescribed and at the outflow boundaries zero order extrapolation is used.

Fig. 3.7 is for a Mach number 20 oblique shock in single uniform grid. The flow properties are slightly below the right values at post-shock position. The computed shock is slightly curved. These problems are due to boundary conditions and narrow computation domain.

By changing the grid spacing we can do some tests on two zones by using the programme for one zone. Fig. 3.8 is for the shock to grid angle 70 degree. Because the shock has more inclination towards the Y direction mesh refinement in Y direction has nearly no effect on the solution. Mesh refinement in X direction improves the shock resolution but induces

overshoot.

For the more general grid boundary, a simple treatment on the interface fluxes is adopted. For example, see Fig. 3.9, the interface flux at 1-2 is $H_{12}(W_c,W_a)$ and at 2-3 is $H_{23}(W_c,W_b)$. To update the coarse cell we need H_{13}, H_{13} is simply taken as the sum of H_{12} and H_{23}.

Coarse zone and fine zone perform one iteration each to count for one iteration for whole domain.

If the fine zone is on the top, we can observe big overshoot at post shock position; however, if the coarse zone is on the top there is no overshoot , see Fig. 3.10 and 3.11. The explanation for this is that the coarse zone on the bottom provides a bad boundary condition for the fine zone on the top. One can see quite clearly from the cross section density plot in Fig. 3.11 the shock transition in the first row of fine zone is staircaselike. On the contrary if the fine zone is on the bottom the transition is smooth. This could influence global solution in practical zonal applications.

We try further two types of interface flux evaluation based on one dimensional interpolation, see Fig. 3.12. For method 3 we can obtain smooth transition at the first row; however, the overshoot is still produced eventually, see Fig. 3.13. This is because it still does not provide correct boundary condition to produce a shock on fine grid despite the transition is smooth.

While the above results are from grids with integer spacing. For grid with noninteger spacing it does not seem to produce extra problem. Fig. 3.14 is for same grid ratio but discontinuous grid lines and Fig. 3.15 for different grid ratio. The results are very similar to the integer spacing cases.

The process of shock evolution is quite smooth for freestream as initial condition, but much harder for post shock condition as initial condition and for local time stepping. We can see from the Fig. 3.16 that very big noises are generated during the evolution process. Fortunately they propagate out of the computational domain very quickly.

3.5 Concluding Remarks

We now understand that for shock moving across two different grids, large disturbances can be generated. Fortunately this phenomena does not hamper the convergence if they propagate out of the boundary quickly. We do not know what will happen if the noise is trapped in a computational domain. It might take time to dissipate.

From the oblique shock results we suggest that where shocks are likely to be present large mesh ratio, say more than 2, should be avoided even for steady state calculation.

CHAPTER 4 : THE IMPLICIT SCHEME FOR SINGLE ZONE

4.1 Introduction

The explicit scheme, especially the TVD scheme, needs thousands of iterations to reach convergence due to the CFL rule restriction. Implicit schemes escape the CFL rule in theory. Although most implicit schemes cannot converge as fast as theory suggests, they still converge faster than explicit schemes in terms of iteration number and CPU time.

To prepare for the next chapter on the implicit zonal method, we investigate the implicit scheme here with emphasis on inviscid hypersonic flow, which is much more difficult to compute than transonic flow.

Section 4.2 introduces the explicit operator and the carbuncle phenomenon. The implicit operator is discussed in section 4.3. Several methods for solving the matrix equation generated by the implicit scheme are briefly described in section 4.4. Explicit and implicit boundary conditions are explained in section 4.5. Section 4.6 presents the results from various solvers of section 4.4. The experience on linear and nonlinear GMRES is describes in section 4.7. Finally concluding remarks are given in section 4.8.

4.2 The Explicit Operator and the Carbuncle Phenomenon

The scheme we use is a 2nd order accurate finite volume scheme with TVD flux limiter and Roe's Riemann solver is adopted. There are several reasons behind this choice.

The finite volume approach is most natural to preserve conservation in the nonoverlapped composite grid. As we will demonstrate in next chapter it is easier to implement than the finite difference approach.

The order of accuracy is another issue. First order is not accurate enough. The so called 3rd order schemes are only true in one dimension; besides, in the zonal calculation we need to store more data of the neighbourhood of the interface due to the wider stencils of 3rd order schemes. Thus the 2nd order schemes are preferred. In the 2nd order scheme category we can have at least three choices, fully upwind, Lax-Wendroff and central difference. However fully upwind and Lax-Wendroff are not 2nd order accurate in two/three dimensions without resorting to operator splitting or predictor-corrector method. The only choice left is the central difference scheme with TVD limiter.

Th explicit operator was first proposed by Osher and Chakravarthy (1984) and later used by Rai (1986); however, its property was not well understood. Roe (1987) gave a clearer insight of this operator with emphasis on Navier-Stoke equations. We will only give a brief description here.

The Euler equations in two dimension are given by

$$\frac{\partial W}{\partial t}+\frac{\partial F}{\partial x}+\frac{\partial G}{\partial y}=0$$

where

$$W=\begin{vmatrix}\rho\\ \rho u\\ \rho v\\ e\end{vmatrix},\quad F=\begin{vmatrix}\rho u\\ \rho uu+p\\ \rho uv\\ u(e+p)\end{vmatrix},\quad G=\begin{vmatrix}\rho v\\ \rho vu\\ \rho vv+p\\ v(e+p)\end{vmatrix},$$

$$p=(\gamma-1)[e-0.5\rho(u^2+v^2)].$$

The semidiscrete finite volume form for a quadrilateral cell i,j is, see Fig. 4.1,

$$A_{ij}\frac{\partial W_{ij}}{\partial t}+H_{i+1/2j}-H_{i-1/2j}+H_{ij+1/2}-H_{ij-1/2}=0$$

where A is the cell area and H is the interface flux. For the latter use we define

$$R(W_{ij}) = (H_{i+1/2j} - H_{i-1/2j} + H_{ij+1/2} - H_{ij-1/2})$$

For first order scheme we have, for example,

$$H_{i+1/2j} = 0.5\,(F_{i+1j} + F_{ij})\,s^x_{i+1/2j} + 0.5\,(G_{i+1j} + G_{ij})\,s^y_{i+1/2j} - 0.5 \sum_{k=1}^{4} |\lambda_k|\,\alpha_k\,e_k\,s_{i+1/2j}$$

$$= h_{i+1/2j}$$

where λ_k, α_k, and e_k are obtained from one dimensional wave decomposition along the normal of the segment ab. The normal is given by

$$\vec{s}_{i+1/2j} = s^x_{i+1/2j}\,\vec{i} + s^y_{i+1/2j}\,\vec{j}$$

$$s^x_{i+1/2j} = y_a - y_b, \qquad s^y_{i+1/2j} = x_b - x_a, \qquad s_{i+1/2j} = |\vec{s}_{i+1/2j}|$$

Define the interface flux Jacobian as

$$J_{i+1/2j}(W_{i+1j} - W_{ij}) = (F_{i+1j} - F_{ij})\,s^x_{i+1/2j} + (G_{i+1j} - G_{ij})\,s^y_{i+1/2j}$$

and $$J_{i+1/2j} = (RDL)_{i+1/2j}$$

where J, R, D and L are 4x4 matrices. R is the matrix of right eigenvector e_k. D is a diagonal matrix with $\lambda_k s_{i+1/2j}$ as diagonal entry. L is the matrix of left eigenvector ℓ_k. The formulae for R, D, and L can be found in Chakravarthy and Osher (1985) for 2D case and Chakravarthy (1987) for 3D case. The wave strength α_k is given by

$$\alpha_k = \ell_k (W_{i+1j} - W_{ij})$$

Therefore we have

$$\sum_{k=1}^{4} \lambda_k \alpha_k e_k s_{i+1/2j} = (F_{i+1j} - F_{ij})\,s^x_{i+1/2j} + (G_{i+1j} - G_{ij})\,s^y_{i+1/2j}$$

The wave speeds λ_k are

$$\lambda_1 = V_n + a, \qquad \lambda_{2,3} = V_n, \qquad \lambda_4 = V_n - a$$

where V_n is the interface velocity normal to the cell boundary.

For central-difference TVD scheme the interface flux is

$$H_{i+1/2,j} = h_{i+1/2,j} + 0.5 \sum_{k=1,4}^{k+} \phi(r^{k+}_{i+1/2,j})\, \Delta f^{k+}_{i+1/2,j} - 0.5 \sum_{k=1,4}^{k-} \phi(r^{k-}_{i+1/2,j})\, \Delta f^{k-}_{i+1/2,j}$$

where

$$\Delta f^{k+}_{i+1/2,j} = \lambda_k \alpha_k e_k s_{i+1/2,j} \quad \text{for } \lambda_k \geq 0$$

$$\Delta f^{k-}_{i+1/2,j} = \lambda_k \alpha_k e_k s_{i+1/2,j} \quad \text{for } \lambda_k < 0$$

$$r^{k+}_{i+1/2,j} = \frac{\Delta f^{k+}_{i-1/2,j}}{\Delta f^{k+}_{i+1/2,j}} \quad , \qquad r^{k-}_{i+1/2,j} = \frac{\Delta f^{k-}_{i+3/2,j}}{\Delta f^{k-}_{i+1/2,j}}$$

ϕ is the limiter function, see section 2.7. One can see immediately that if when the flow is smooth ϕ is about 1 then this scheme becomes central difference.

The semidiscrete form can be approximated to high order of accuracy in time by using Runge-Kutta scheme. To preserve the TVD property in time not all classes of Runge-Kutta scheme can be used, see Shu (1988) for more details. The TVD preserving R-K scheme can not increase the time step size. With minmod and superbee limiter the CFL number allowed are only 2/3 and 1/2 respectively for this central-difference TVD scheme.

The above scheme does not satisfy entropy condition, thus it might produce nonphysical solution. Yee's method [1987], which is derived from Harten's method, is the most popular solution for breaking nonphysical expansion shocks. Here Yee's formula is adopted. The $Q(\lambda_k)$, which replaces λ_k, is given by

$$Q(\lambda_k) = \begin{cases} \lambda_k & \text{if } |\lambda_k| > \delta_k \\ \frac{1}{2}\left(\text{sign}(\lambda_k) \frac{\lambda_k^2 + \delta_k^2}{2\delta_k} + \lambda_k \right) & \text{if } |\lambda_k| \leq \delta_k \end{cases}$$

where

$$\delta_k = \tilde{\delta}_k (|V_n| + |V_t| + a)$$

V_n, V_t, and a are the normal velocity, the tangential velocity with respect to the grid interface, and the interface sound

speed respectively. Note that a more appropriate extension of Harten's dissipation in section 2.6 is to use

$$\delta_k=\tilde{\delta}_k(|V_n|+a)$$

The dissipation is not necessary for V_n waves for breaking expansion shocks; however, in the hypersonic blunt body calculation we do need it for the V_n waves. It has been observed by some people that Roe's and Osher's Riemann solvers produce instability when they are used to compute supersonic flow over blunt bodies, see Fig 4.2. During the shock evolution there is no problem. It is when shock reaches its final position the instability begins to appear although in Fig. 4.2 the residuals are not small. The cause is not clear. For the 2nd order scheme, we have to set the dissipation coefficient for V_n waves to a quite large value to overcome this instability. The convergence rate is quite dependent on the magnitude of the dissipation. With ONERA's IAPYX2 code (Borrel and Montagne 1985) which uses Van Leer's flux vector splitting, we find that no extra dissipation is required. As it is known flux vector splitting is very dissipative for the V_n waves, this explains why it works. We need larger number for $\tilde{\delta}_2$ and $\tilde{\delta}_3$ than that for the symmetric TVD used by Yee. The symmetric TVD is also quite dissipative in the V_n waves.

It is after one year since we finished the work contained in this and next chapters that we discovered the paper of Peery and Imlay (1988) which could be the first to report this instability in the literature. According to them this instability was called "carbuncle phenomenon" by the researchers at NASA. Peery and Imlay also reported the flux vector splitting of Steger-Warming has no such problem. They suggested another formula for this problem, which we will discuss it

together with our modification later in section 6.7. Another interesting paper by Pfitzner et al (1989) reported that even for the 1st order scheme the $\tilde{\delta}_k$ has to be greater than 0.25, which agrees with our results, although 0.25 seemed to be the limit value Yee (1987) employed. Lastly, we would like to draw readers' attention to the paper by Muller (1989), who reported considerable problems in computing hypersonic flow over ramp.

To add dissipation to the V_n waves is not a good idea especially for viscous calculation. We will demonstrate this point in section 6.6.

The other problem associated with hypersonic calculations is the evaluation of r. The equation we mentioned previously is appropriate for transonic calculation. Nevertheless to have monotone shock transition in hypersonic cases we have to scale it by square of sound speed, as suggested by Yee (1987). Thus it becomes

$$r^{k+}_{i+1/2,j} = \frac{\Delta f^{k+}_{i-1/2,j}\, a^2_{i-1/2,j}}{\Delta f^{k+}_{i+1/2,j}\, a^2_{i+1/2,j}} \qquad r^{k-}_{i+1/2,j} = \frac{\Delta f^{k-}_{i+3/2,j}\, a^2_{i+3/2,j}}{\Delta f^{k-}_{i+1/2,j}\, a^2_{i+1/2,j}}$$

which is in effect proportional to pressure gradient.

4.3 The Implicit Operator

Since we are only interested in steady state calculations we only consider first order Euler implicit equation,

$$W^{n+1}_{ij} - W^n_{ij} + \mu_{ij} R(W^{n+1}_{ij}) = 0 \qquad \text{where} \quad \mu_{ij} = \frac{\Delta t_{ij}}{A_{ij}}$$

After linearisation it becomes

$$(I + \mu \frac{\partial R(W)}{\partial W})\, \delta W_{ij} = -\mu_{ij} R(W_{ij}) \qquad \text{where} \quad \delta W_{ij} = W^{n+1}_{ij} - W^n_{ij}$$

Follow Yee's work, two approximations for $\partial R/\partial W$ can be made,

nonconservative and conservative forms. The "conservation" here is for the time conservation which is not important for steady state calculation.

The nonconservative form is

$$-\mu_{IJ}\,J^{+}_{I-1/2,J}\delta W_{I-1J} - \mu_{IJ}\,J^{+}_{IJ-1/2}\delta W_{IJ-1} + \mu_{IJ}\,J^{-}_{I+1/2,J}\delta W_{I+1J} + \mu_{IJ}\,J^{-}_{IJ+1/2}\delta W_{IJ+1}$$
$$+[I+\mu_{IJ}\,(J^{+}_{I-1/2J}-J^{-}_{I+1/2J}+J^{+}_{IJ-1/2}-J^{-}_{IJ+1/2})\,\delta W_{IJ} = -\mu_{IJ}R(W_{IJ})$$

where

$$J^{+}_{I+1/2J}=(RD^{+}L)_{I+1/2J} \qquad J^{-}_{I+1/2J}=(RD^{-}L)_{I+1/2J}$$

D^{+} and D^{-} contain the positive and negative entries of D respectively.

The conservative form is

$$-0.5\mu_{IJ}(J^{E}_{I-1J}+|J_{I-1/2J}|)\,\delta W_{I-1J} - 0.5\mu_{IJ}(J^{S}_{IJ-1}+|J_{IJ-1/2}|)\,\delta W_{IJ-1}$$
$$+0.5\mu_{IJ}(J^{W}_{I+1J}-|J_{I+1/2J}|)\,\delta W_{I+1J} + 0.5\mu_{IJ}(J^{N}_{IJ+1}-|J_{IJ+1/2}|)\,\delta W_{IJ+1}$$
$$+[I+0.5\mu_{IJ}(|J_{I-1/2J}|+|J_{I+1/2J}|+|J_{IJ-1/2}|+|J_{IJ+1/2}|)\,\delta W_{IJ} = -\mu_{IJ}R(W_{IJ})$$

where

$$J^{E}_{IJ}=J_f S^{x}_{I+1/2J}+J_g S^{y}_{I+1/2J}\,, \quad J^{W}_{IJ}=J_f S^{x}_{I-1/2J}+J_g S^{y}_{I-1/2J}\,, \quad |J|=R(D^{+}-D^{-})L$$

$$J^{N}_{IJ}=J_f S^{x}_{IJ+1/2}+J_g S^{y}_{IJ+1/2}\,, \quad J^{S}_{IJ}=J_f S^{x}_{IJ-1/2}+J_g S^{y}_{IJ-1/2}\,, \quad J_f=\frac{\partial F}{\partial W}\,, \quad J_g=\frac{\partial G}{\partial W}$$

Initially our experience was on the nonconservative form, later we switch to conservative form. The convergence speed, as stated by Yee, is much improved for hypersonic flow application.

Both forms can be cast as

$$M_{I-1J}\,\delta W_{I-1J} + M_{IJ-1}\,\delta W_{IJ-1} + M_{I+1J}\,\delta W_{I+1J} + M_{IJ+1}\,\delta W_{IJ+1}$$
$$+D_{IJ}\,\delta W_{IJ} = -\mu_{IJ}R(W_{IJ})$$

Using this form we solve the matrix equation once then update the solutions. With small modifications one can choose to do several subiterations inside every time step to obtain time accuracy. Since we only want steady state solutions, we do not consider the subiteration approach here.

The pentadiagonal matrix equation is too expensive to solve directly. There are some options to solve it approximately. Several methods are tested.

4.4 Different Solvers

The backward and forward line Gauss-Seidel line relaxation can be expressed as

Backward sweep :

$$M_{i,j-1}\,\delta W^{\bullet}_{i,j-1} + D_{i,j}\,\delta W^{\bullet}_{i,j} + M_{i,j+1}\,\delta W^{\bullet}_{i,j+1} = -\mu_{i,j} R(W_{i,j}) - M_{i+1,j}\,\delta W^{\bullet}_{i+1,j}$$

Forward sweep :

$$M_{i,j-1}\,\delta W_{i,j-1} + D_{i,j}\,\delta W_{i,j} + M_{i,j+1}\,\delta W_{i,j+1} = -\mu_{i,j} R(W_{i,j}) - M_{i+1,j}\,\delta W^{\bullet}_{i+1,j} - M_{i-1,j}\,\delta W_{i-1,j}$$

LU scheme is a symmetric Gauss-Seidel relaxation. It can be expressed as

$$D_{i,j}\,\delta W^{\bullet}_{i,j} = -\mu_{i,j} R(W_{i,j}) - M_{i-1,j}\,\delta W^{\bullet}_{i-1,j} - M_{i,j-1}\,\delta W^{\bullet}_{i,j-1}$$

$$D_{i,j}\,\delta W_{i,j} = -\mu_{i,j} R(W_{i,j}) - M_{i-1,j}\,\delta W^{\bullet}_{i-1,j} - M_{i,j-1}\,\delta W^{\bullet}_{i,j-1} - M_{i+1,j}\,\delta W_{i+1,j} - M_{i,j+1}\,\delta W_{i,j+1}$$

The sweep is along i+j=constant.

The most widely used is perhaps the approximate factorisation scheme (AF) or ADI scheme:

i sweep :

$$M_{i-1,j}\,\delta W^{\bullet}_{i-1,j} + D^{i}_{i,j}\,\delta W^{\bullet}_{i,j} + M_{i+1,j}\,\delta W^{\bullet}_{i+1,j} = -\mu_{i,j} R(W_{i,j})$$

j sweep :

$$M_{i,j-1}\,\delta W_{i,j-1} + D^{j}_{i,j}\,\delta W_{i,j} + M_{i,j+1}\,\delta W_{i,j+1} = \delta W^{\bullet}_{i,j}$$

where D^{i}/D^{j} contains only the Jacobians in the i/j direction.

The other AF scheme by Lombard (1983) called DDADI (diagonal dominant ADI) is:

i sweep :

$$M_{i-1,j}\,\delta W^{\bullet}_{i-1,j} + D_{i,j}\,\delta W^{\bullet}_{i,j} + M_{i+1,j}\,\delta W^{\bullet}_{i+1,j} = -\mu_{i,j} R(W_{i,j})$$

j sweep :

$$M_{i,j-1}\,\delta W_{i,j-1} + D_{i,j}\,\delta W_{i,j} + M_{i,j+1}\,\delta W_{i,j+1} = D\,\delta W^{\bullet}$$

Unlike AF there is no three dimension extension of DDADI.

The last scheme we will explain immediately later does not belong to the approximate solver category. It is essentially quite different from the above four methods.

For all the above schemes the values of W are not updated until the sweeps complete. We can also choose to update the W immediately One of these approaches by Bardina and Lombard (1985) and Chakravarthy (1987) is

back/forward marching:

$$M_{i-1,j}\,\delta W_{i-1,j} + D_{i,j}\,\delta W_{i,j} + M_{i+1,j}\,\delta W_{i+1,j} = -\mu_{i,j} R(W_{i,j})$$

for/backward marching:

$$M_{i-1,j}\,\delta W_{i-1,j} + D_{i,j}\,\delta W_{i,j} + M_{i+1,j}\,\delta W_{i+1,j} = -\mu_{i,j} R(W_{i,j})$$

The marching direction is usually chosen as the streamwise direction. Here we call one single sweep as one iteration. The matrix equation is only tridiagonal, which can be solved exactly. This method is usually used with AF or DDADI in three dimension calculation. AF and DDADI are used on the cross plane while this method is used on the streamwise direction. The advantage is that one can work with three/five planes at one time for 1st/2nd scheme. The core memory is easier to manage, see Bardina and Lombard (1985) and Chakravarthy (1987) for more details. Since different researchers tend to call this method by different names we will call it as method 5 for later reference.

4.5 Boundary Conditions

For the supersonic inflow we put halo cells in the inflow. The values of halo cells are fixed for explicit part, therefore the change δW for the implicit part is zero. For the supersonic outflow we set the flow values in the halo cell equal to the values upstream, thus the Jacobian M is zero. $M\delta W$ is therefore zero. For subsonic inflow and outflow farfield we can set the values of halo cells to the free stream, since the interface fluxes obtain from upwind scheme are automatically characteristics based. Because we fix the halo cell the change δW is zero.

For the solid wall we use simple reflected boundary condition, the halo cell is assigned to have same but negative normal momentum to the boundary cell. The change δW in the halo cell is

$$\begin{vmatrix} \delta\rho \\ -\delta\rho V_n \\ \delta\rho V_t \\ \delta e \end{vmatrix}_{\text{halo}} = \begin{vmatrix} \delta\rho \\ \delta\rho V_n \\ \delta\rho V_t \\ \delta e \end{vmatrix}_{\text{inside}}$$

From the above relation we can work out $\delta\rho u$ and $\delta\rho v$. This is only first order accurate which is consistent with the implicit operator. Without this boundary condition the implicit scheme converges much slower. For the explicit part we need a better interface flux, we simply extrapolate the pressure from the interior to the boundary. This can be further refined.

4.6 Results from Different Solvers

Before we present the results we would like to discuss the definition of residual. The residual is defined as

$$\text{Residual} = \left[\sum_{i=1}^{imax}\sum_{j=1}^{jmax} |R(\rho_{ij})| / A_{ij}\right]/(imax \cdot jmax)$$

This is better than

$$\text{Residual} = \left[\sum_{i=1}^{imax}\sum_{j=1}^{jmax} |\delta\rho_{ij}| / \Delta t_{ij}\right]/(imax \cdot jmax)$$

The residual defined by the second equation could be misleading if large CFL number is used. Although we advance solution by a certain time, the flow does not evolve so fast due to the errors from linearisation and approximate solver. The residual evaluated from the second equation is normally smaller than that from the first equation. The residual from the first equation reflects the state of the flow and it is independent of the time step size. For example if the CFL number is increased suddenly during the iterations the residual should go up instead of going down suddenly. In this situation the first definition gives the right residual jump while the second definition gives the wrong residual jump.

Through out this work local time step is used for convergence acceleration. The optimum CFL number is about 10-20, which is quite modest. The initial conditions are always the free stream conditions. For the hypersonic blunt body calculations the shock appears initially at the solid wall, which usually causes programs to generate negative pressure. Some researchers use the initial condition which contains a detached shock. A trick we found works very well is to set the CFL number at a smaller value and the $\tilde{\delta}_k$ at a higher value then gradually adjust to their final values in about 50 time steps.

There are four different test cases. The M=0.85 GAMM bump is used as transonic flow test. The bump height is 0.042 chord, channel height is 2.073 chords, the length from inflow to leading edge is 1.5 chord, and the length from trailing edge to outflow is 2.5 chords. The grid used is 72x21 nodes with 41 nodes on the bump. The reentry body grid is provided by ONERA. The slope tangent to the blunt nose is 30 degree. This is used for Mach 5 flow test. The quarter cylinder is used for Mach 2 and 20 flow test.

For 1st order scheme all solvers works reasonably well, we will not discuss the 1st order results here.

For the GAMM bump test, the line Gauss-Seidel and LU schemes have difficulty to drive residual down for the second order scheme. For blunt body it is worse. We will not discuss these scheme anymore.

In general method 5 and DDADI perform quite well, but for AF we have problem at high Mach number flow.

The CPU time required for Method 5 depends on the grid size and marching direction. If the grid has more cells in i direction than in j direction then marching in i direction implies solving the matrix equation in j direction. In this case CPU time required is smaller than DDADI. If it marches in j direction then the CPU time required will be much longer. Our codes are not optimised, especially for the method 5, therefore no exact comparison of CPU time will be given. The data management method mentioned in section 4.4 is not used since we can afford to store all data in small calculations. This method works well except that for blunt body calculations it generates negative pressure at the shock apex if the radial direction is

chosen as the marching direction.

DDADI is able to converge with nonconservative implicit operator but not with conservative implicit operator. To be able to converge with conservative operator we found the sweep directions need to be changed alternatively. More precisely for odd iterations we use i sweep then j sweep and for even iterations we use j sweep then i sweep.

At low Mach number AF works quite well. But for higher Mach number the performance of AF begins to degrade. It needs extra dissipation to push residual down. In contrast to the excellent results of AF by Yee (1987) our AF is not successful for high Mach number. We suspect the difference might come from boundary conditions and blunt nose instability problem.

Van Albada's limiter gives slightly better convergence rate than minmod. All the results shown later are from using van Albada's limiter. Some researchers have difficulties to drive the residual down when using implicit scheme with nonsmooth limiters such as minmod and superbee. We do not have this problem. As we are aware the explicit operator of Borrel and Montagne (1985) which uses a direct MUSCL approach has such problem. We assume this problem is related to the explicit operator. With the direct MUSCL approach the flow data is preprocessed to piecewise linear data. The slope of linear variation is directly decided by one value of the limiter function. In contrast with our flux limiter approach each wave has its own limiter values. It is rare that all the values that the limiters operate are just in the discontinuity points thus the flux limiter is less susceptible to the discontinuity of the limiters.

Fig. 4.3, 4.4, 4.5 and 4.6 show results of Mach 0.85, 2, 5, and 20 flows from various solvers. The convergent speed is reasonable when compared with other researchers' results.

4.7 Experience with GMRES Solver

The linear GMRES (generalised minimal residual algorithm) solver by Saad and Schultz (1986) is a conjugate gradient-like method for solving linear systems of equations. Since we only solve the matrix equation approximately and the factorisation error is not small, we could possibly solve it with same or more accuracy by GMRES with only few iterations. From the numerical experiments only a few subiterations inside GMRES for each iteration are required initially, however when residual reduces by three orders of magnitude the subiterations required increase very quickly. We conclude that to use linear GMRES as approximate solver is not competitive. If we solve the matrix equation very accurately at the expanse of long CPU time only few hundred iterations is able to drive the residual to machine zero. This incidently indicates our boundary conditions are sufficient good at least for DDADI.

To better use high accurate approximate or exact solvers one should use Newton method which could possibly reach convergence in few iterations (Venkatakrishnan 1990). The objection of using direct solver in our study is that the convergent rate in term of iterations can be too fast for zonal calculation, see Chapter 5 for the reason.

The nonlinear GMRES by Brown and Saad (1985) is a clever combination of inexact Newton method and linear GMRES for solving the nonlinear systems of equations. According to Wigton (1985), with any solvers such as AF as preconditioner,

the nonlinear GMRES will help convergence in the difficult case and help to stabilise scheme. In our experience we are not able to have any gain. We need to do more works about the use of nonlinear GMRES.

4.8 Concluding Remarks

The hypersonic flow calculation turns out to be much more difficult than we thought and extra dissipation is usually needed.

Several approximate matrix solvers are tried but not all reach the success other researchers have in transonic calculations and when the flux vector splitting scheme, instead of the flux difference splitting scheme, is used on both explicit and implicit operators.

Nevertheless we have produced basic implicit codes by DDADI and method 5 for hypersonic calculations. Although we are not successful with AF we believe our implicit codes provide a reasonable start for our next objective of investigating zonal methods.

CHAPTER 5 : THE IMPLICIT ZONAL METHOD

5.1 Introduction

To ease the grid generation difficulty in three dimension and to improve the grid quality the most flexible approach except unstructured grid is to use overlapped grid. The biggest obstacle to use the overlapped grid is to maintain the flux conservation. As pointed out by Berger (1987a) it is extremely difficult to achieve exact conservation. A good example of bad result from nonconservative interpolation algorithm was given by Benek et al (1983).

Nevertheless it is perhaps not necessary to have EXACT flux conservation, if the flux conservation is met to certain degree of accuracy. The approach suggested by Thomas et al (1988) seems to meet this condition. They conserved the conservative variable times cell area, A·W, instead of interface flux. Their results on nonoverlapped composite grid were quite encouraging. Moon and Liou (1989) made significant refinement on this technique and applied it to overlapped grid in two dimension showing very promising result. One inherent problem of this approach is that the complexity of programming and computing overhead is larger than nonoverlapped approach especially in three dimension.

Here we only pursue the nonoverlapped grid approach, that is grids with common boundaries.

We first categorise the zonal boundaries, see Fig. 5.1. Type B1 has continuous grid lines, it can be either continuous or discontinuous in slopes. Type B2 has integer grid spacing, while type B3 has noninteger grid spacing.

The composite grid can be classified as two types. Type G1 is globally structured, therefore the zonal boundaries can only be the B1 type. Type G2 is globally unstructured which is more realistic in practice , thus the zonal boundaries consist of all three types. One important advantage of G2 type grid is that it allows local grid refinement. For the flow solvers, we can have either explicit (S1) or implicit (S2) solver. The explicit solver uses only local grid data to march in time, while the implicit scheme needs all data in the computational domain to march in time. This difference has important implication on the zonal method.

For data management we assume the data stores in both the primary and secondary memories, which is the situation for realistic 3D calculation. Type M1 uses the data in the primary and secondary memory at the same time, see Fig. 5.2. The time spent on the data access is in general too long. Type M2 uses only the data in the main memory, the data in the main memory and secondary memory exchanges periodically. Type M2 is the usual case.

Combine the grid, solver, and data management we have several options.

M1/M2+S1+G1 is simply the case for single zone grid. M1+S1+G2 is easy in the finite volume formulation. M2+S1+G2 adds some problems on the data exchange. M1+S2+G1 is trivially the case for single zone. M1+S2+G2 can be done but the matrix

from implicit scheme becomes unstructured, for which no efficient solver is available. The most challenging combination is M2+S2+G1/G2. The matrix is structured for using G1 grid for which efficient approximate solver can be used; however, the order of the matrix equation is very large. One does not wish to solve it as a whole. The situation for G2 grid is even more difficult since the matrix is not only very large but also highly unstructured. One will prefer to form the matrix equation and solve it zone by zone. But with this approach the implicit scheme now can not receive all the data, which violate the underlying principle of implicit scheme. This will be the centre issue of our research.

Section 5.2 reviews some works which we consider are more related to our experiences. Section 5.3 and 5.4 describe the treatment of explicit and implicit operators at the zonal boundaries respectively. The results and discussion are presented in section 5.5. Section 5.6 describes possible problems in three dimension. Section 5.7 concludes the chapter.

5.2 Selected Literature Review

There are so many papers about the zonal method that an complete review is impossible. Here we only concentrate on some works.

Rai (1986) used AF finite difference scheme on G2 type grid. We consider his treatment on the conservation is more complicated due to the finite difference setting. The implicit zonal boundary condition he used was not stable for one subiteration, however by relaxation method one subiteration was stable (Rai 1985). The implicit zonal boundary condition he chose was simply to set the δW in the other zone to zero. Mach

2 was the maximum tested Mach no.

Belk and Whitfield (1987) used LU finite volume scheme on G1 type grid. The implicit zonal boundary condition was either to set the $\delta W = 0$ in the other zone or took the $\delta W_{new} = \delta W_{old}$, where the δW_{old} was the δW from previous iteration. With the M2 case one can choose to use the old data or to use the newest data available from the other updated zone. They named the synchronisation (SYN) as using only the old data and unsynchronisation (UNSYN) as using the newest available data. The test problem was transonic flow past a wing. The main conclusion from their work was that the convergence speed in order is UNSYN+$\delta W = 0$ first, SYN+$\delta W = 0$ second, and UNSYN+$\delta W_{old} = 0$ last. The SYN+$\delta W_{old} = 0$ approach was not stable.

Morice (1988) used a noncentred finite volume scheme on G1 grid. The test case was M=0.85 GAMM bump. His implicit characteristic boundary condition is perhaps the most reasonable among others in our opinion. However it is still not genuinely implicit because of intrinsic restriction of the M2 case. He showed a striking result that two-zone calculation could have the same convergent rate as one zone case.

Kathong (1988) first applied Ramshaw's algorithm (1985) to find the overlapped areas in the 3D block boundary. This point will be addressed later.

Eriksson and Rai (1988) gave the first numerical stability analysis of the Jameson type scheme and upwind scheme. They concluded the upwind scheme was superior in stability for all B1, B2, B3 type zonal boundaries. For nonupwind schemes extra dissipation was required for using B2 and B3 type boundaries.

5.3 The Explicit zonal boundary condition

As we stated earlier the explicit part calculation only needs local data therefore there is basically no difficulty in theory. With the finite volume and the flux limiter approach one can assume the flow is locally uniform inside the computational cell. With reference to Fig. 5.3 one can work out the 1st order flux across ab by simply solving the Riemann problem with W_1 and W_2 as the left and right states. For the 2nd order flux, we need to compare Δf^{k-} at mn with Δf^{k-} at ab to obtain r^{k-}. When the $r^{k\pm}$ is evaluated we scale the $\Delta f^{k\pm}$. The $r^{k\pm}_{ab}$ for limiter function is therefore equal to

$$r^{k+}_{ab} = \frac{\Delta f^{k+}_{de} a^2_{de} S_{ab}}{\Delta f^{k+}_{ab} a^2_{ab} S_{de}} \qquad r^{k-}_{ab} = \frac{\Delta f^{k-}_{mn} a^2_{mn} S_{ab}}{\Delta f^{k-}_{ab} a^2_{ab} S_{mn}}$$

After all interface fluxes are found the R(W) for cell 1 is equal to $H_{ab}+H_{bc}-H_{de}+H_{ad}-H_{ce}$

In the above approach we assume there is a common boundary running through different zones. One needs a table of the data at the neighbourhood of zone boundary. The table is most convenient to produce during the grid generation stage. In the grid generator one first establishes all the boundaries, such as solid boundaries, far field boundaries, and zonal boundaries etc. These boundaries are usually represented in parametric from. In two dimension one parameter is enough. By comparing the number of the parameter one can establish the table quickly. Three dimension case will be discussed in section 5.6.

Because the assumption of common boundary the cells at the boundaries are not quadrilateral in general. In our calculation, for example, the area of the cell abcde is assumed to have the same area of abcd. Note that we still keep flux

conservation. The error will be insignificant if the zonal boundary is quite straight with respect to each cell. If one decides to use exact area it is most conveniently supplied from the grid generator.

5.4 The Implicit Zonal Boundary Condition

With the M2 data management and the basic implicit scheme we use in chapter 4 there will be no real implicit zonal boundary condition if one does not want to solve the complete matrix equation. With this understanding we believe the success of implicit zonal schemes come from the coupling of explicit part.

Since the implicit schemes still need hundreds of iterations to reach convergence in single grid calculation, during the iteration process the explicit boundary condition can couple different zones effectively. Therefore we adopt the simplest $\delta W = 0$ approach.

All the works mentioned in section 5.2 were quite obscure about how they treated the diagonal term D. We find the diagonal term D has to treated properly especially when the G2 grid is used.

Use similar approach as in the explicit part we can work out the interface Jacobian. Take the conservative form for example the diagonal term for cell abcde, see Fig. 5.4, is

$$D = I + 0.5\mu \left(|J_{ab}| + |J_{bc}| + |J_{de}| + |J_{ad}| + |J_{ae}|\right)$$

A try which does not include the Jacobian in the zonal interface turns out to be unstable.

5.5 Results and Discussion

Before the results are presented we have to explain how to view our contour plottings. Since we use finite volume formulation the flow data is cell-centred. We plot the contours zone by zone and inside each zone we do not try to extrapolate the contour lines. Therefore at the zonal boundary the contour lines are not connected. Sometimes the appearance generated is a little unusual, e.g. Fig. 5.9 and Fig. 5.18 where the noses of bow shocks just lie on the zonal boundaries, but in all case the actual solution is well behaved. Nevertheless it is easy to use imagination to connect the lines.

Various positions of zonal boundary will be presented to see what sort of situation is difficult. The results are presented from low to high Mach number range. Most results are obtained using conservative DDADI schemes unless specified.

Fig. 5.5 is the Morice's GAMM bump test with zonal boundary covering subsonic and supersonic regions using UNSYN and SYN approaches. The convergent rate of UNSYN approach is as good as single zone calculation and the SYN approach is only slightly slower. Fig. 5.6 is again for the GAMM bump but with the zonal boundary lying inside the shock. The convergence speed is not influenced at all.

Fig. 5.7 shows the results for Mach 2 flow past quarter cylinder with two different kinds of zonal boundary using DDADI and UNSYN and SYN approaches. The convergent speed is again not degraded at all. The AF scheme was unstable without using subiteration approach according to Rai (1986); however, our AF (result not shown) has no such problem. We believe the

difference comes from the treatment of diagonal term.

Fig. 5.8 to 5.13 are for Mach 5 flow past reentry body.

The zonal boundary in Fig. 5.8 is away from the bow shock. The convergent rates are obviously slower in Fig.5.8 when compared with Fig 4.5, especially for SYN, which might due to the narrow domain near the body.

Fig. 5.9 and 5.10 have zonal boundaries inside the nose of bow shock. The zonal boundary of Fig. 5.10 is one more cell away from the body then that of Fig. 5.9. Fig. 5.9 also shows the convergent history with method 5. In these cases which shocks lie on the zonal boundaries SYN approach are UNSTABLE for CFL no. 10. Lower CFL no. has to be used.

Fig. 5.11 has small shock to zonal boundary angle. Fig. 5.12 has zonal boundary in the supersonic region. Fig. 5.12 is by method 5 with marching in the streamwise direction and the zonal boundary is perpendicular to the bow shock. Of these results shock positions do not seem to produce problems with UNSYN approach. The SYN approaches are not tested.

Fig. 5.13 is for the integer grid spacing case with mesh ratio 2 using UNSYN approach. The convergence speed can not be compared with one zone result.

Fig. 5.14 to 5.18 are examples for Mach 20 flow past quarter cylinder using UNSYN approach.

The convergent speed is quite good in Fig. 5.15. Fig. 5.15 and 5.16 have noninteger grid spacing. The convergence is exceptionally fast in Fig. 5.16 because the grid which contains

the shock is very coarse.

Fig. 5.17 and 5.18 have shock close to zonal boundary with CFL number 10 and 20. For Fig. 5.17 the residual can not go down at CFL number 20. For Fig. 5.18 with the boundary inside the shock using CFL number 20 shows faster convergence than using CFL number 10. The test in Fig. 5.17 is perhaps too severe for the whole bow shock lies at the boundary of left zone.

Some general observations can be made from above results.

Firstly, the UNSYN approach converges faster and is more robust than the SYN approach especially when there is a shock in/near the zonal boundary. The first reason might be that in the UNSYN approach the number of explicit coupling DOUBLES. If the solutions in different zones do not match each other the UNSYN approach can tolerate such difference while the SYN approach, which does not use the newest data, needs the solutions to be compatible.

Secondly, low Mach number flow is easier to compute. This might be because the change at shock layer is not much bigger than that in the smooth flow.

Thirdly, shock following the zonal boundary will cause problem when Mach number increase especially for SYN approach. This is due to the fact that most change is on the same row near the zonal boundary. If shock crosses zonal boundary it does not seem to a problem. This is because that near the boundary the big change due to the shock is in a small region.

We believe the reason that the $\delta W=0$ method works well is partly due to the optimum CFL number of our implicit codes is quite modest and also the diagonal dominant characteristics of upwind implicit scheme allow us to discard the off-diagonal terms if the diagonal term is treated properly.

Although our explicit operator is a central-difference operator with TVD limiter, we believe other explicit operators can be used if the 1st order implicit operator is treated as before.

A benefit from using the implicit zonal method is that the size of matrix equation reduces. If the overhead from doing the extra calculation for the zonal boundary is not counted the overall computing cost should decrease because of smaller size of matrix equation to solve.

5.6 Generalisation to Three Dimension

The method we use can be generalised to 3D in principle.

To keep the conservation we need to have the overlapped areas on the zonal plane. If the zone boundary is a straight plane Ramshaw's conservative re-zoning algorithms can be implemented efficiently, e.g. Kathong (1988). However the zone boundary is generally a curved plane no efficient method exists to the author's knowledge. One possible solution is to apply Ramshaw's technique on (s,t) parameter plane after the curved boundary is parameterised, see Fig. 5.19, and this should be integrated to grid generation procedure.

To compute the volume of multiface cell abutting on the zonal boundary extra effort is required. If the boundary is quite straight, one can again calculate the cell volume as if it is a hexahedron. Some of the cell surfaces intersecting the zonal boundaries might have more than four edges. The area vector of these surfaces is required for the finite volume scheme. Again if the zonal boundary is quite straight we can calculate it as a four-edge surface.

Another problem associated in a 3D patched-grid was addressed in Thomas et al (1989). Near a solid wall the grid could be unable to match each other especially for highly stretched mesh for thin-layer N-S calculation, see Fig. 5.20. We will prefer to avoid this situation.

5.7 Concluding Remarks

In this chapter we have demonstrated a robust and simple finite volume approach for using the implicit scheme in the zonal setting. The convergent rates are quite satisfactory for most test cases. Proper treatment of the diagonal Jacobian turns out to be crucial for stability while the unsynchronised approach which uses the newest data helps convergence.

Although promising result is obtained in 2D three dimensional test still has to be done.

CHAPTER 6 : VISCOUS CALCULATIONS AND ITS GRID ADAPTION

6.1 Introduction

After studying the inviscid calculation in previous chapters we move to viscous calculations. The main concern is on the grid adaption for viscous computation. Two problems with Roe's Riemann solver are also examined in viscous flow.

A general discussion on the Navier-Stokes calculation and grid adaption are given at sections 6.2 and 6.3 respectively. The linear advection-diffusion equation is studied at section 6.4. Section 6.5 gives some suggestions on the grid adaption of viscous flow. The dissipation effect on the numerical boundary layer thickness is examined at section 6.6. A better cure for the carbuncle phenomenon is proposed at section 6.7. Section 6.8 discusses the pressure kink problem first observed by Venkatakrishnan (1990). Section 6.9 concludes this chapter.

6.2 General Discussion of Navier-Stokes Calculations

Adding the viscous terms to the Euler equations of section 4.1 we obtain the Navier-Stokes equations,

$$\frac{\partial W}{\partial t}+\frac{\partial F}{\partial x}+\frac{\partial G}{\partial y}+\frac{\partial F^v}{\partial x}+\frac{\partial G^v}{\partial y}=0$$

with

$$F^v=\begin{vmatrix} 0 \\ -\tau_{xx} \\ -\tau_{xy} \\ -u\tau_{xx}-v\tau_{xy}+Q_x \end{vmatrix}, \quad G^v=\begin{vmatrix} 0 \\ -\tau_{xy} \\ -\tau_{yy} \\ -u\tau_{xy}-v\tau_{yy}+Q_y \end{vmatrix}$$

where

$$\tau_{xx}=\frac{2}{3}\frac{\mu}{Re_L}\left(2\frac{\partial u}{\partial x}-\frac{\partial v}{\partial y}\right), \quad Q_x=\frac{-\mu}{(\gamma-1)M_\infty^2 Re_L Pr}\frac{\partial T}{\partial x}$$

$$\tau_{yy}=\frac{2}{3}\frac{\mu}{Re_L}\left(2\frac{\partial v}{\partial y}-\frac{\partial u}{\partial x}\right), \quad Q_y=\frac{-\mu}{(\gamma-1)M_\infty^2 Re_L Pr}\frac{\partial T}{\partial y}$$

$$\tau_{xy}=\frac{\mu}{Re_L}\left(\frac{\partial u}{\partial y}+\frac{\partial v}{\partial x}\right),$$

$$\mu=T^{\frac{3}{2}}\frac{(1+C/T_\infty)}{(T+C/T_\infty)}\,,\quad C=110.4^\circ K\,,\qquad T=\gamma M_\infty^2 P/\rho$$

In the above equations the velocity, density, temperature, and viscosity are nondimensionalised by their free stream values, and x,y,z by the characteristic length L. For more details see Anderson et al. (1984).

The inviscid terms can be discretised as before by the TVD schemes. The viscous terms are usually discretised by using central difference. The semidiscrete finite volume scheme for the cell i,j is therefore

$$A_{i,j}\frac{\partial W_{i,j}}{\partial t}+H_{i+1/2,j}-H_{i-1/2,j}+H_{i,j+1/2}-H_{i,j-1/2}$$
$$+H^v_{i+1/2,j}-H^v_{i-1/2,j}+H^v_{i,j+1/2}-H^v_{i,j-1/2}=0$$

The viscous interface flux is, for example,

$$H^v_{i,j+1/2}=F^v_{i,j+1/2}s^x_{i,j+1/2}+G^v_{i,j+1/2}s^y_{i,j+1/2}$$

To calculate $F^v_{i,j+1/2}$ and $G^v_{i,j+1/2}$ we need to evaluate the derivatives $\partial f/\partial x$, $\partial f/\partial y$ at the cell interfaces (f=u, v, and T). For example to evaluate derivatives at (i,j+1/2) we construct an auxiliary cell centered at (i,j+1/2), see Fig. 6.1, using the Gauss law we have,

$$\frac{\partial f}{\partial x}=+\frac{1}{A_{i,j+1/2}}\oint_{1234} f\,dy$$
$$=+\frac{1}{A_{i,j+1/2}}\left(f_{i+1/2,j+1/2}\Delta y_{12}+f_{i,j+1}\Delta y_{23}+f_{i-1/2,j+1/2}\Delta y_{34}+f_{i,j}\Delta y_{41}\right)$$
$$\frac{\partial f}{\partial y}=-\frac{1}{A_{i,j+1/2}}\oint_{1234} f\,dx$$
$$=-\frac{1}{A_{i,j+1/2}}\left(f_{i+1/2,j+1/2}\Delta x_{12}+f_{i,j+1}\Delta x_{23}+f_{i-1/2,j+1/2}\Delta x_{34}+f_{i,j}\Delta x_{41}\right)$$

with

$$\Delta x_{ab}=x_b-x_a\,,\quad \Delta y_{ab}=y_b-y_a\,,\qquad A_{i,j+1/2}=0.5(A_{i,j+1}+A_{i,j})\,,$$

$$f_{i+1/2,j+1/2}=0.25(f_{i,j}+f_{i+1,j}+f_{i,j+1}+f_{i+1,j+1})$$

This is a standard finite volume technique, see Peyret and Taylor (1983) for more discussions.

For the high Reynolds number computation the viscous diffusion parallel to the wall can be neglected without losing much accuracy if there is no massive flow separation. Dropping the viscous terms along the wall we obtain the thin layer Navier-Stokes equations first proposed by Steger (1978). For example the $H^{v}_{i+1/2j}$ and $H^{v}_{i-1/2j}$ terms are discarded if the i direction is parallel to the wall. To further exploit the thin layer concept we can simplify the evaluation of derivatives by neglecting the $f_{i+1/2j+1/2}$ and $f_{i-1/2j+1/2}$ contributions since both terms are relative small in the case of high aspect mesh and low streamwise diffusion. In fact this is equivalent to the finite difference approach which works on body conformed coordinates.

The finite volume approach is slightly more accurate; however, the finite difference approach is good enough with the thin layer assumption. The finite difference approach is easier to implement, especially in the zonal setting. To evaluate derivatives at zonal boundary, see Fig. 6.2, FV approach will need interpolation to find $f_{i+1/2j+1/2}$ while for FD approach the stencils do not involve the data from the other zone.

The implicit schemes for the Euler equations in Chapter 4 are used as bases for Navier-Stokes equations. For constructing implicit part of viscous terms the linearisation suggested by Steger (1978) is used in our study. Only the DDADI conservative scheme is tested on viscous problems. Its performance we found depends critically on the aspect ratio of the mesh near the body. The allowed CFL number compared with inviscid calculation reduces significantly if the mesh aspect ratio is greater than 50. More experiences on viscous calculations using different schemes are required.

6.3 General Discussion of Grid Adaption

It has been widely demonstrated that by attracting the grid lines to the high error regions (moving grid point approach) or by refining the meshes locally in such regions (embedded grid approach) one can gain great accuracy with economy, see Fig. 6.3. The combination of both approaches has also been demonstrated.

The main difference between both approaches is that the former approach tries to obtain most accurate result for a fixed cost and the latter tries to attain a fixed accuracy for a minimum cost (Berger 1987a). Note that for the embedded grid approach the cost is not known beforehand. For the 3D calculation the computing resources required are so large that one usually can only afford the first approach. The latter approach is usually used in 2D unsteady calculations for complex gas dynamics problems. It also has been used on steady state solutions but it generally prevents one from using some acceleration technique, such as implicit schemes.

Here we will only discuss the first approach. There are several review papers available, for recent ones see Thompson (1985), and Eiseman (1987).

The first step of grid adaption is to obtain error estimate. Knowing where the large error is, we can move the grid lines to such region. The most popular approach is to use the equidistribution concept, i.e., redistribution of grid points such that a positive weight function, w_i, is equally distributed over a grid line

$$w_i \Delta s_i = \text{const.}$$

where Δs_i is the grid interval and w_i the weight function which

should be proportional to the error estimate. The problem of choosing the weight function will be discussed in later section.

After a suitable weight function is obtained one can then choose either the smoothness or spring analogy approach to generate a new grid, see the text book by Thompson (1985). With smoothness approach the grading function is simply

$$\xi(s)=\int_0^s w dt \Big/ \int_0^{s_{max}} w dt \ , \qquad \xi\in[0,1]$$

where s is the arc length along the grid line. If the grid point index J ranges between 1 and N we have the relation

$$J=(N-1)\xi+1$$

To extend this idea to two or three dimension, one often need to consider the smoothness and orthogonality of grid. To extend one dimensional approach to higher dimensions the simplest choice is to do adaption along one coordinate and interpolate the solution to the new grid then use the same procedures for the other coordinates. Usually the final grid needs to be smoothed. More sophisticated algebraic adaption techniques have also been developed, see Eiseman (1987). Recently Anderson (1986) showed the equidistribution law can be seen as an elliptic equation with a forcing term. He integrated the equidistribution law into the elliptic grid generator and also developed a method with cell area control (Anderson 1987). With variational formulation an optimum grid with respect to weight function, smoothness, orthogonality and volume variations can be obtained at relative high cost. Here we do not intend to consider the grid quality problems.

The mesh size can be out of control if the weight function is not properly scaled. Nakahashi and Deiwert (1986) showed one can control the RATIO of maximum and minimum spacings by

adjusting the weight function. If the original weight function is called M using the relation

$$\Delta S_{max} W_{min} = \Delta S_{min} W_{max}$$

the new weight function is

$$w = 1 + cM$$

where

$$c = \frac{R-1}{M_{max} - M_{min} R}, \quad R = \frac{\Delta S_{max}}{\Delta S_{min}}$$

They (1987) also showed one can control exactly the specified minimum and maximum specified mesh spacings. Their weight function was

$$w = 1 + af^b$$

a can be computed directly but b needs to be adjusted iteratively.

The above two methods can be used if one has only one variable to adapt with. If one wants to use two or more variables, e.g. density and temperature gradients, an immediate problem is how to scale them since they are not of the same physical dimensions. This multivariable adaption problem can be solved by using the fraction control technique. Dwyer (1984) first suggested to use

$$w = 1 + aw_1 + bw_2$$

where a and b can be adjusted to obtain the specified weight on w_1 and w_2. His method needs iterations to find a and b. It is however easier to work directly on the grading function (Eiseman 1987). Eiseman's formula was used by Abolhassani (1987) for multivariable adaption.

The fraction control technique uses a linear weight function

$$w=c_0+c_1w_1+c_2w_2+\ldots+c_nw_n$$

The c's are adjusted such that

$$\int_0^{S_{max}} c_0\,dt = f_0\int_0^{S_{max}} w\,dt$$

$$\int_0^{S_{max}} c_1w_1\,dt = f_1\int_0^{S_{max}} w\,dt$$

$$\vdots$$

$$\int_0^{S_{max}} c_nw_n\,dt = f_2\int_0^{S_{max}} w\,dt$$

$$\sum(f_0+f_1+f_2+\ldots+f_n)=1.0$$

With the fraction f specified the grading function can be defined without knowing the values of c's. It is

$$\xi(s)=\frac{s}{S_{max}}\left[1-\sum_{j=1}^{n}f_j\right]+\sum_{j=1}^{n}f_j\frac{F_j(s)}{F_j(S_{max})}$$

where

$$F_j(s)=\int_0^s w_j\,dt$$

6.4 Study on the model Equation

In this section we use the linear advection-diffusion equation to validate some ideas. We first produce an implicit scheme. It is used to test different limiters on uniform grid. A modification on nonuniform grid is then attempted. Finally we try to find a good criterion for grid stretching.

The linear advection-diffusion equation

$$U_t+aU_x=bU_{xx}$$

with boundary conditions

$$U=U_L \text{ at } x=0$$

$$U=U_R \text{ at } x=L$$

is used as a model equation for studying the viscous and grid adaption problems. The exact solution for the steady equation $aU_x=bU_{xx}$ is

$$U=\frac{U_Le^{(aL/b)}-U_R}{e^{(aL/b)}-1}+\frac{(U_R-U_L)e^{(ax/b)}}{e^{(aL/b)}-1}$$

which has a boundary-layer-like profile if **b** is much smaller than **a**.

We will introduce the notation $\nu=\frac{a\Delta t}{\Delta x}$ and $R=\frac{a\Delta x}{b}$ where ν is the CFL number and **R** is the mesh Reynolds number.

One way to solve it is by using the FTCS scheme which uses forward-time and centre-space difference. The resulting scheme is

$$\frac{U_i^{n+1}-U_i^n}{\Delta t}+a\frac{U_{i+1}^n-U_{i-1}^n}{2\Delta x}=b\,\frac{U_{i+1}^n-2U_i^n+U_{i-1}^n}{(\Delta x)^2}$$

Using the Fourier analysis the stability bound is

$$2\nu\leq R\leq 2/\nu$$

It is also well known that for $2\leq R\leq 2/\nu$ one obtains oscillatory exponential solution. This can be analysed by using the normal mode analysis.

If one uses TVD schemes on the convection term, aU_x, and central difference on diffusion term, bU_{xx}, the stability bound is not clear since TVD condition does not imply stability in this situation and the limiter involved prevents the Fourier analysis. For the oscillatory solution problem Roe (1987a) managed to show that it will not occur if limiters are used. This is confirmed by numerical experiments, see Fig. 6.4 for a mesh Reynolds number 4 result. Since the explicit scheme is bound to have very small time step size, following what we did for the Euler equations an implicit scheme is used in this study.

The semidiscrete finite volume scheme is

$$\frac{dU_i}{dt}+\lambda_i(H_{i+1/2}-H_{i-1/2})=0$$

The interface flux, for a>0, is

$$H_{i+1/2}=a\{U_i+\frac{1}{2}\phi(U_{i+1}-U_{i-1})\}-b\{\frac{U_{i+1}-U_{i-1}}{0.5(\Delta x_{i+1}+\Delta x_i)}\}$$

where ϕ is the limiter function. The implicit scheme is

$$U_i^{n+1}+\lambda_i[H_{i+1/2}^{n+1}-H_{i-1/2}^{n+1}]=U_i^n$$

After some manipulations we have

$$(-a\lambda_i-\lambda_i\frac{2b}{\Delta x_i+\Delta x_{i-1}})\delta U_{i-1}+(1+a\lambda_i+\lambda_i(\frac{2b}{\Delta x_i+\Delta x_{i-1}}+\frac{2b}{\Delta x_i+\Delta x_{i+1}})\delta U_i$$

$$+(-\lambda_i\frac{2b}{\Delta x_i+\Delta x_{i+1}})\delta U_{i+1}=\lambda_i(H_{i+1/2}-H_{i-1/2})$$

where $\delta U=U^{n+1}-U^n$

which can be solved directly by a scalar tridiagonal matrix solver. Numerical tests show it is unconditionallystable.

The theory suggests superbee limiter should gives the best result among other limiters. Numerical experiments confirms superbee limiter is as accurate as pure central difference.

Since stretched grid is usually used in viscous calculation we try to improve the evolution of advection and diffusion terms on nonuniform grid. For the advection term a simple modification is made. For the diffusion we first evaluate U_x and then fit a parabola locally for U_x therefore the U_{xx} value at the grid interface is obtained by differentiating the parabola, see Fig. 6.5. Numerical experiments with this method on stretched grid show both worse and better results than those with original scheme. The results are proved disappointing.

Now we turn to grid adaption. To find a good error estimate or weight function is the first difficulty with mesh adaption. To use the truncation error as weight function is not practical in more general cases. The usual choice is to use 1st derivative, 2nd derivative or curvature of the solution. Thompson suggested to use $1+b^2|k|\sqrt{1+a^2U_x}$, where k is the curvature, which combines gradient and curvature of solution. However all the possible combinations have constants to be adjusted

and no universal constants can be given.

It is more reasonable that the weight function should also depend on the numerical schemes used. Carey and Dinh (1985) responded to this by posing the best interpolation for U : for a given fixed N determine the mesh $\{x_i\}$, i=0,1,2,...N such that the associated interpolant of U is optimum in some sense. For using piecewise linear interpolation with respect to minimum L_∞ norm the weight function is simply $U_{xx}^{2/5}$.

Numerical experiments with this weight function show very good result on the model problem. Especially the L_∞ error norm is quite close to L_1 norm despite U_{xx} is optimum in L_∞ norm. With the weight function suggested by Thompson after fine tuning the constants the result is also quite good but the L_1 and L_∞ norm cannot be so close. Fig. 6.6 shows an example from using this weight function.

Carey and Dinh derived their formula by using the Fourier series. It is very easy to follow their approach to derive the formula for obtaining minimum error for two or more variables. The resulting weight function is

$$[\sum c_n (U_n)_{xx}]^{2/5}$$

As a final note initially we consider the gradient $r_{i+1/2} = \frac{U_i - U_{i-1}}{U_{i+1} - U_i}$ used for the limiter function could be a good candidate for setting up a weight function. The magnitude of weight function depends on how far r deviate from 1.0. The idea is that if one can obtain a grid such that r is very close to 1 at every cell interface one should obtain a very good solution. The other advantage is that r is nondimensional and one can possibly generalise this to system of equation. Nevertheless numerical experiments proved disappointing.

6.5 Grid adaption of viscous solution

The results from the model equation are not quite applicable to the complex Navier-Stokes equations. Again the problem of choosing the right weight function comes first. What variables should we use? The thickness of thermal boundary layer is about $1/\sqrt{Pr}$ times the thickness of viscous boundary. For air Pr=0.72 the thermal boundary is thicker! Should we treat the adiabatic wall and isothermal wall differently? These problems can not be answered by studying the simple linear advection-diffusion equation.

The other problem which is not encountered in Euler adaption is that the grid scale difference is very large for inviscid and viscous regions. If the grid scale change by the order of 3 the value of weight functions should also have such variation to preserve the fine grid near wall. Our experience shows none of the mesh size control techniques mentioned in sections 6.3 and 6.4 are capable of generating reasonable grid.

Some researcher (Nakahashi 1986, C.Hsu 1987, and A.Hsu 1989) have recognised this difficulty and solved it by essentially changing the basic equidistribution law to

$$\Delta s_i w_i / c_i = \text{const}$$

where c_i is the original grid spacing. One can understand the original weight function is now scale by the original grid. A more general formula was given by Hsu (1989).

It is possible to combine the techniques of controlling ratio of spacing and fraction of variables and the scaled equidistribution law together to provide more control of mesh.

One can obtain an approximate formula for the grading function, which is

$$\xi(J)\sim f_0\frac{J-1}{N-1}+\frac{f_1}{\sum_{k=2,N-1} w_1(k)}\sum_{k=2}^{J-1} w_1(k)+\ldots+\frac{f_n}{\sum_{k=2,N-1} w_n(k)}\sum_{k=2}^{J-1} w_n(k)$$

where w_j is control by the specified ratio R_j.

As an example Fig. 6.7 shows the pressure contours of viscous flow past quarter cylinder with free stream Mach number 2 on a 35x51 grid. We could not afford to study the accuracy problem, i.e. to decide how to choose the best weight function. We will only demonstrate the mesh size control technique. Pressure gradient is used as the basic weight function, M, to cluster the grid around the bow shock. The adaption is done along the radial grid lines only. The weight function is

$$w=1+c_1w_1$$

where $w_1=1+c^1M$, $c^1=\frac{R_1-1}{M_{max}-M_{min}R_1}$

with fractions, f_0 and f_1 ,and ratio of M, R_1, to be specified. With $f_0=0.5$, $f_1=0.5$ and $R_1=10$ and the unscaled equidistribution law the grid near the wall becomes unreasonably coarse, see Fig. 6.8, while with the scaled law the fine grid near the wall is able to retain (Fig. 6.9). Since the pressure gradient is evaluated with respect to the arc length it is relative small around the shock near the outflow. This can be improved by evaluating the pressure gradient with respect to the grid index, for example the M at point J can be set to $\max\{|P_{J+1}-P_J|, |P_J-P_{J-1}|\}$. Using this the grid in the shock region is better clustered (Fig. 6.10). The grid quality of Fig. 6.8 to 10 can be further improved by one or two passes of a smoothing operator.

Since the value of weight function is proportional to the inverse of mesh spacing the mesh spacing produced by above simple method can be used as input for more sophisticated methods using original equidistribution law.

For more complex flow the embedded mesh approach is obviously a much safer approach. In our opinion if one wish to do adaption covering both viscous and inviscid regions it will need heavy human intervention to guarantee the adapted grid is reasonable.

A possible way to avoid the above problem is to separate the flow region into two. The one near the wall uses fine grid while another one away from the wall uses coarse grid. The adaption is done in the individual grid. However it is not clear if the sudden mesh size change will bring any problem and if this approach needs more grid points.

6.6 Dissipation effect on numerical boundary layer thickness

It is well known that Roe's Riemann solver, which includes informations about all waves, can give very accurate representation of boundary layers in quite coarse mesh while Van Leer's flux-vector splitting, which ignores the linear waves, badly diffuses the boundary layer (Van Leer et al 1987).

As we pointed out in Chapter 4 the formula suggested by Yee (1987) introduces large dissipation into the linear waves which might degrade the solution significantly for viscous calculations.

An easy demonstration is to check the numerical boundary thickness on a flat plate. A numerical scheme with more dissipations will give thicker numerical boundary layer.

The test Mach number is 0.5 with Reynolds number 10668 and adiabatic wall condition. Along the streamwise direction there are ten cells before the leading edge and 20 cells on the plate with uniform mesh spacing. The residuals are reduced by 10 orders of magnitude after 1000 iterations for all meshes used. Fig. 6.11 shows the velocity profiles at the last column cells on the plate from first order and second order schemes on three different grids. The coarse grid result is very close to fine grid result even for first order scheme; however, with $\tilde{\delta}_{2.3}=0.25$ the calculated boundary layer is unacceptable even on the fine grid. Although in this case we do not need to use dissipation any boundary layers must have such low Mach number region in high Mach number viscous flow.

We therefore do not recommend Yee's dissipation for viscous calculations and any methods proposed for curing the blunt nose instability should pass this test case.

There are two more interesting things we can learn from this simple boundary layer calculation. The singularity at the leading edge can never be resolved by refining the meshes and the grid near the L.E. should be very fine; however, one does not obtain bad solutions downstream of the L.E.. This implies the singularity is not very important. The other thing is that the worse region of the solution is where the curvature of velocity profile is large, i.e. near the edge of boundary layer. The velocity profile near the wall is very accurate. This might justify the use of simple forms of stretched grids in viscous

calculations if one only needs the viscous stress.

6.7 The carbuncle phenomenon revisit

As demonstrated in section 6.6 the formula of Yee is not suitable for viscous calculation. This problem was also understood by Peery and Imlay (1988). They proposed a formula which uses pressure gradient to tune the magnitude of dissipation. They changed the eigenvalues (wave speeds) to

$$\lambda_k' = \frac{1}{2}\left(\frac{\lambda_k^2+\epsilon_k^2}{\epsilon_k}\right)$$

where

$$\epsilon_{1,4} = \begin{cases} 1.2(|V_\infty|+a)+\dfrac{\Delta\Delta p}{4\bar{p}}V_\infty & \text{in i direction} \\ 0.2(|V_\infty|+a)+\dfrac{\Delta\Delta p}{4\bar{p}}V_\infty & \text{in j direction} \end{cases}$$

$$\epsilon_{2,3} = \begin{cases} |V_\infty|+a+\dfrac{\Delta\Delta p}{4\bar{p}}V_\infty & \text{in i direction} \\ \dfrac{\Delta\Delta p}{4\bar{p}}V_\infty & \text{in j direction} \end{cases}$$

in their words, $\Delta\Delta p$ is a second difference of pressure averaged at the cell face, $\bar{p}$ is an averaged local pressure, and V_∞ is the free stream total velocity. They used a Mach 2 flow past a flat plat to demonstrate their formula is suitable for viscous calculation if the j direction is normal to the wall. Nevertheless their formula is still not suitable for viscous blunt-body calculation because the i direction, which has bigger dissipation, is normal to the body. Another problem of their formula is that, again in their words, the shock was captured with approximately three internal points, although the outer two points were nearly equal to the conditions at the edges of the shock. This is due to the excessive dissipation at supersonic part of flow.

Their idea of using pressure gradient to tune the dissipation seems to a good idea. We still uses the $Q(\lambda_k)$ in section 4.2 but change the δ_k. Our modification is

$$\delta_{i,i}=(|V_n|+a)(\kappa_1+\kappa_2\kappa_p)$$
$$\delta_{i,j}=(|V_n|+a)(\kappa_3\kappa_p)$$

k_p is similar to $\Delta\Delta p$. The k_p at interface (i+1/2,j) for example is equal to the average of k_p at (i+1,j) and (i,j). The k_p at (i,j) is chosen as

$$(\kappa_p)_{ij}=0.5\left(\left|\frac{p_{i+1,j}-2p_{ij}+p_{i-1,j}}{p_{i+1,j}+2p_{ij}+p_{i-1,j}}\right|+\left|\frac{p_{ij+1}-2p_{ij}+p_{ij-1}}{p_{ij+1}+2p_{ij}+p_{ij+1}}\right|\right)$$

and if the local Mach number at cell (i,j) is greater than 1.0 the k_p is divided by the Mach number.

Our modification removes the direction dependency of Peery and Imlay's formula and decreases the dissipation at supersonic region.

There are at most most two internal points in the shock layer with our formula. Fig. 6.12 shows the result for Mach 8 calculation with $k_1=0.25, k_2=0,$ and $k_3=15$ with CFL no.5. Fig. 6.13 is obtained with $k_2=5$. Fig. 6.14 and 6.15 show the results for Mach 20 using same parameters of Fig. 6.12 and 6.13 respectively. From these graphs the solutions converge better with $k_2=5$. The optimum CFL no. is lower than using Yee's formula, which is more dissipative in the smooth flow.

Using this formula the magnitude of k_p is about the order of 10^{-4} in smooth flow, which is quite small.

6.8 The grid-dependent characteristic of current upwind schemes

The scheme which is based on one dimensional Riemann solver can only partially model the physics in multidimensional flow. This is because the Riemann solvers only consider the flow normal to the cell interfaces.

Roe (1986b) gave some examples that how the important physics can be totally missed and suggested a discrete model which better mimicked the physics. Hirsch (1987) also proposed a similar scheme. Powell and Van Leer (1989) designed a third order scheme which utilises Hirsch's method. Overall the so-called genuinely multidimensional upwind scheme is still under development.

Such grid dependent Riemann solvers not only can miss the important physics but even give abnormal interface conditions. For example choose a set of data which meet the condition shown in Fig. 6.16a the usual Riemann solver gives lower pressure in the interface while in Fig. 6.16b it gives higher pressure.

Although the usual upwind scheme has its theoretical deficiency it works very well generally and no obvious problem appears from using it until recently Venkatakrishnan (1990) showed the pressure contours exhibited kinks from the laminar calculation of NACA 0012 at Mach number 0.5 and Reynolds number 5000 with adiabatic wall conditions. The flow separated at 81.4% cord according to Swanson and Turkel (1987) using a very fine grid. Venkatakrishnan also showed that with central-difference scheme the kink disappeared. However he was not sure the reason it occurred for upwind schemes. He was in favor of false viscous effect due to the truncation error of

viscous term despite it can not explain the pure central difference scheme on the advection term generats no kinks.

We tend to consider it is due to mesh dependent problem of current Riemann solvers, i.e. the inviscid term is the cause. Our results are shown in Fig. 6.17, 18 and 19 for pressure contours, streamlines and density contours respectively. The flow and mesh conditions before trailing edge are similar to Fig. 6.16a and after the trailing edge are similar to Fig. 6.16b; however, the pressure kinks point to the left above the trailing edge and to the right after the trailing edge (Venkatakrishnan did not observe this behind the trailing edge). Since the pressure is increasing from the left to the right we should obtain kinks pointed to opposite directions.

The pressure kinks can be altered by changing the grid locally between 80% and 100% chord region such that we can have the Fig. 6.16b case. Fig. 6.20 shows the pressure kinks now point to right after 80% cord. From this example one can expect if the grid line follow very closely with the streamlines the pressure kinks should disappear.

Venkatakrishnan also showed the kinks disappeared with fine grid. This can also be explained since the conditions between two cells are closer the pressure difference from the Riemann becomes very smaller.

The results are obtained using minmod limiter. The grid is a 101X33 C mesh with 66 points on the aerofoil. It is generated by using the author's grid generator which is based on the method of Eagle code (Thompson 1987a and 1987b). Although it is capable to generate an elliptic grid with surface normal control only transfinite interpolation solution with Hermite

interpolation normal to the wall is used. The flow in Fig. 6.17 separates at 85% chord while it separates at 80% chord in Fig. 6.20. The second grid is slightly finer than the first grid near the aerofoil.

6.9 Concluding remarks

We have studied the model equation extensively to validate some ideas although the results are unfortunately not directly applicable to Navier-Stokes equations. A simple method which combines three mesh control techniques suitable for multivariable adaption on viscous flow is proposed and demonstrated. We consider the moving grid point approach needs heavy human intervention to produce a better adaptive grid especially for viscous problems.

The dissipation effect on the boundary layer calculation is shown to be undesired. We also show a better formula to cure the carbuncle phenomenon, which is based on pressure gradient. Finally we are able to demonstrate the grid-dependent characteristic of current Riemann solver.

APPENDIX : A CELL-VERTEX TVD SCHEME

A.1 Introduction

In the search for effective numerical solution techniques for the compressible Euler equations (or any other set of equations having the same mathematical form) significant differences arise from taking different views as to what the computations mean.

In the cell-centre approach (Fig. a) the solution is sought as AVERAGE values of the conserved variables WITHIN each computational cell. The flux between two cells is assumed to be $0.5(W_1+W_2)$ which is likely to be inaccurate if the two cells are of very different size.

In the cell-vertex approach (Fig. b) the solution is sought as POINT values of the conserved variables at NODES of the computational mesh. The flux through an edge is assumed to be $0.5(W_a+W_b)$ which is accurate regardless of mesh distortion.

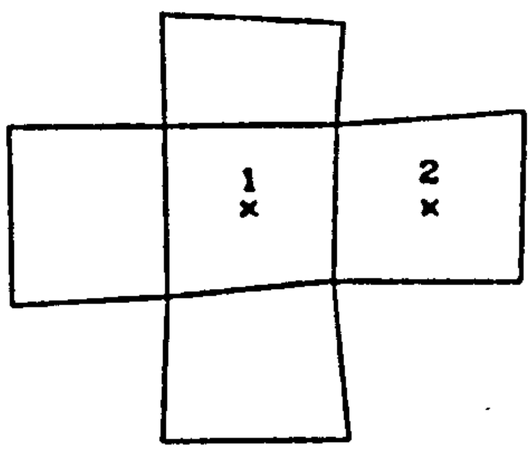

Fig. a cell-centre

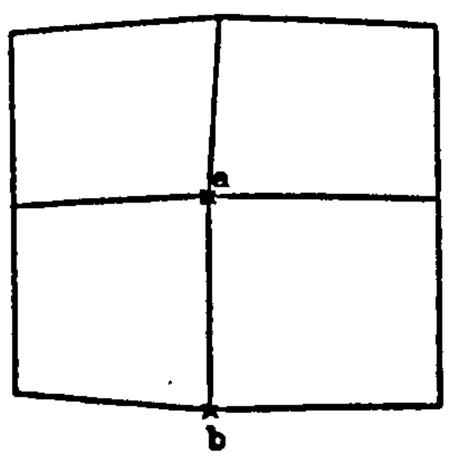

Fig. b cell-vertex

These simple considerations incline one to assume that cell-vertex schemes should be more accurate than cell-centre (finite volume) schemes on distorted grids, and more detailed mathematical analysis (Roe 1987b, Paisley 1986) and numerical experiments (Lin 1987) support this view.

In the previous chapters we use a TVD scheme which approximates the cell-centre scheme of Jameson (1981) without artificial dissipation in smooth flow. We hope to developed a cell-vertex TVD scheme which gives cell-vertex residual in smooth flow.

Powell and Van Leer (1987) proposed a third order cell-vertex scheme based on multidimensional upwinding; however, their scheme was not TVD.

A.2 A cell-vertex TVD scheme

Take the control volume for point 0 as A_0, Jameson (1986) proposed a cell vertex scheme, see Fig. c,

$$A_0\frac{dW_0}{dt}+\frac{1}{2}\sum_{k=1}^{8}\{(F_k+F_{k-1})(y_k-y_{k-1})-(G_k+G_{k-1})(x_k-x_{k-1})\}=0$$

which is equivalent to

$$A_0\frac{dW_0}{dt}+\sum_{k=1}^{8}\{(F_k-F_0)\Delta y_k-(G_k-G_0)\Delta x_k\}=0$$

where

$$\Delta x_k=\frac{1}{2}(x_{k+1}-x_{k-1})\qquad \Delta y_k=\frac{1}{2}(y_{k+1}-y_{k-1})\qquad k=1,8$$

For later use we define

$$\Delta x_0=\frac{1}{2}(x_1-x_5)\qquad \Delta y_0=\frac{1}{2}(y_1-y_5)\qquad k=0$$

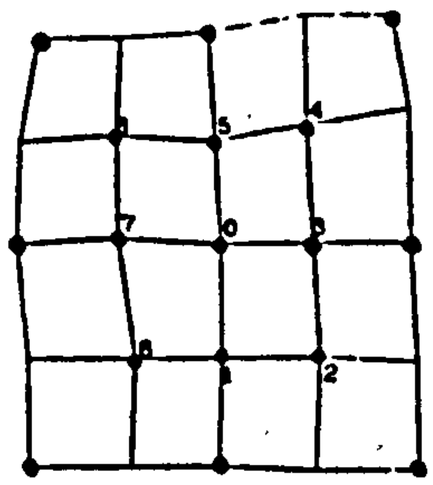

Fig. c

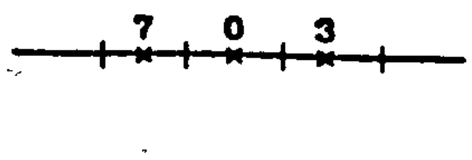

Fig. d

To make this scheme TVD the main difficulty is the stencils involved 9 points. However we can at least make it TVD in four directions 7→3, 1→5, 8→4, and 2→6. Take 7→3 for example, let

$$\mathcal{F}_{37} = (F_3-F_0)\Delta y_3-(G_3-G_0)\Delta x_3 + (F_7-F_0)\Delta y_7-(G_7-G_0)\Delta x_7$$

if $\Delta y_3=-\Delta y_7$ and $\Delta x_3=-\Delta x_7$ we have

$$\mathcal{F}_{37} = (F_3-F_7)\Delta y_3-(G_3-G_7)\Delta x_3$$

which is simply central-differencing.

For one dimensional cell-centre central difference TVD scheme we have, refer to Fig. d,

$$\Delta x\frac{dW_0}{dt}+\frac{1}{2}\{[F_3+F_0+\sum_{k=1.3}^{k+}(\phi-1)\Delta F_{30}^{k+}-\sum_{k=1.3}^{k-}(\phi-1)\Delta F_{30}^{k-}]$$
$$-[F_7+F_0+\sum_{k=1.3}^{k+}(\phi-1)\Delta F_{07}^{k+}-\sum_{k=1.3}^{k-}(\phi-1)\Delta F_{07}^{k-}]\}=0$$

Denote the terms involved with limiter ϕ as Φ_{30} and Φ_{07} we have

$$2\Delta x\frac{dW_0}{dt}+(F_3-F_0)+(F_0-F_7)+\Phi_{30}-\Phi_{07}=0$$

Similarly for cell-vertex scheme we can add $\Phi_{30}-\Phi_{07}$ to $\mathcal{F}_{37}$. Therefore we have

$$A_0\frac{dW_0}{dt}+\mathcal{F}_{37}+\Phi_{30}-\Phi_{07}+\mathcal{F}_{51}+\Phi_{50}-\Phi_{01}+\mathcal{F}_{48}+\Phi_{40}-\Phi_{08}+\mathcal{F}_{62}+\Phi_{60}-\Phi_{02}=0$$

If we evaluate Φ_{30} according to Δx_3 and Δy_3 and Φ_{03} according to Δx_0 and Δy_0, usually we would have $\Phi_{30}\neq\Phi_{03}$ which would make this scheme nonconservative. However if these terms are evaluated according to $\pm\frac{1}{2}(\Delta x_3-\Delta x_0)$ and $\pm\frac{1}{2}(\Delta y_3-\Delta y_0)$ we will have a conservative scheme (similarly for Φ_{07}, Φ_{60}, and Φ_{01}).

There are several disadvantages of this scheme. Firstly, it needs to compute Riemann problems twice as often than the cell-centre scheme does and for three dimension case it will be 10/3 times more. Second, it needs to evaluate limiter function in the diagonal directions. This is not easy to implement near the boundary and besides the limiter function is very grid dependent. A possible way to cut down the cost is probably to estimate $\Phi_{40}-\Phi_{08}+\Phi_{60}-\Phi_{02}$ as const. $(\Phi_{30}-\Phi_{07}+\Phi_{60}-\Phi_{01})$. That will bring the work down to about the same as the cell-centre

scheme. We will called this as simplified approach.

A.3 Result and discussion

The Ni's bump is chosen as the test problem. The bump height is 10 percent chord and Mach number is 0.675. We do not test the original approach because even if it works it is too expensive to use in practice. Only the simplified one is tested. To make it simple the boundary is implemented in the first order. Only the interior points are in second order. If we set ϕ equal 0.0 for the gridwise terms but ϕ equal 1.0 for the diagonal terms, which is more accurate than 1st order scheme but less accurate than 2nd order scheme, the scheme converges to the correct solution and no oscillation near the shock. However with second order scheme the residual is unable to go down after it is reduced by 3 orders of magnitude. This simplified approach is thus pessimistic.

REFERENCE

Abolhassani, J.S. et al. (1987), "Grid Adaption for Hypersonic Flow", AIAA paper 87-1169.

Anderson, D.A. et al. (1984), "Computational Fluid Mechanics and Heat Transfer", McGraw-Hill.

Anderson, D.A. and J. Steinbrenner (1986), "Generating Adaptive Grids with Conventional Grid Scheme", AIAA paper 86-0427.

Anderson, D.A. (1987), "Adaptive Grid Scheme Controlling Cell Area/Volume", AIAA paper 87-0202.

Bardina, J. and C.K. Lombard (1985), "Three Dimensional CSCM Method for the Compressible Navier-Stokes Equations with Application to Multi-Nozzle Exhaust Flow Field", AIAA-85-1193.

Belk, D.M. and D.L. Whitfield (1987), "Three-dimensional Euler Solutions on Blocked Grids Using an Implicit Two-pass Algorithm", AIAA-87-0450.

Bell, J. et al. (1989), "Higher-Order Godunov Methods for General Systems of Hyperbolic Conservation Laws", J. Comput. Physics, 82, pp. 362-397.

Benek, J.A. et al (1983), "A Flexible Grid Embedding Technique with Application to the Euler Equations", AIAA-83-1944.

Berger, M. (1987a), "Adaptive Finite Difference Methods in Fluid Dynamics", in Computational Fluid Dynamics, VKI Lecture Series 1987-04.

Berger, M. (1987b), "On Conservation at Grid Interfaces", SIAM J. Numer. Anal., Vol.24, No. 5.

Berger, M. and Colella, P. (1989), "Local Adaptive Mesh Refinement for Shock Hydrodynamics", J. Comput. Physics 82, 64-84.

Boris, J.P. and P.L.Book (1973), "Flux Corrected Transport: I. SHASTA, a Fluid Transport Algorithm That Works", J. Comput. Phy., 11, pp. 38-69.

Borrel, M and J.L.Montagne (1985), "Numerical Study of a Non-centered scheme with Application to Aerodynamics, AIAA-85-1497.

Brown, P.N. and Y.Saad (1987), "Hybrid Krylov Method for Nonlinear Systems of Equations", preprint.

Carey, G.F. and H.T. Dinh (1985), "Grading Functions and Mesh Redistribution", SIAM J. Numer. Anal., Vol.22, No. 5.

Chakravarthy, S.R. and S. Osher (1985), "A New Class of High Accuracy TVD Schemes for Hyperbolic Conservation Laws", AIAA-85-0363.

Chakravarthy, S.R. and K-Y Szema (1987), "Euler Solvers for Three Dimensional Supersonic Flow With Subsonic Pockets", J. Aircraft, Vol 24, No. 2.

Colella, P and P.R. Woodward (1984), "The Piecewise Parabolic Method (PPM) for Gas Dynamical Simulation", J. Comput. Physics, 54, pp. 174-201.

Dwyer, H.A. (1984), "Grid Adaption for Problems in Fluid Dynamics ", AIAA J., Vol. 22, No. 12, pp. 1705-1712.

Eiseman, P.R. (1987), "Adaptive Grid Generation", Computer Meth. in Appl. Mech. and Eng., 64, pp. 321-376.

Engquist,B. and S. Osher (1980), "Stable and Entropy Satisfying Approximations for Transonic Flow Calculations", Math. Comp., 34, pp.45-75.

Eriksson, L-E and M.M. Rai (1988), "A Stability Analysis of Various Patched Grid Interface Conditions for Hyperbolic equations", FFA report 144, 1988.

Godunov, S.K. (1959), "Finite-Difference Method for Numerical Computation of Discontinuous Solution of the Equations of Fluid Dynamics", Math. Sbornik, 47, pp. 217-306.

Harten, A. (1983a), "Self Adjusting Grid Methods For One-Dimensional Hyperbolic Conservation Laws", J. Comput. Physics 50, pp. 235-269.

Harten, A. (1983b), "High Resolution Schemes for Hyperbolic Conservation Laws", J. Comput. Physics, 49, pp. 357-393.

Hemker, P.W. and S.P. Spekreijse (1986), "Multiple Grid and Osher's Scheme for the Efficient Solution of the Steady State Euler Equations", Applied Num. Math. 2., pp. 475-493.

Hirsch, C. et al. (1987), "Convection Algorithms Based on a Diagonalization Procedure for the Multidimensional Euler Equations" , AIAA paper 87-1173.

Hirsch, C. (1988), "Numerical Computation of Internal and External Flows", Vol. 1, John Wiley and Sons, Chichester.

Hirsch, C. (1990), "Numerical Computation of Internal and External Flows", Vol. 2, John Wiley and Sons, Chichester.

Hsu, A.T. an d J.K. Lytle (1989), "A Simple Algebraic Grid Adaption Scheme With Applications to Two- and Three-Dimensional Flow Problems", AIAA paper 89-1984-CP.

Hsu, C-C and C-G Tu (1987), "A Self-Adaptive Gridding for Inviscid Transonic Projectile Aerodynamics Computation", Int J. for Numer. Meth. in Fluids, Vol. 7, pp. 567-579.

Jameson, A., Schmidt, W., and Turkel, E. (1981), "Numerical Solution of the Euler Equations by Finite Volume Methods Using Runge-Kutta Time Stepping Scheme", AIAA paper 81-1259.

Jameson, A. (1986), "Multigrid Algorithms for Compressible Flow Calculations", in the Proccedings of the Second European Conference on Multigrid Methods, in Lecture Notes in Mathematics, Vol. 1228, Edited by Trottenberg and Hackbusch, Springer-Verlag.

Jennings, G. (1974), "Discrete Shocks", Comm. Pure and Appl. Math., Vol. 27, pp. 25-37.

Kathong, M. et al. (1988), "A Conservative Approach for Flow Field Calculations on Multiple Grids", AIAA-88-0224.

Kim, H-Y and Thompson, J.F. (1988), "Three Dimensional Adaptive Grid Generation on a Composite Block Grid", AIAA paper 88-0311.

Lax, P.D. (1954), "Weak Solutions of Nonlinear Hyperbolic Equations and Their Numerical Computation", Comm. Pure and Appl. Math., vol. 7, pp. 159-93.

Lax, P.D. (1973), "Hyperbolic Systems of Conservation Laws and the Mathematical Theory of Shock Waves", SIAM, Philadelphia.

Lin, H-C (1987), "Accuracy of Various Schemes for the Numerical Solution of the Euler Equations Governing Inviscid Compressible Flow", M.Sc. Thesis, College of Aeronautics, Cranfield Inst. of Technology.

Lombard, C.K. (1983), "Multi-Dimensional Formulation of CSCM - an Upwind Eigenvector Split Method for the Compressible Navier-Stokes Equations", AIAA-83-1985.

Moon, Y-J and M-S Liou (1989), "Conservative Treatment of Boundary Interface for Overlaid Grids and Multi-level Grid Adaptions ", AIAA-89-1980-CP.

Morice, Ph. (1988), "Transonic Computations by Multidomain Techniques with Potential and Euler Solvers", ONERA T.P. no. 1988-78.

Muller, B. (1989), "Simple Improvements of an upwind TVD scheme for Hypersonic Flow", AIAA-89-1977-CP.

Nakahashi, K and G.S. Deiwert (1986), "Three-Dimensional Adaptive Grid Method", AIAA J., Vol. 24, pp. 949-954.

Nakahashi, K and G.S. Deiwert (1987), "Self-Adaptive-Grid Method with Application to Airfoil Flow", AIAA J., Vol. 25, pp. 513-20.

Ni, R-H (1982), "A Multiple Grid Scheme for Solving the Euler Equations", AIAA Journal, Vol. 21, pp. 1565-1571.

Osher, S. and F. Solomon (1982), "Upwind Difference Schemes for Hyperbolic Systems of Conservation Laws", Math. Comp., Vol. 18, no. 158, pp. 339-374.

Osher, S. and S. Chakravarthy (1984), "High Resolution Schemes and the Entropy Conditions", SIAM J. Numer. Anal. Vol.21, no. 5.

Paisley, M.F. (1986), "A Comparison of Cell Centre and Cell Vertex Scheme for the Steady Euler Equations", Oxford University Computing Laboratory Numerical Analysis Group Report 86/1.

Pandolfi, M. (1987), "Upwind Formulations for the Euler Equations ", Computational Fluid Dynamics, VKI lecture Series 1987-04.

Peery, K.M. and Imlay, S.T. (1988), "Blunt-Body Flow Simulations", AIAA paper 88-2904.

Peyret, R. and Taylor, T.D. (1983), "Computational Methods for Fluid Flow", Springer-Verlag.

Pfitzner, M. et al (1989), "Three-Dimensional Simulation of Hypersonic Flows", in Proc. of Int. Conf. on Hypersonic Aerodynamics, Royal Aeronautical Society.

Pike, J. (1987), "Grid Adaptive Algorithms for the Solution of the Euler Equations on Irregular Grids", J. Comput. Physics, 71, pp. 194-223.

Powell, K.G. and Van Leer, B. (1989), "A Genuinely Multidimensional Upwind Cell-Vertex Schemes for Euler Equations", AIAA paper 89-0095.

Rai, M.M. (1985), "A Relaxation Approach to Patched-Grid Calculations with the Euler Equations", AIAA-85-0295.

Rai, M.M. (1986), "An Implicit, Conservative, Zonal Boundary Scheme for Euler Equation Calculations", Computer and Fluids, 14, no. 3, pp. 295-319.

Ramshaw, J.D. (1985), "Conservative Rezoning Algorithm for Gener alized Two-Dimensional Meshes", J. Comput. Physics 59, pp. 193-199.

Roberts, T.W. (1988), "The Behaviour of Flux Difference Splitting Schemes Near Slowly Moving Shock Waves", in "Numerical Methods for Fluid Dynamics III", eds by K.W. Morton and M.J. Baines, Oxford University Press.

Roe, P.L. (1981a), "The Use of the Riemann Problem in Finite difference Schemes", Lecture Notes in Physics, 141, Spring-Verlag, New York, pp. 354-559.

Roe, P.L. (1981b), "Approximate Riemann Solvers, Parameter Vectors and Difference Schemes", J. Comput. Physics, 43, pp. 357-372.

Roe, P.L. and J. Pike (1984), "Efficient Construction and Utilization of Approximate Riemann Solutions", in "Comput. Methods. Appl. Science Engrg, VI", North-Holland.

Roe, P.L. (1986a), "Characteristic-based schemes for the Euler Equations", Ann. Rev. Fluid Mech., vol. 18, pp. 337-65.

Roe, P.L. (1986b), "Discrete Models for the Numerical Analysis of Time Dependent Multidimensional Gas Dynamics", J. of Comput. Physics, 63, pp. 458-76.

Roe, P.L. (1987a), "Finite-Volume Methods for the Compressible Navier-Stokes equations", 5th International Conf. on Numerical Methods on Laminar and Turbulent Flow.

Roe, P.L. (1987b), "Error Estimates for Cell-vertex Solutions of the Compressible Euler Equations", ICASE Report 87-6.

Saad, Y and M.H. Schultz (1986), "GMRES: A Generalized Minimal Residual Algorithm for Solving Nonsymmetric Linear Systems", SIAM J. Sci. Stat. Comput., Vol. 9, no. 3.

Shu, Chi-Wang and S. Osher (1988), "Efficient Implementation of Essentially Non-Oscillatory Shock-capturing Scheme", J. Comp. Physics, Vol.77, pp. 439-471.

Steger, J.L. (1978), "Implicit Finite-Difference Simulation of Flow about Arbitrary Two-Dimensional Geometries", AIAA J., Vol. 16, No. 17.

Swanson, R.C. and E.Turkel (1987), "Artificial Dissipation and Central Difference Schemes for the Euler and Navier-Stokes Equations", AIAA paper 87-1107.

Sweby, P.K. (1983), "High Resolution Schemes Using Flux Limiters For Hyperbolic Conservation Laws", SIAM J. NUMER. Anal., Vol 24 , No. 5, pp. 995-1011.

Thomas, J.L. et al. (1988), "Patched-grid Computations of High Speed Inlet Flows", in ASME Symposium: Advances and Applications in Comp. Fluid. Dyn., Vol. 66, pp. 11-22.

Thomas, J.L. et al. (1989), "A Patched-Grid Algorithm for Complex Configurations Directed Towards the F-18 Aircraft", AIAA paper 89-0121.

Thompson, J.F. et al. (1985a), "Numerical Grid Generation, Foundations and Applications", North-Holland.

Thompson, J.F. (1985b), "A Survey of Dynamically Adaptive Grids in the Numerical Solutions of Partial Differential Equations", Appl. Numer. Math., Vol. 1, pp. 3-27.

Thompson, J,F. (1987a), "A General Three-Dimensional Elliptic Grid Generation Systems on a Composite Block Structure", Computer Methods in Applied Mechanics and Engineering, 64, pp. 377-441.

Thompson, J,F. (1987b), "A Composite Grid Generation Code for General 3-D Regions", AIAA paper 87-0275.

Turkel, E. (1985), "Accuracy of Schemes with Nonuniform Meshes for Compressible Fluid Flows", ICASE Report 85-43.

Van Leer, B. (1973), "Toward the Ultimate Conservative Difference Scheme I. the Quest of Monotinicity", in Lecture Notes in Phys. , Vol. 18, pp. 163-68, Springer-Verlag, Berlin.

Van Leer, B. (1984), "On the Relation between the Upwind-Difference Scheme of Godunov, Engquist-Osher and Roe", SIAM J. Sci. Stat. Comput., Vol. 5, No. 1, pp. 1-20.

Van Leer, B. et al (1987), "A Comparison of Numerical Flux Formulas for the Euler and Navier-Stokes Equations", AIAA-87-1104.

Venkatakrishnan, V. (1990), "Viscous Computations Using a Direct Solver", Computer and Fluids, Vol.18, No. 2, pp. 191-204.

Wigton, L.B. et al. (1985), "GMRES Acceleration of Computational Fluid Dynamics Codes", AIAA-85-1495.

Yee, H-C (1987), "Upwind and Symmetric Shock-Capturing Scheme", NASA TM89464.

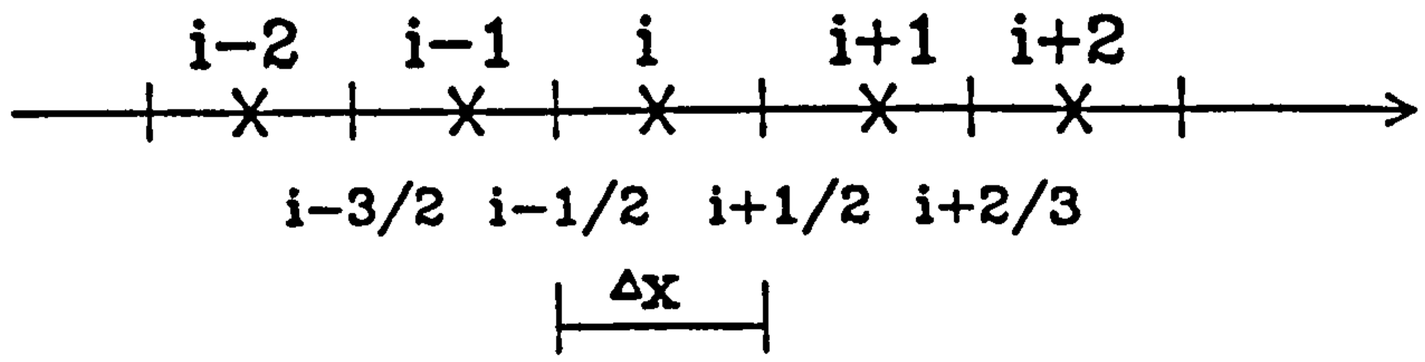

Fig. 1.1 Mesh for 1D calculation

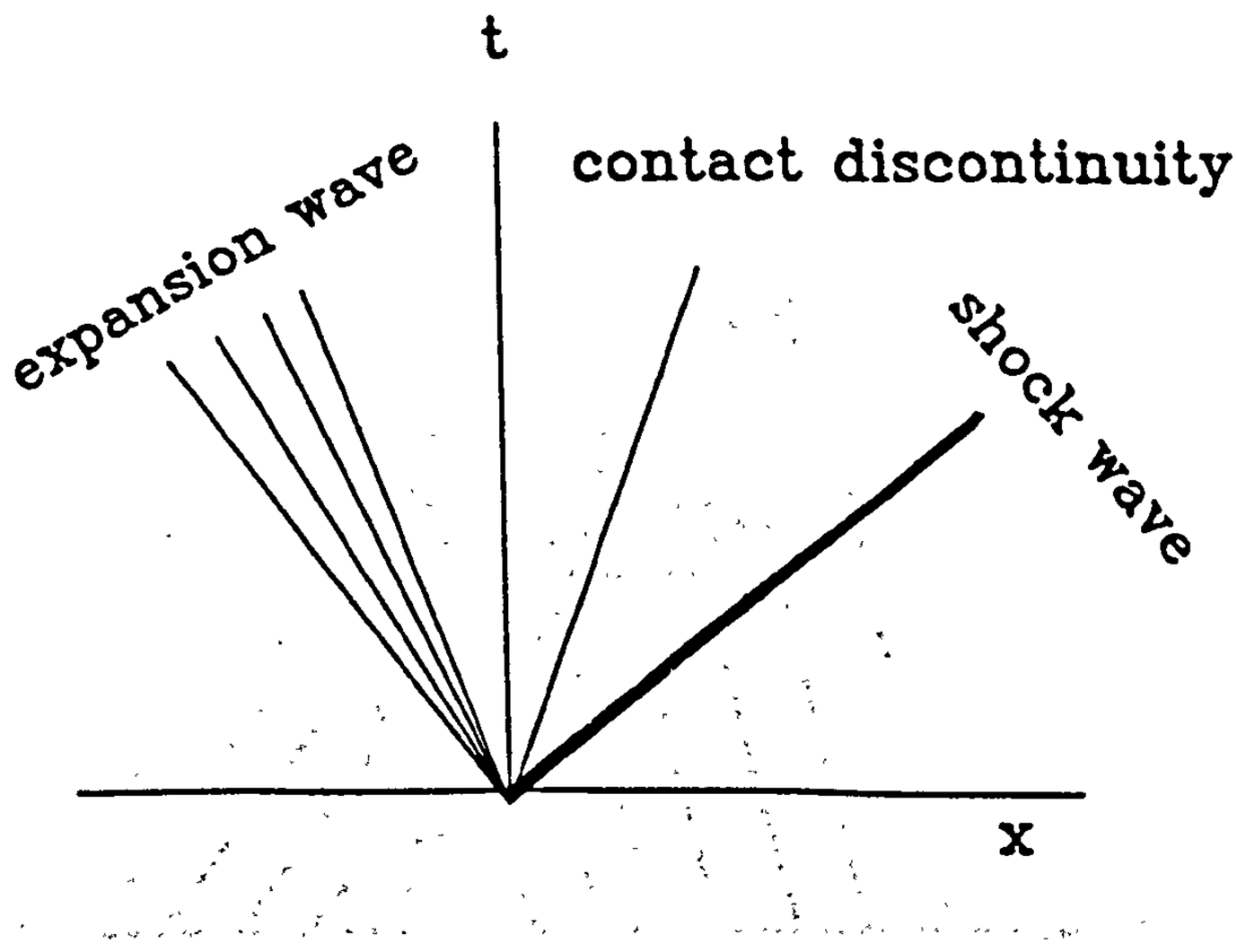

Fig. 1.2 An example of Riemann problem

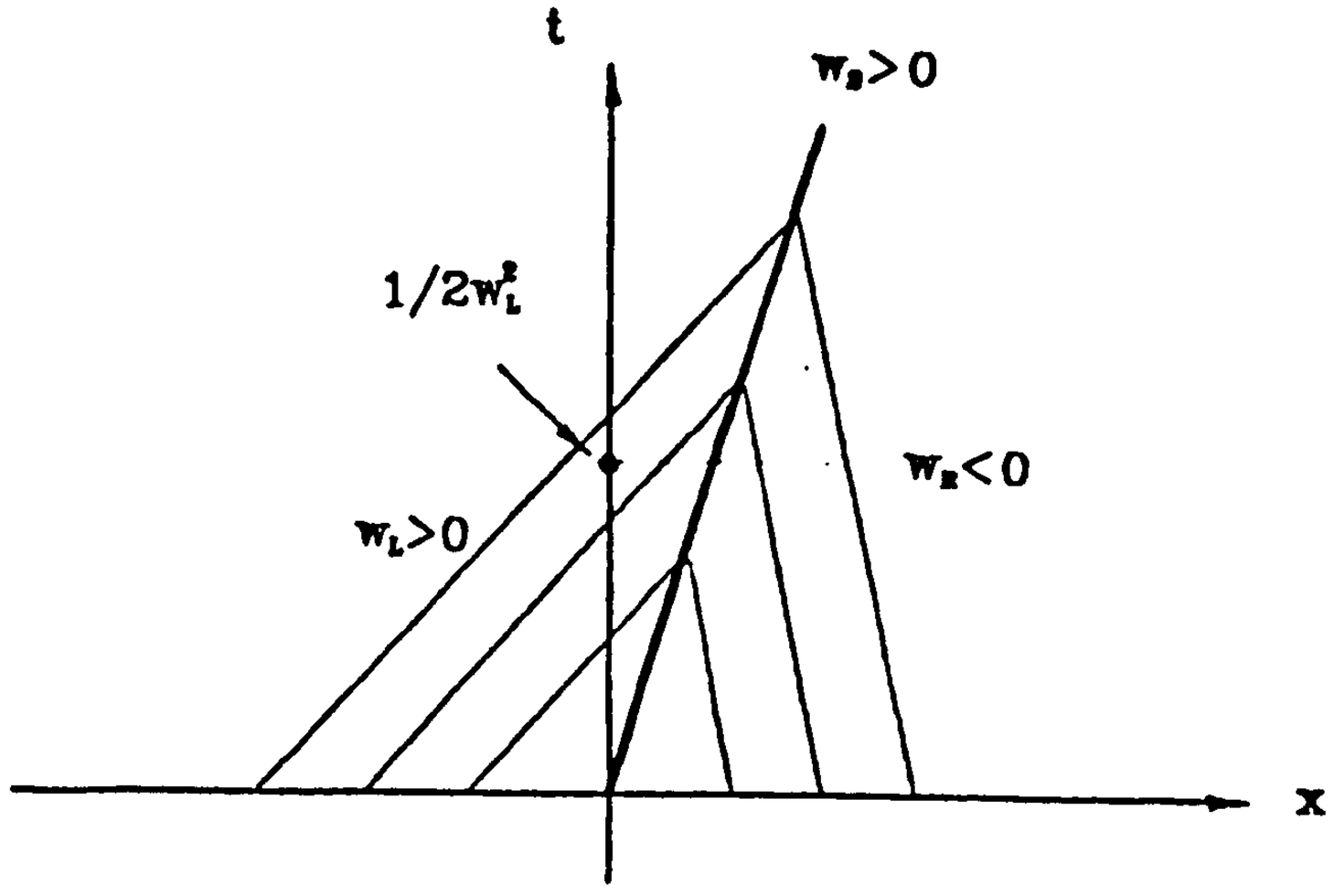

(a)

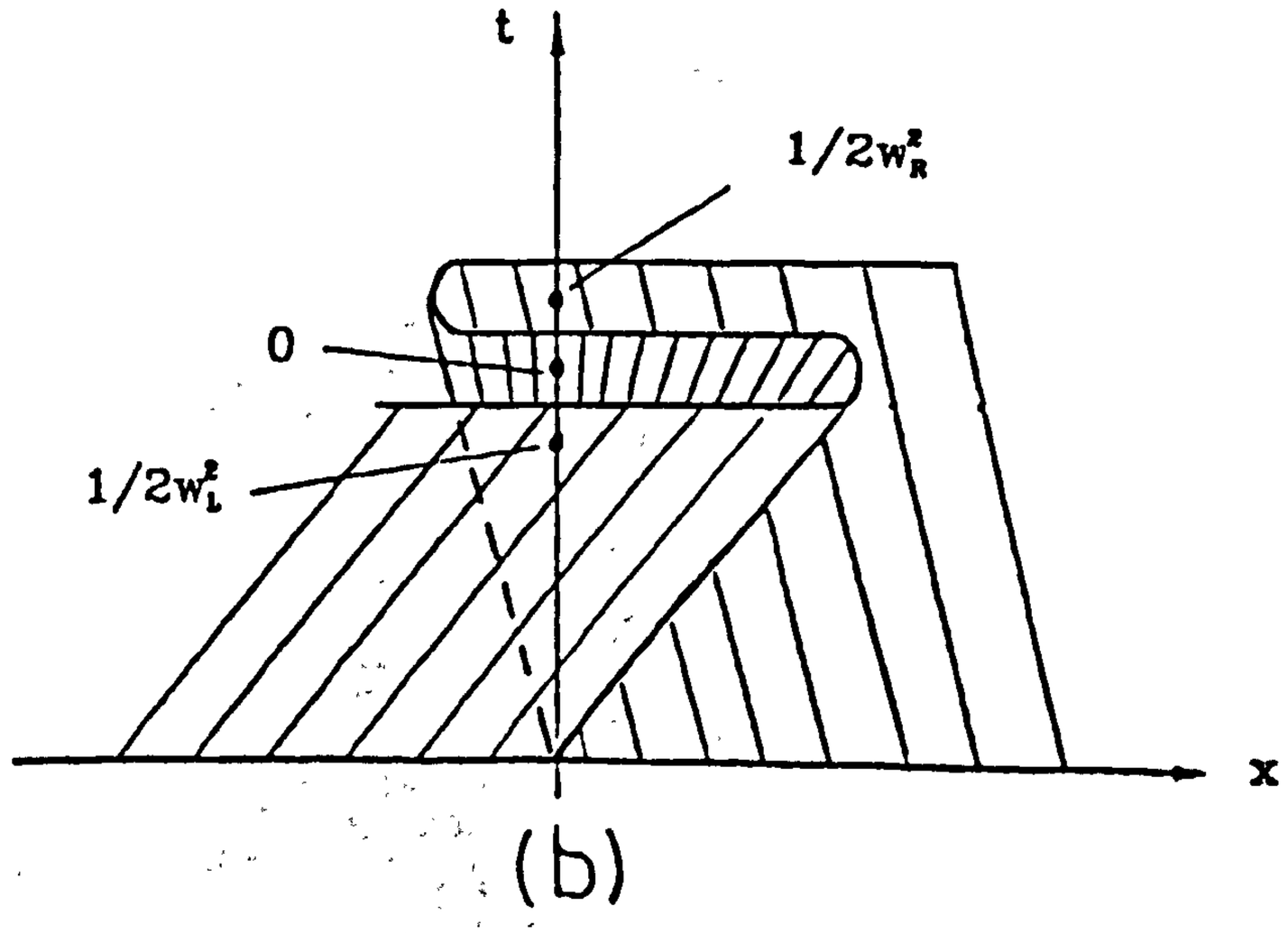

(b)

Fig. 2.1 Waves diagram for a right moving shock

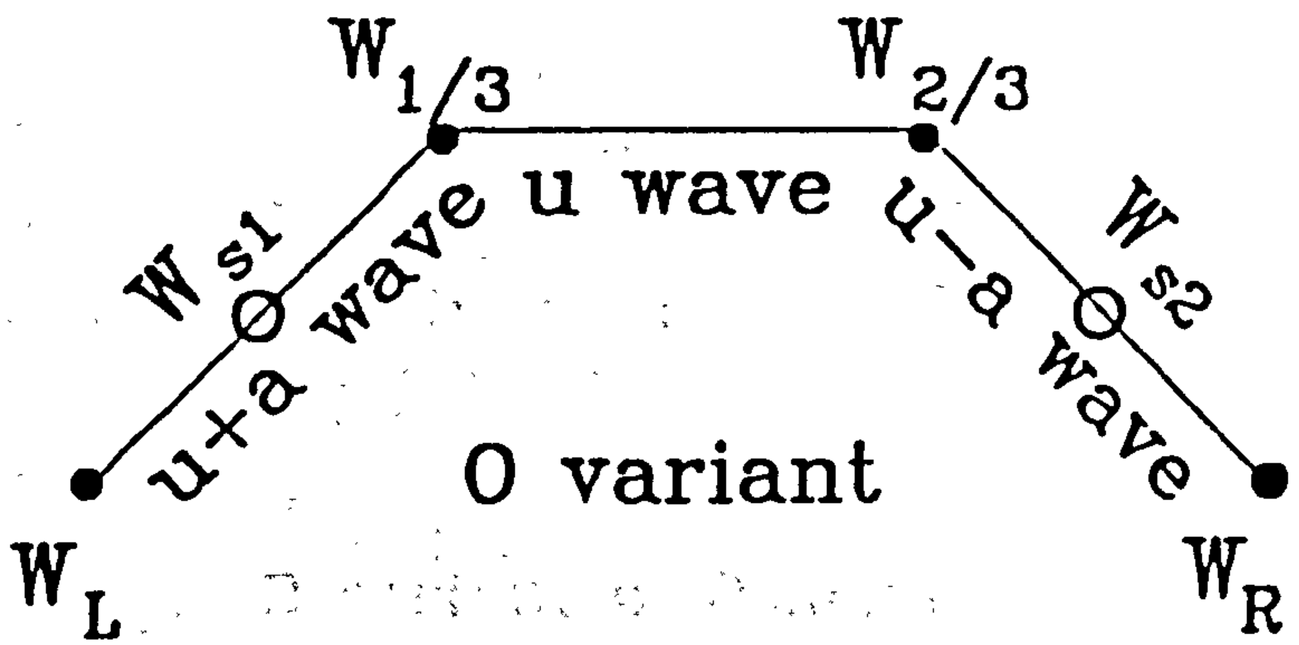

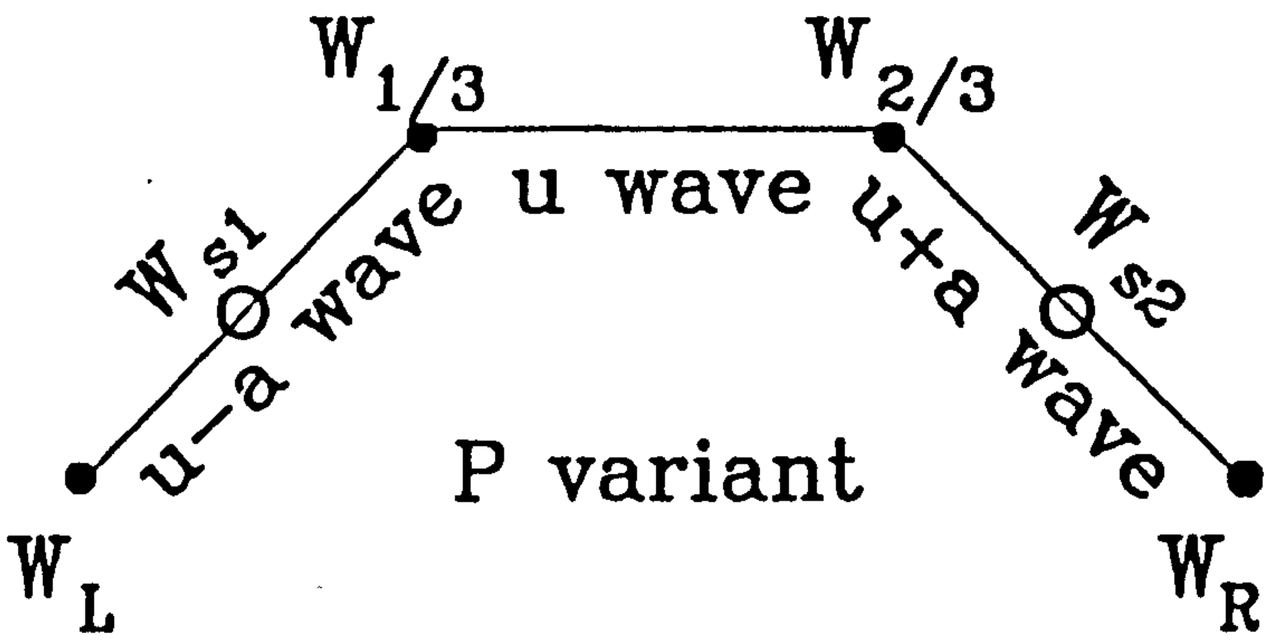

Fig. 2.2 Wave paths for O and P variants of Osher's scheme

Godunov's

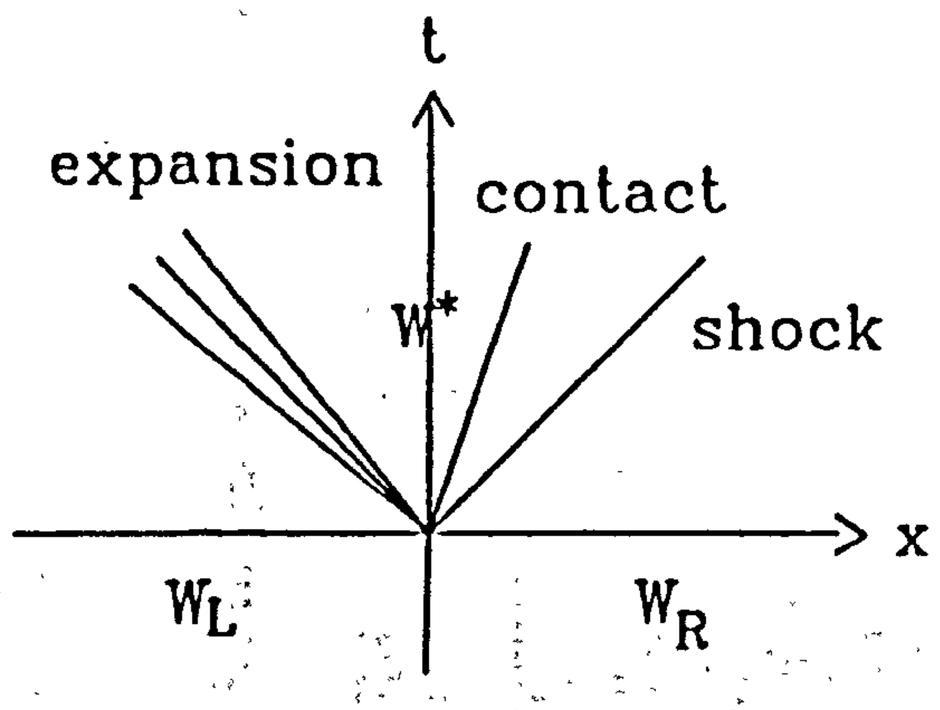

Roe's

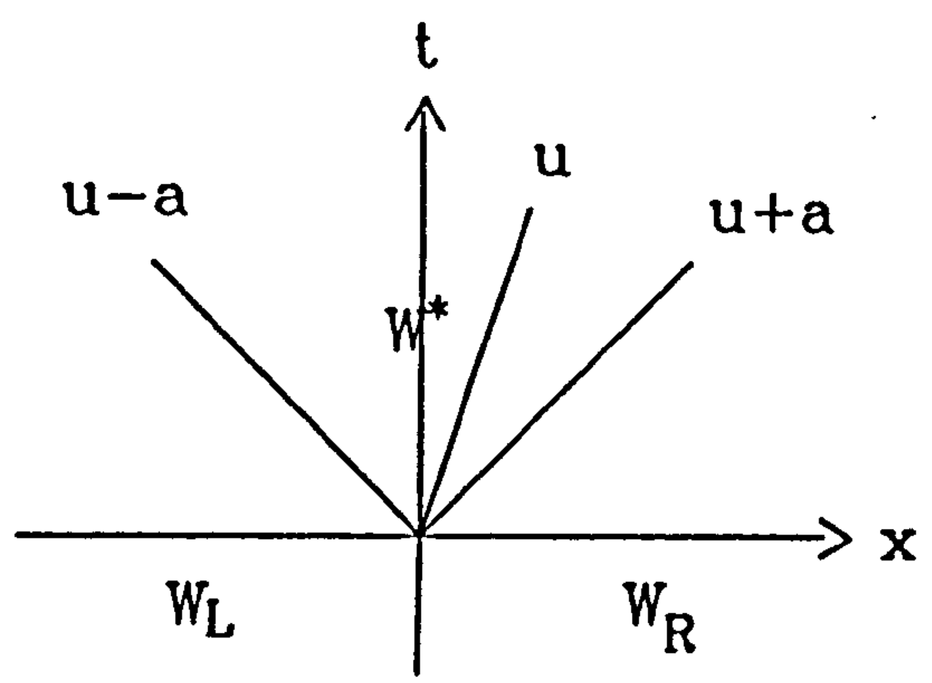

O variant of Osher's

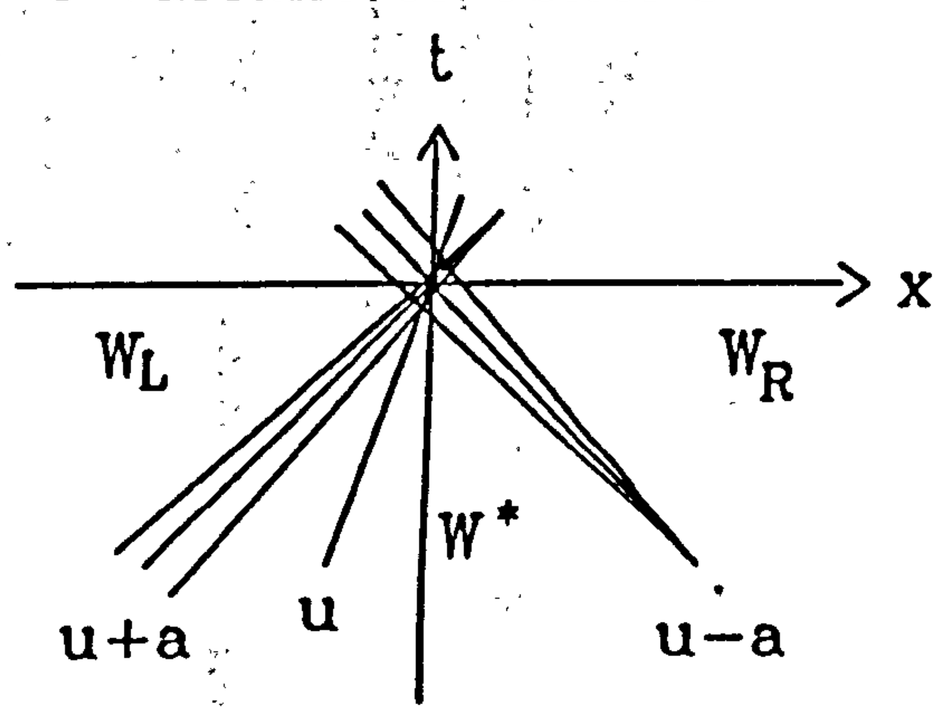

P variant of Osher's

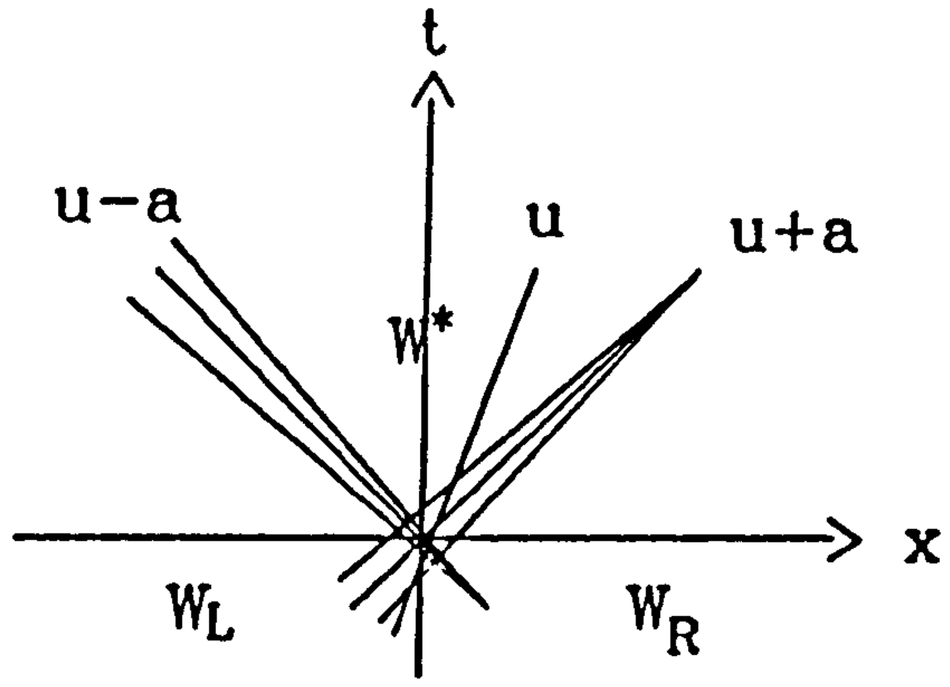

Fig. 2.3 Wave diagrams for various Riemann solvers

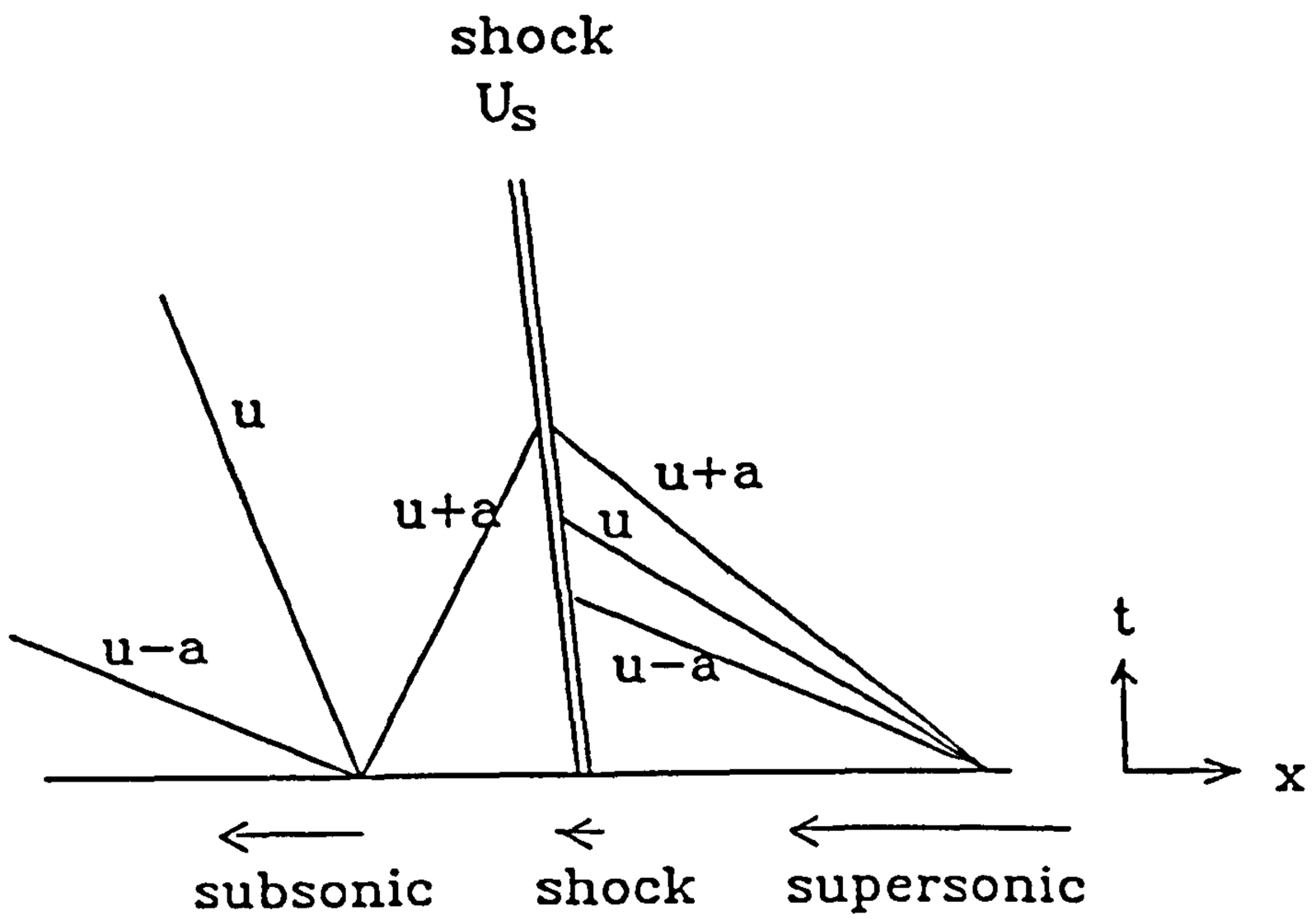

Fig. 2.4 Wave diagram of Woodward and Colllela's test.

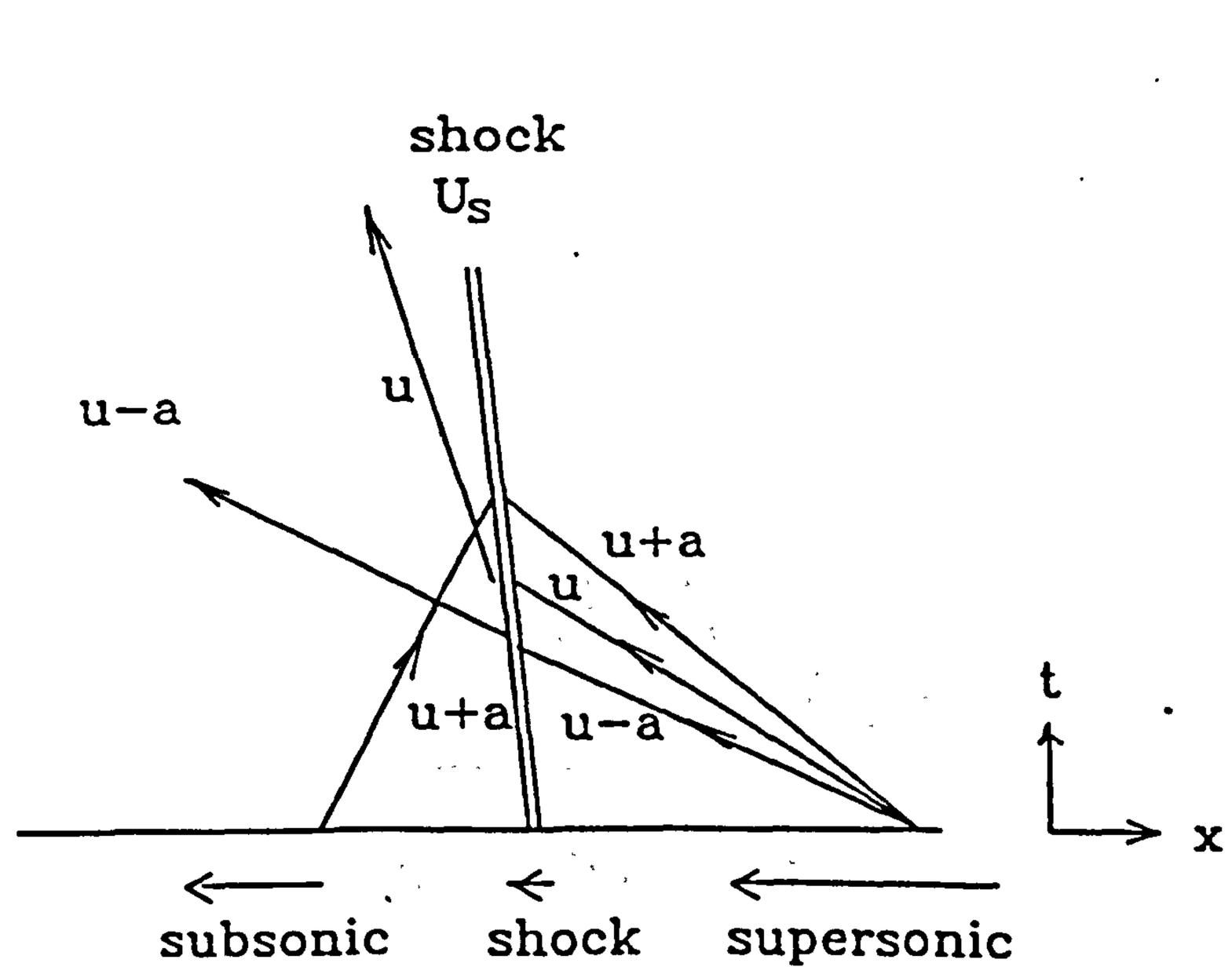

Fig. 2.5 Wave diagram for explaining the post-shock behaviour.

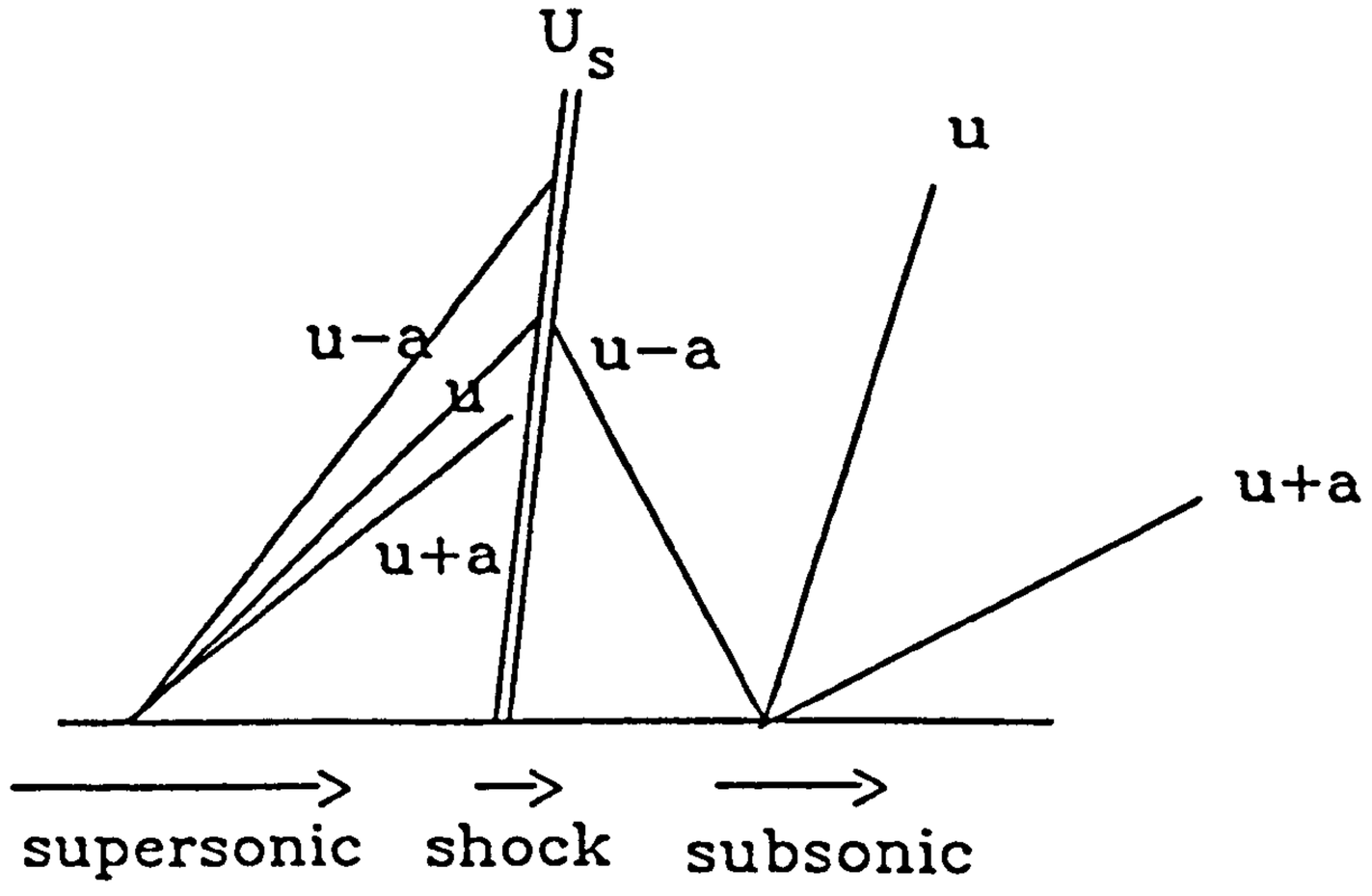

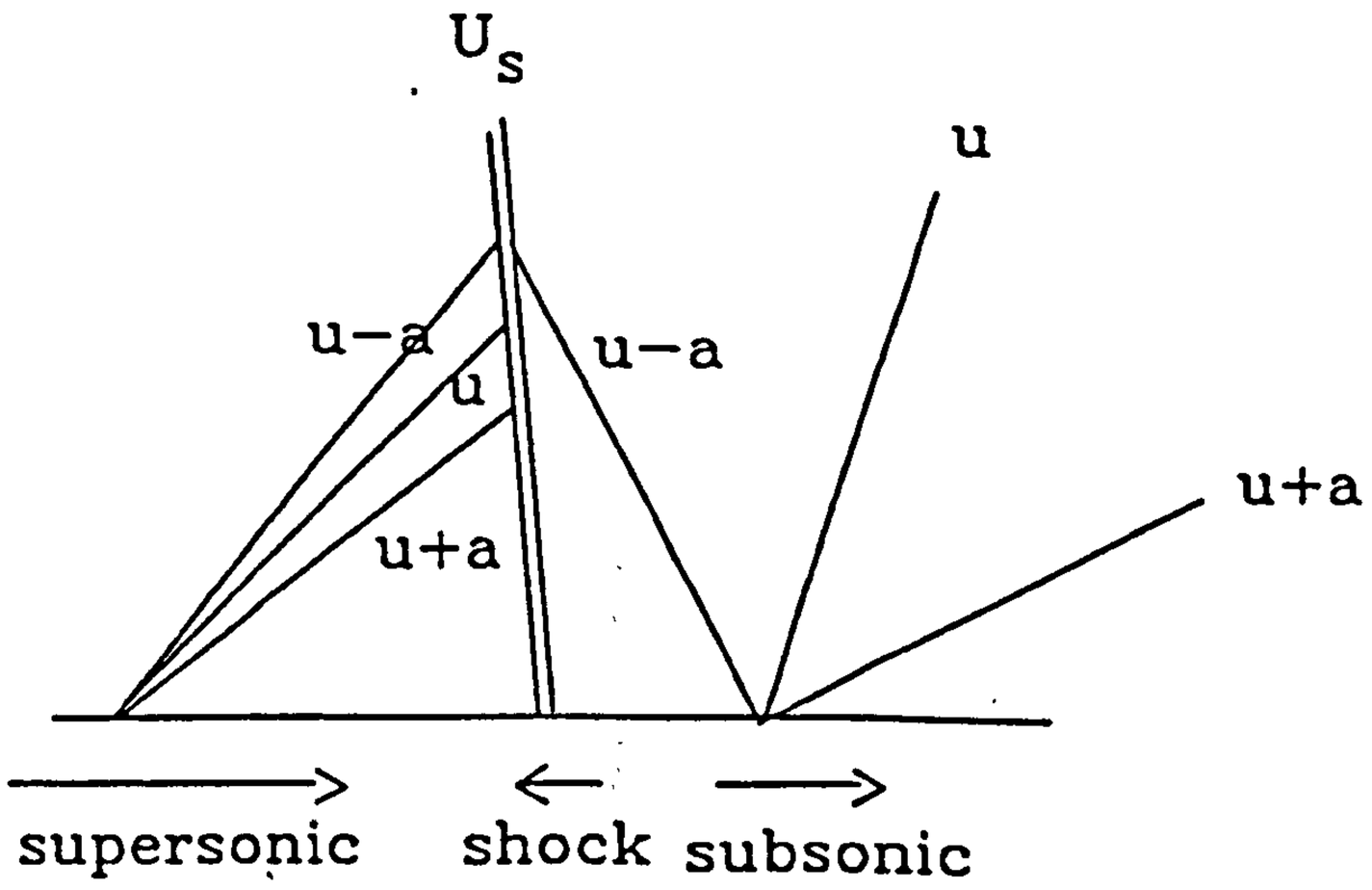

Fig. 2.6 Test case wave diagrams

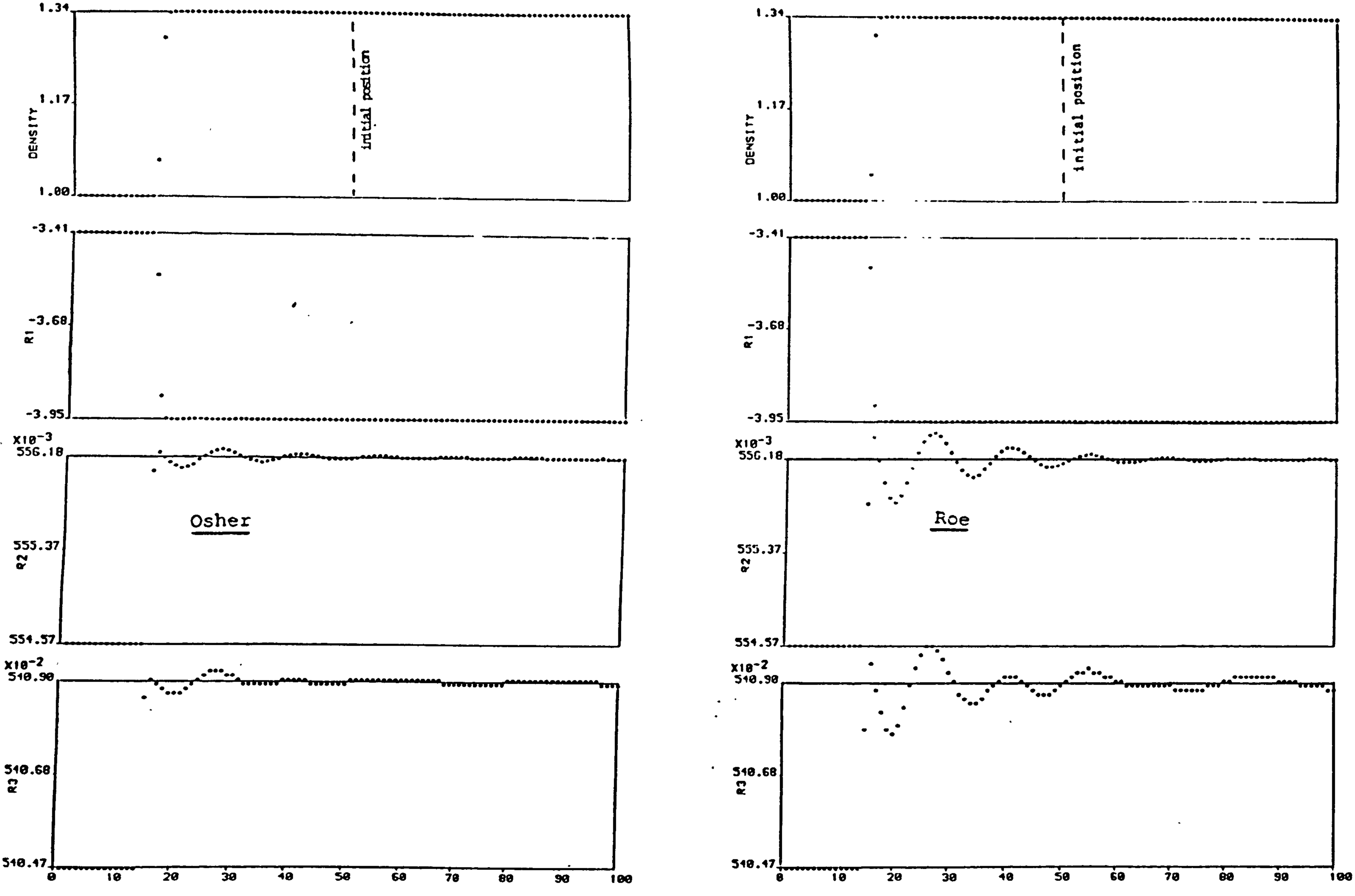

Fig. 2.7 Numerical solutions for M=1.2 shock with SR=-0.035

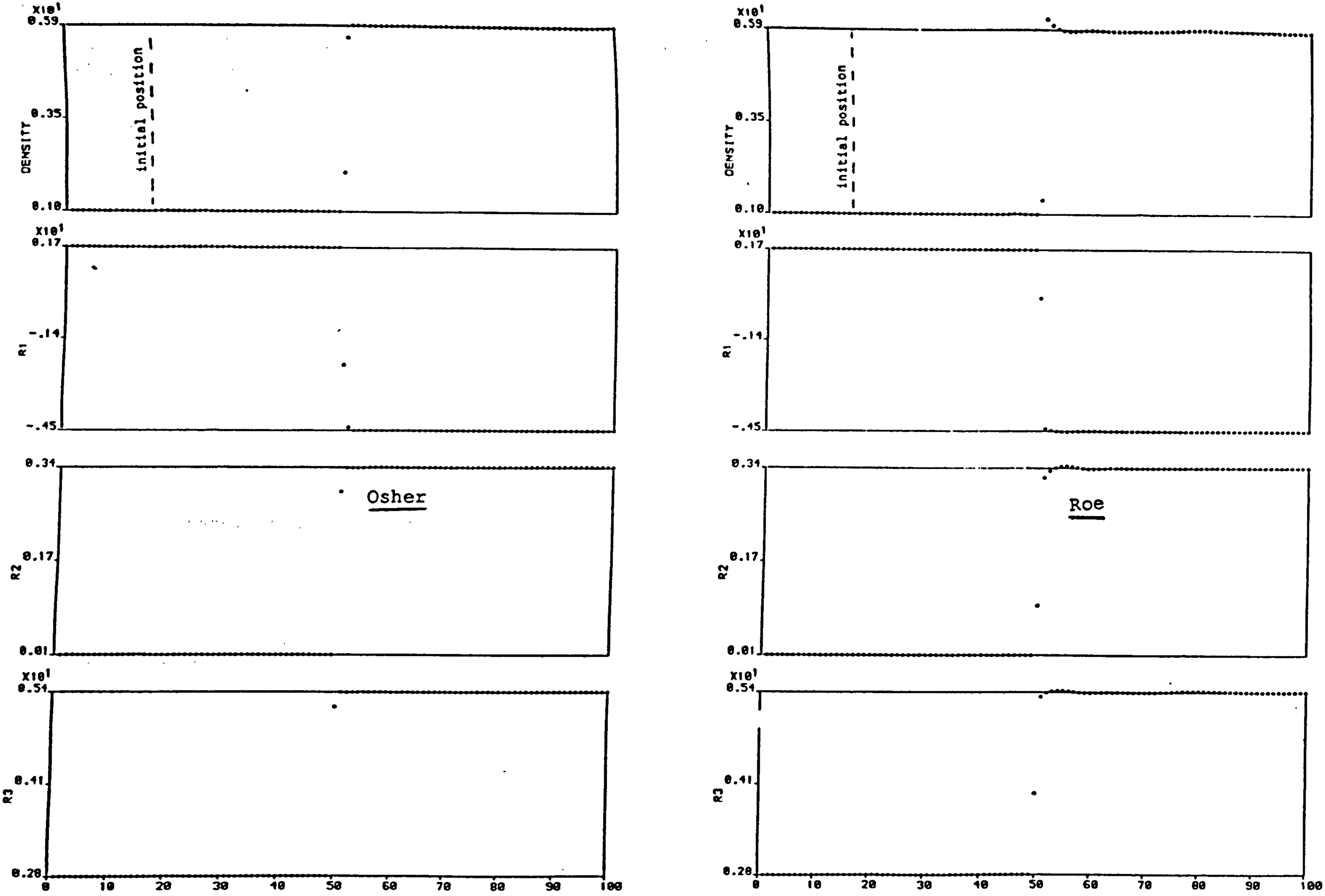

Fig. 2.8 Numerical solutions for M=20 shock with SR=+0.035

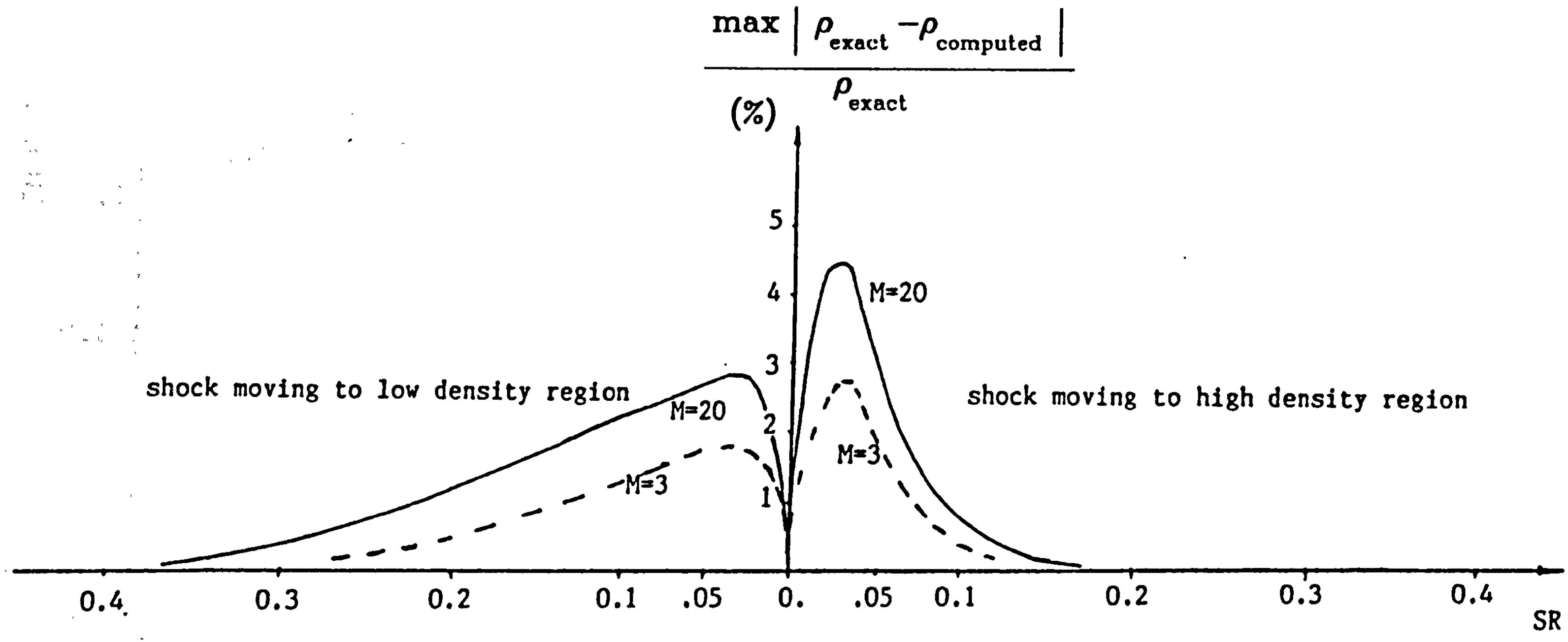

Fig. 2.9 Density oscillation magnitude vs. SR for Roe's scheme

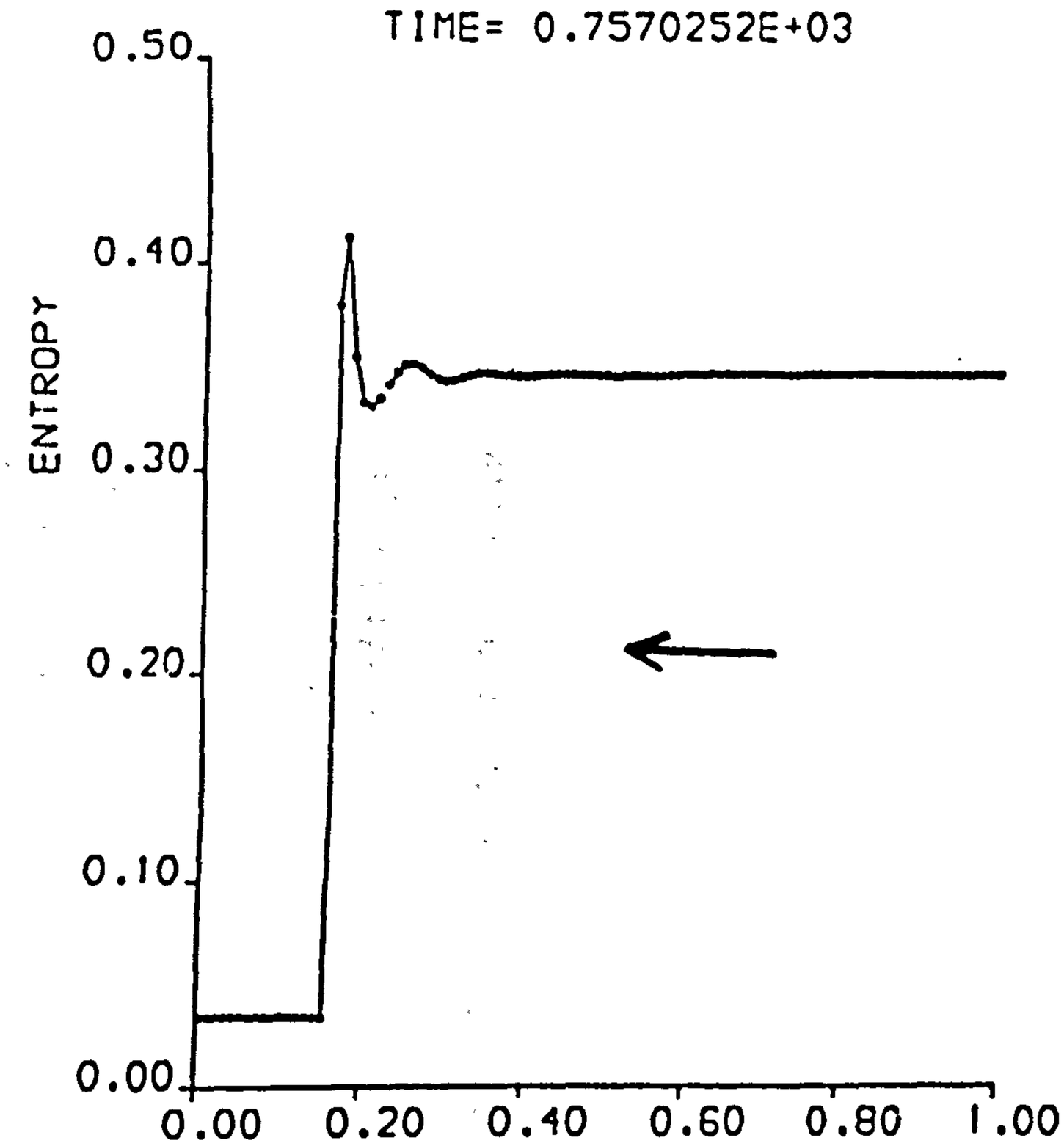

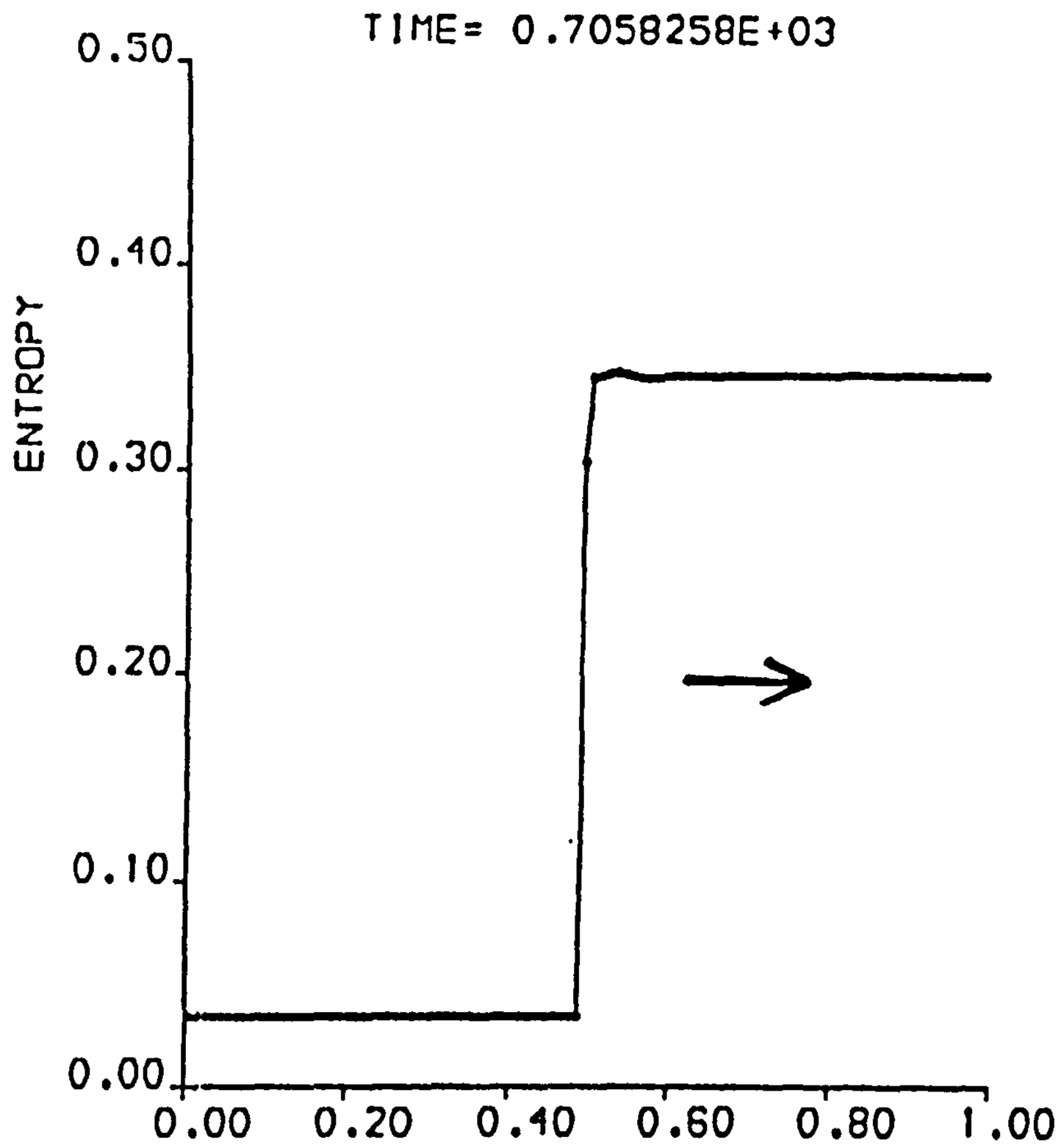

Fig. 2.10 moving shock results from P variant.

in phase space

——— Osher's scheme

..... Bell's scheme
with linear interpolation of λ

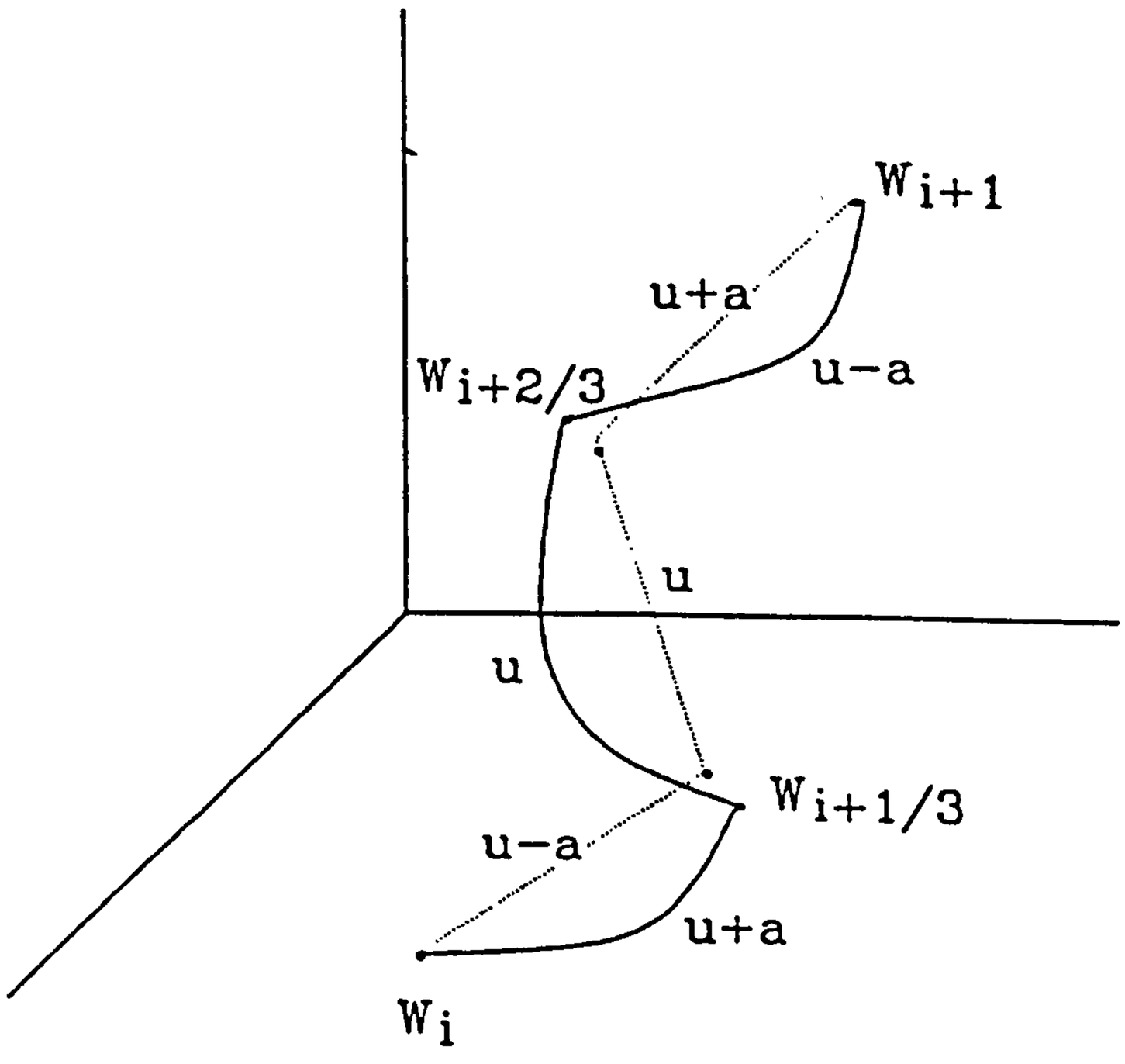

Fig. 2.11 wave paths of Osher's and Bell's schemes

in the phase space

Lax's shock tube problem : ρ_L=0.445, ρ_R=0.5; u_L=0.6991, u_R=0.0; P_L=3.528, P_R=0.571

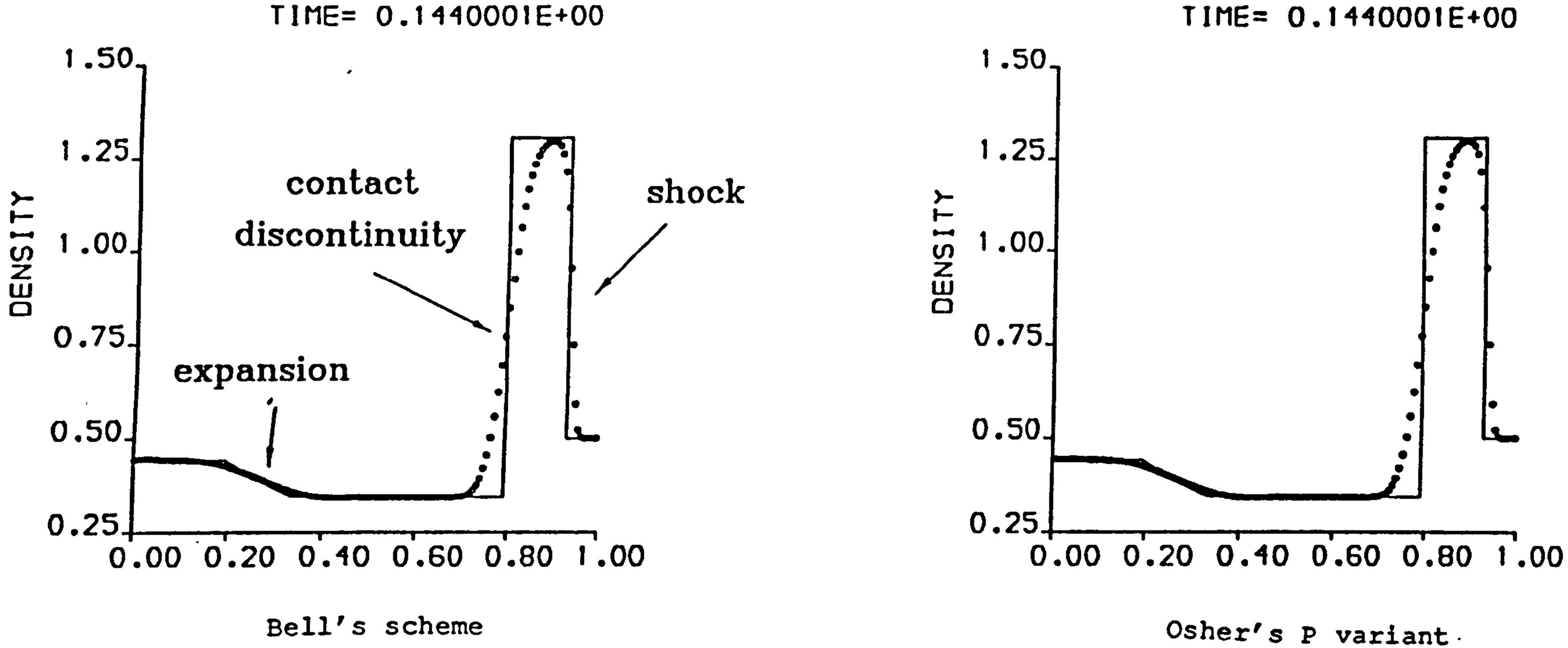

Fig. 2.12 Lax's shock tube result of Bell's scheme and Osher's P variant

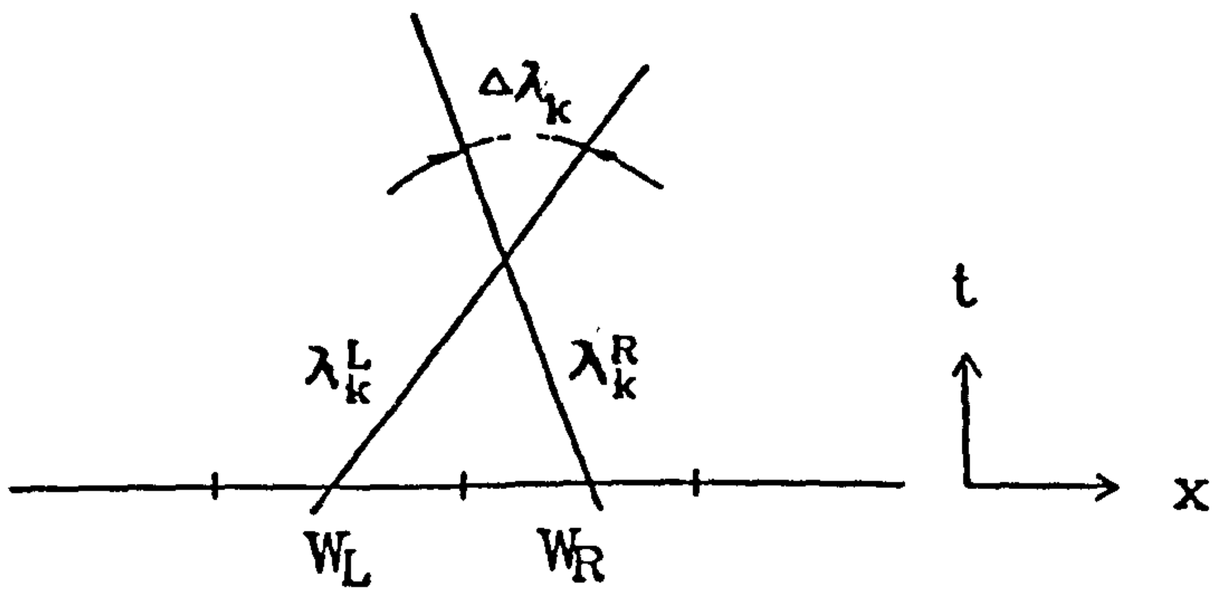

Fig. 2.13 Wave diagram for dissipation

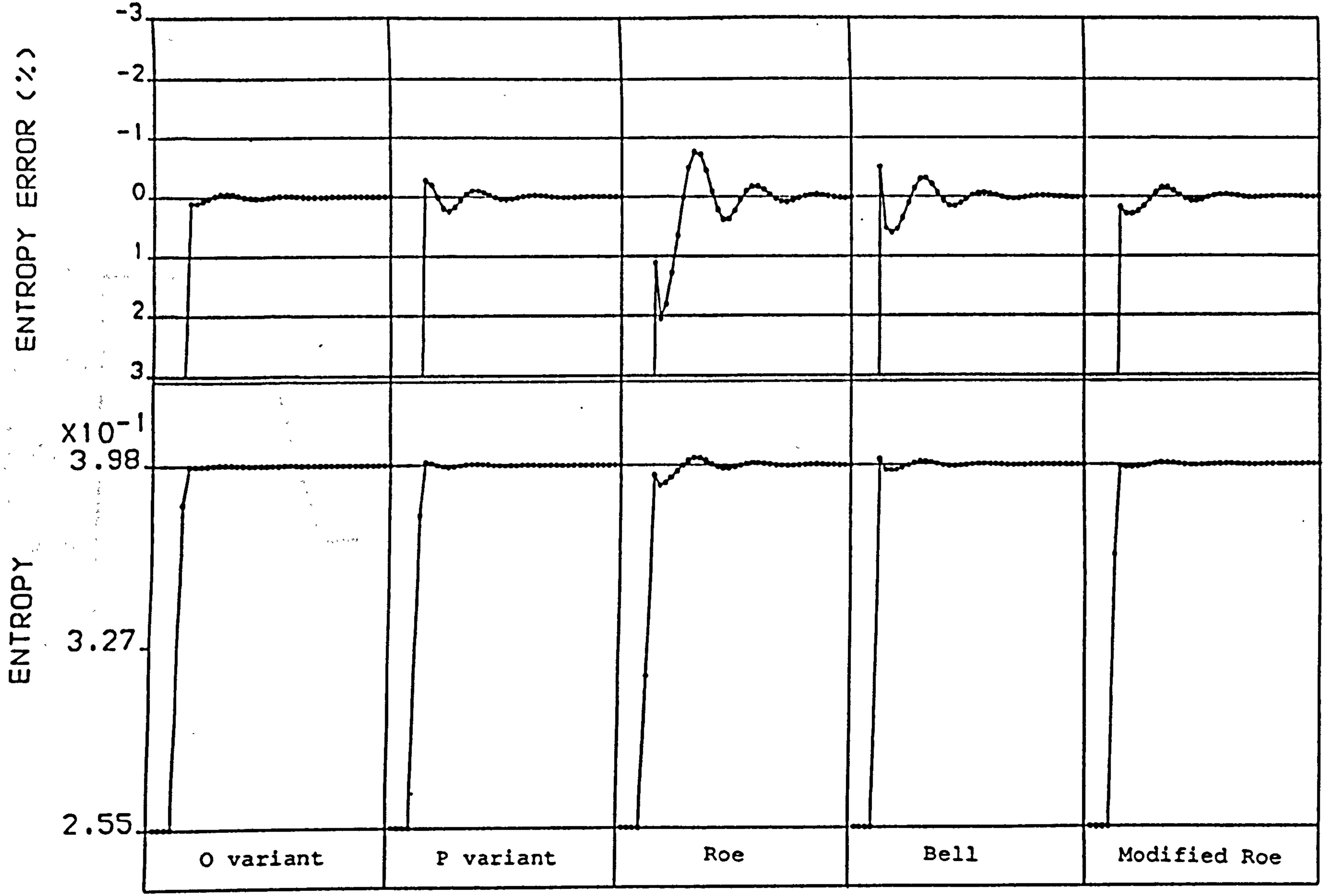

M=3 SR=-.035 50 ITER/CELL FOR CFL NO=.95

Fig. 2.14 Comparison of entropy oscillations for 1st order results

Sod's shock tube problem : $\rho_L=1.0$ $\rho_R=0.125$, $u_L=0.0$ $u_R=0.0$, $P_L=1.0$ $P_R=0.1$

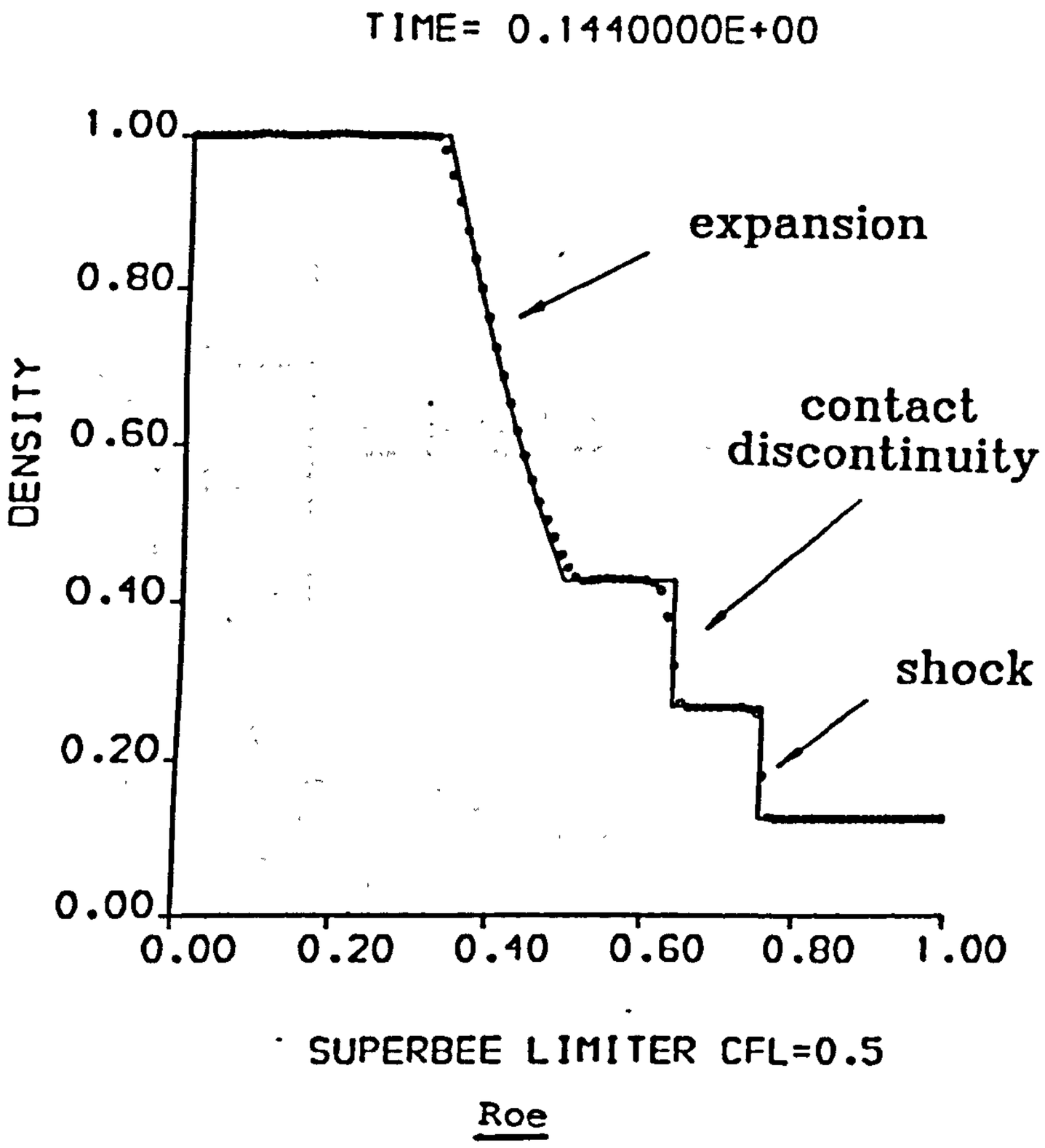

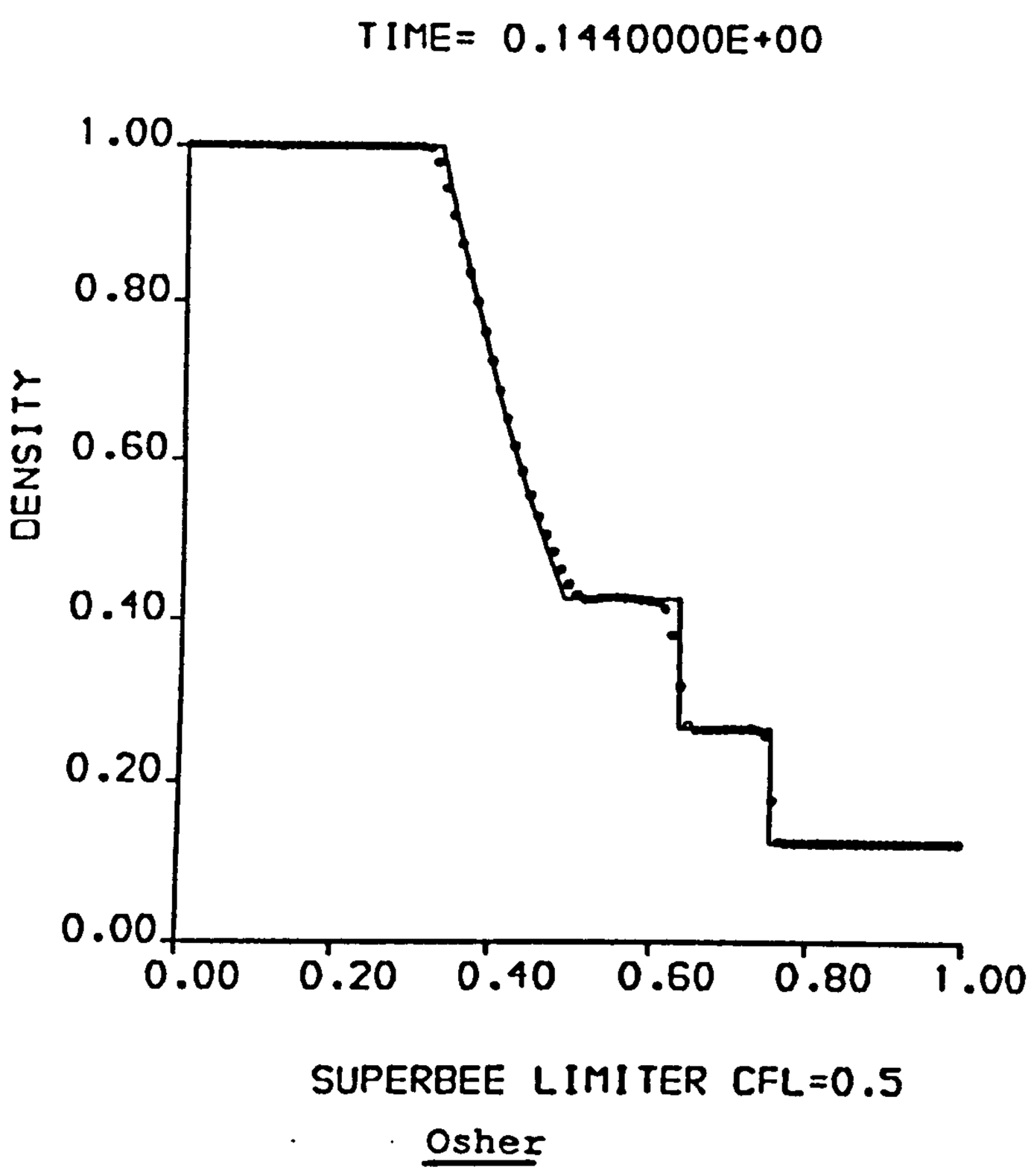

Fig. 2.15 Sod's shock tube results for 2nd order scheme

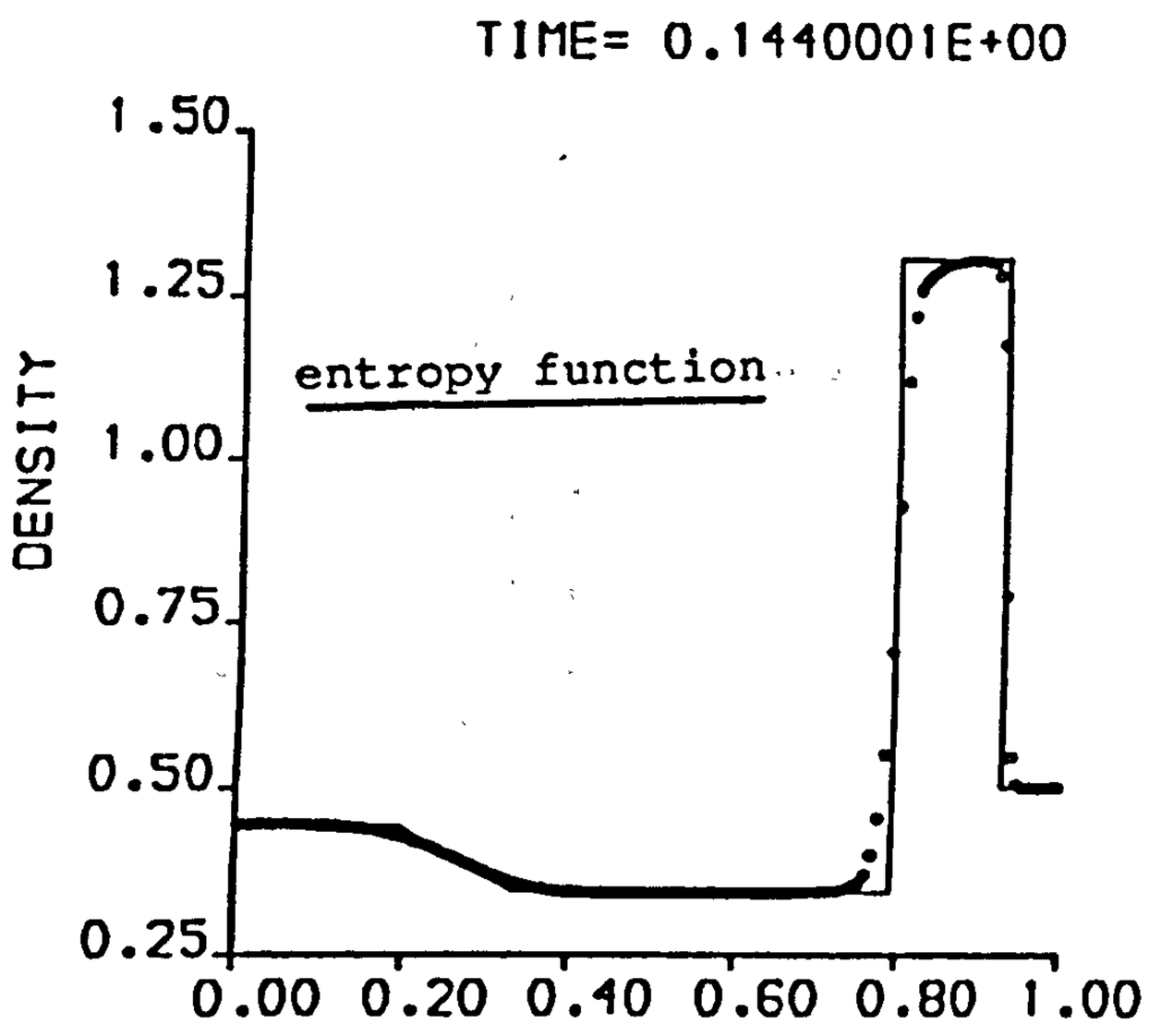

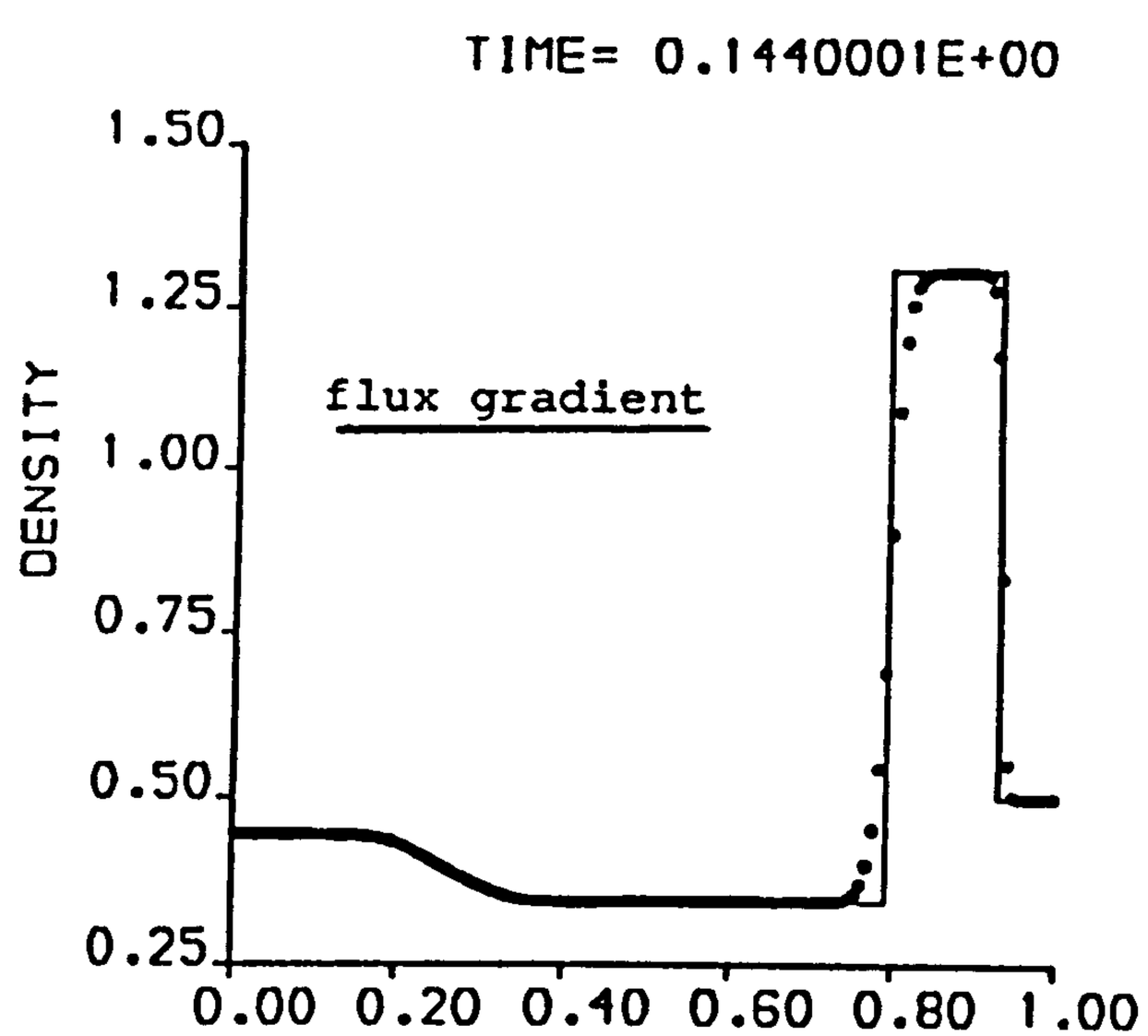

Fig. 2.16 Lax's shock tube results using different methods of evaluating r

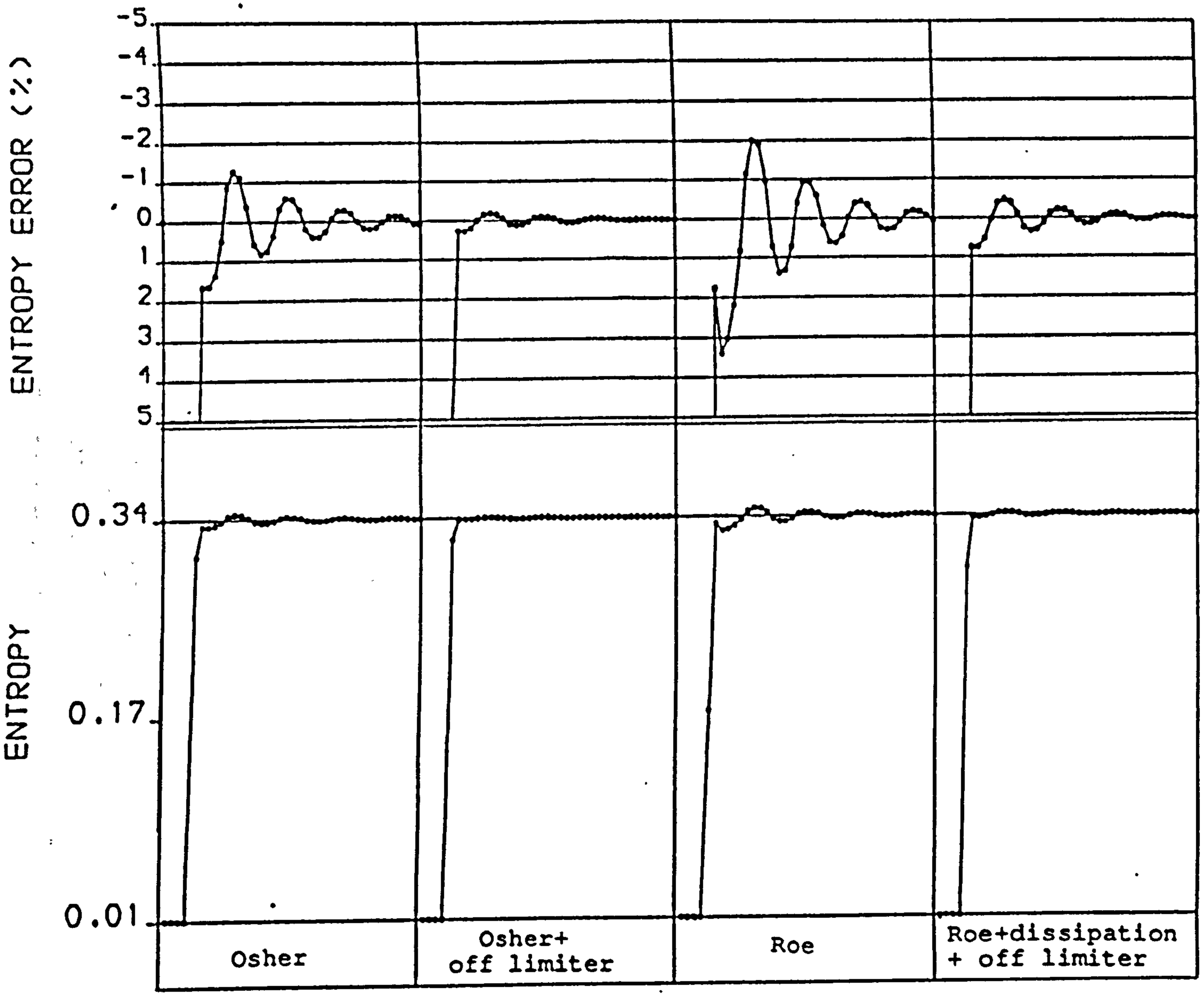

Fig. 2.17 Comparison of entropy oscillations for 2nd order results
(Lax-Wendroff scheme with minmod limiter)

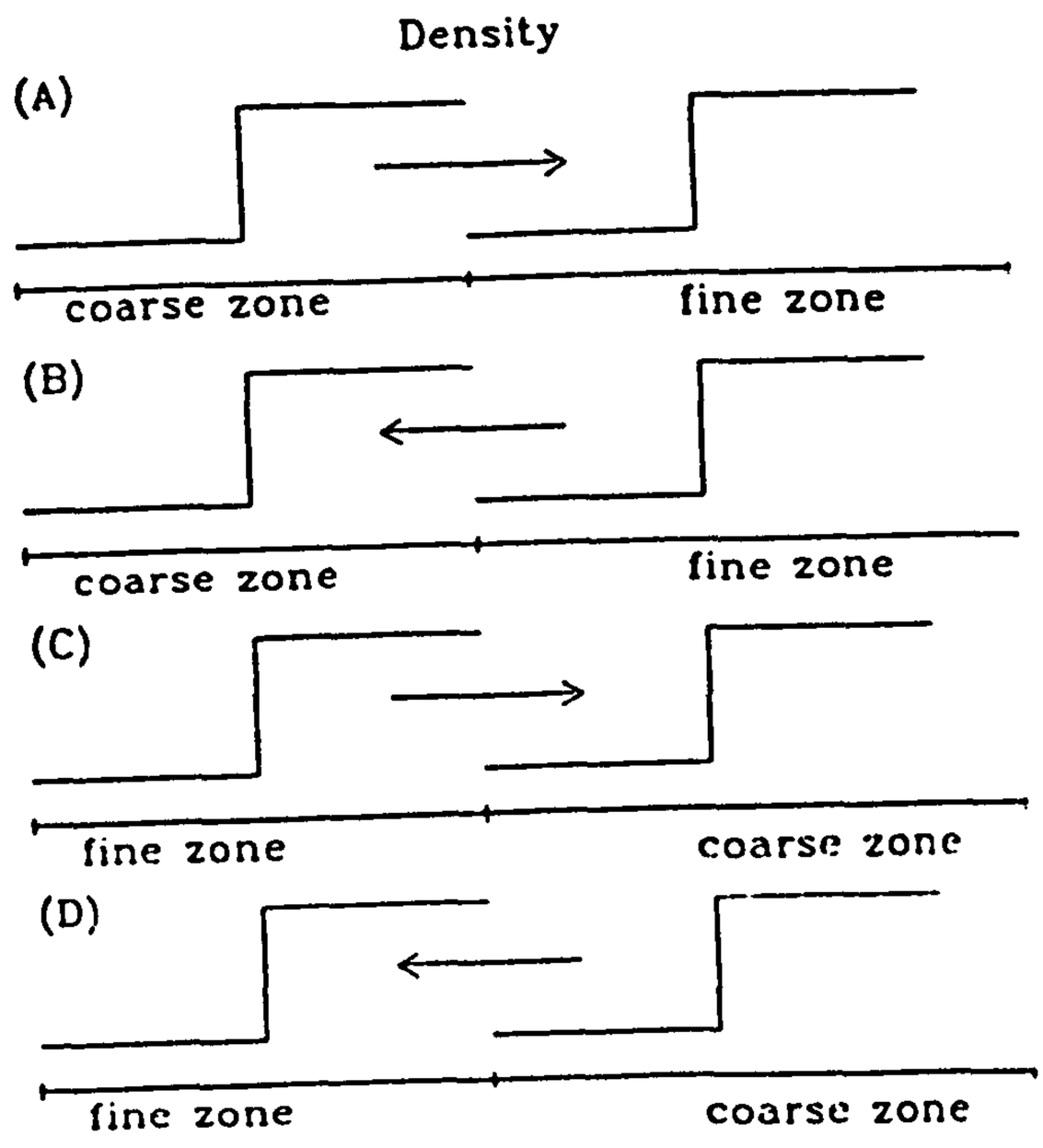

Fig. 3.1 Moving shock test cases

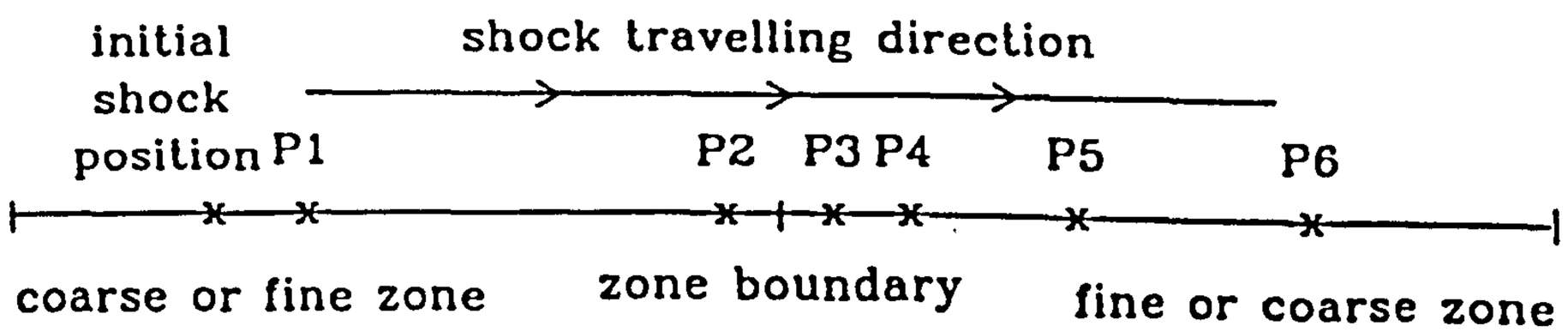

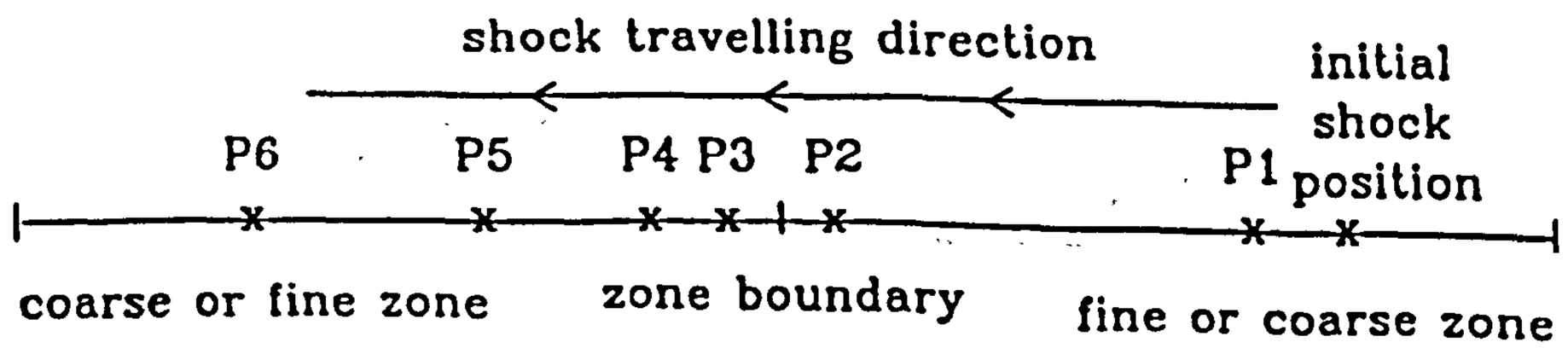

Fig. 3.2 Monitored points for the moving shock test

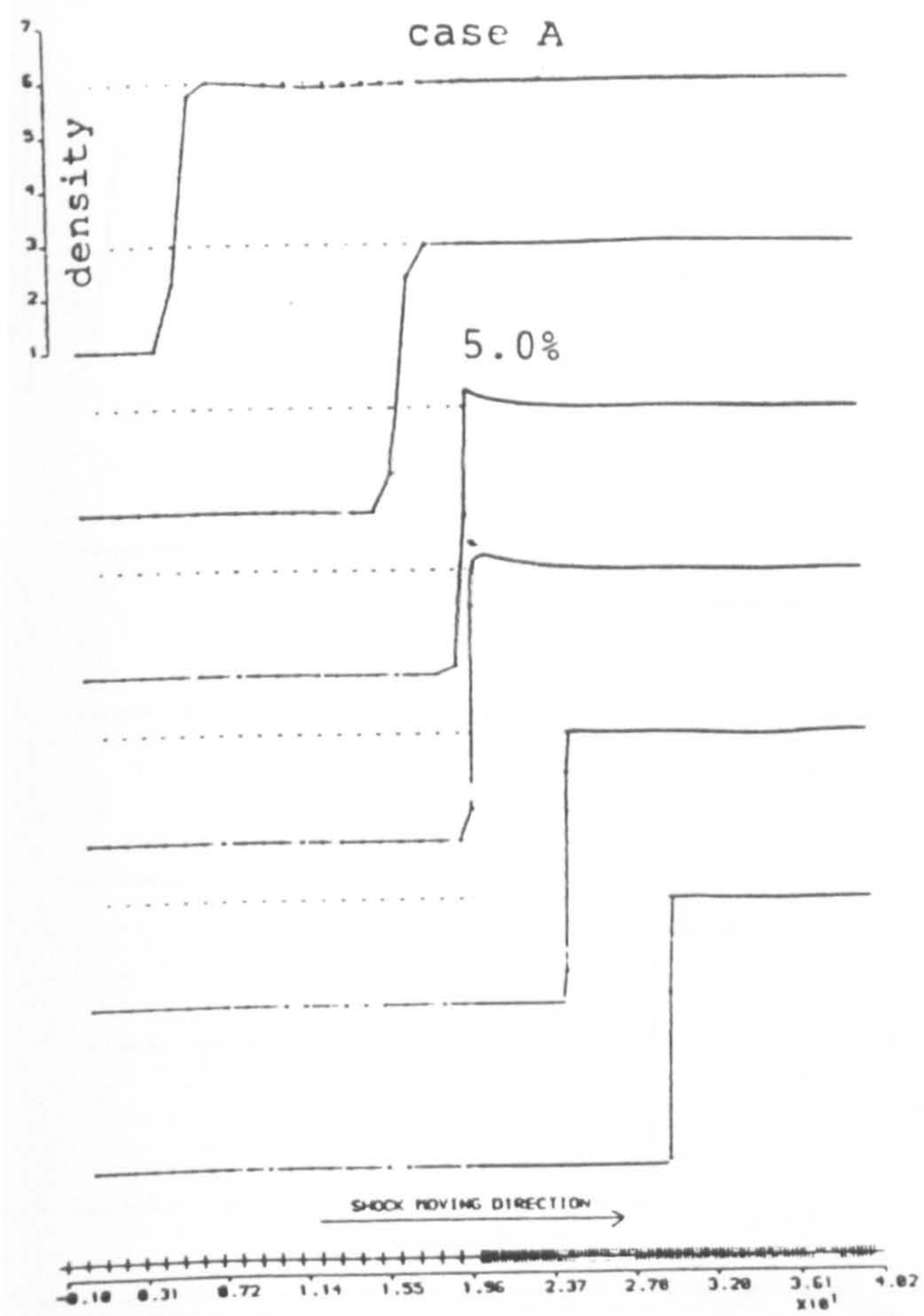

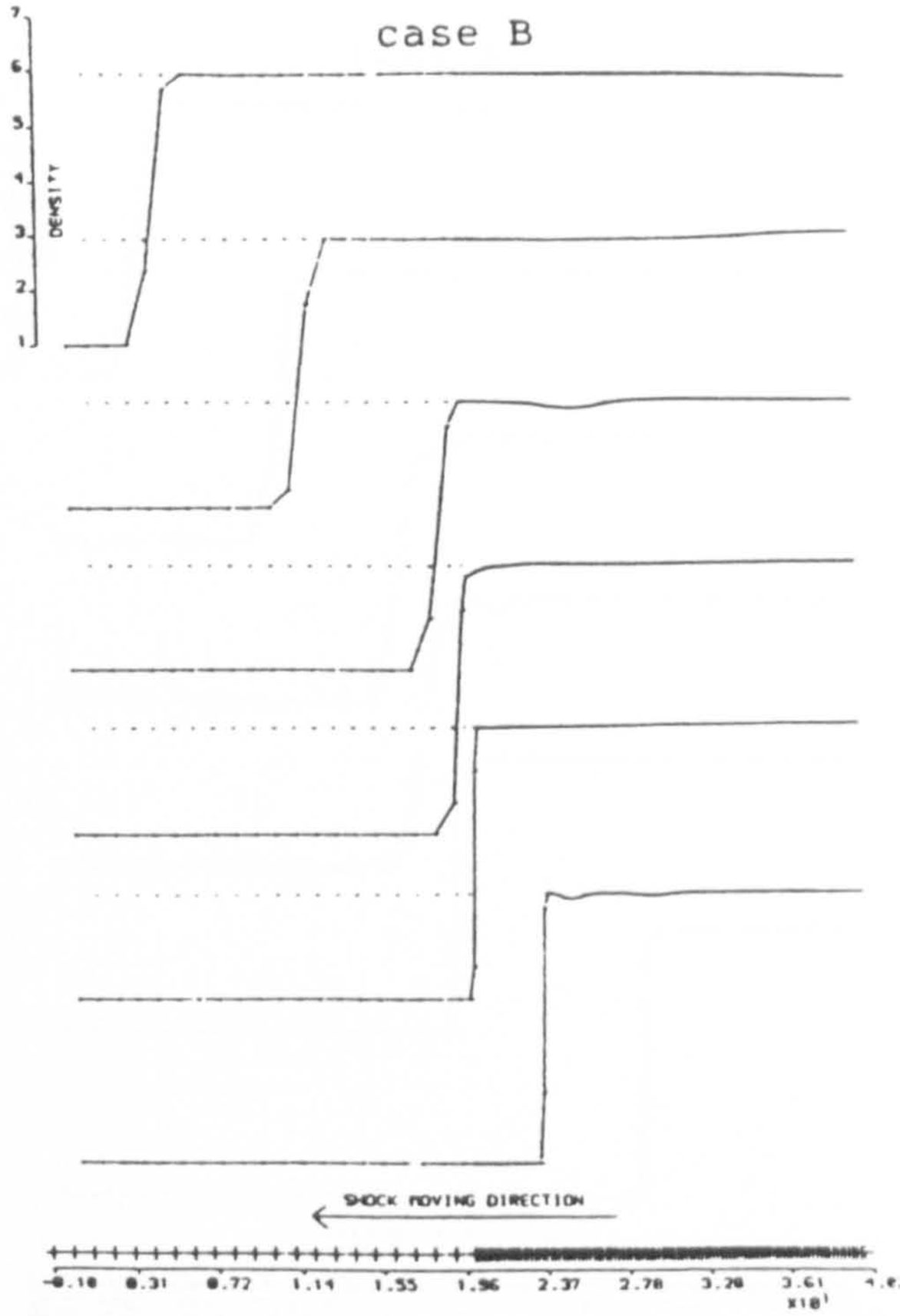

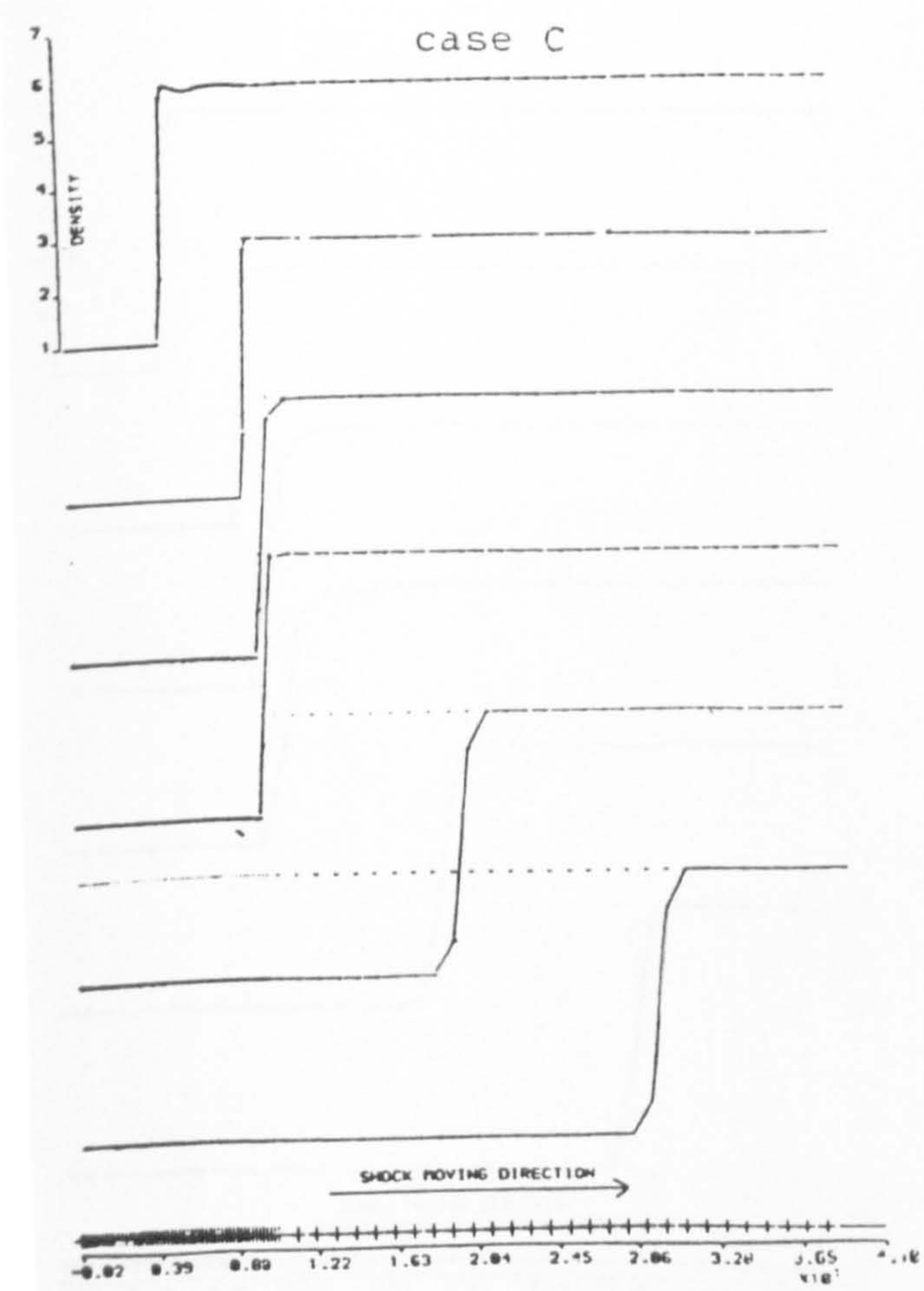

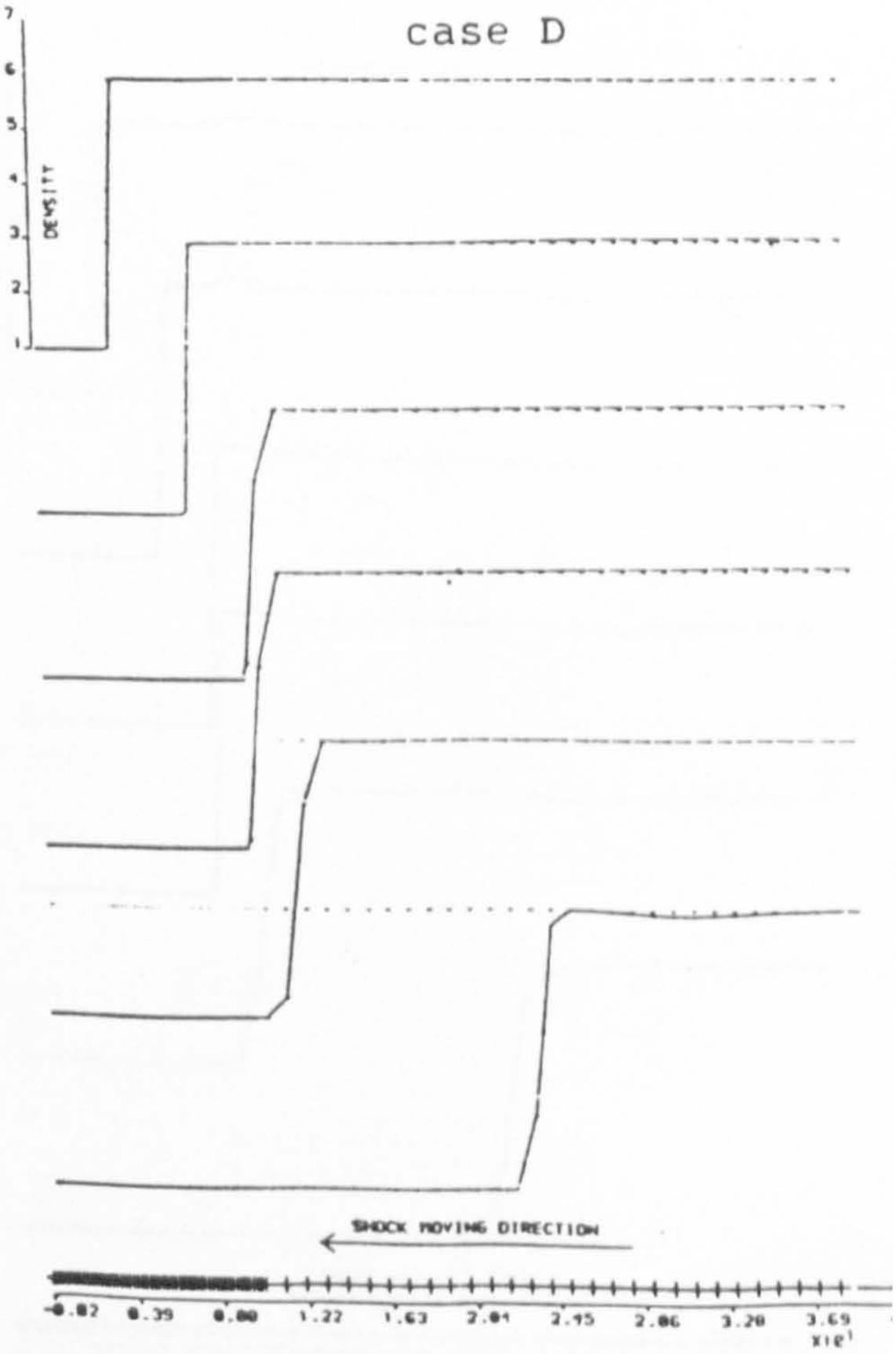

Fig. 3.3 Results from Osher's scheme with M=20, SR=$\pm$0.035, and mesh ratio 5:1

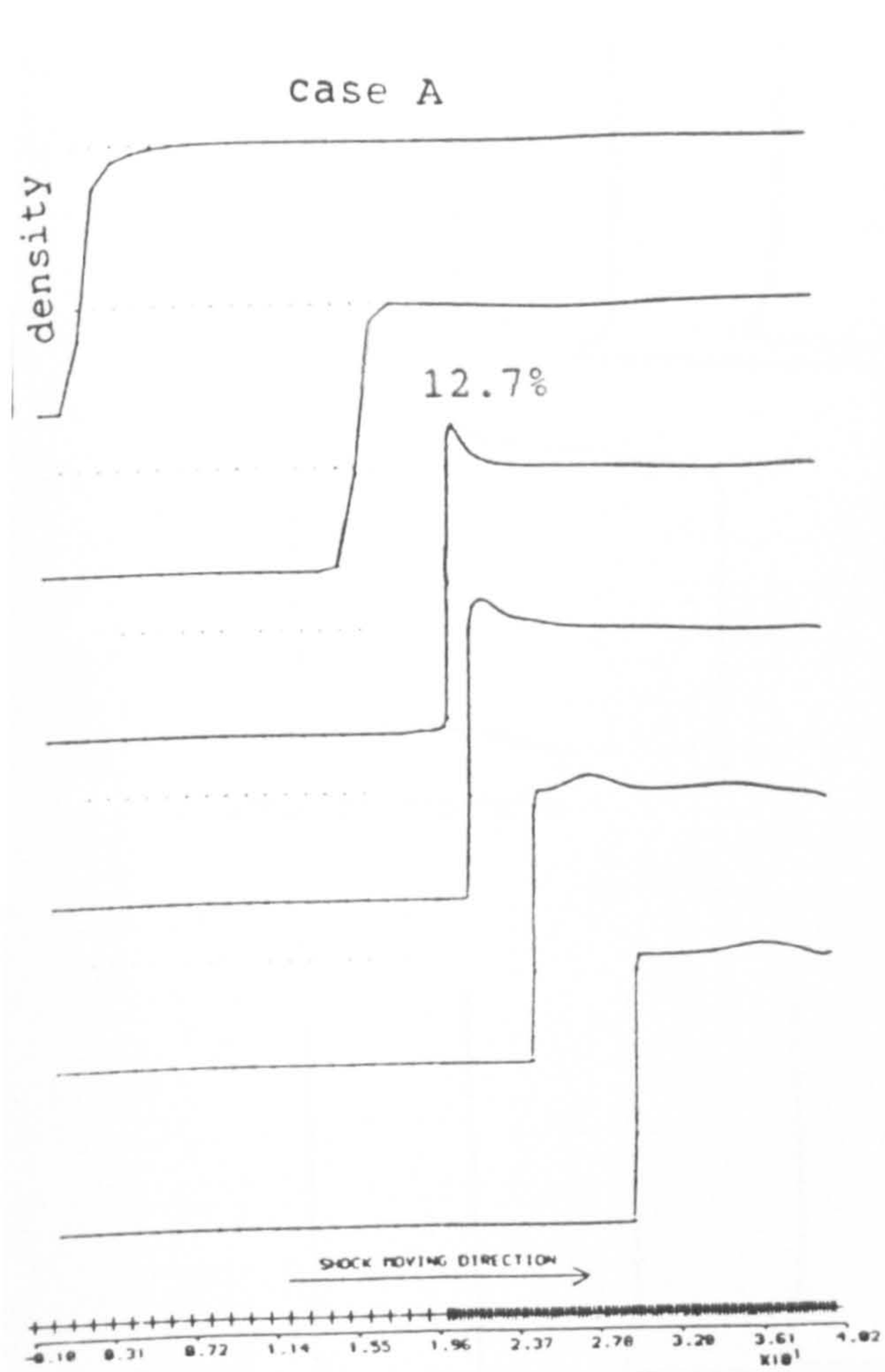

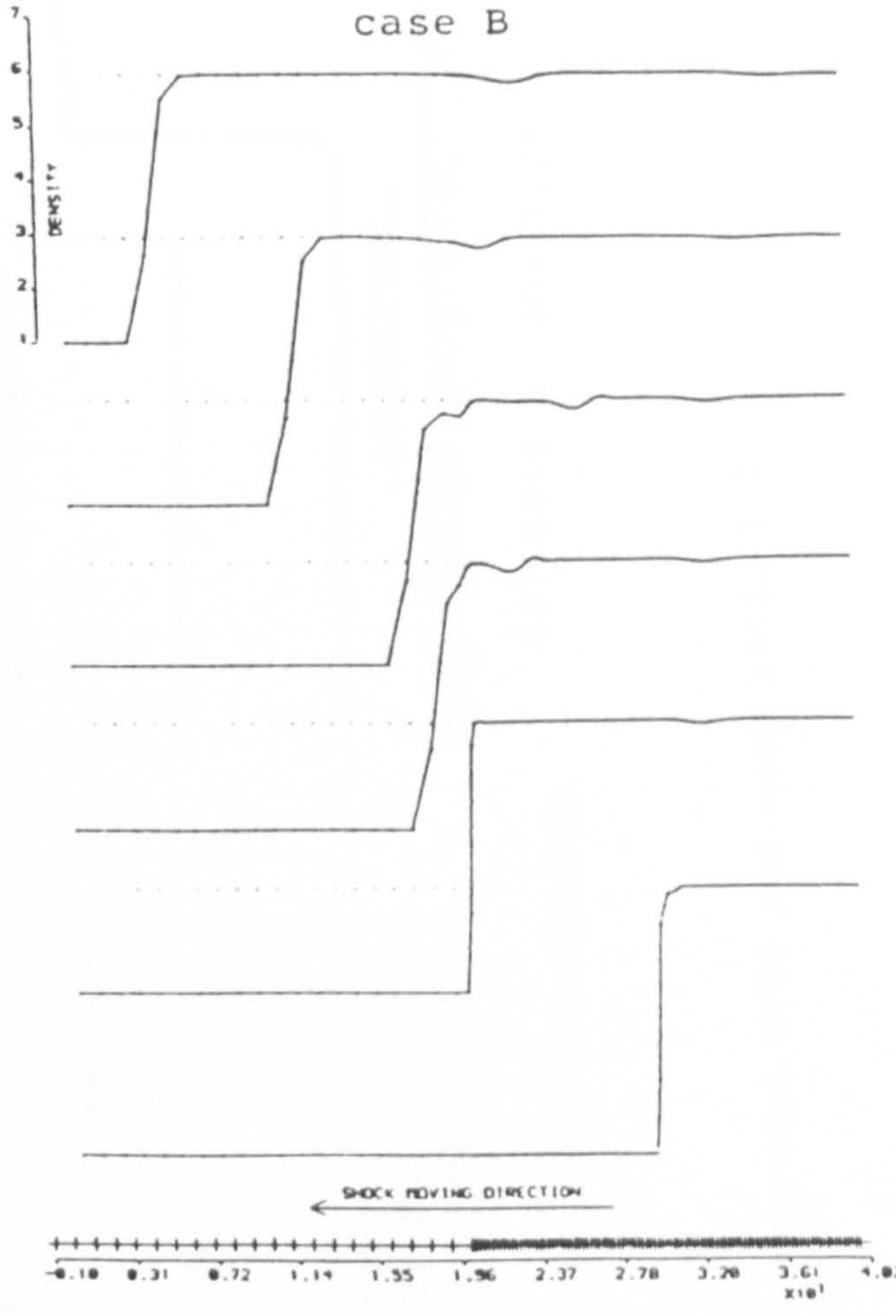

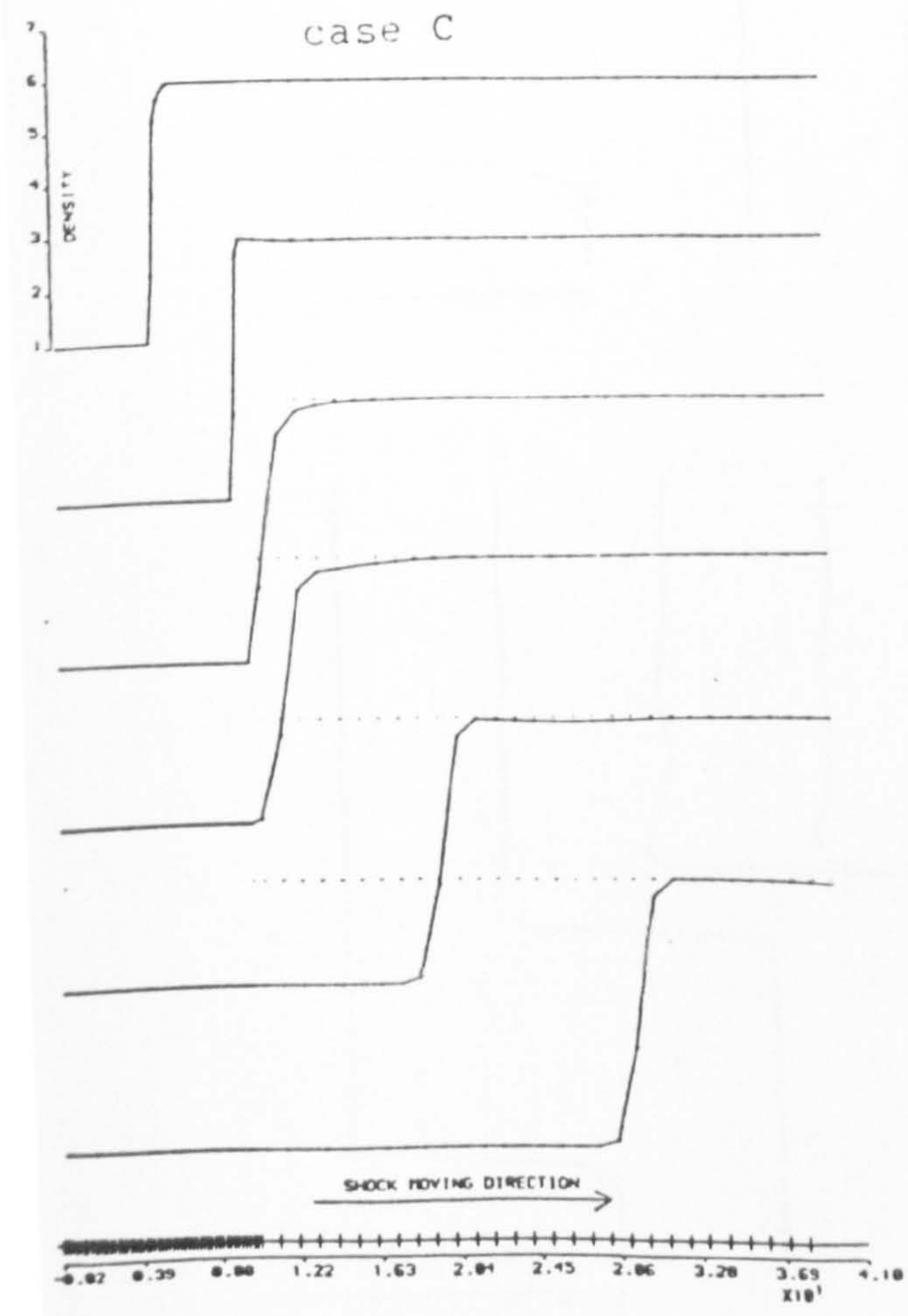

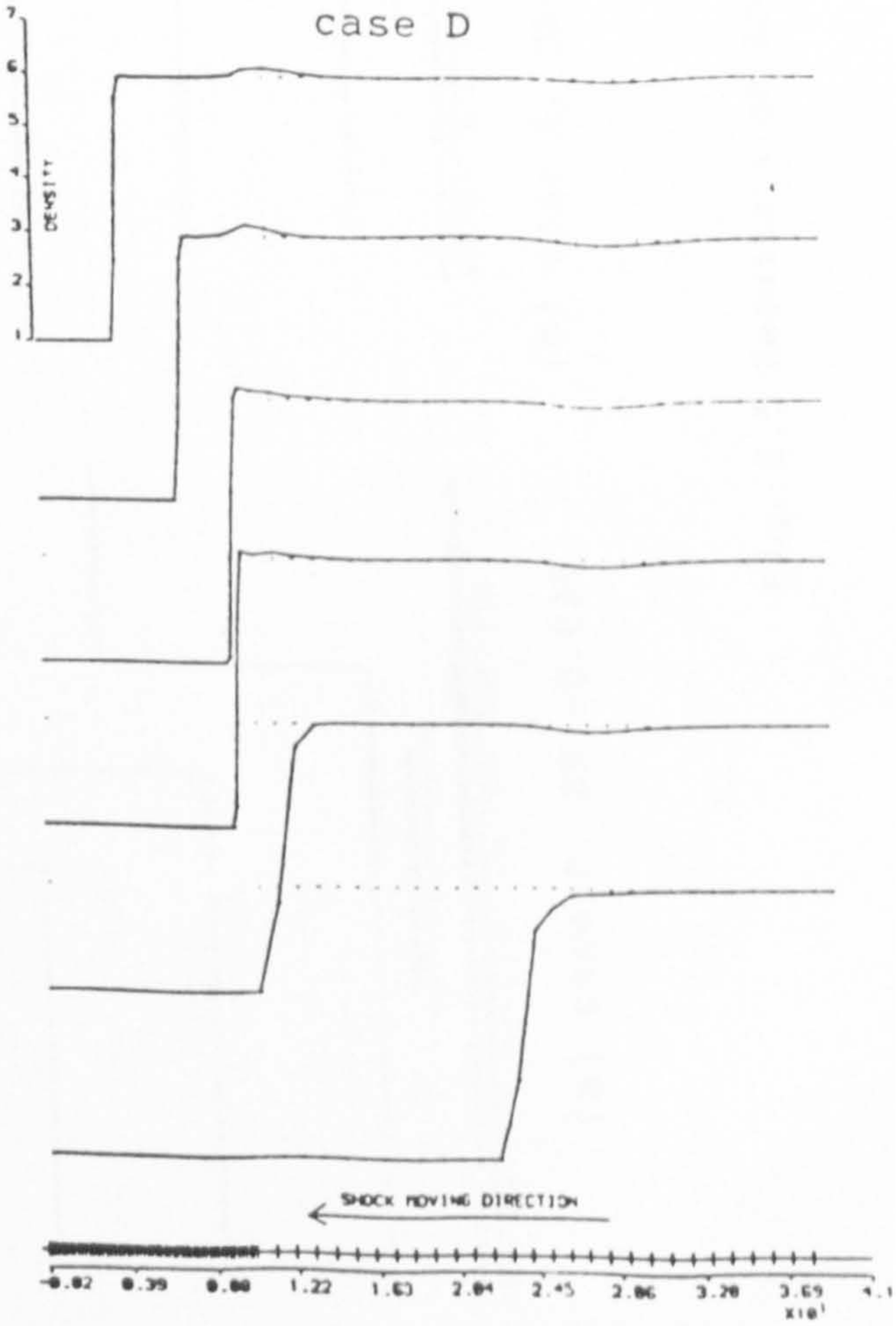

Fig. 3.4 Results from Osher's scheme with M=20, SR=±0.28, and mesh ratio 5:1

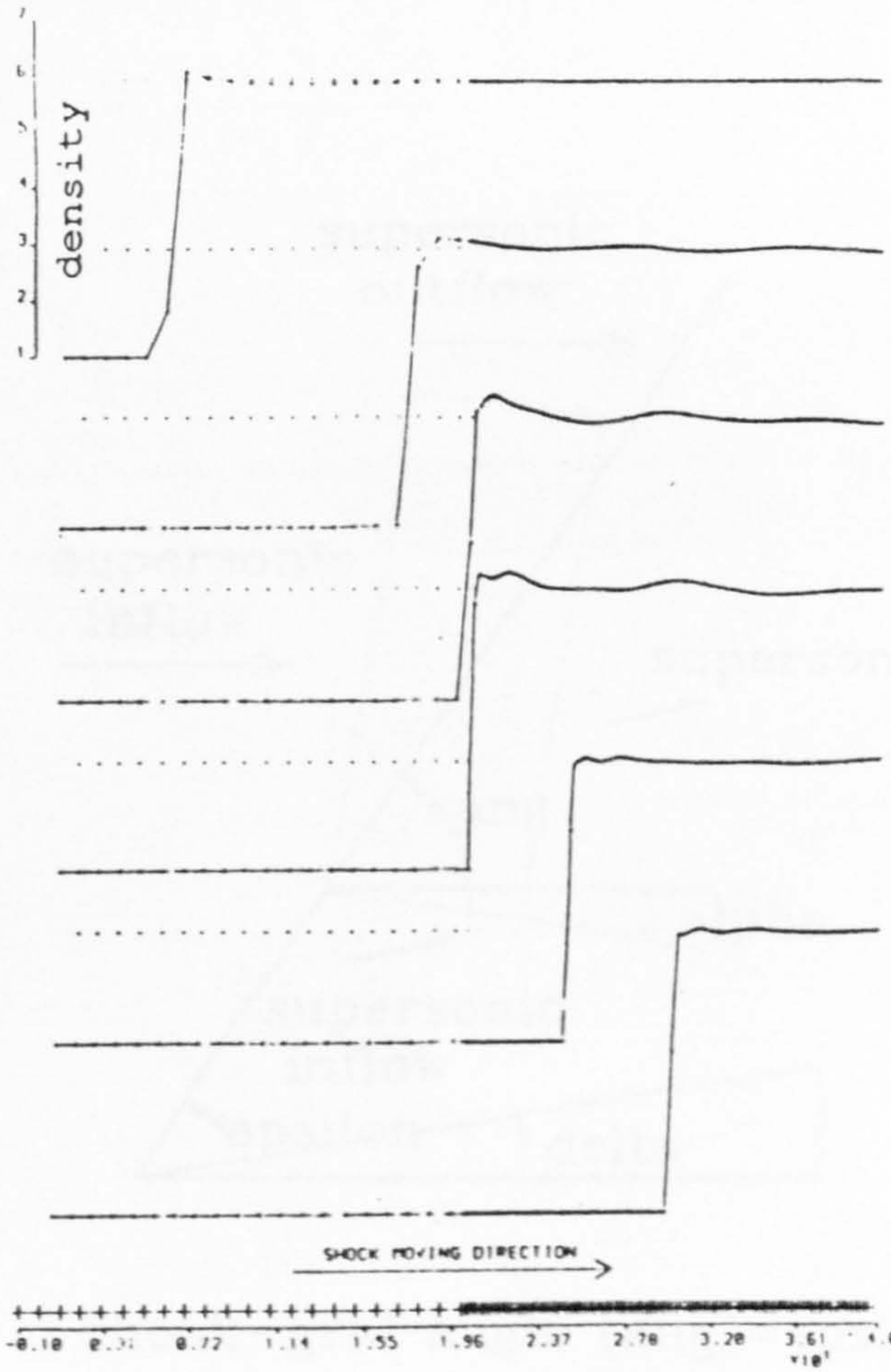

(a) case A, SR=+0.035

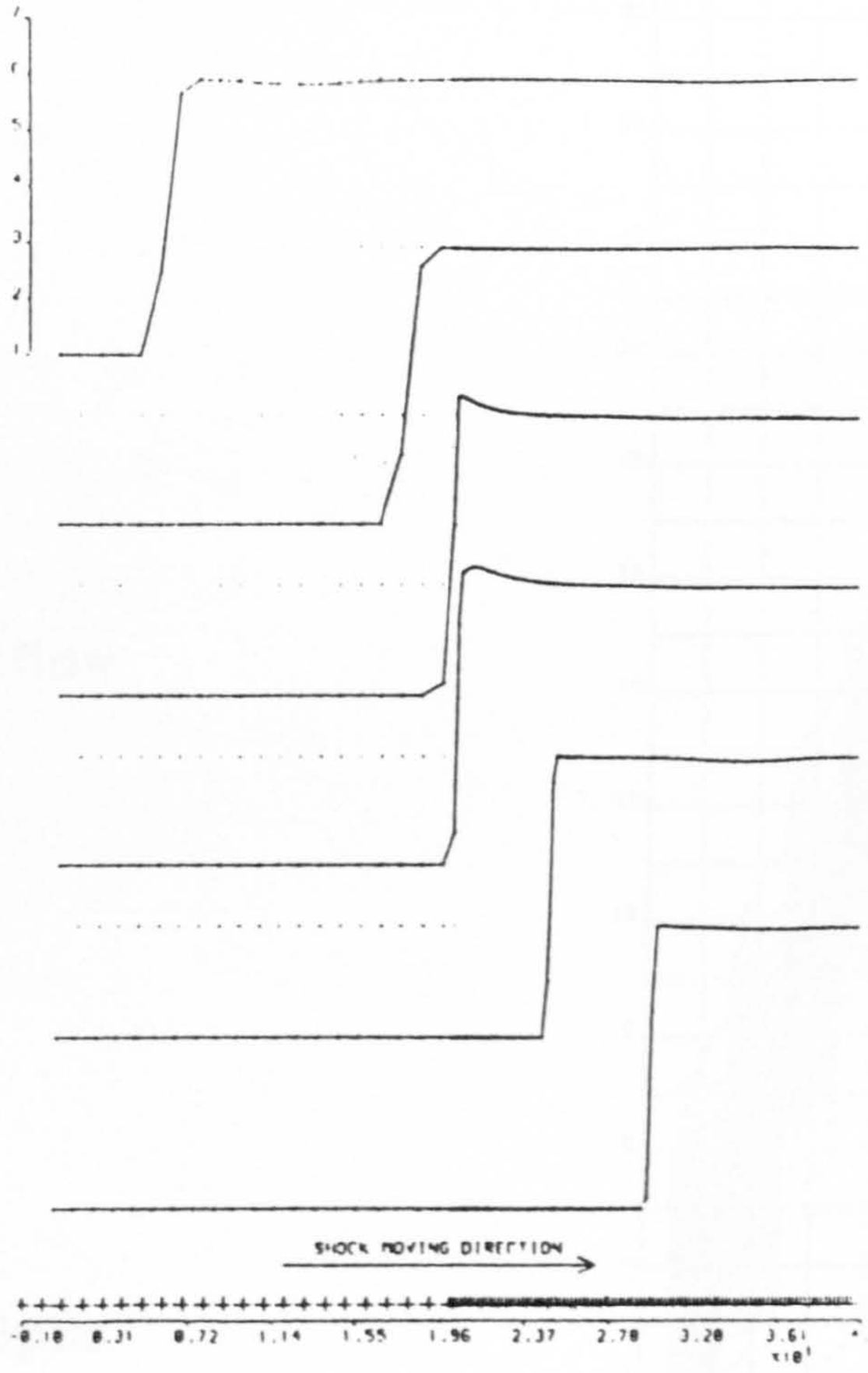

(b) case A, SR=+0.035, with dissipation

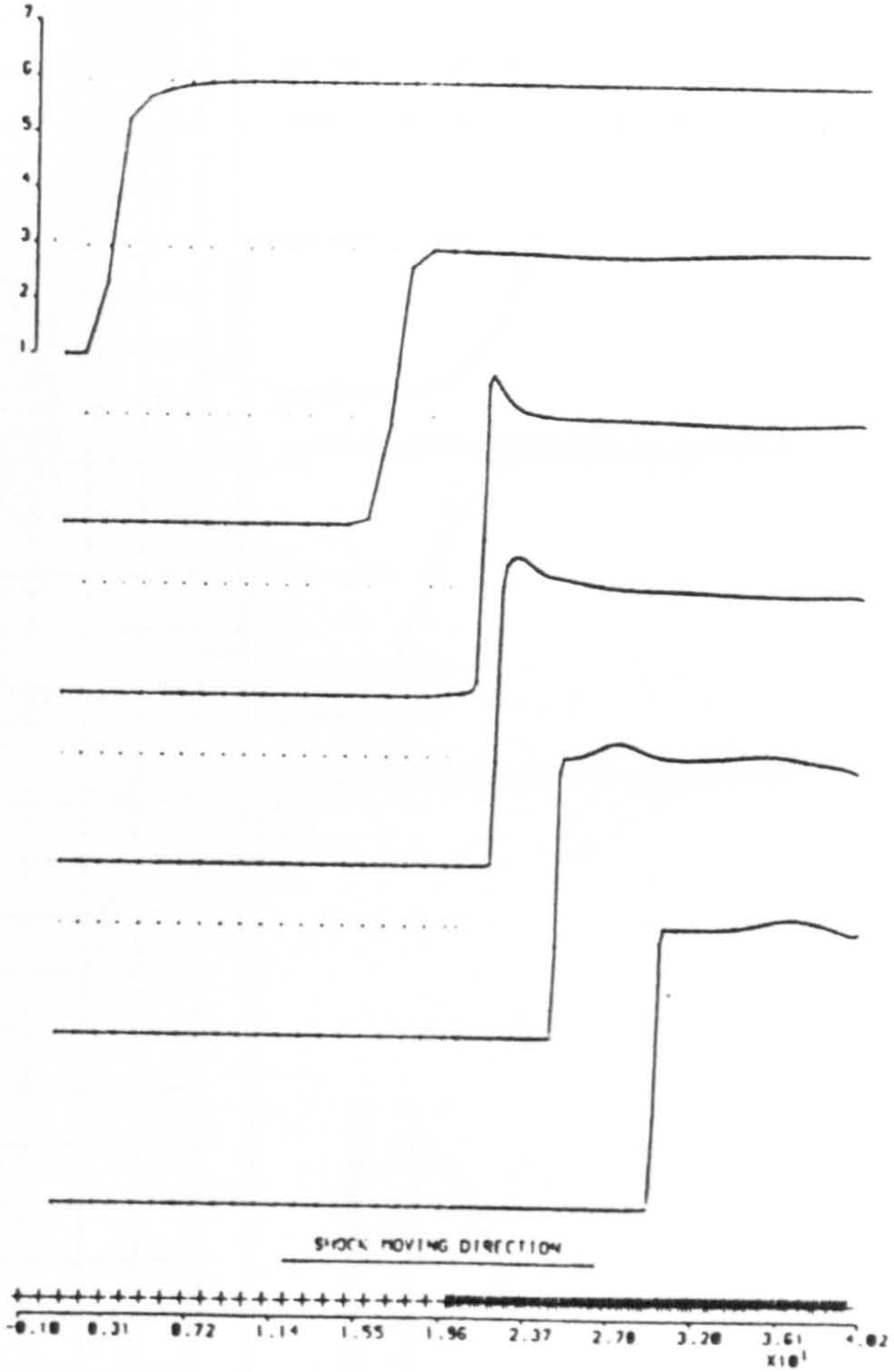

(c) case A, SR=+0.28

Fig. 3.5 Results from Roe's scheme with M=20 and mesh ratio 5:1

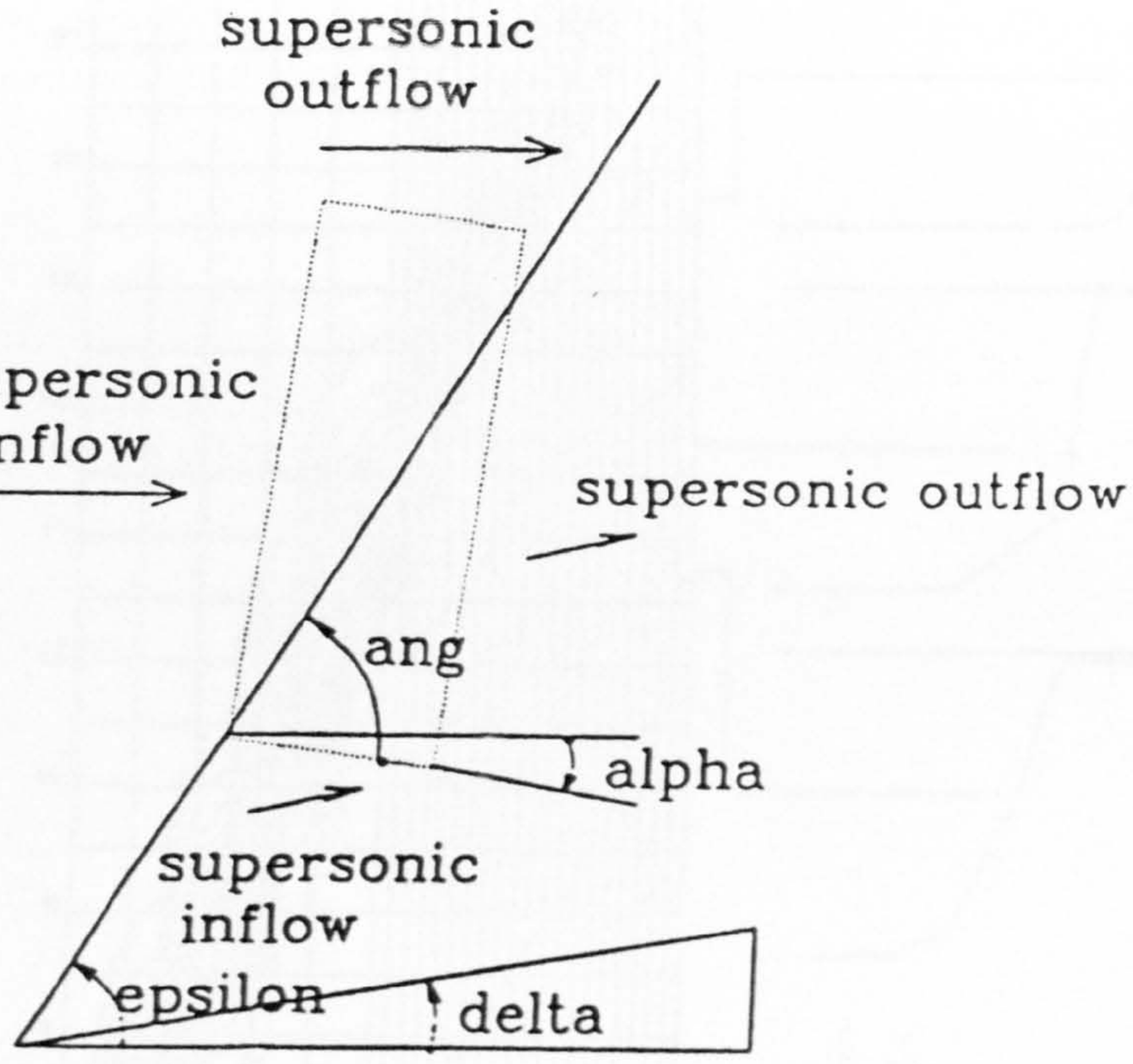

shock-grid angle (ang)=epsilon+alpha

Fig. 3.6 Test case for an oblique shock

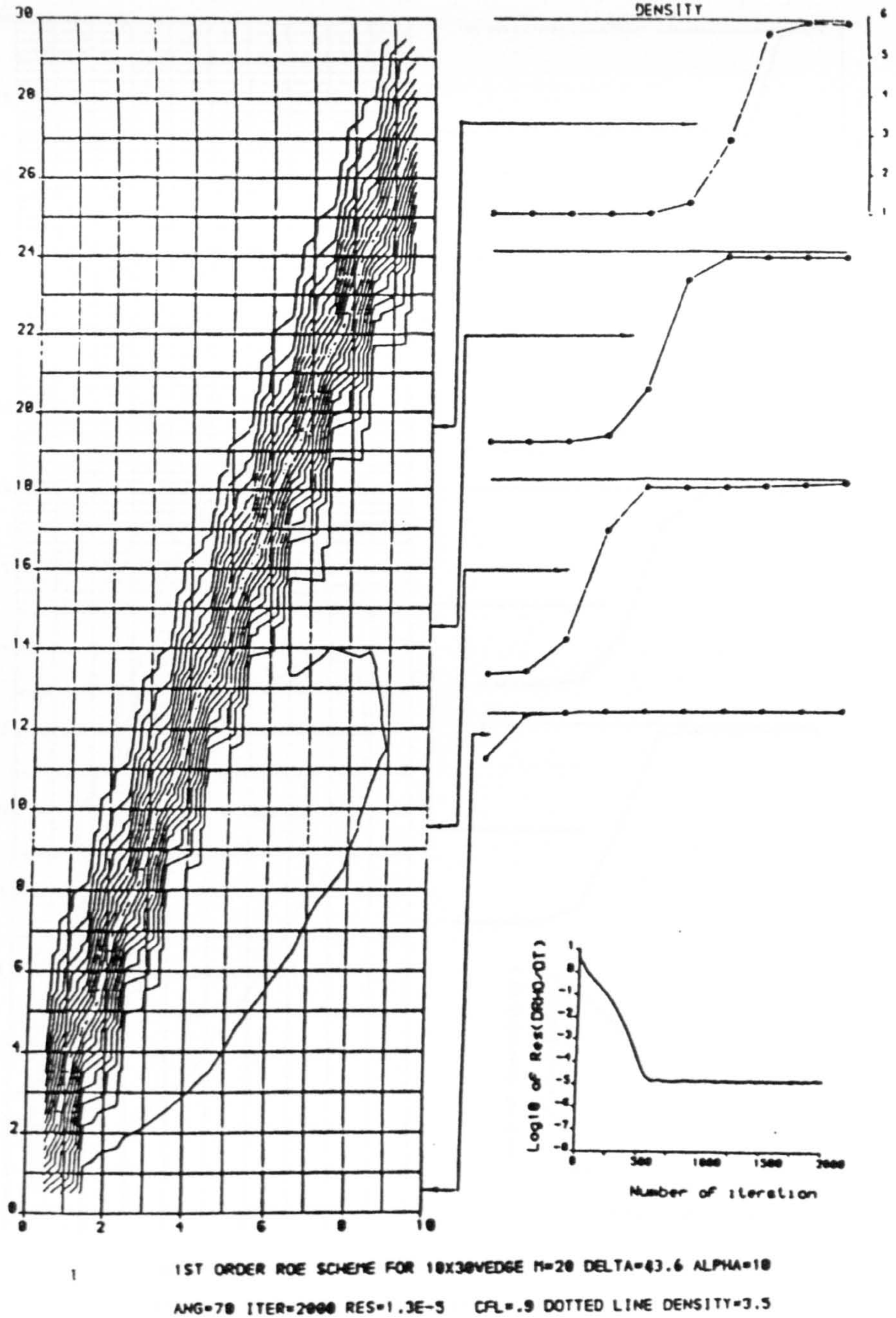

Fig. 3.7 Uniform grid result for M=20 shock

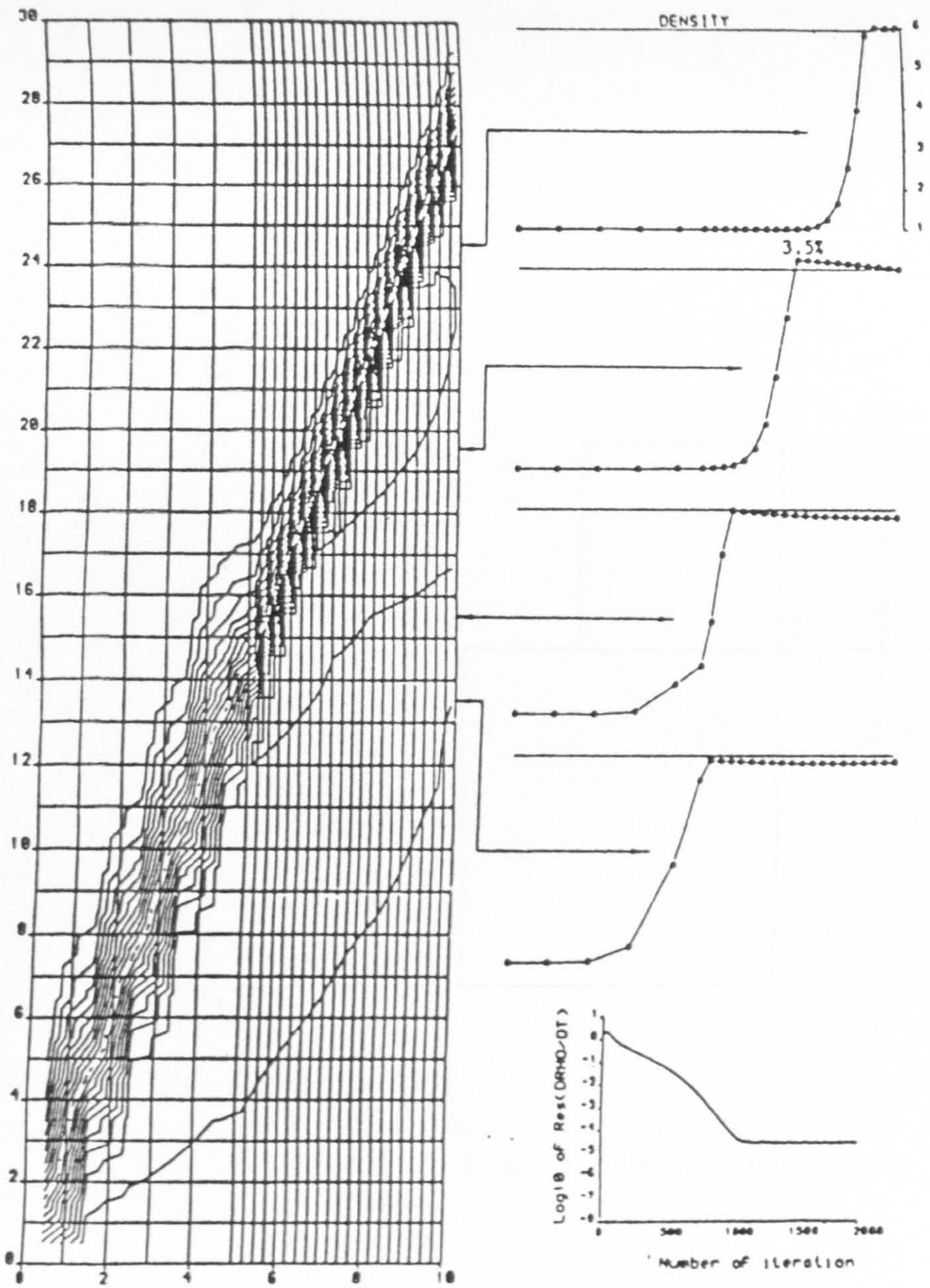

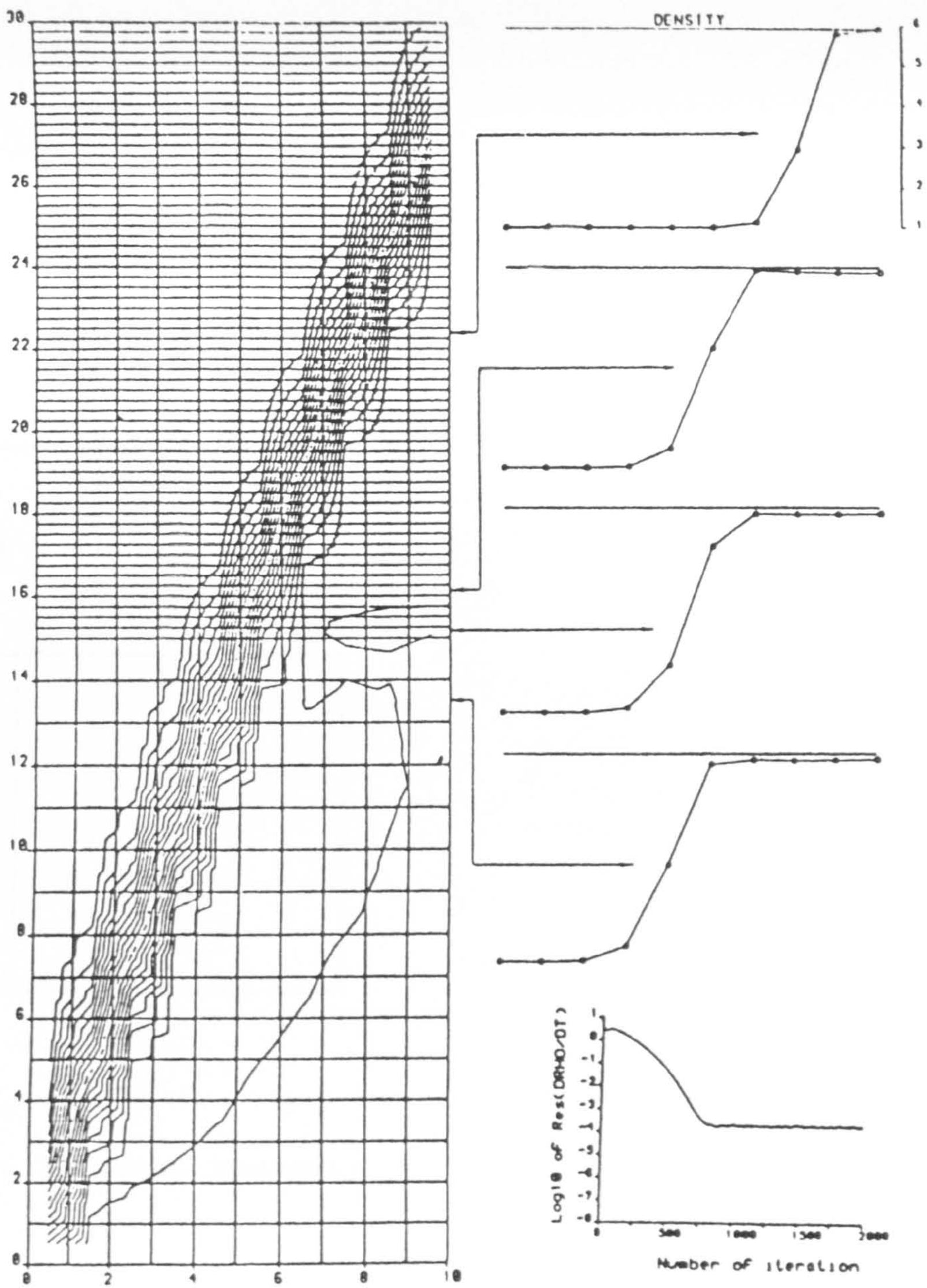

Fig. 3.8 Nonuniform grid results for M=20 shock

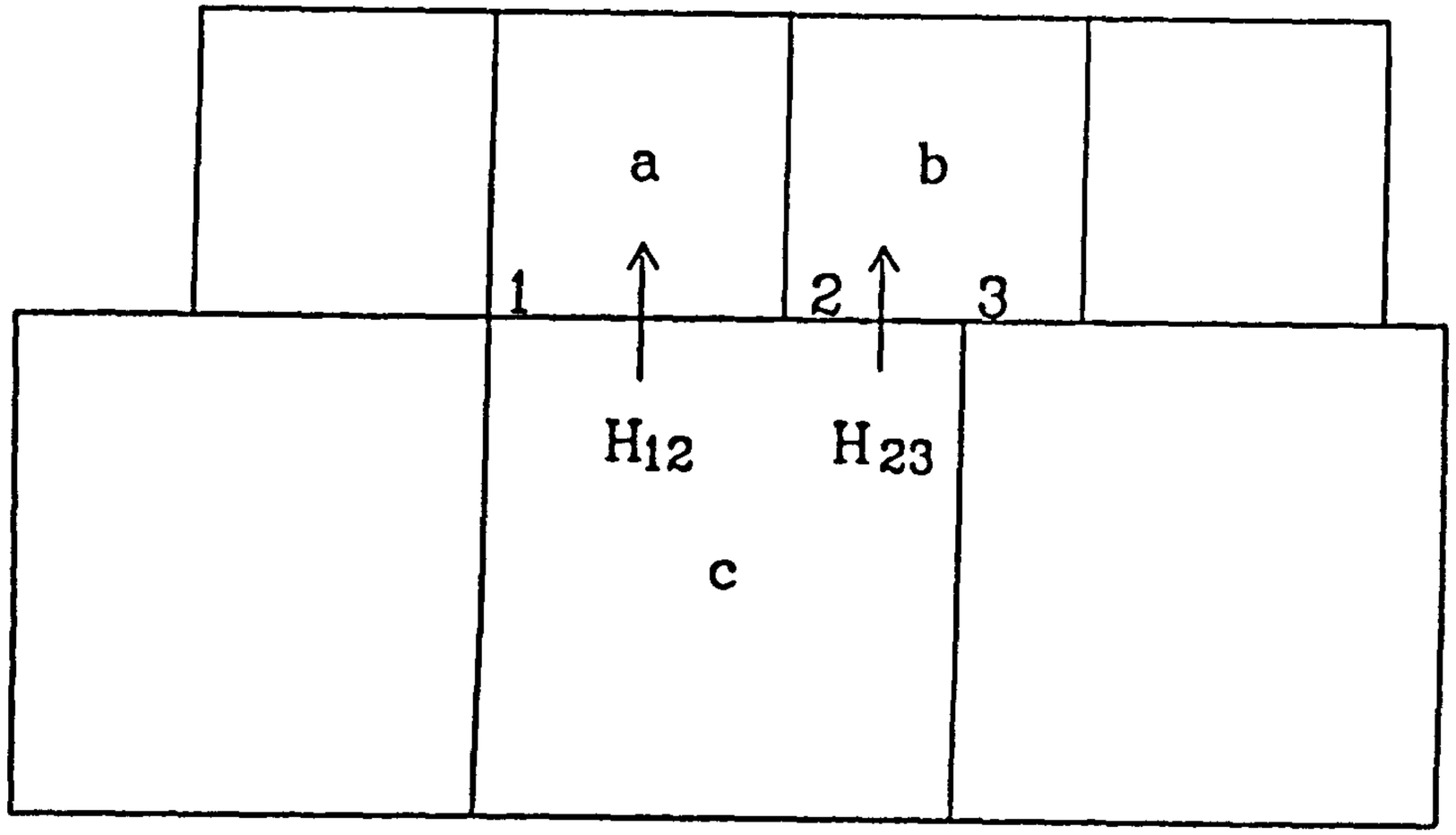

Fig. 3.9 Basic interface treatment at zonal boundary

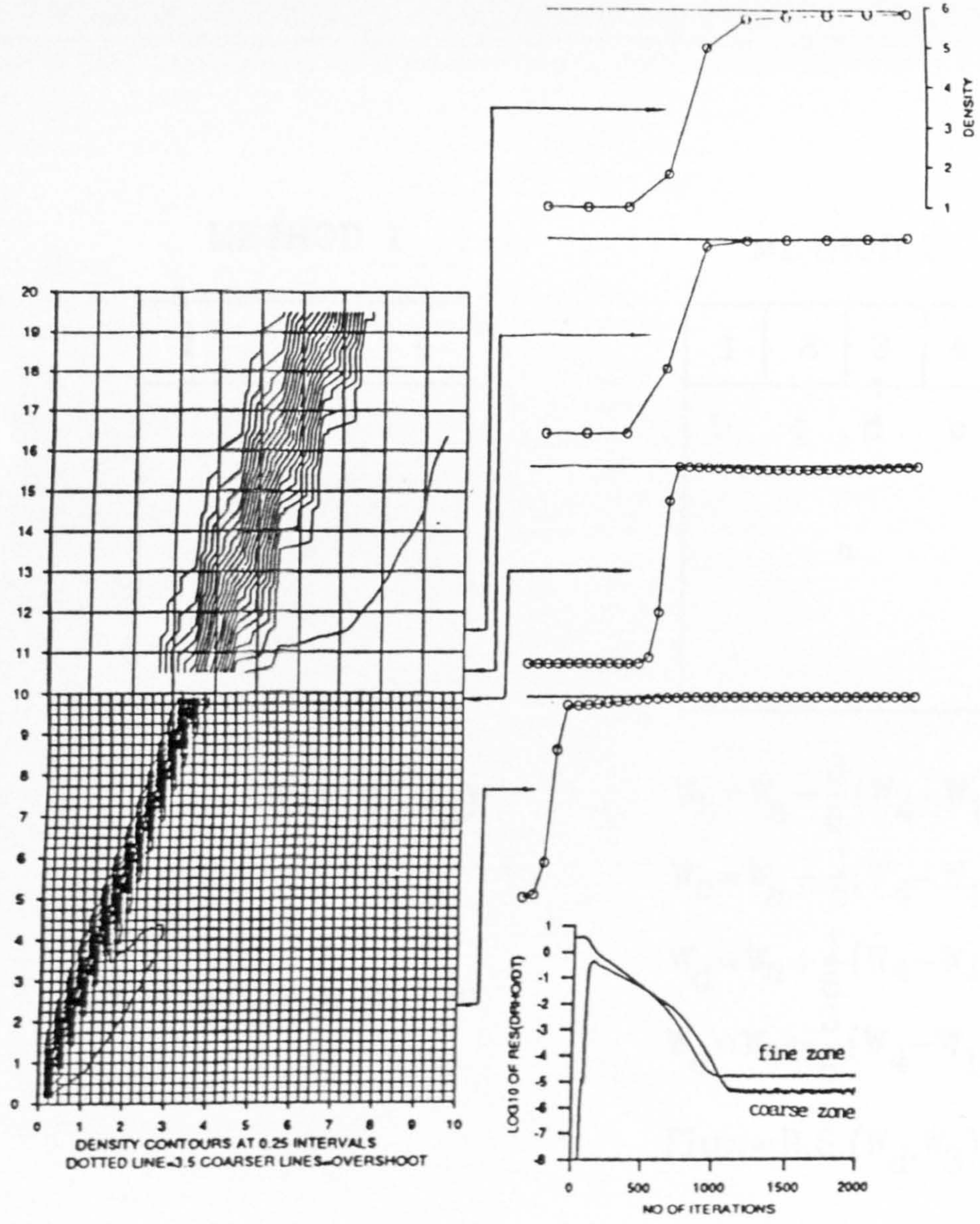

1ST ORDER ROE SCHEME FOR AN OBLIQUE SHOCK M=20 DELTA=43.64 EPSILON=60 ALPHA=10
LOCAL CFL=0.9 N=2000 PRE-SHOCK COND. AS INITIAL COND.

Fig. 3.10 M=20 calculation with fine-coarse grid

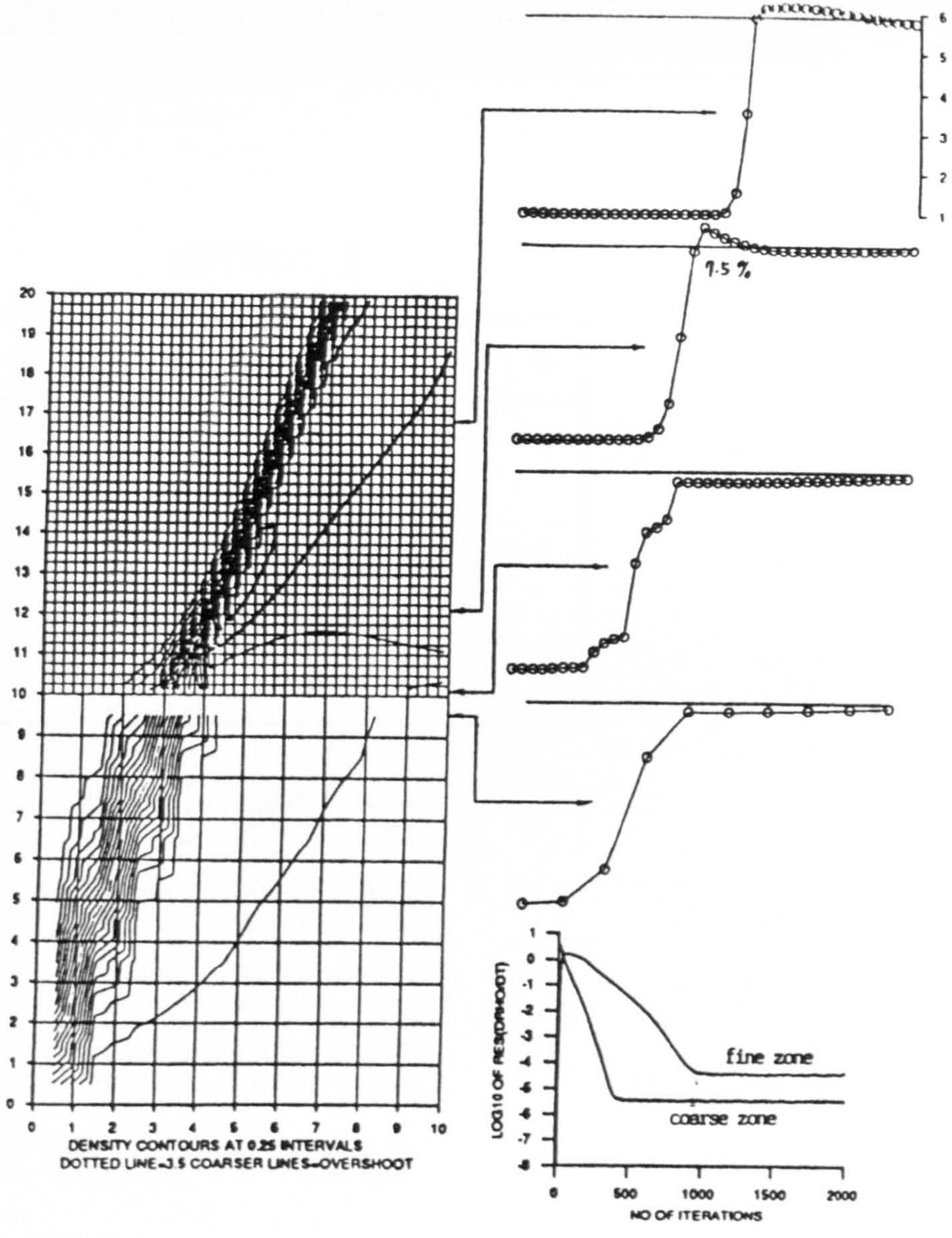

1ST ORDER ROE SCHEME FOR AN OBLIQUE SHOCK M=20 DELTA=43.64 EPSILON=60 ALPHA=10
LOCAL CFL=0.9 N=2000 PRE-SHOCK COND. AS INITIAL COND.

Fig. 3.11 M=20 calculation with coarse-fine grid

METHOD 1

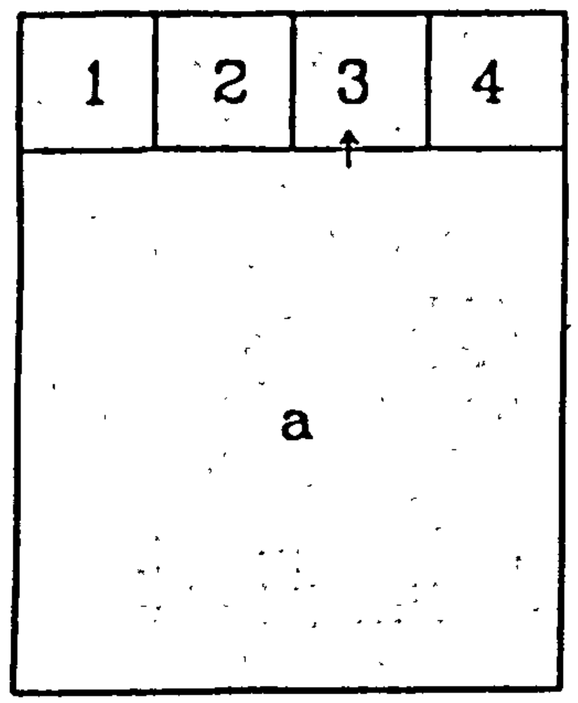

Flux=R.S.(W_a,W_3)

R.S.=Riemann Solver

METHOD 2

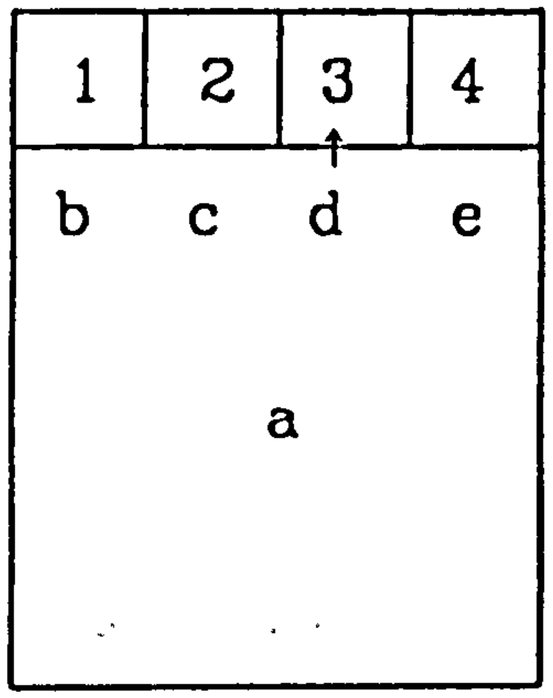

$$W_b = W_a - \frac{3}{6}(W_4 - W_1)$$

$$W_c = W_a - \frac{1}{6}(W_4 - W_1)$$

$$W_d = W_a + \frac{1}{6}(W_4 - W_1)$$

$$W_e = W_a + \frac{3}{6}(W_4 - W_1)$$

Flux=R.S.(W_d,W_3)

METHOD 3

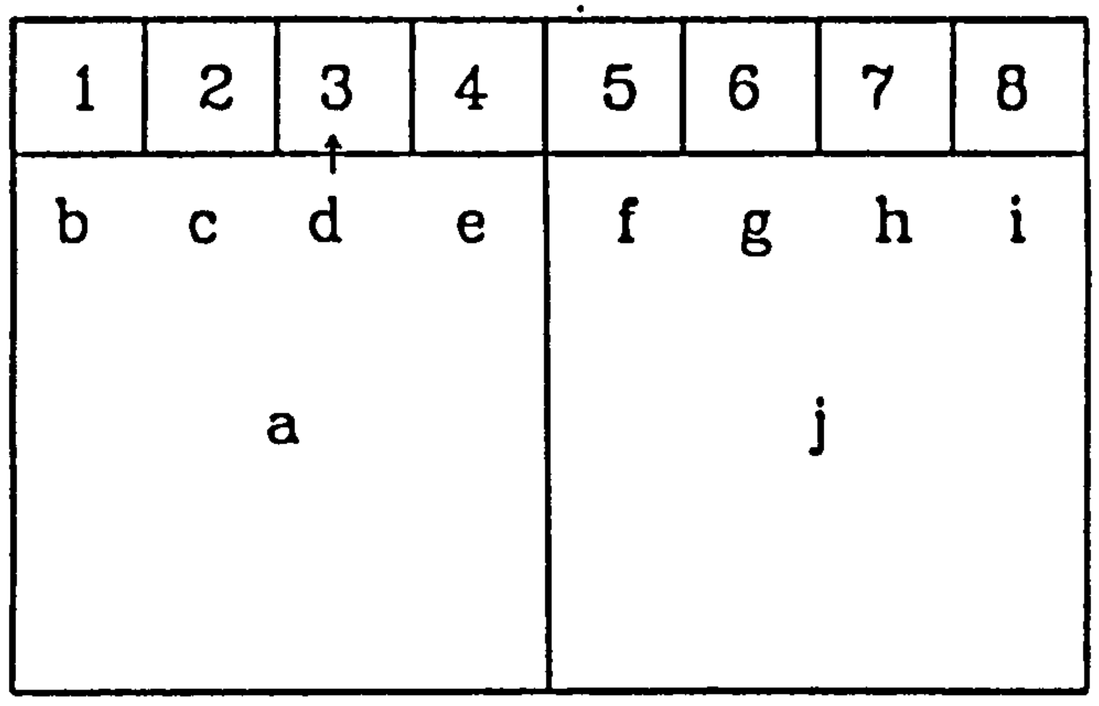

$$W_g = W_j - \frac{1}{8}(W_j - W_a)$$

$$W_f = W_j - \frac{3}{8}(W_j - W_a)$$

$$W_e = W_j - \frac{5}{8}(W_j - W_a)$$

$$W_d = W_j - \frac{7}{8}(W_j - W_a)$$

Flux=R.S.(W_d,W_3)

Fig. 3.12 Various interpolations for flux calculation

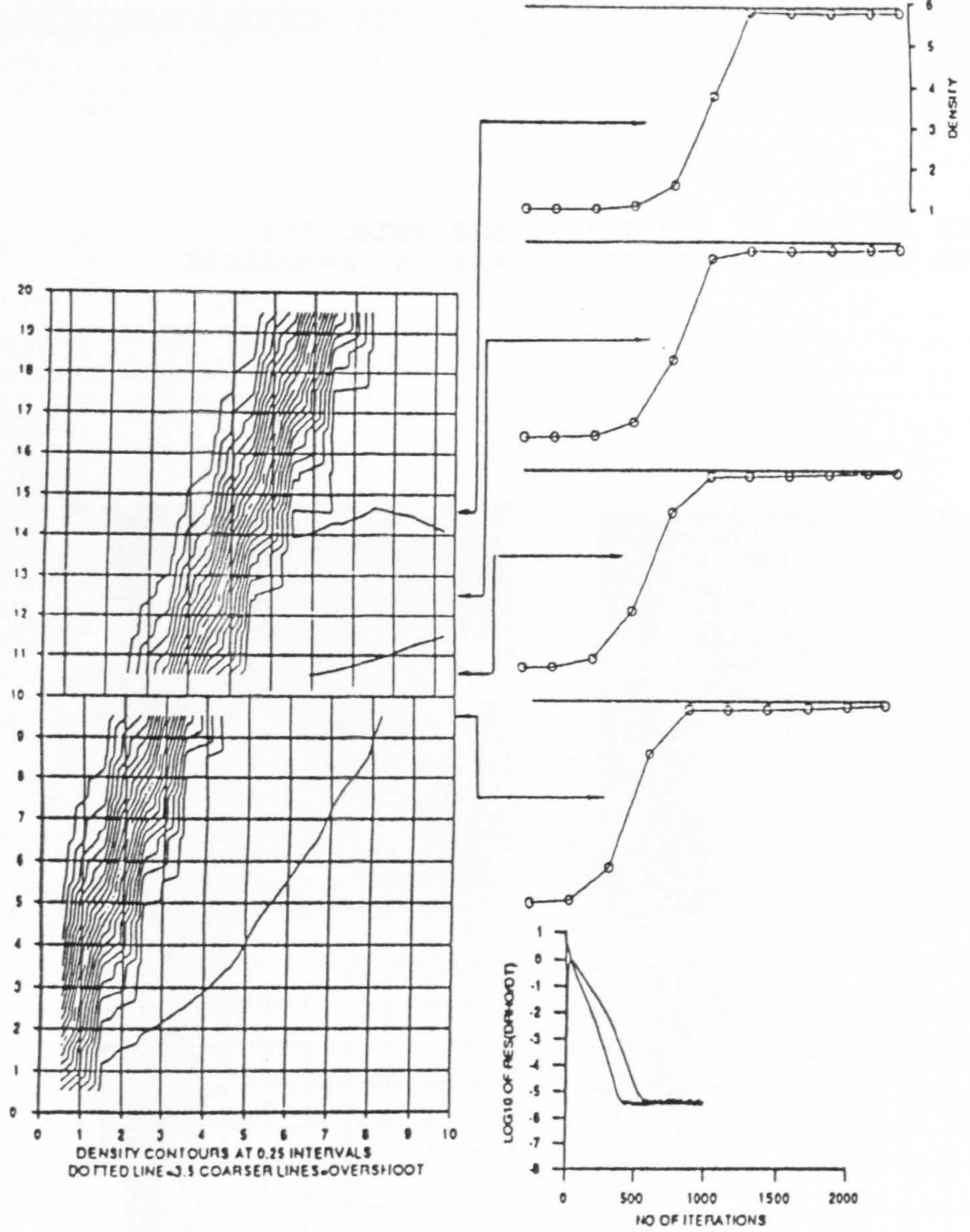

1ST ORDER ROE SCHEME FOR AN OBLIQUE SHOCK M=20 DELTA=43.64 EPSILON=60 ALPHA=10
LOCAL CFL=0.9 N=1000 PRE-SHOCK COND. AS INITIAL COND.

Fig. 3.14 Result from discontinuous grid with equal spacing

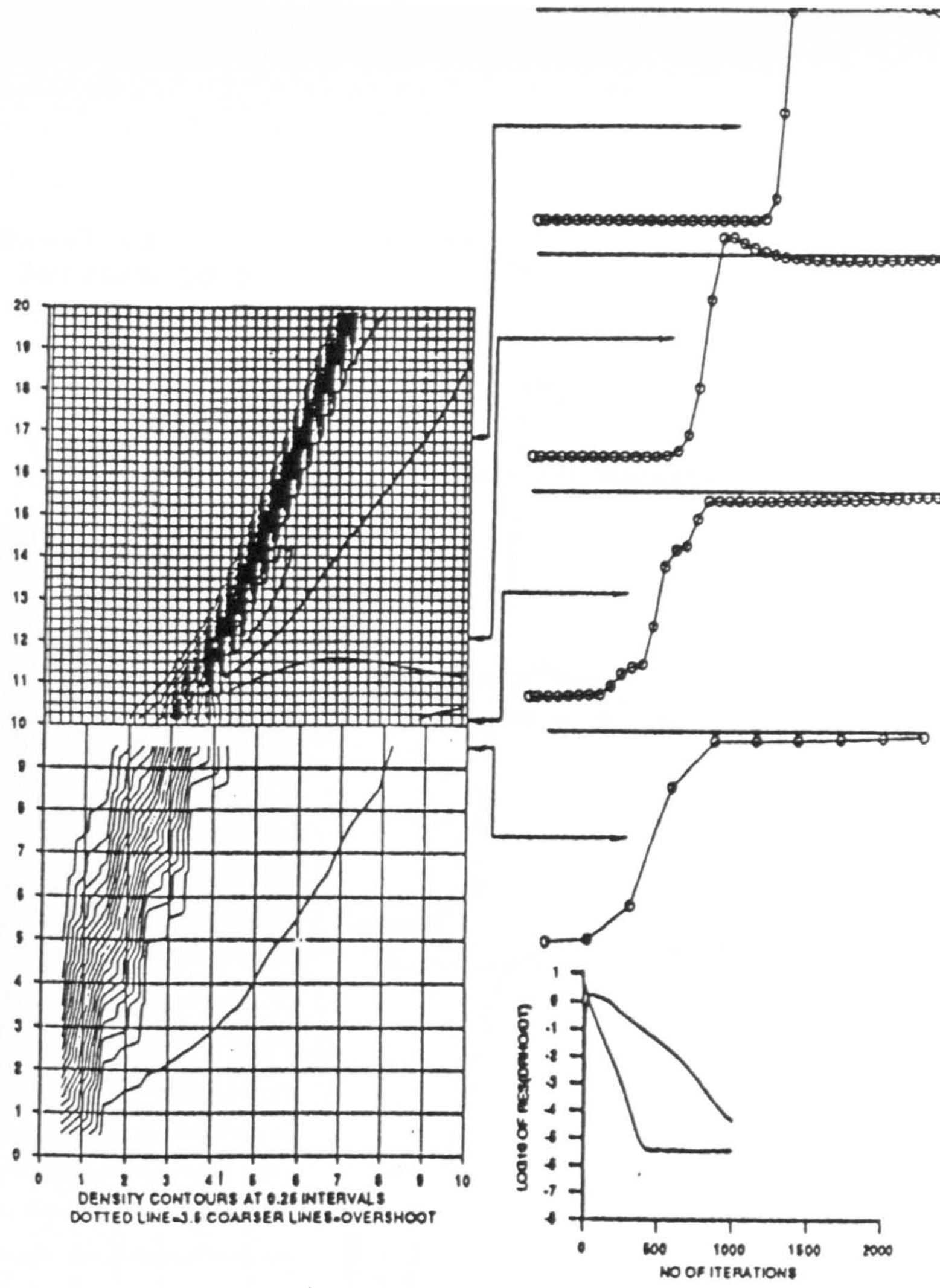

1ST ORDER ROE SCHEME FOR AN OBLIQUE SHOCK M=20 DELTA=43.64 EPSILON=60 ALPHA=10
LOCAL CFL=0.9 N=1000 PRE-SHOCK COND. AS INITIAL COND.

Fig. 3.15 Result from grid with noninteger spacing

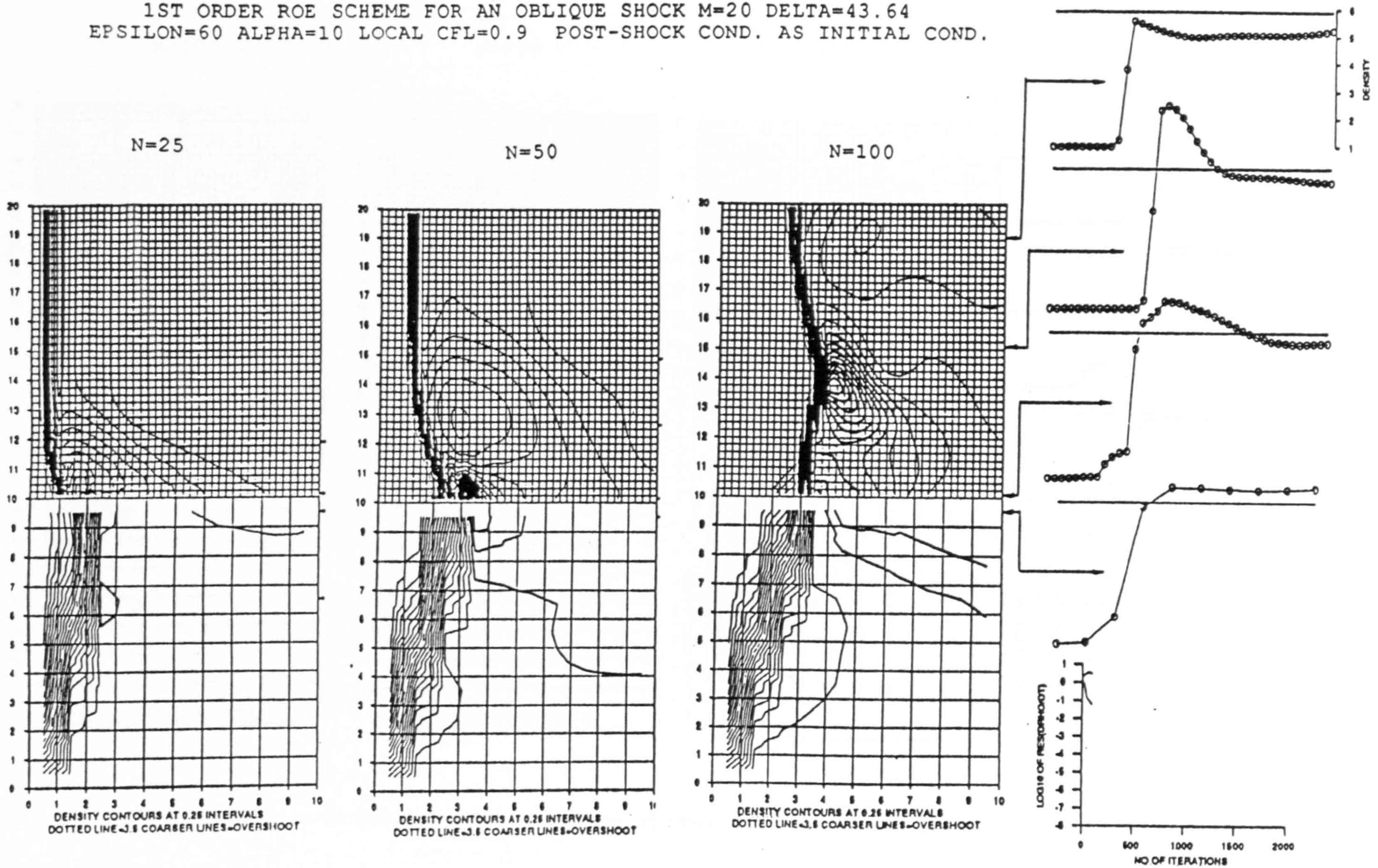

Fig. 3.16 Shock evolution from local time stepping results (continued)

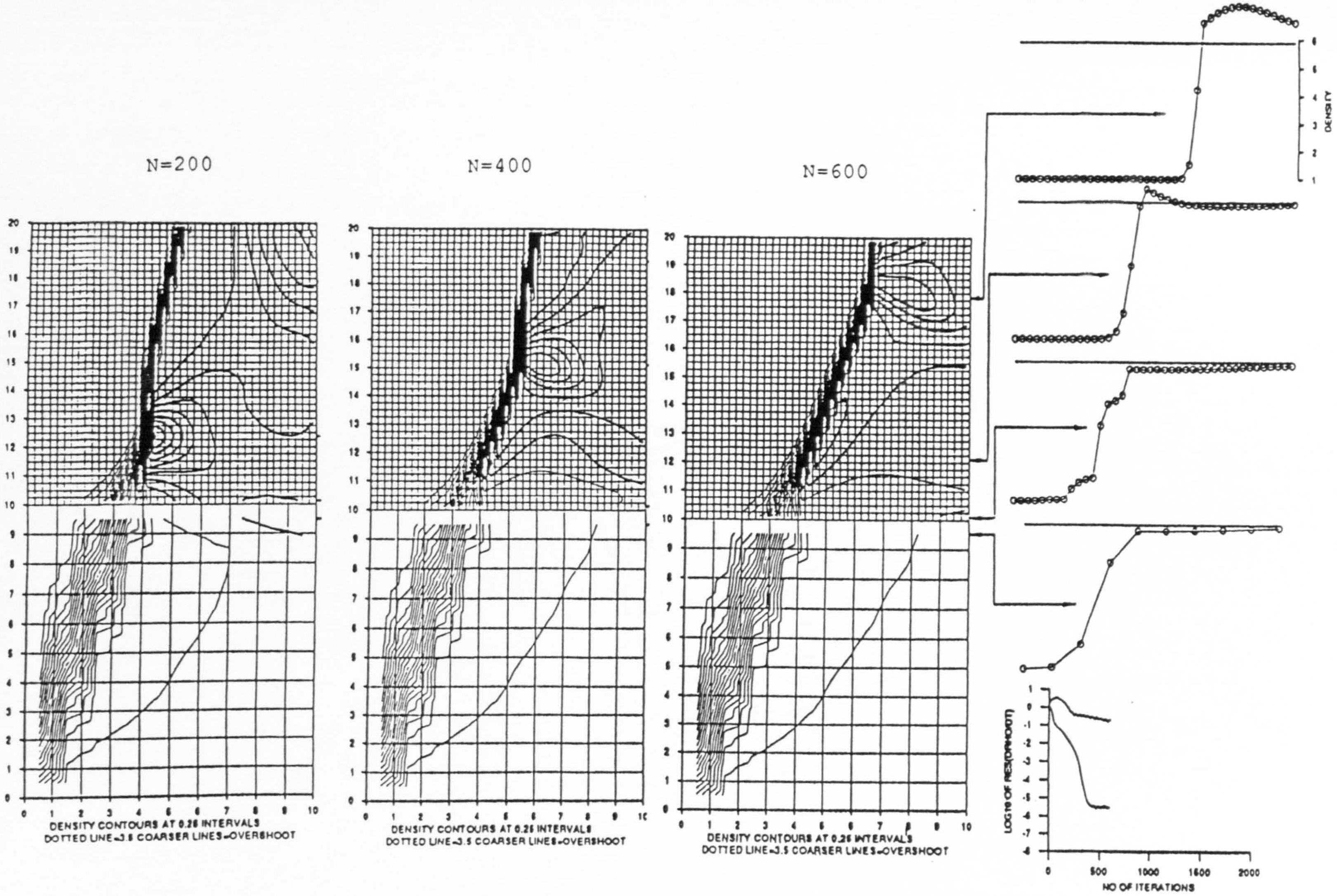

shock evolution from local time stepping results

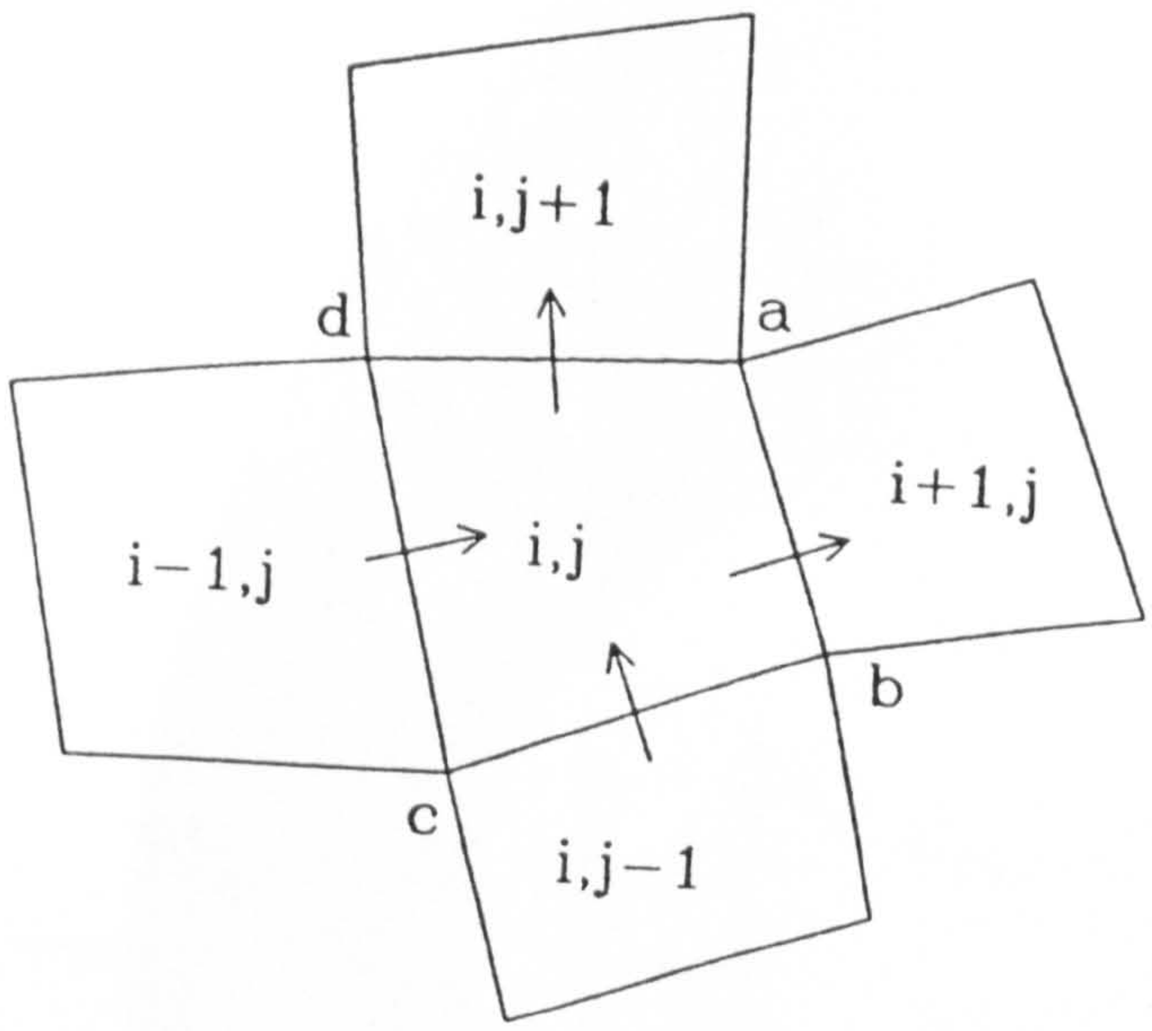

Fig. 4.1 Grid index system

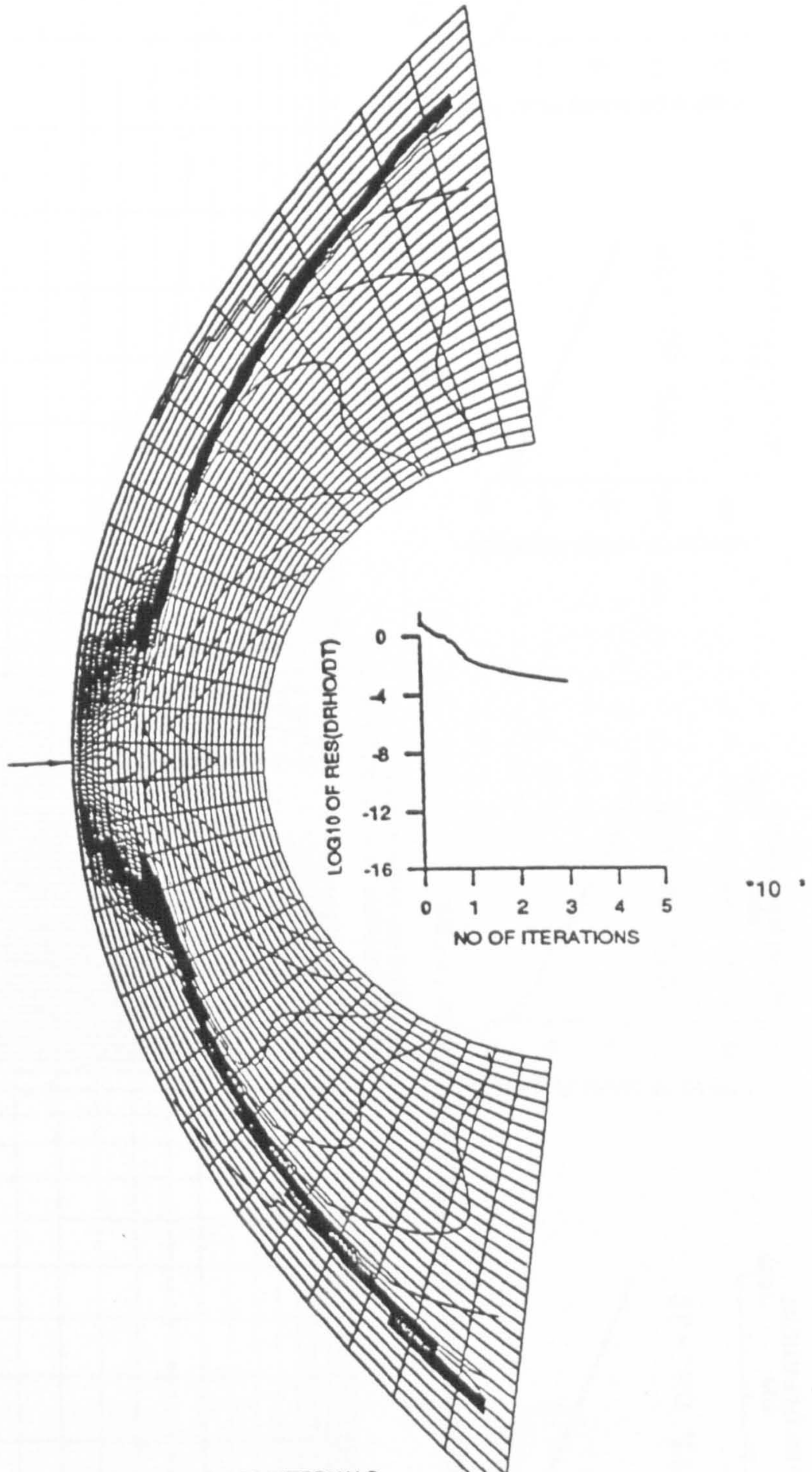

EXPLICIT 1ST ORDER SCHEME WITH ROE'S RIEMANN SOLVER
MACH NO.=8 LOCAL CFL=0.8

Fig. 4.2 Blunt nose instability

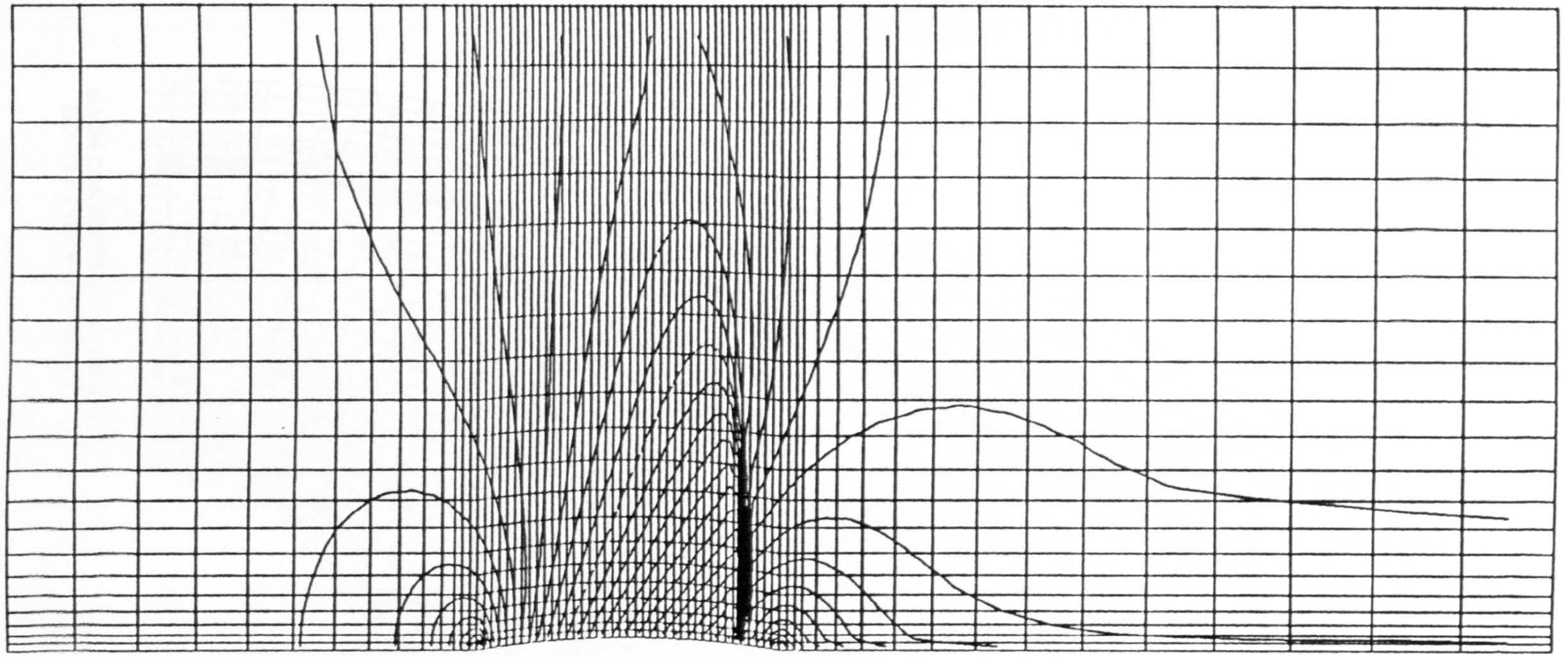

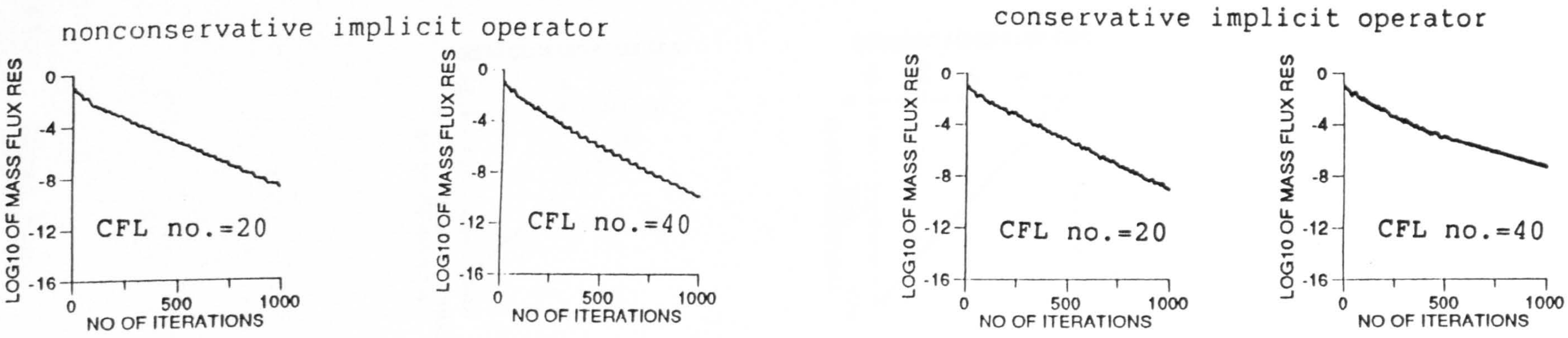

nonconservative/conservative implicit operator with DDADI
21x71 cells Van Albada limiter Mach no.=0.85

Fig. 4.3 Mach 0.85 past GAMM bump

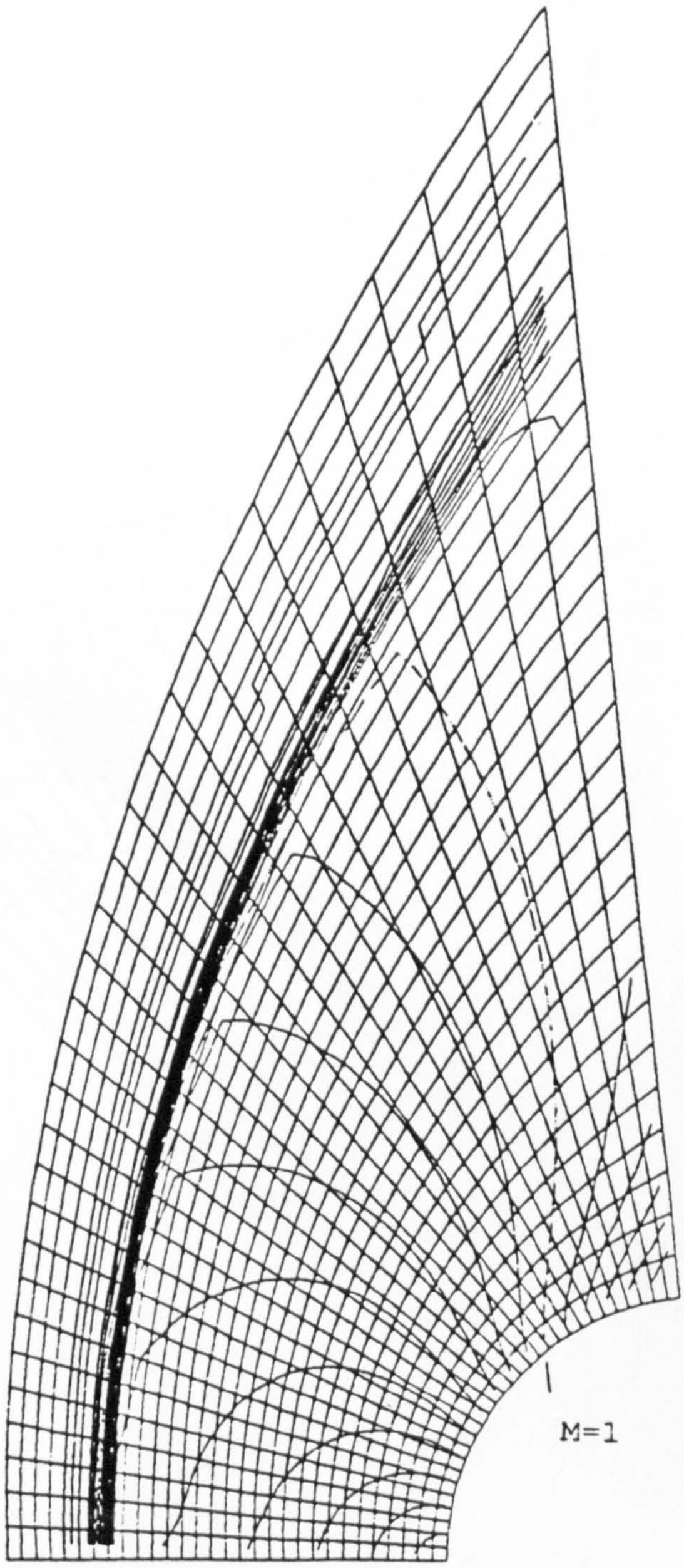

MACH CONTOURS AT 0.1 INTERVALS
DOTTED LINE MACH NO=1.0

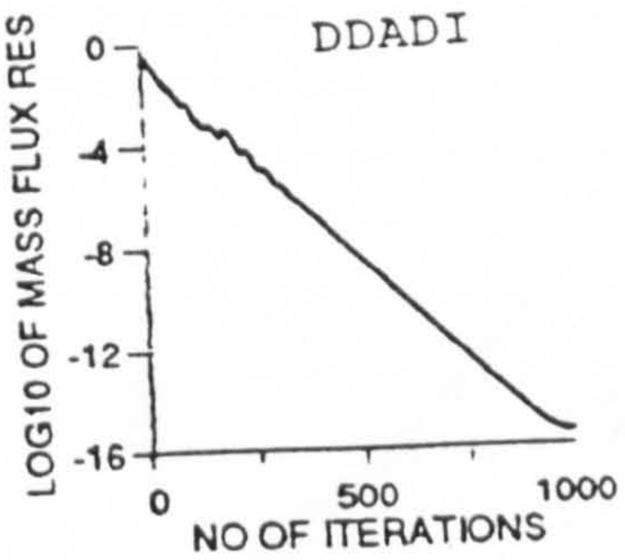

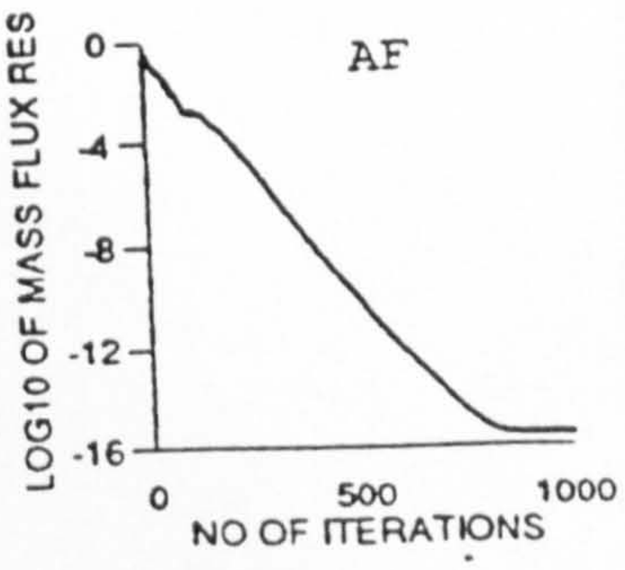

CONSERVATIVE IMPLICIT OPERATOR 30X30 CELLS
VAN ALBADA LIMITER MACH NO.=2. LOCAL CFL=20 $\tilde{\delta}_{1,4}=0.25$ $\tilde{\delta}_{2,3}=0.25$

Fig. 4.4 Mach 2 flow past quarter cylinder

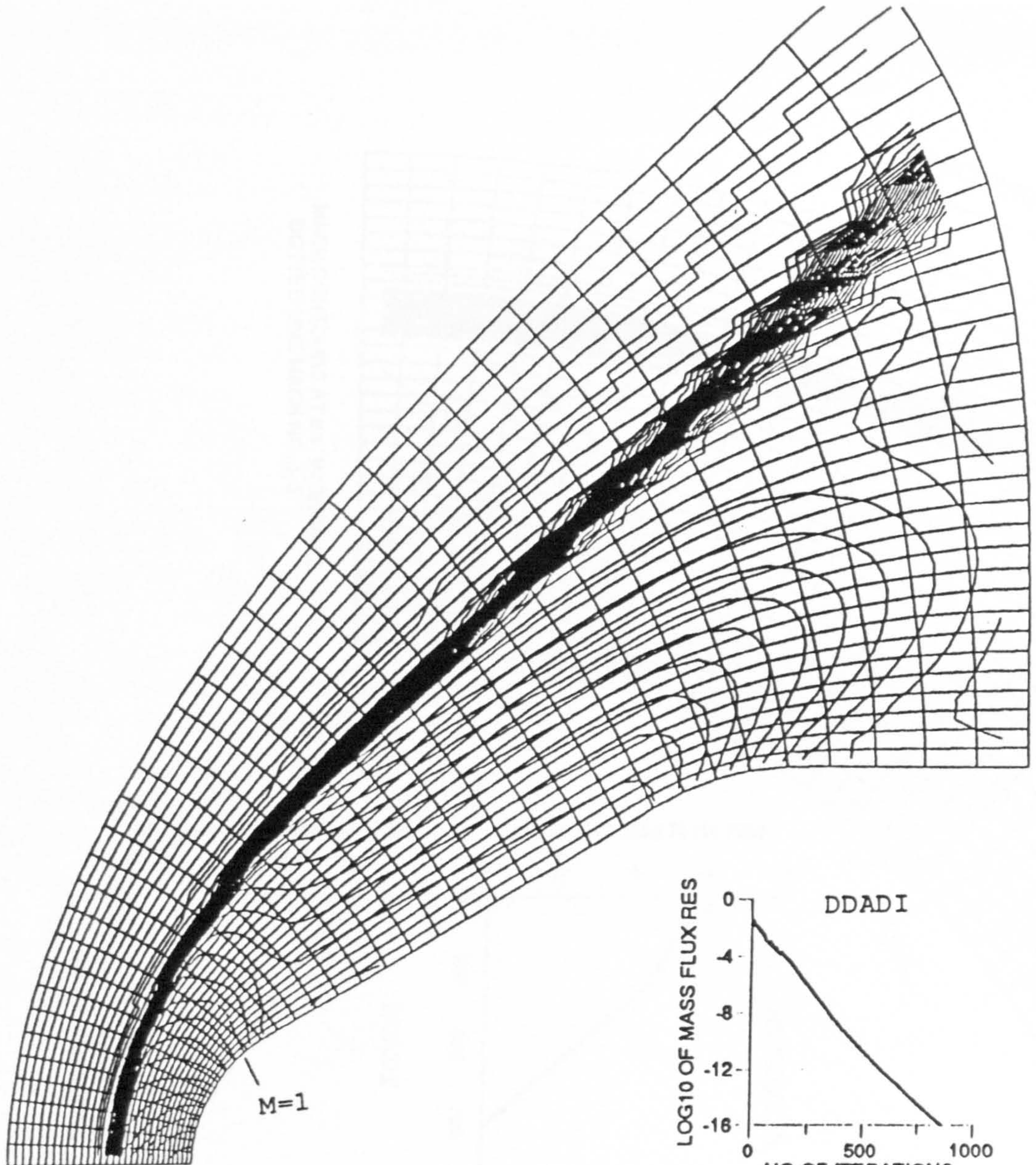

MACH CONTOURS AT 0.1 INTERVALS
DOTTED LINE MACH NO=1.0

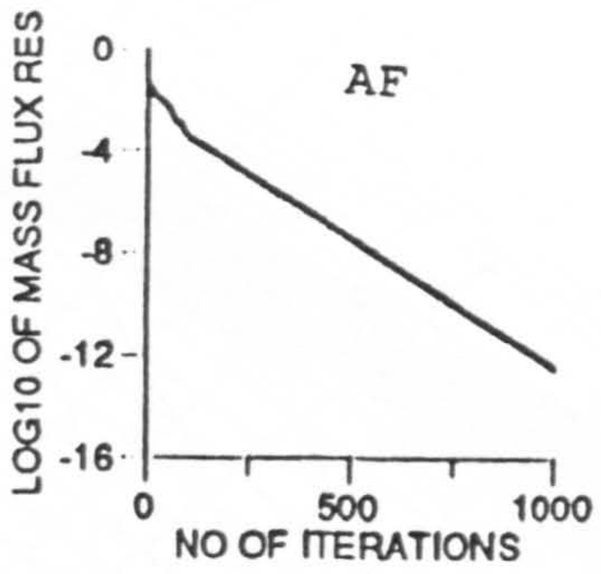

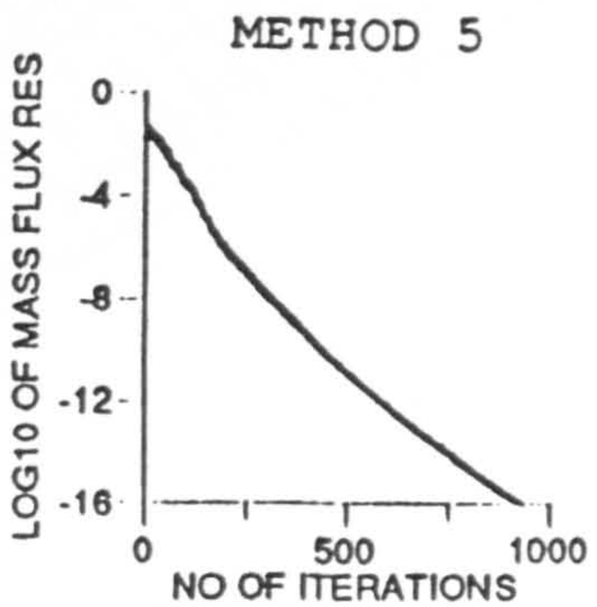

CONSERVATIVE IMPLICIT OPERATOR 30X35 CELLS
VAN ALBADA LIMITER MACH NO.=5. LOCAL CFL=10 $\tilde{\delta}_{1,4}=0.25$ $\tilde{\delta}_{2,3}=0.5$

Fig. 4.5 Mach 5 flow past reentry body

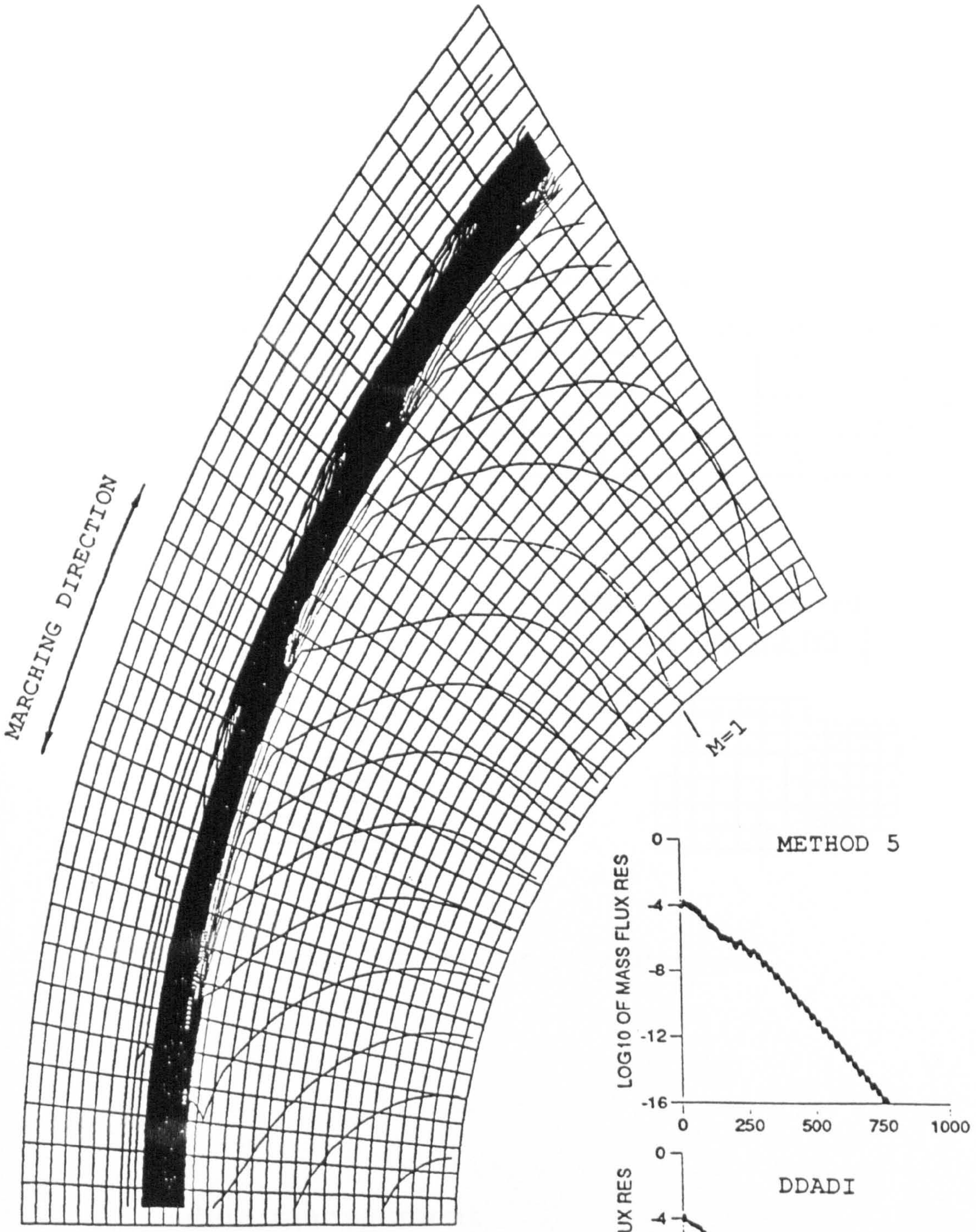

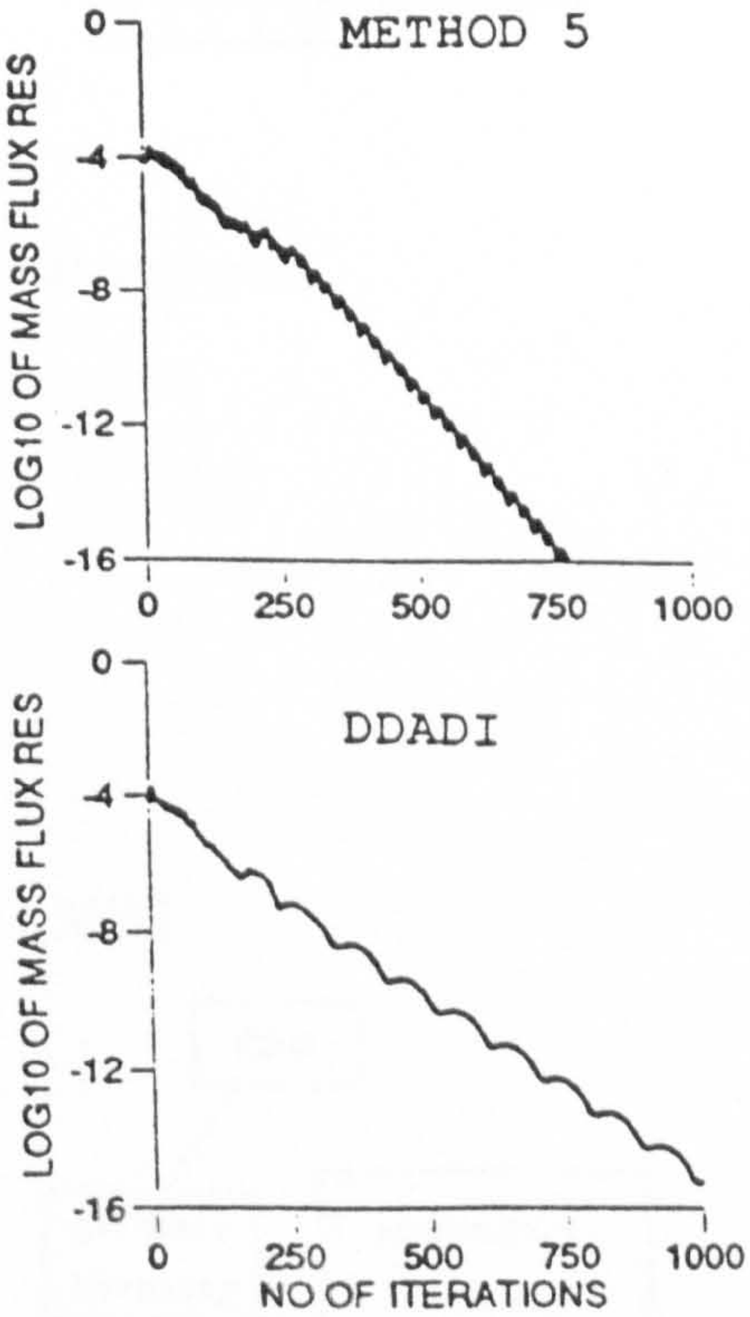

CONSERVATIVE IMPLICIT OPERATOR 30X30 CELLS
VAN ALBADA LIMITER MACH NO.=20. LOCAL CFL=10 $\tilde{\delta}_{1,4}=0.25$ $\tilde{\delta}_{2,3}=0.8$

Fig. 4.6 Mach 20 flow past quarter cylinder

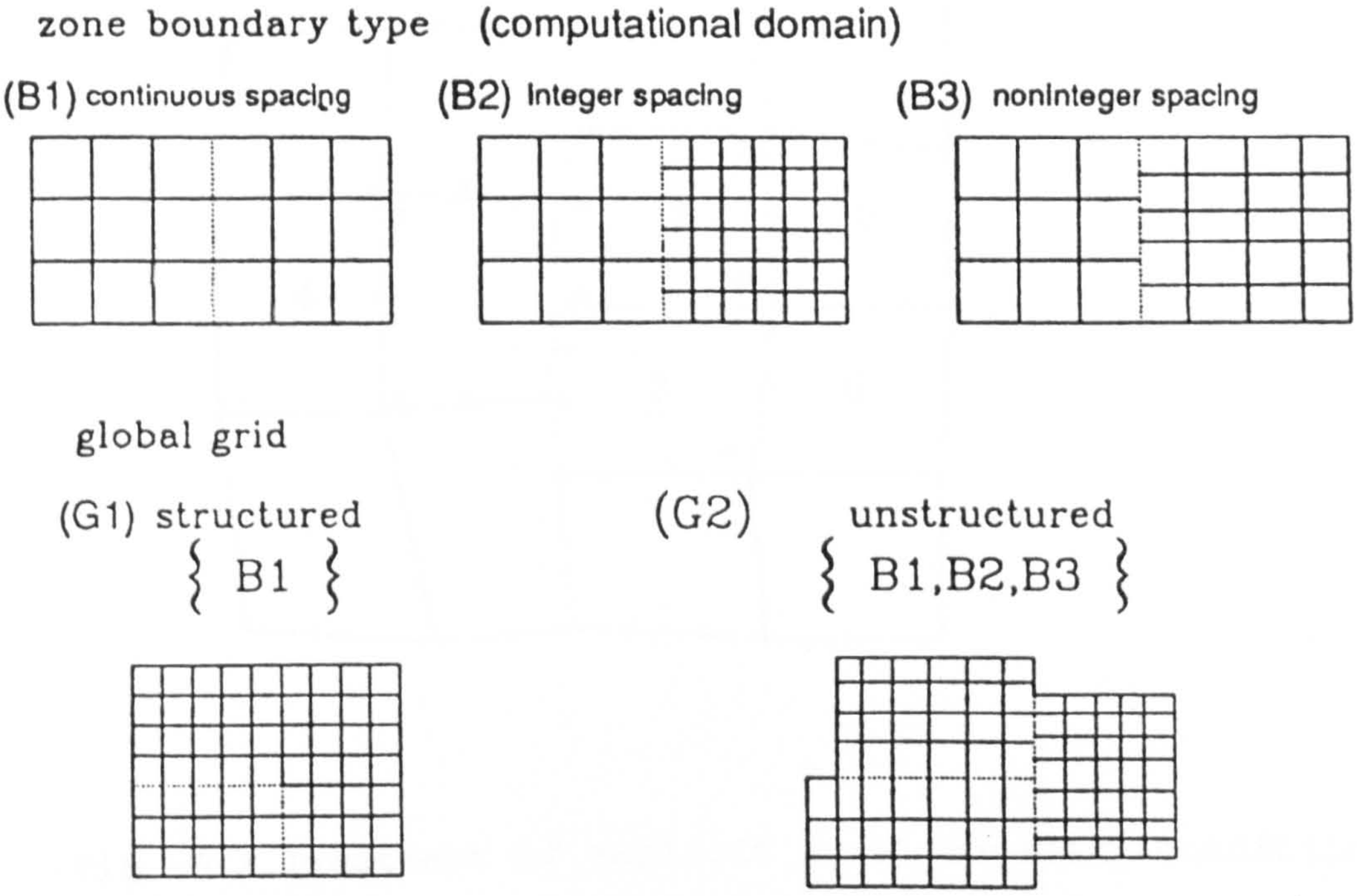

Fig. 5.1 Various grid structure

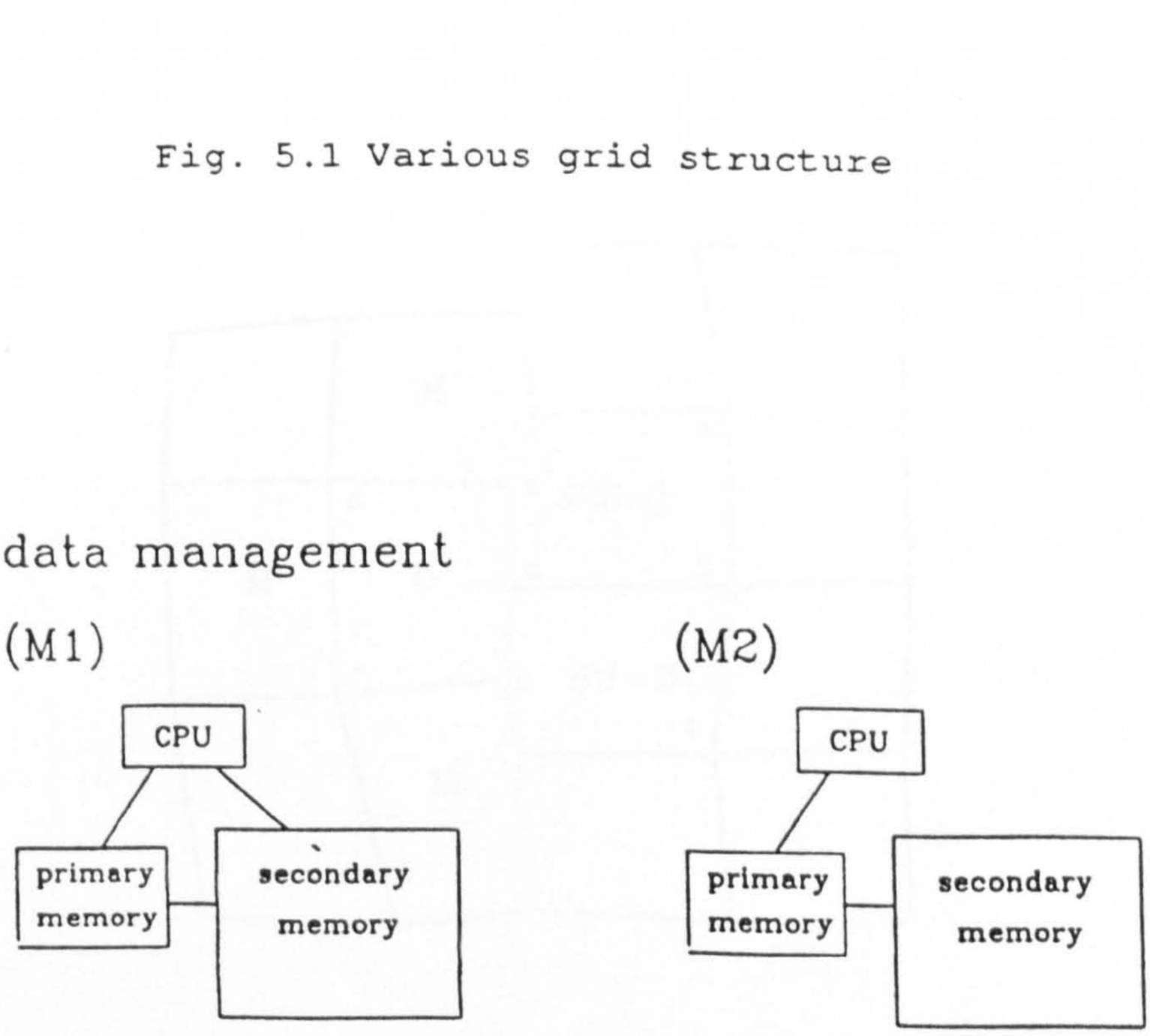

Fig. 5.2 Data management

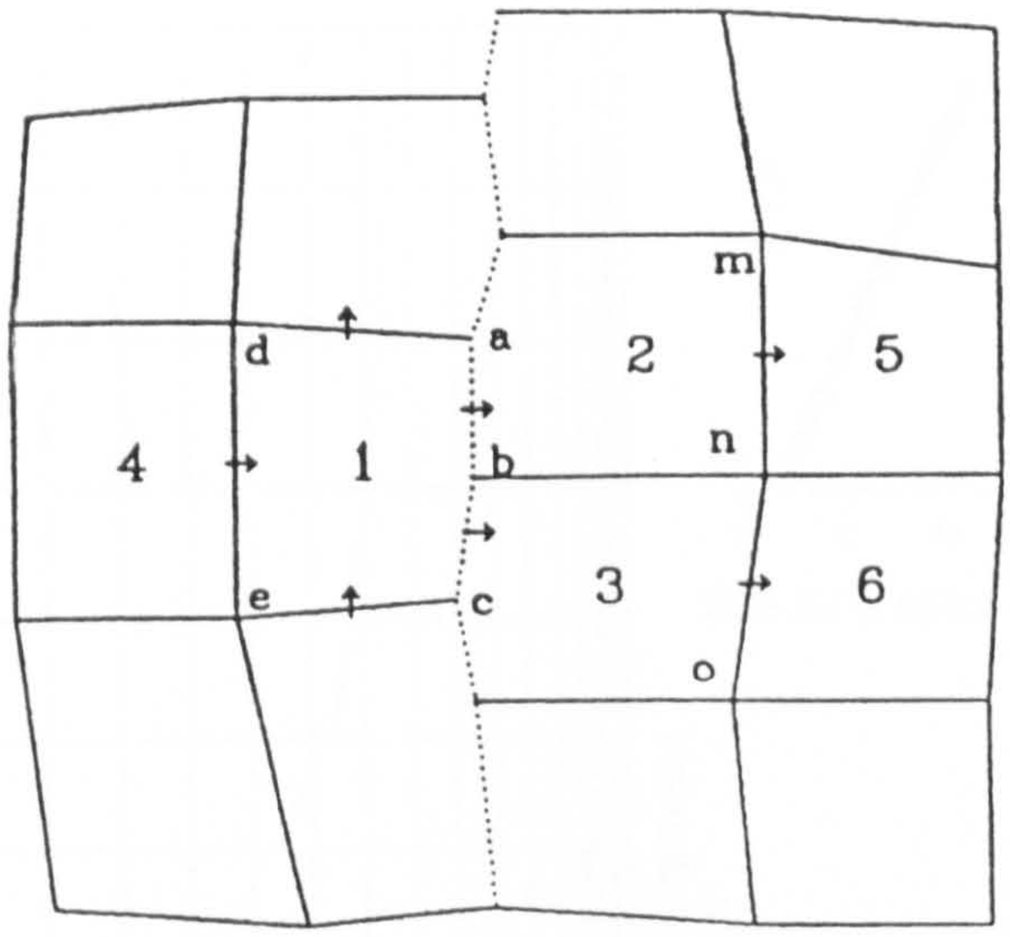

Fig. 5.3 Treatment of explicit zonal boundary condition

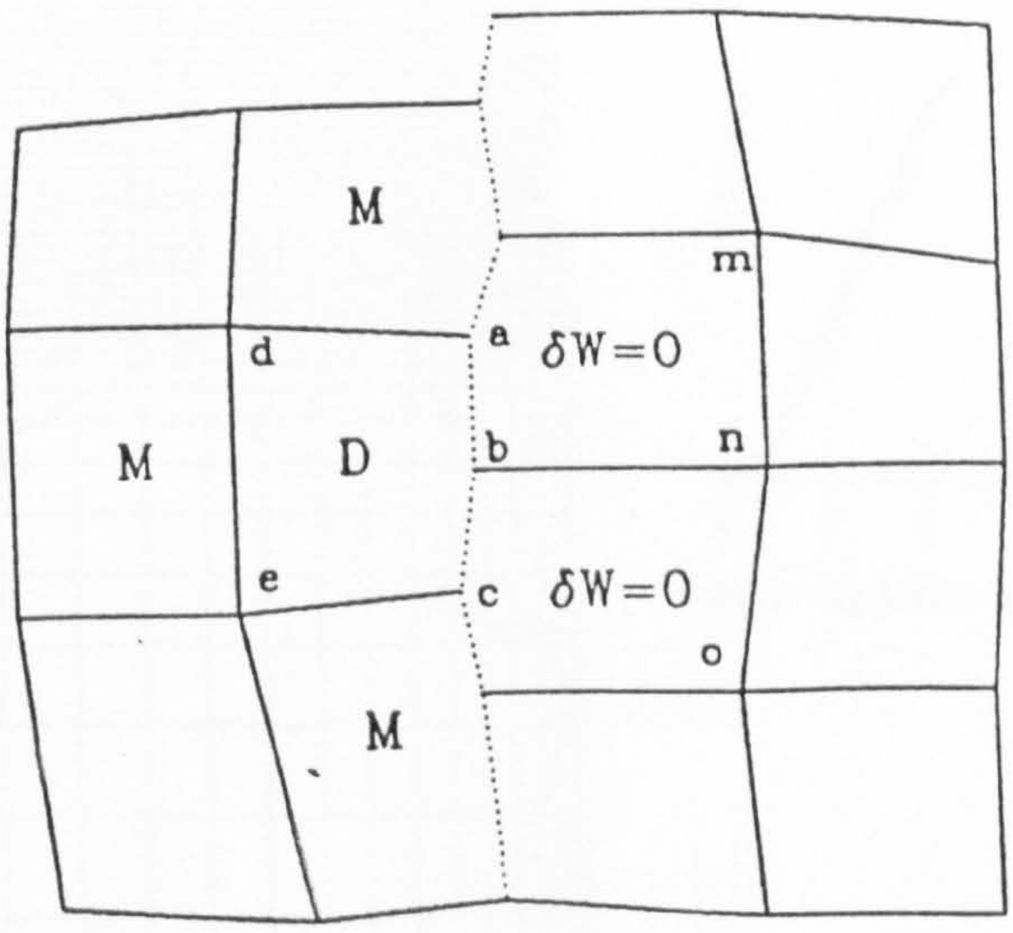

Fig. 5.4 Treatment of implicit zonal boundary condition

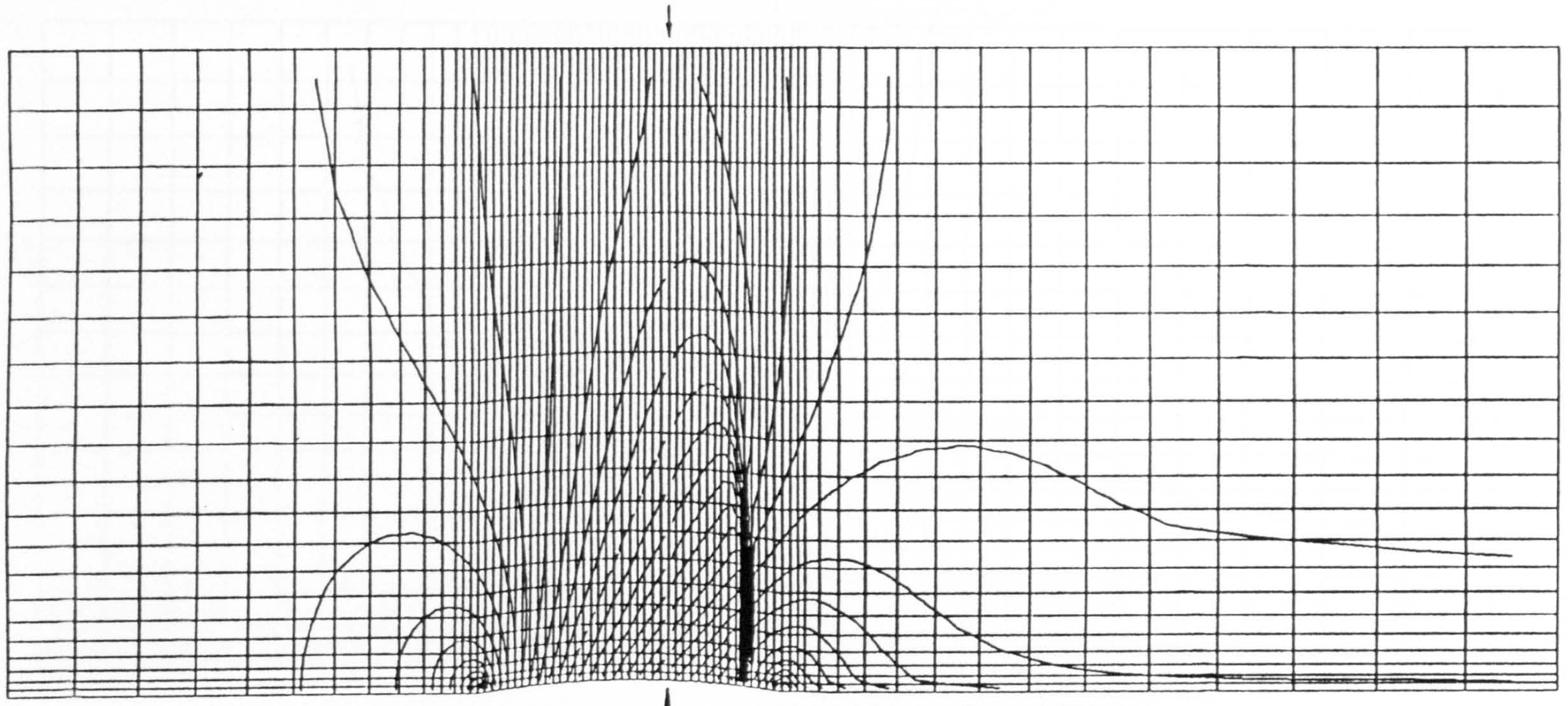

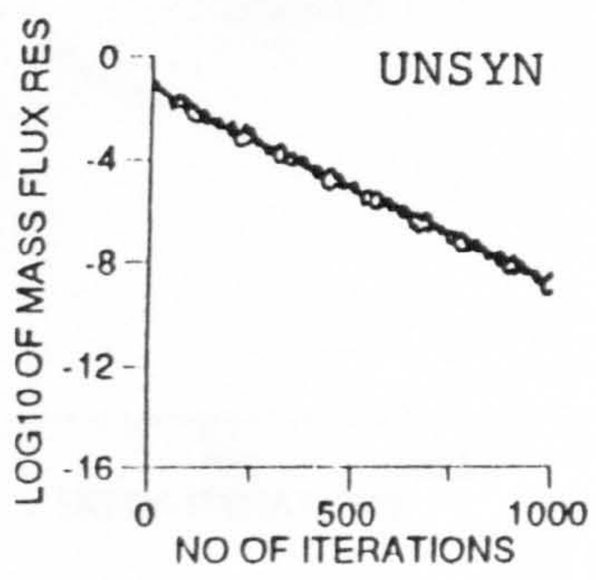

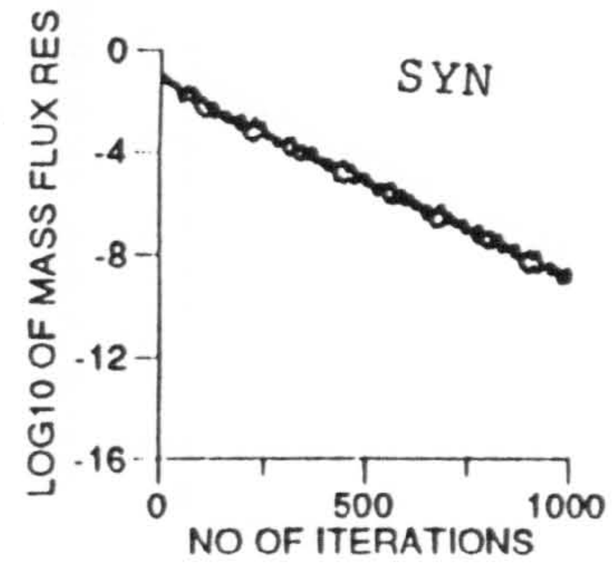

conservative implicit operator with DDADI local CFL no.=20
21x39+21x32 cells Van Albada limiter Mach no.=0.85

Fig. 5.5 GAMM bump calculation with zonal boundary covering subsonic and supersonic flow

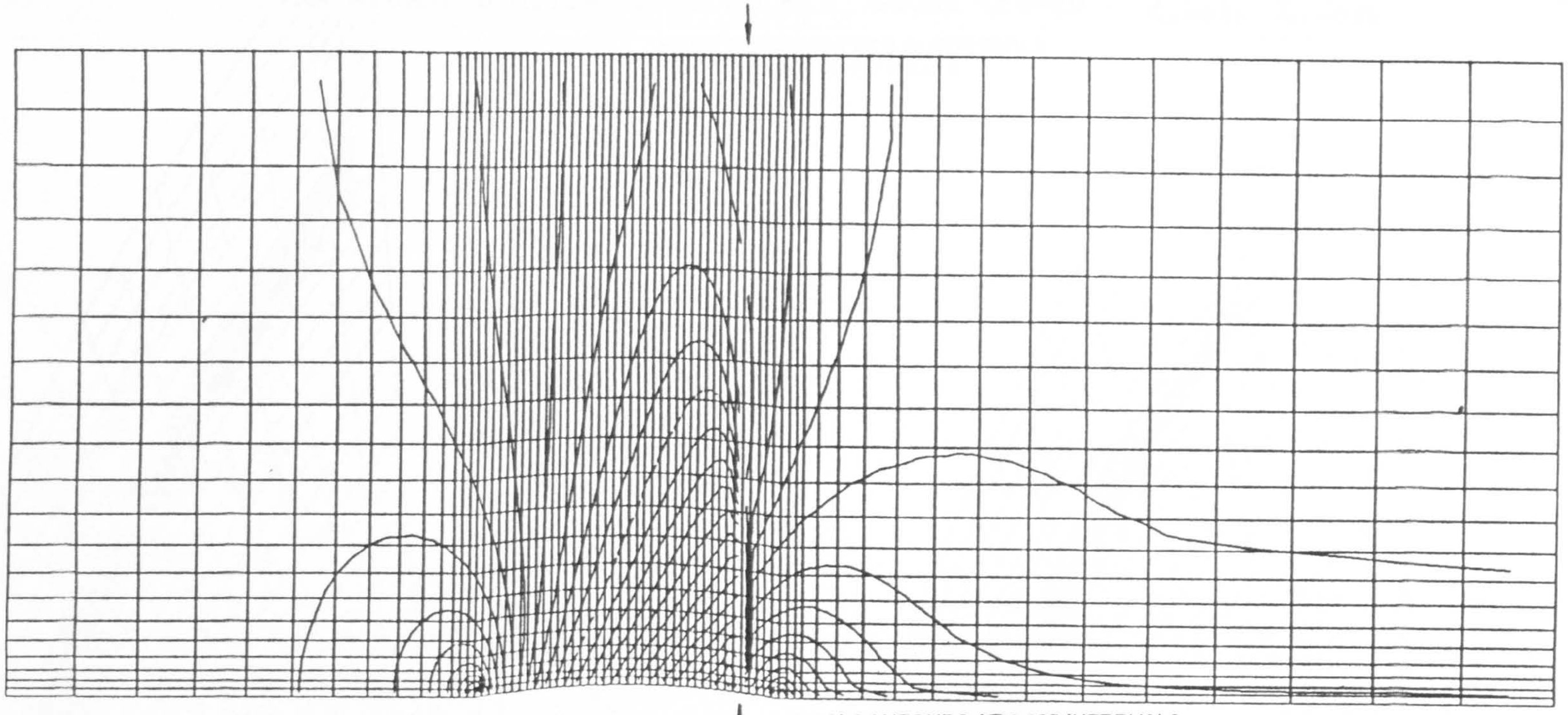

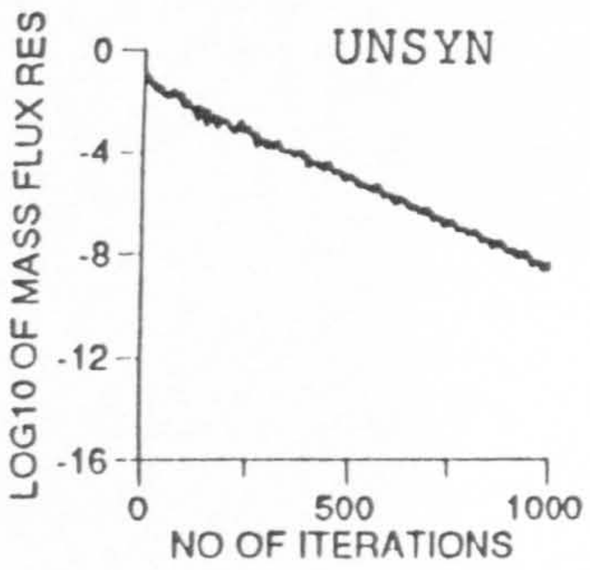

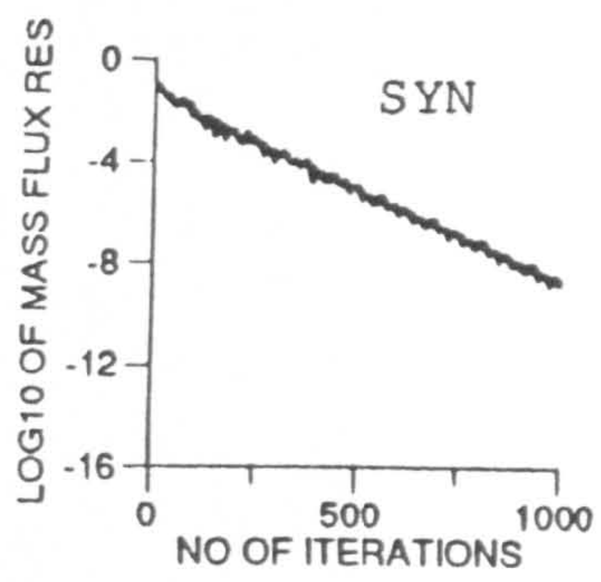

conservative implicit operator with DDADI local CFL no.=20
21x49+21x22 cells Van Albada limiter Mach no.=0.85

Fig. 5.6 GAMM bump calculation with zonal boundary inside shock

CONSERVATIVE IMPLICIT OPERATOR WITH DDADI 15X30+15X30 CELLS
VAN ALBADA LIMITER MACH NO.=2. LOCAL CFL=20 $\tilde{\delta}_{1,4}=0.25$ $\tilde{\delta}_{2,3}=0.25$

MACH CONTOURS AT 0.05 INTERVALS
DOTTED LINE MACH NO=1.0

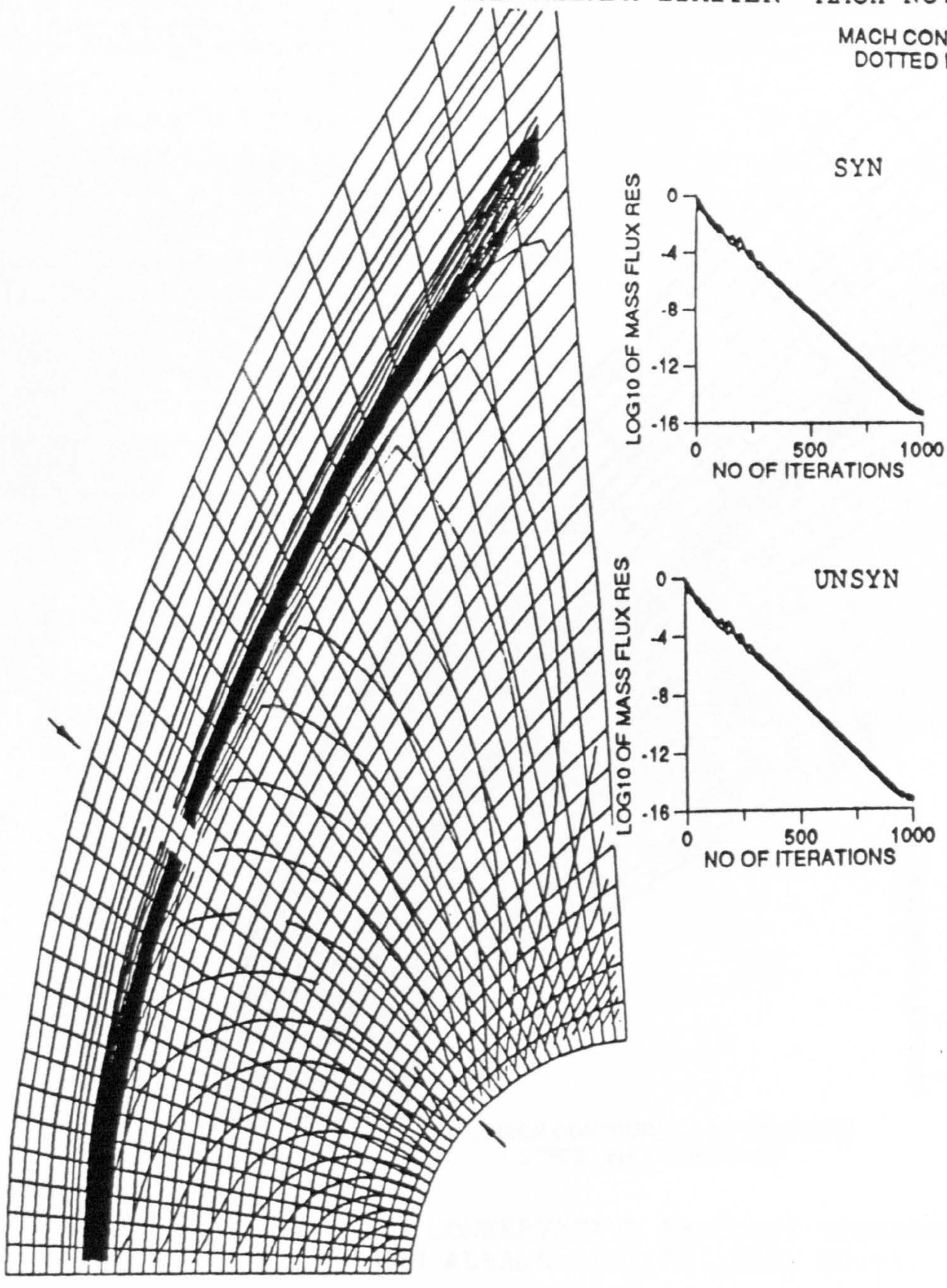

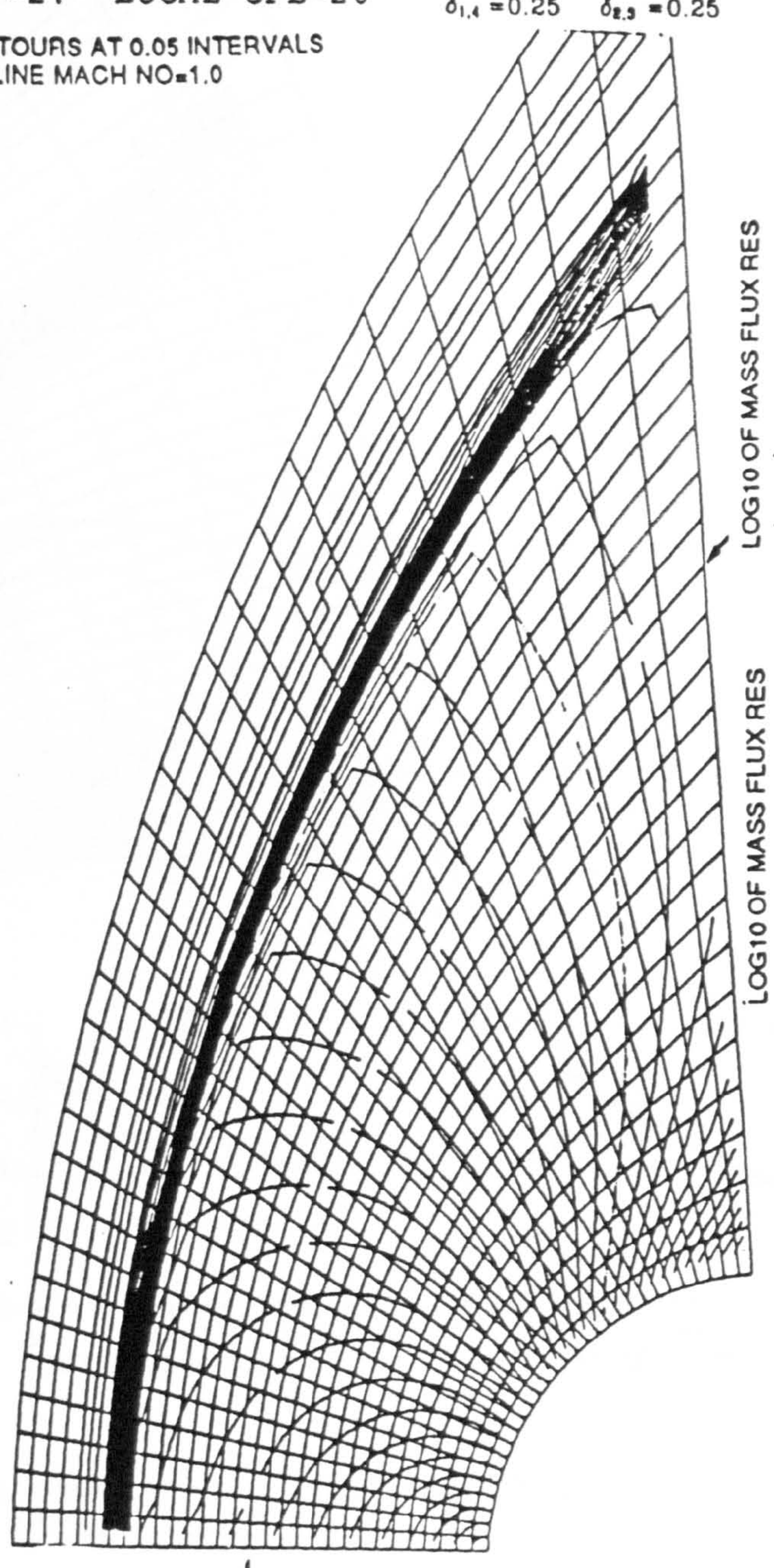

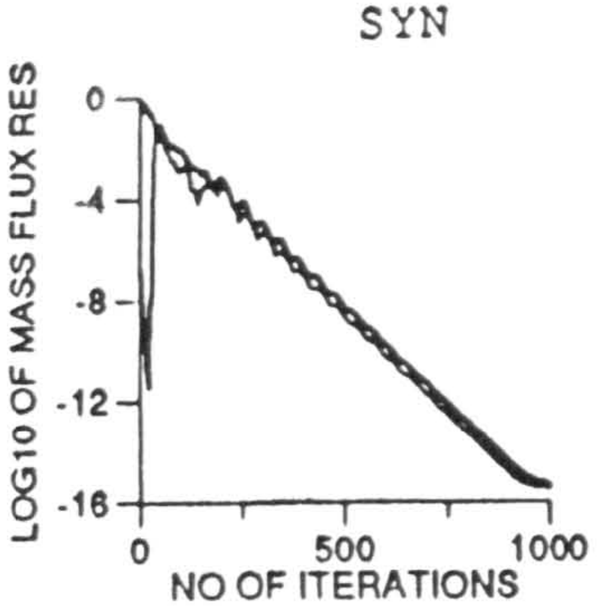

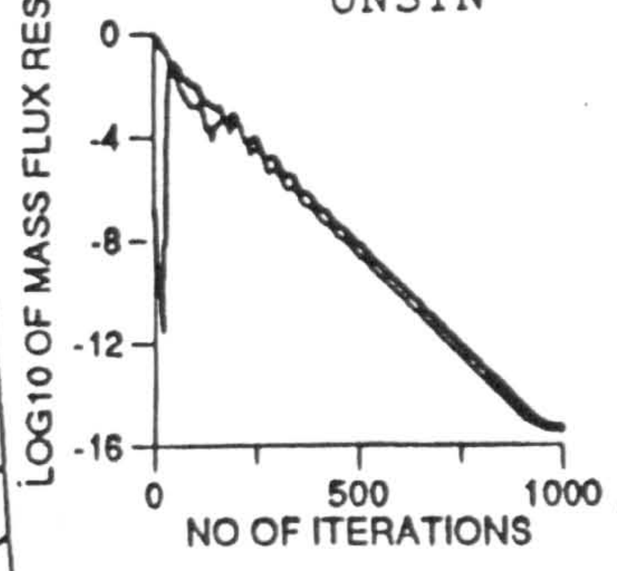

Fig. 5.7 Two-zone calculation of Mach 2 flow past quarter cylinder

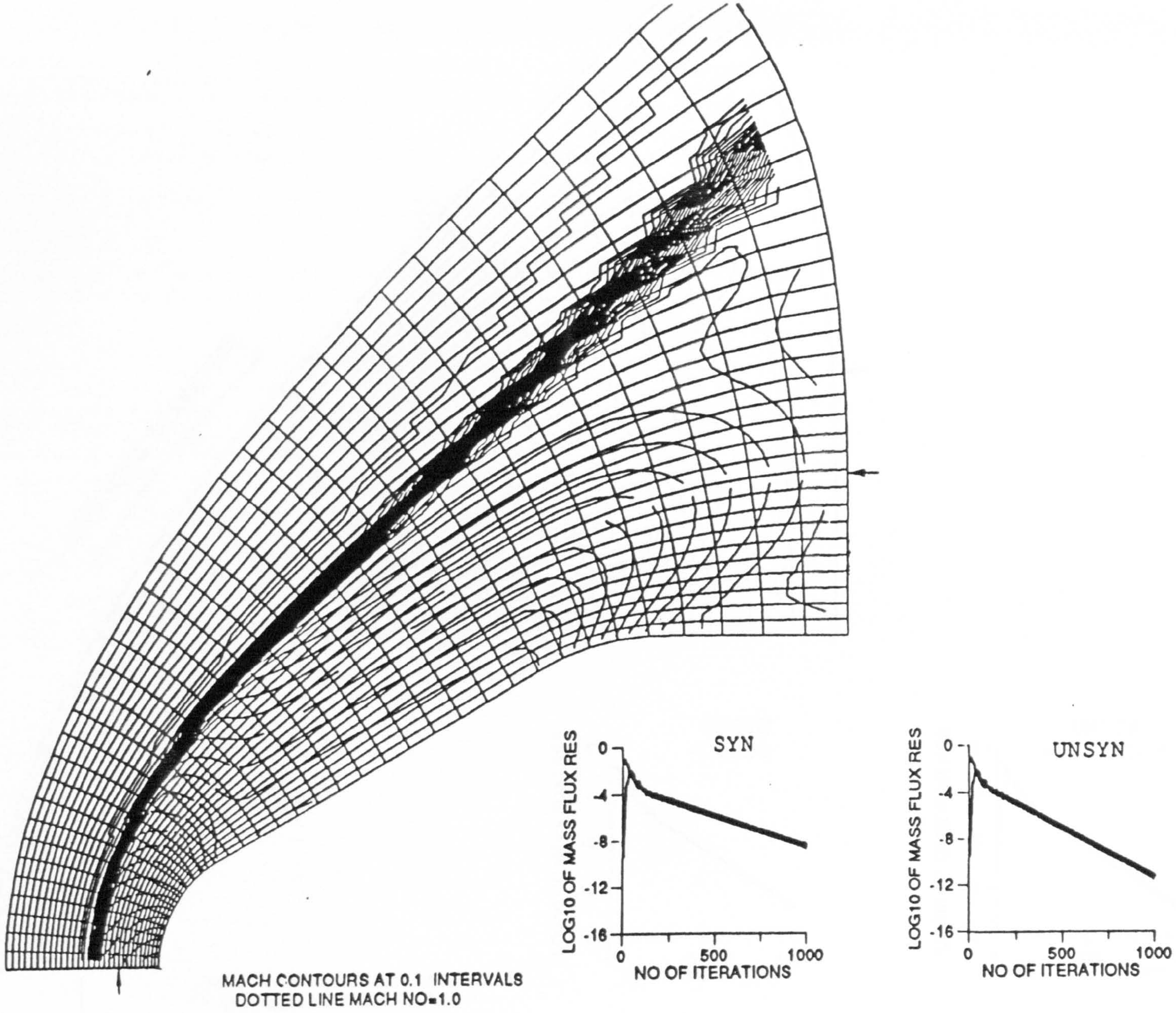

CONSERVATIVE IMPLICIT OPERATOR WITH DDADI 20X35+10X35 CELLS
VAN ALBADA LIMITER MACH NO.=5. LOCAL CFL=10

Fig. 5.8 Two-zone calculation of Mach 5 flow past reentry body (A)

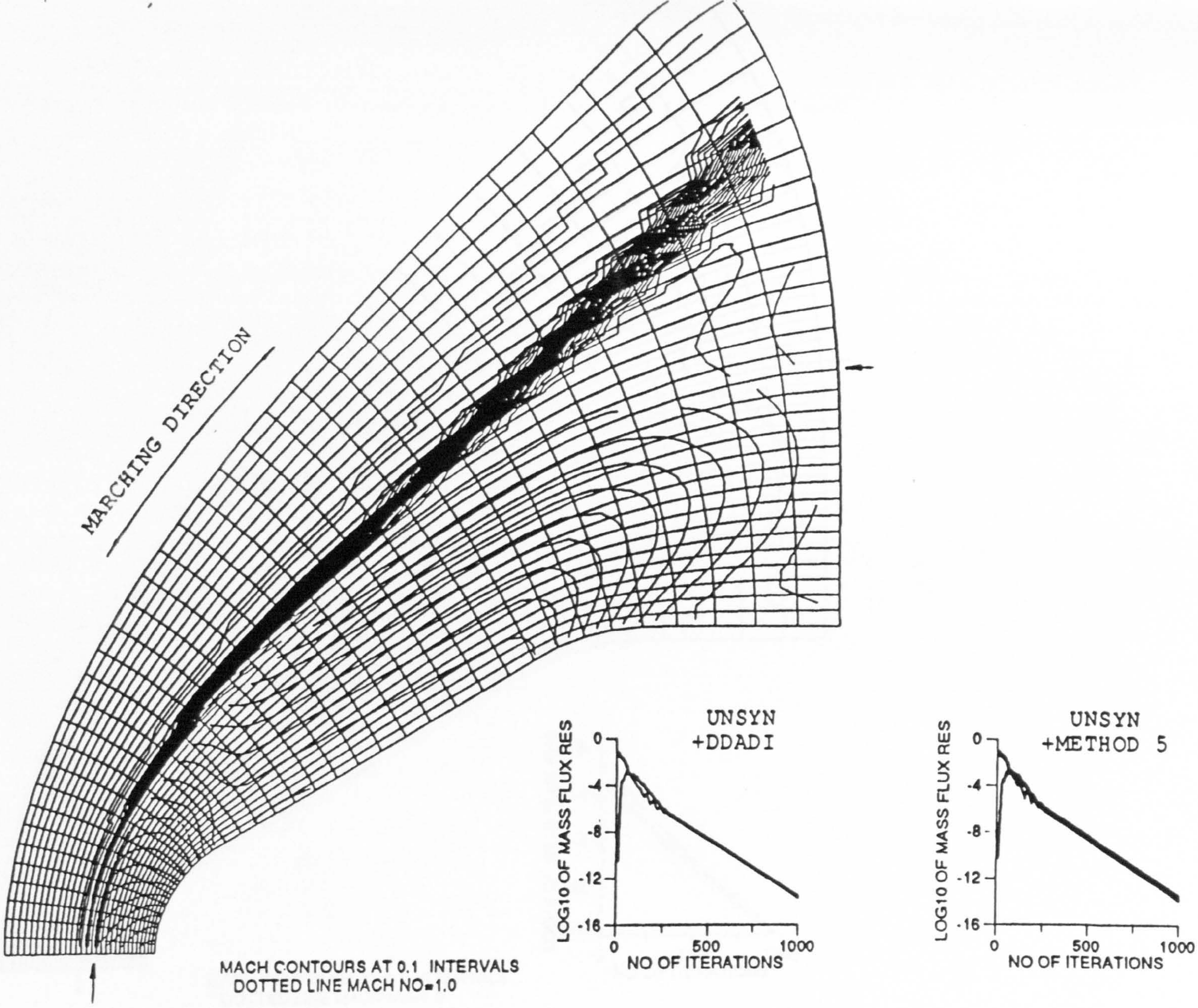

CONSERVATIVE IMPLICIT OPERATOR 15X35+15X35 CELLS
VAN ALBADA LIMITER MACH NO.=5. LOCAL CFL=10 $\tilde{\delta}_{1,4}=0.25$ $\tilde{\delta}_{2,3}=0.5$

Fig. 5.9 Two-zone calculation of Mach 5 flow past reentry body (B)

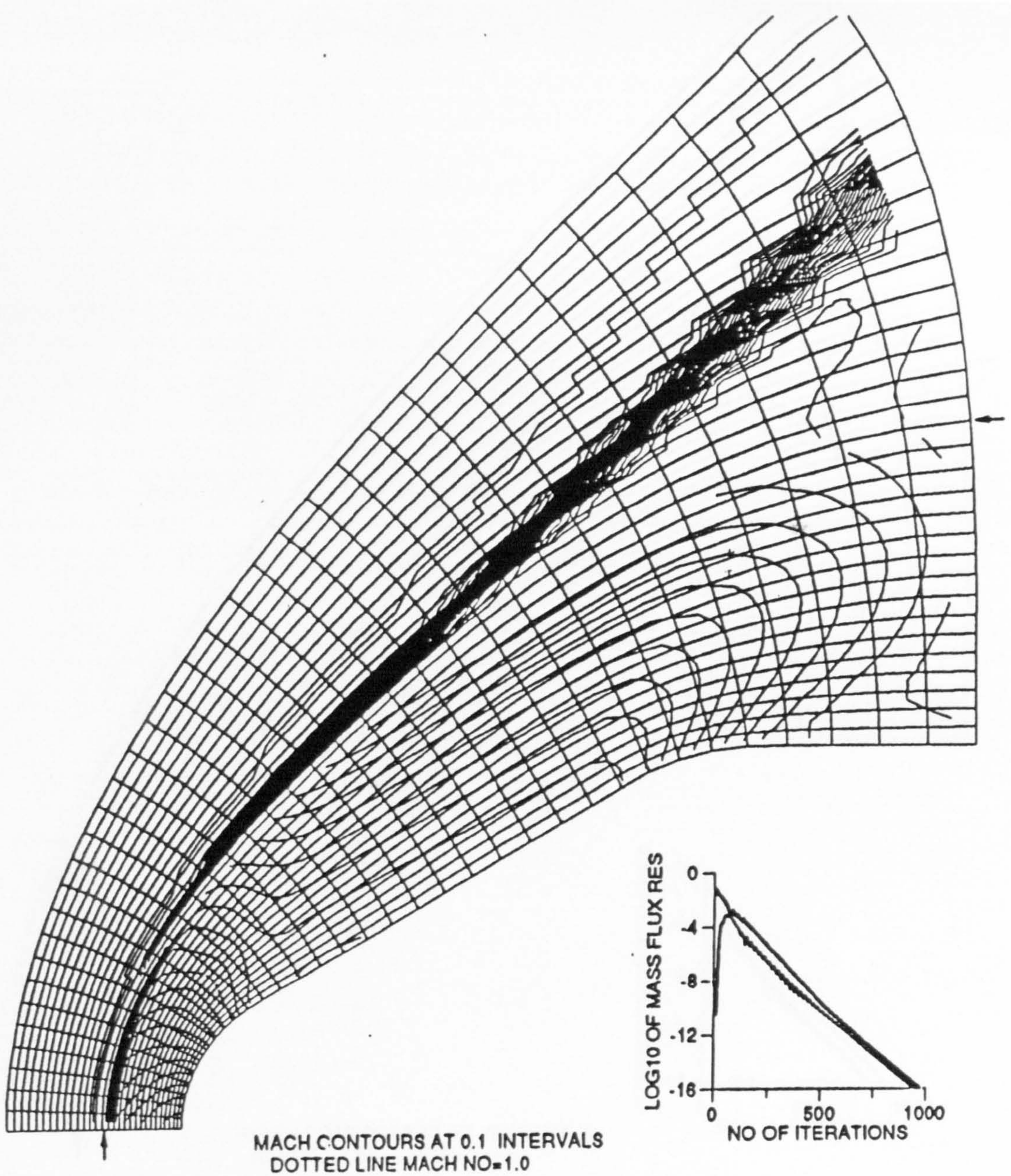

CONSERVATIVE IMPLICIT OPERATOR WITH DDADI+UNSYN 14X35+16X35 CELLS
VAN ALBADA LIMITER MACH NO.=5. LOCAL CFL=10 $\tilde{\delta}_{1,4}=0.25$ $\tilde{\delta}_{2,3}=0.5$

Fig. 5.10 Two-zone calculation of Mach 5 flow past reentry body (C)

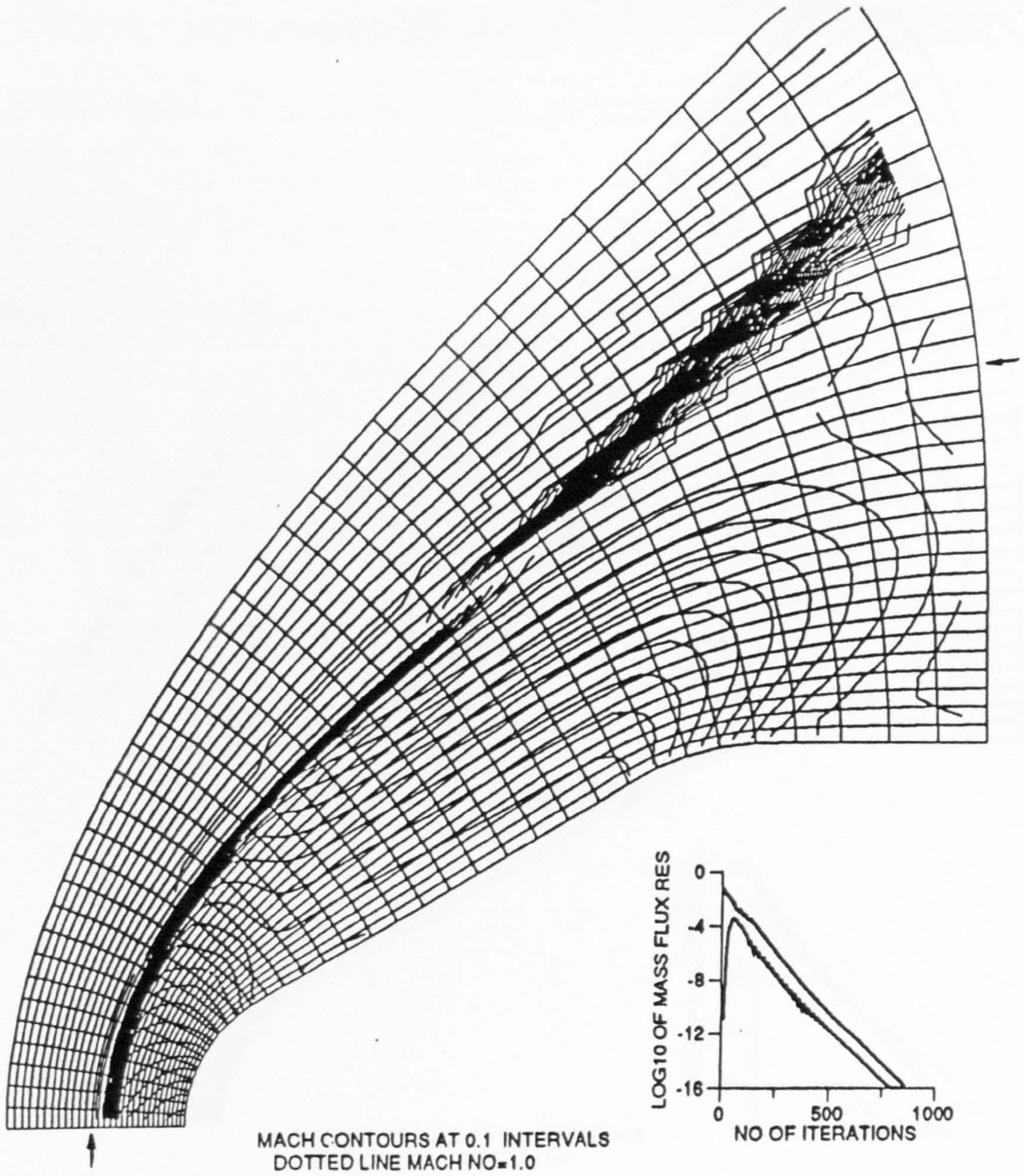

CONSERVATIVE IMPLICIT OPERATOR WITH DDADI+UNSYN 12X35+18X35 CELLS
VAN ALBADA LIMITER MACH NO.=5. LOCAL CFL=10 $\delta_{1,4}=0.25$ $\delta_{2,3}=0.5$

Fig. 5.11 Two-zone calculation of Mach 5 flow past reentry body (D)

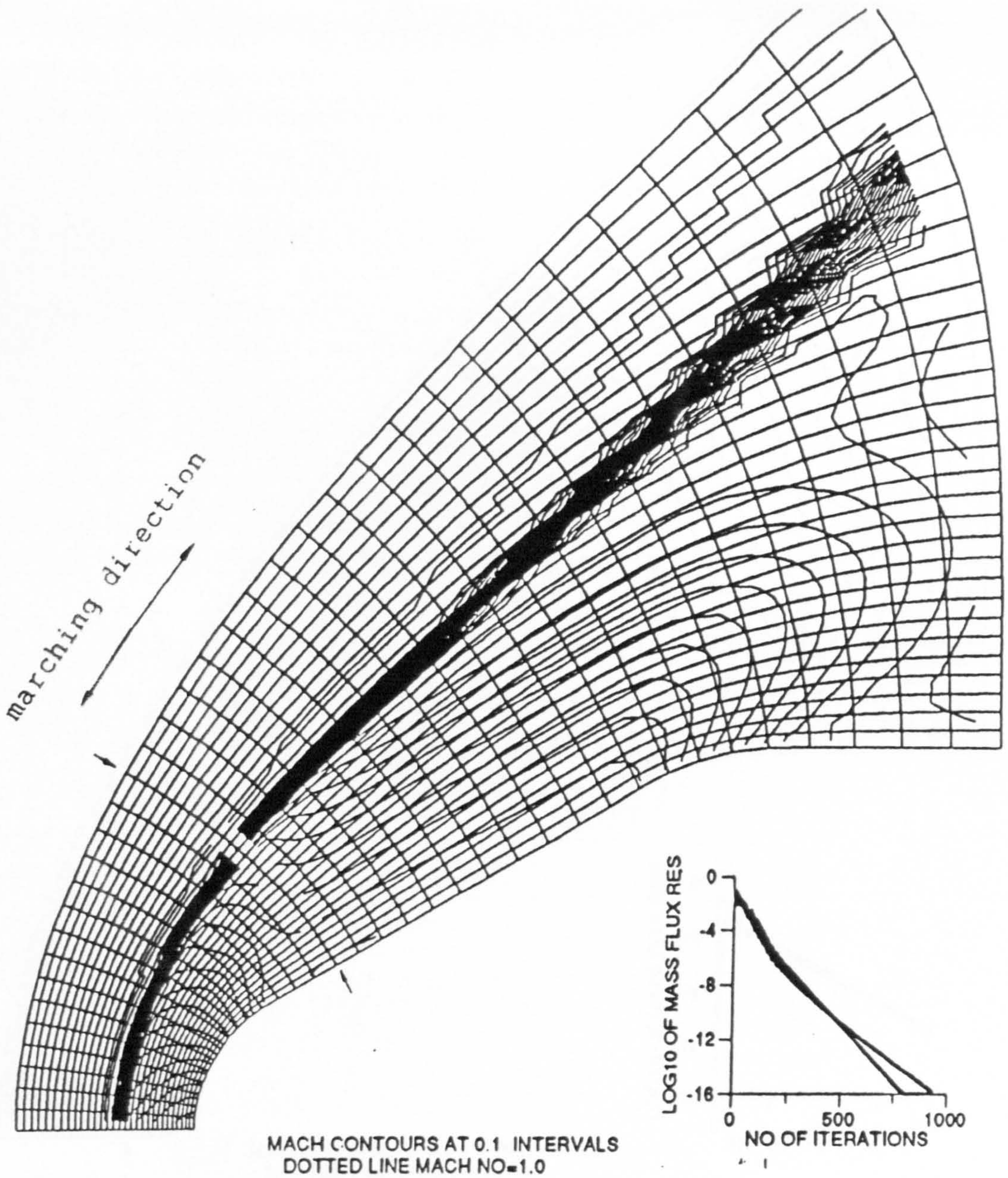

CONSERVATIVE IMPLICIT OPERATOR WITH METHOD 5+UNSYN 30X15+30X20 CELLS
VAN ALBADA LIMITER MACH NO.=5. LOCAL CFL=10 $\delta_{i,j}=0.25$ $\gamma_{e,s}=0.5$

Fig. 5.12 Two-zone calculation of Mach 5 flow past reentry body (E)

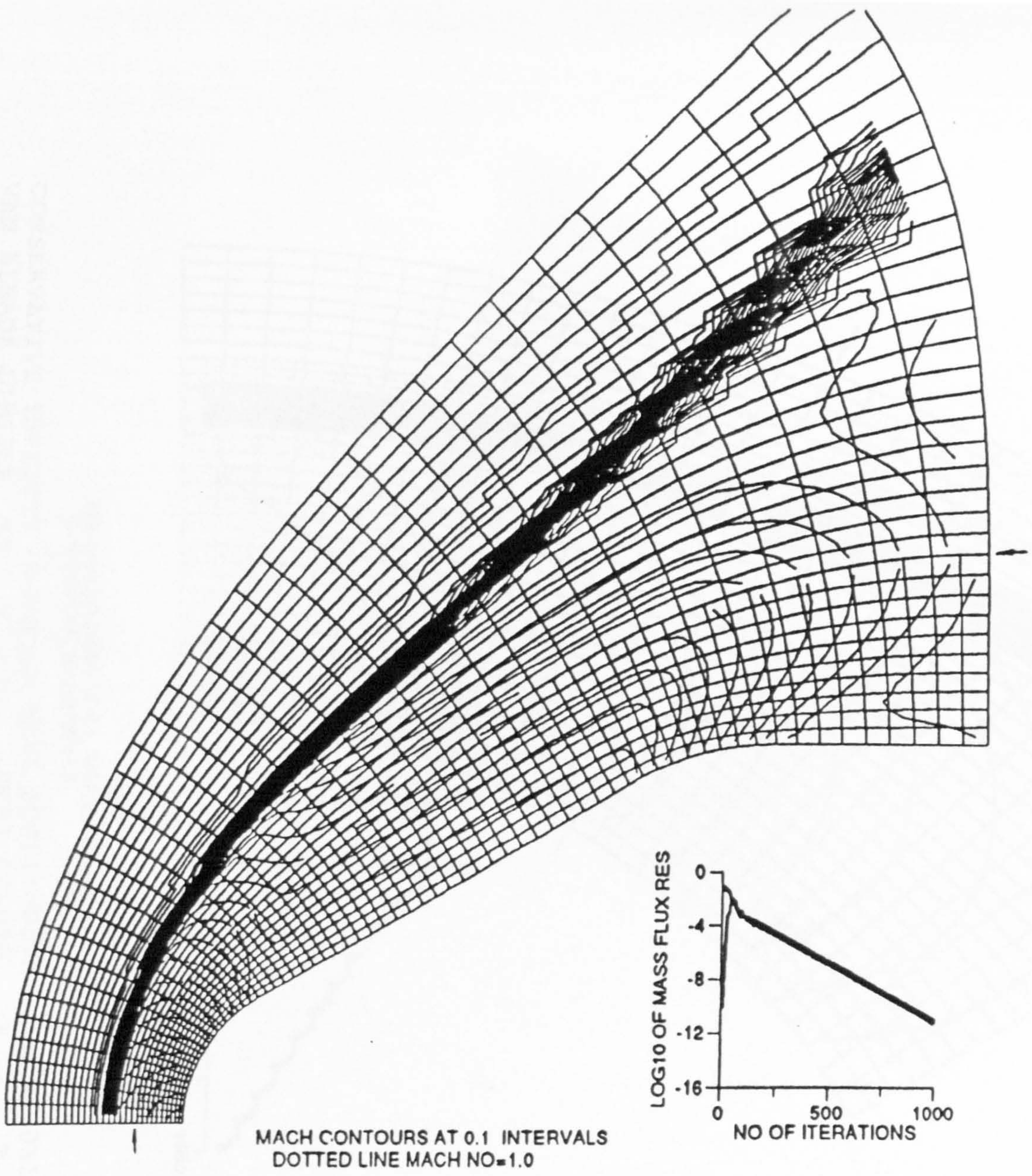

CONSERVATIVE IMPLICIT OPERATOR WITH DDADI+UNSYN 20X35+10X70 CELLS
VAN ALBADA LIMITER MACH NO.=5. LOCAL CFL=10 $\delta_{1,4}=0.25$ $\delta_{2,3}=0.5$

Fig. 5.13 Two-zone calculation of Mach 5 flow past reentry body (F)

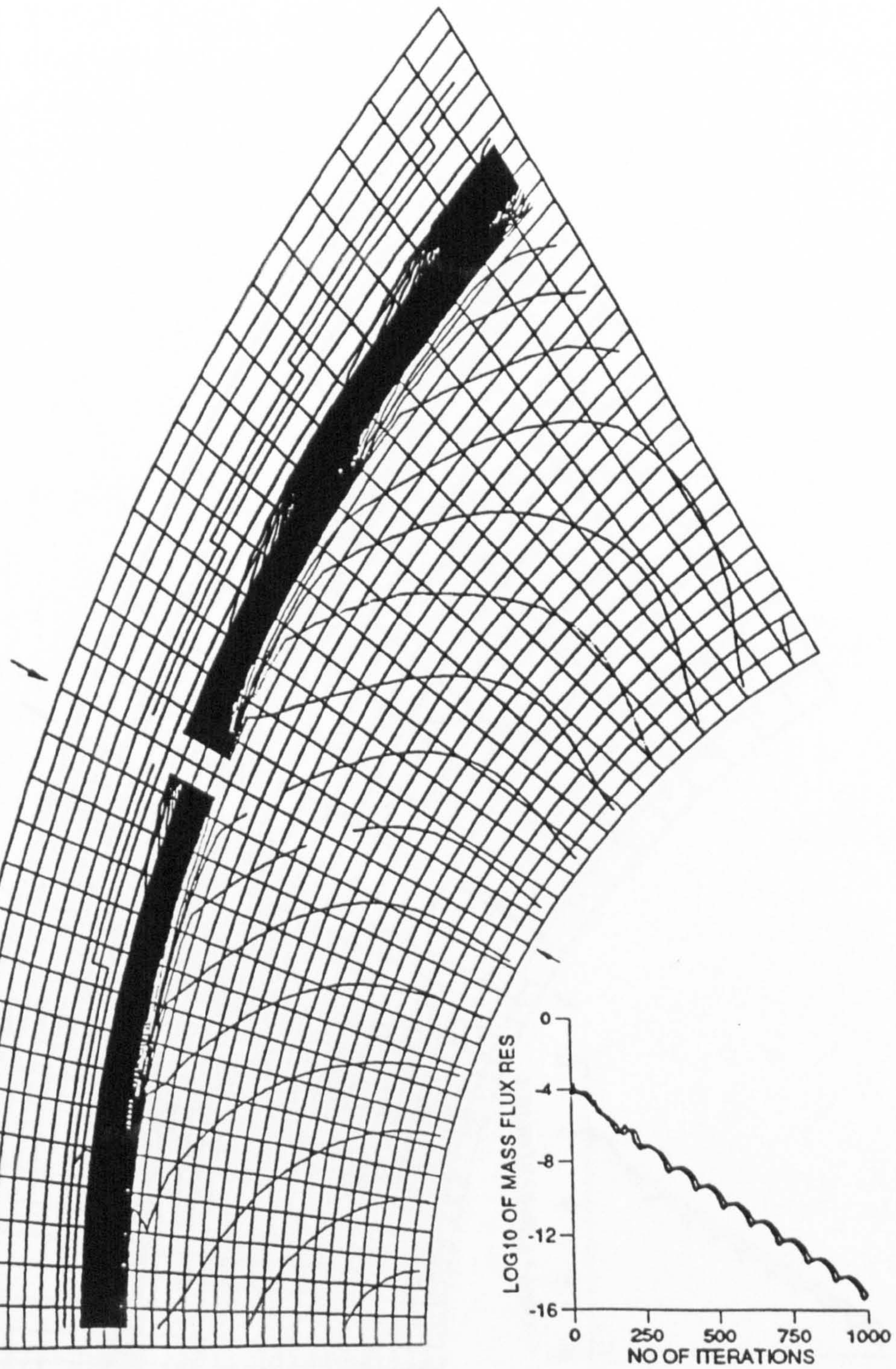

MACH CONTOURS AT 0.1 INTERVALS
DOTTED LINE MACH NO=1.0

CONSERVATIVE IMPLICIT OPERATOR WITH DDADI+UNSYN 30X15+30X15 CELLS
VAN ALBADA LIMITER MACH NO.=20. LOCAL CFL=10 $\tilde{\delta}_{1,4}=0.25$ $\tilde{\delta}_{2,3}=0.8$

Fig. 5.14 Two-zone calculation of Mach 20 flow past quarter cylinder (A)

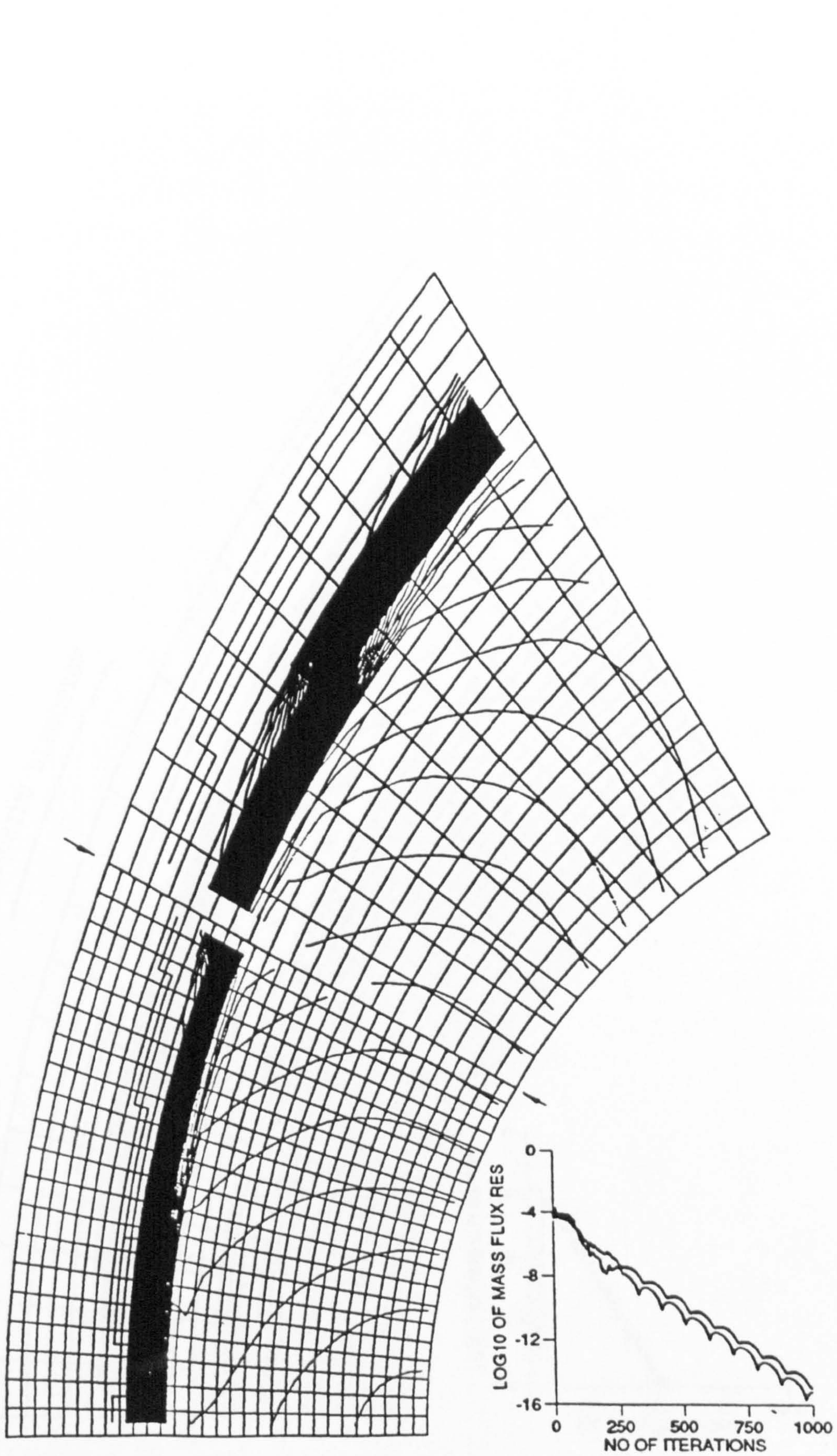

MACH CONTOURS AT 0.1 INTERVALS
DOTTED LINE MACH NO=1.0

CONSERVATIVE IMPLICIT OPERATOR WITH DDADI+UNSYN 30X20+20X10 CELLS
VAN ALBADA LIMITER MACH NO.=20. LOCAL CFL=10 $\tilde{\delta}_{1,4}=0.25$ $\tilde{\delta}_{2,3}=0.8$

Fig. 5.15 Two-zone calculation of Mach 20 flow past quarter cylinder (B)

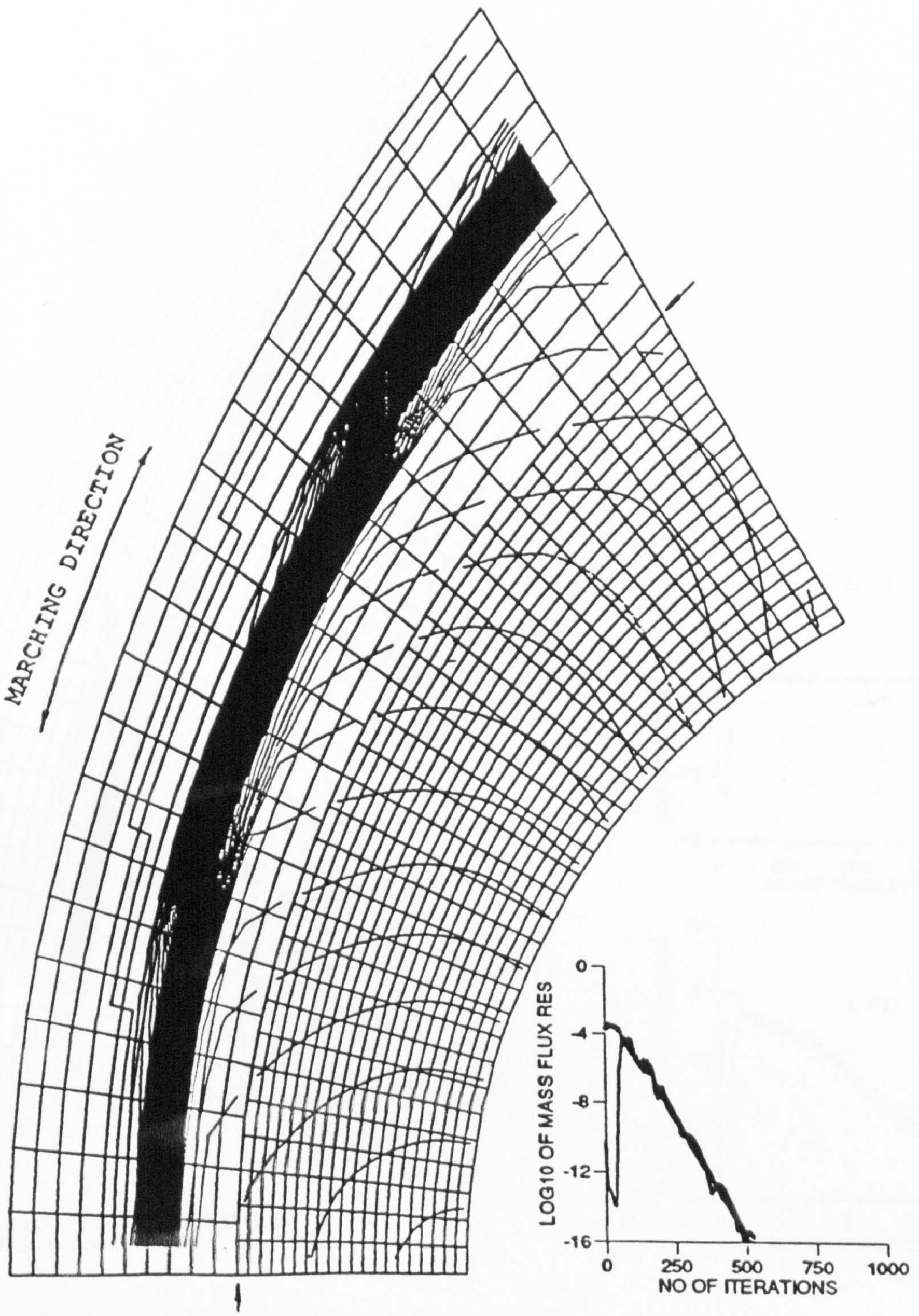

MACH CONTOURS AT 0.1 INTERVALS
DOTTED LINE MACH NO=1.0

CONSERVATIVE IMPLICIT OPERATOR WITH METHOD 5+UNSYN 10X20+20X30 CELLS
VAN ALBADA LIMITER MACH NO.=20. LOCAL CFL=10 $\tilde{\delta}_{1,4}=0.25$ $\tilde{\delta}_{2,3}=0.8$

Fig. 5.16 Two-zone calculation of Mach 20 flow past quarter cylinder (C)

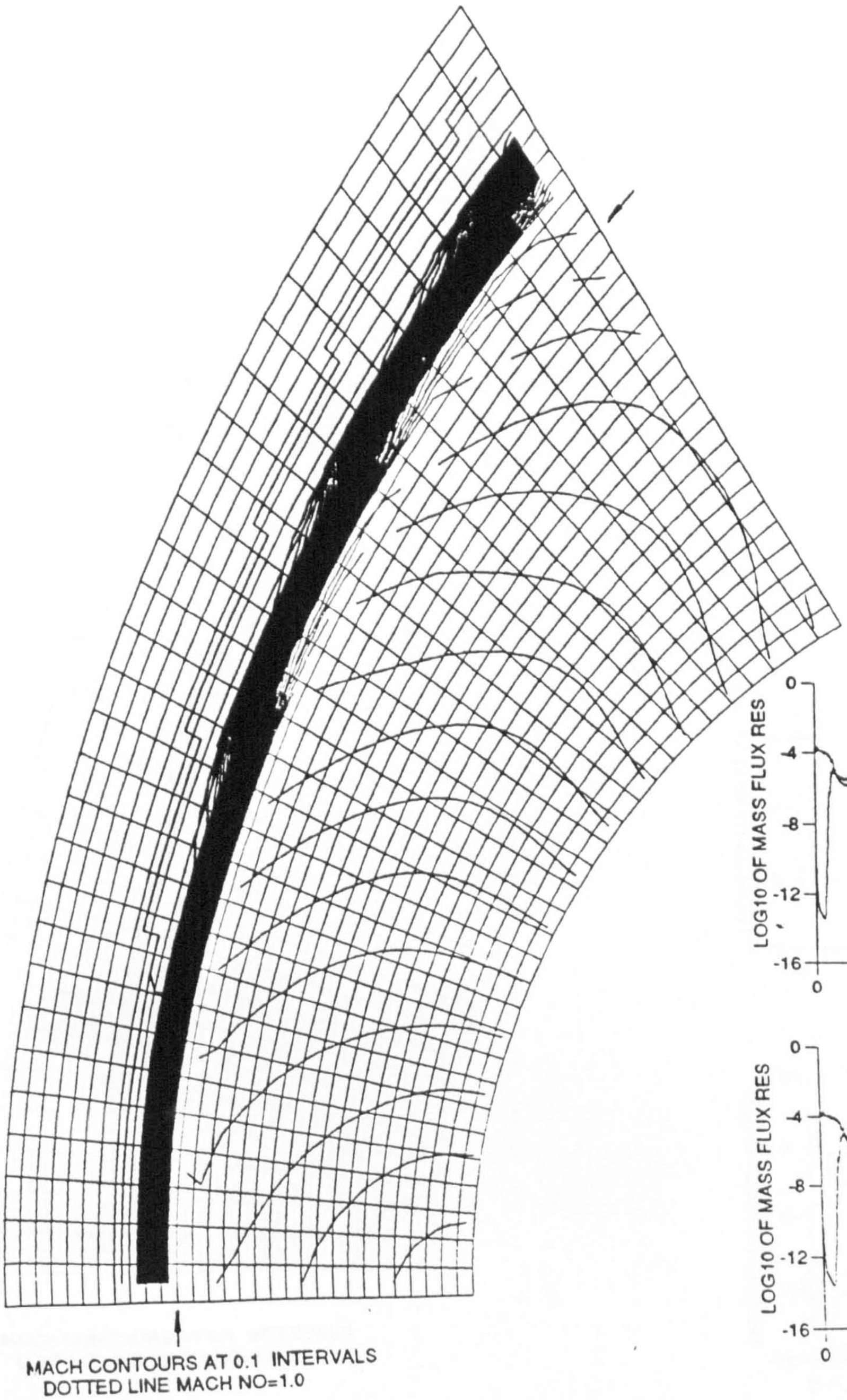

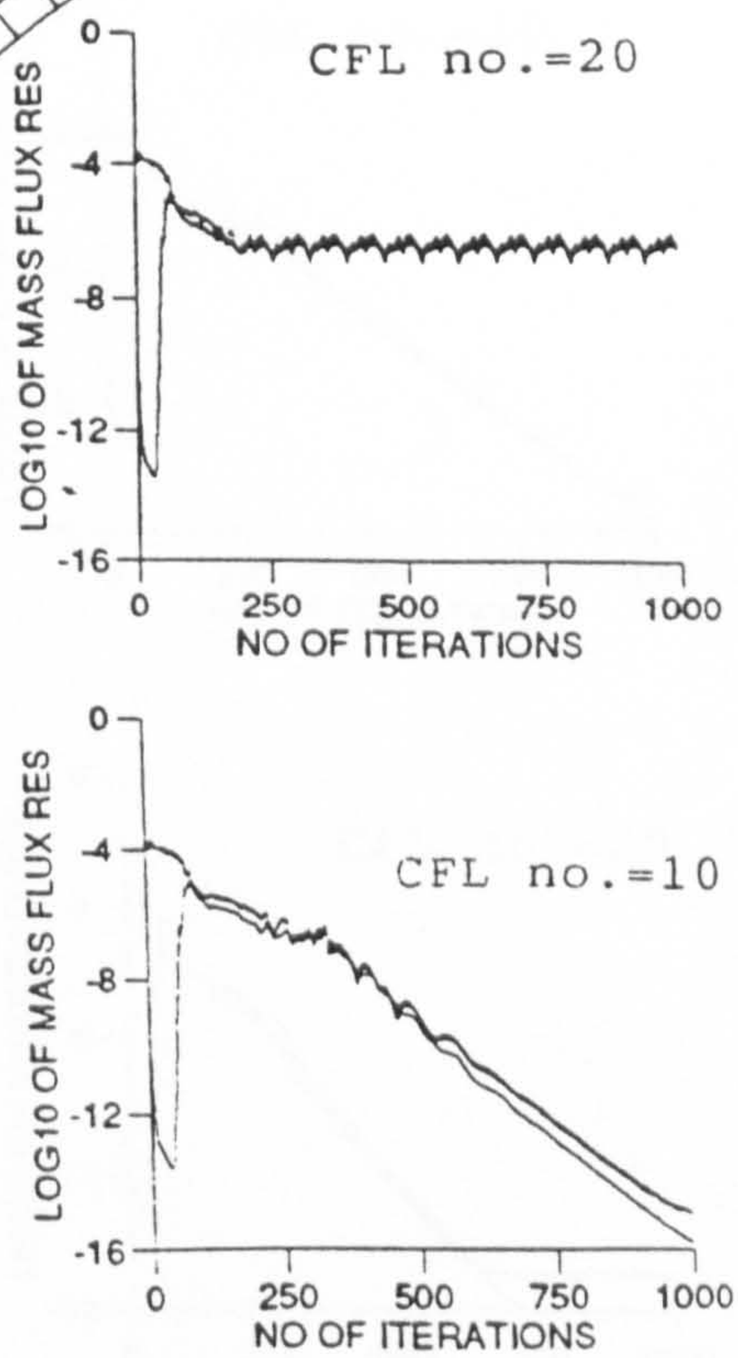

conservative implicit operator with DDADI+UNSYN
11x30+19x30 cells Van Albada limiter Mach no.=20.

$\tilde{\delta}_{1,4}=0.25 \quad \tilde{\delta}_{2,3}=0.8$

Fig. 5.17 Two-zone calculation of Mach 20 flow past quarter cylinder (D)

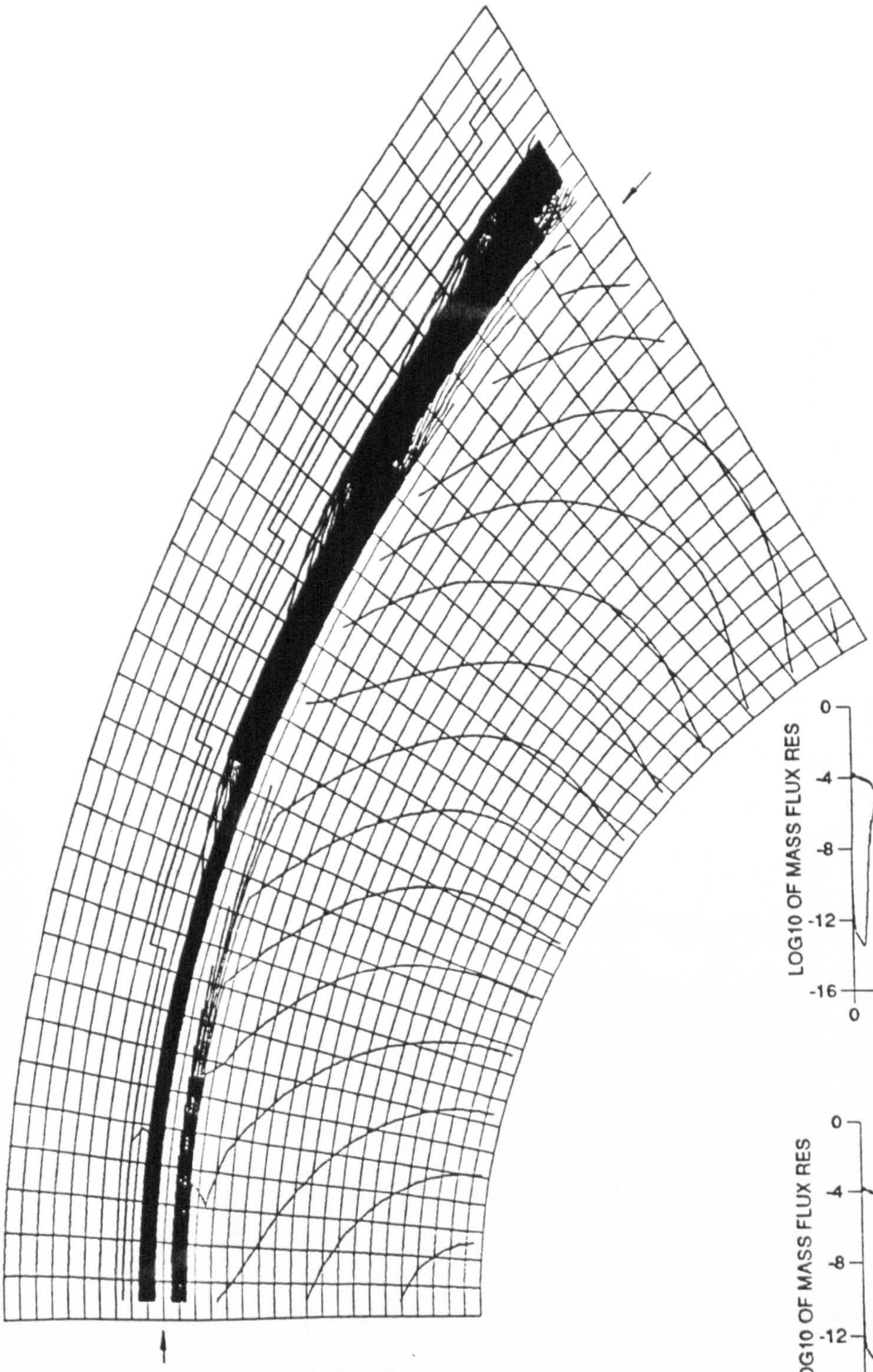

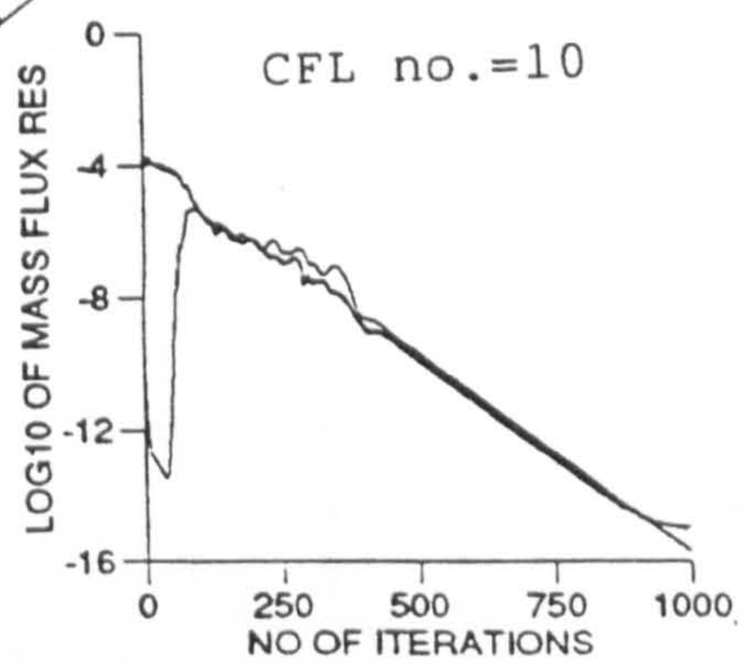

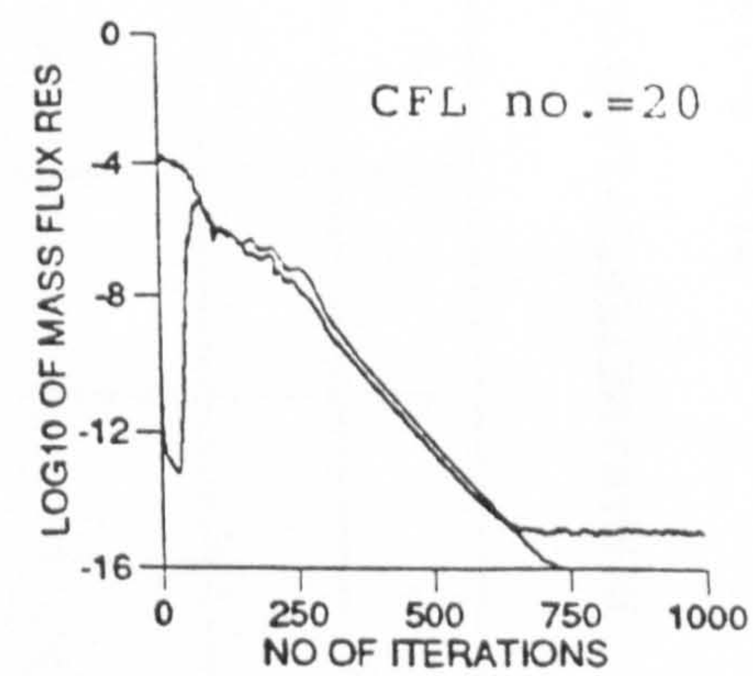

conservative implicit operator with DDADI+UNSYN
10x30+20x30 cells Van Albada limiter Mach no.=20.

$\tilde{\delta}_{1,4}=0.25 \quad \tilde{\delta}_{2,3}=0.8$

Fig. 5.18 Two-zone calculation of Mach 20 flow past quarter cylinder (E)

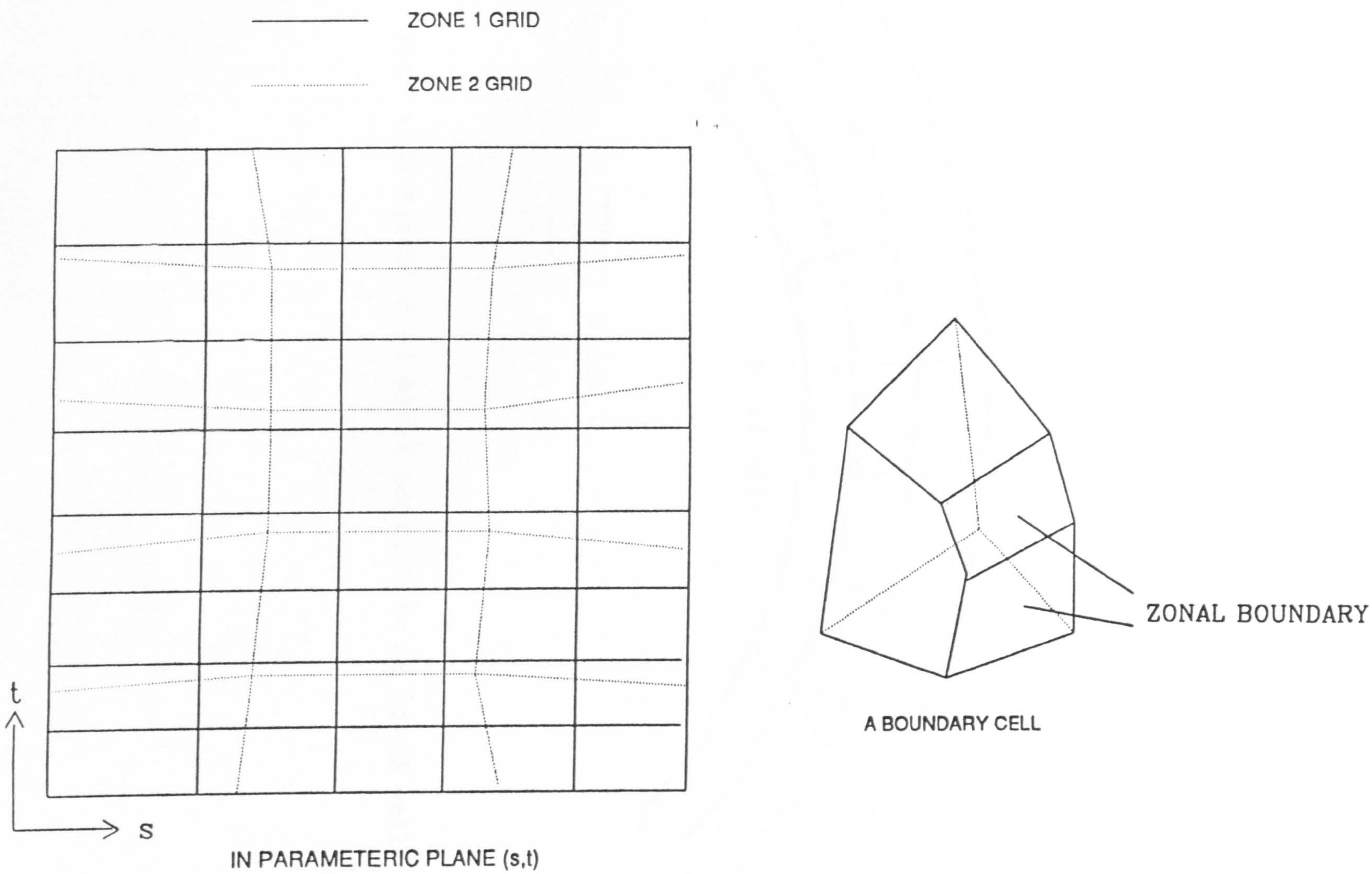

Fig. 5.19 Three dimensional zonal boundary

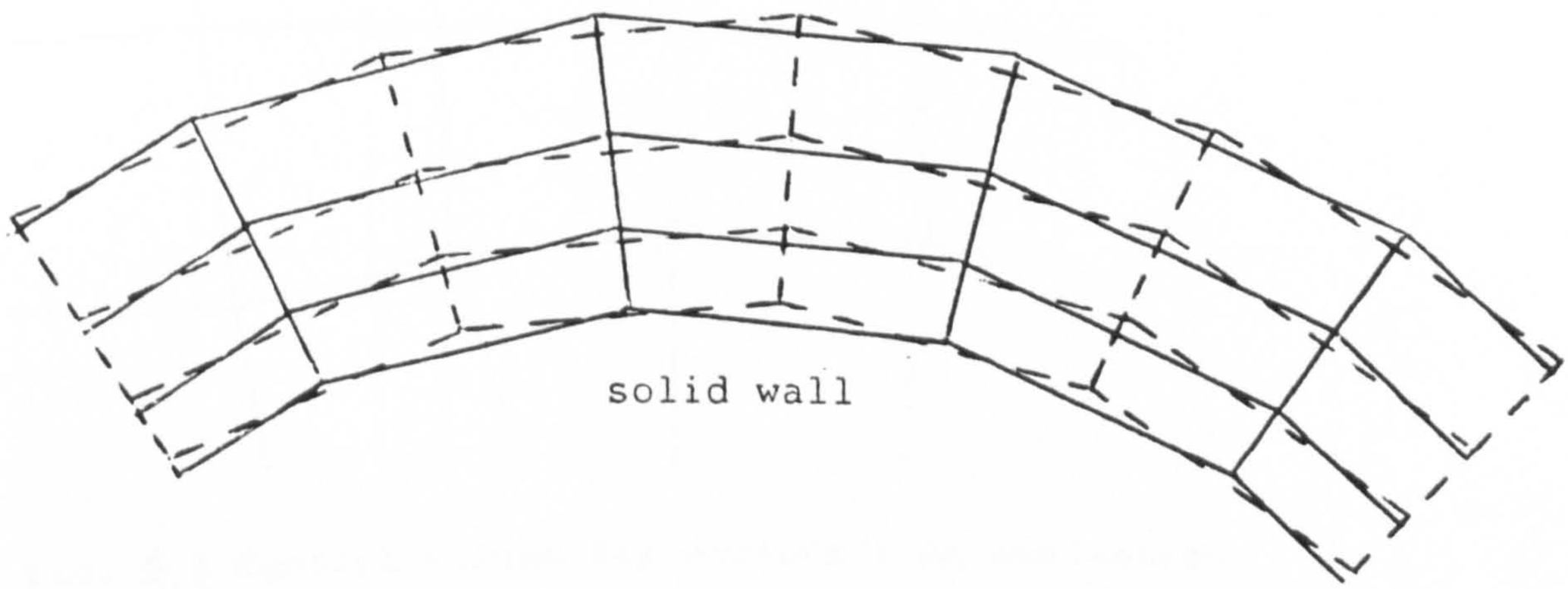

fig. 5.20 Mismatch of block boundaries at solid wall

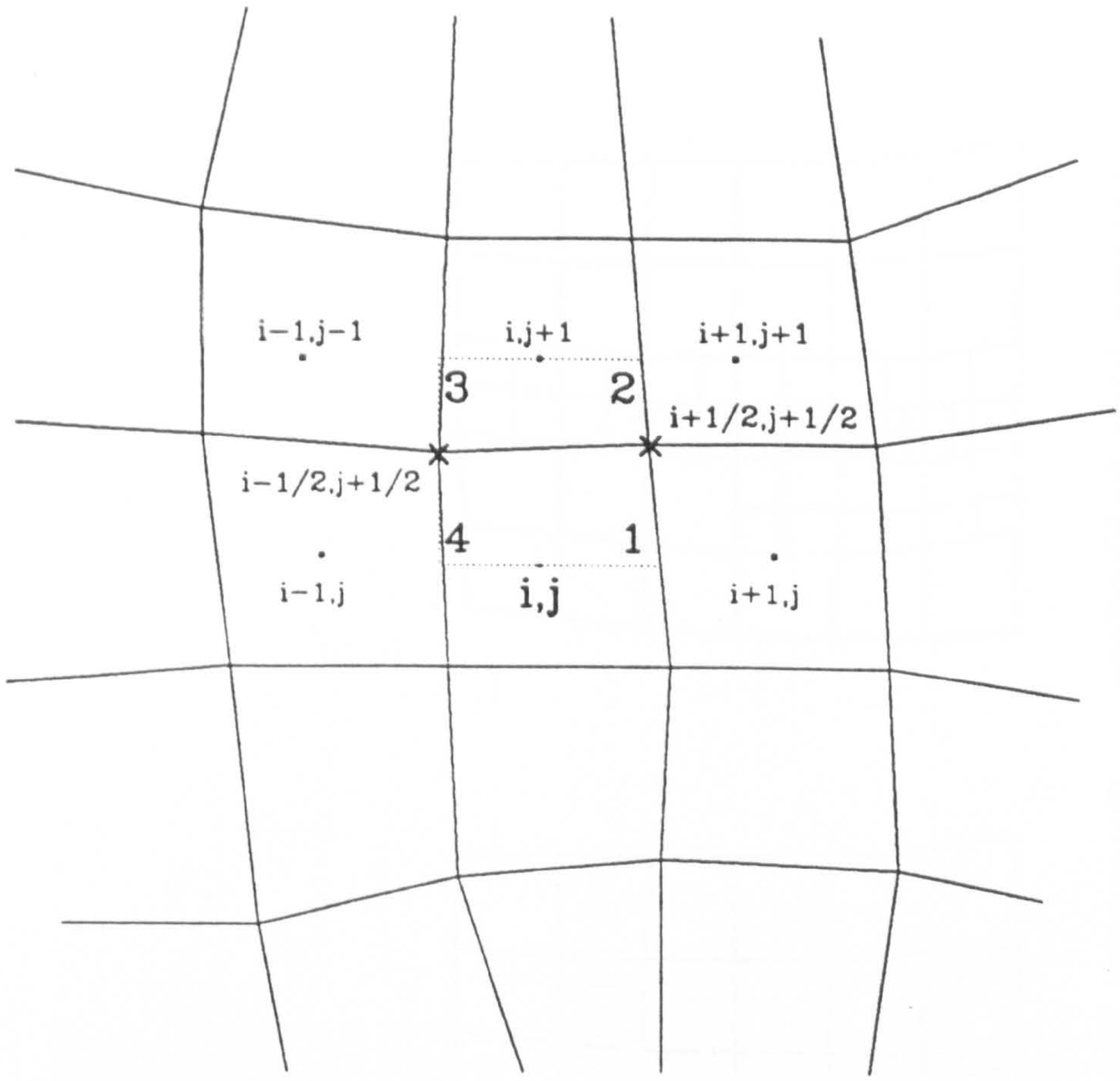

Fig. 6.1 Control volume for viscous flux evaluation

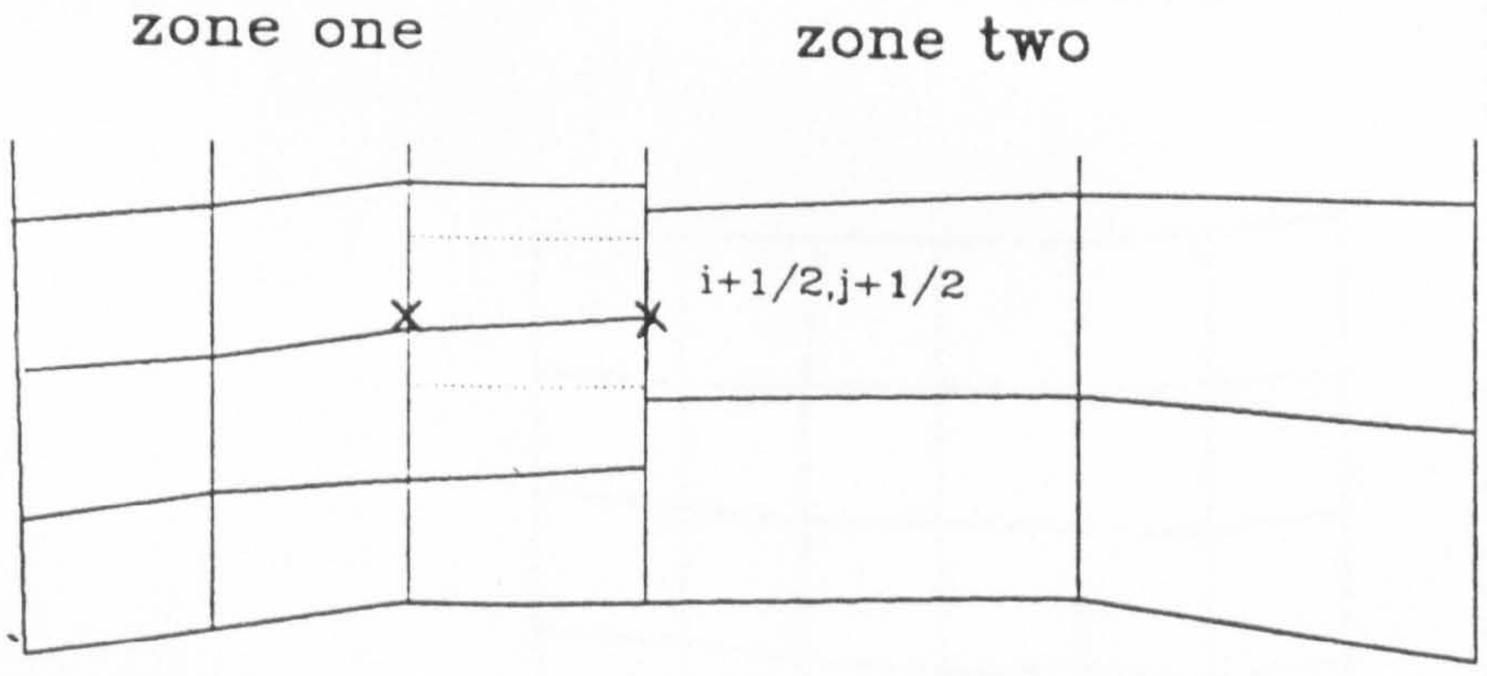

Fig. 6.2 Control volume near the zonal boundary

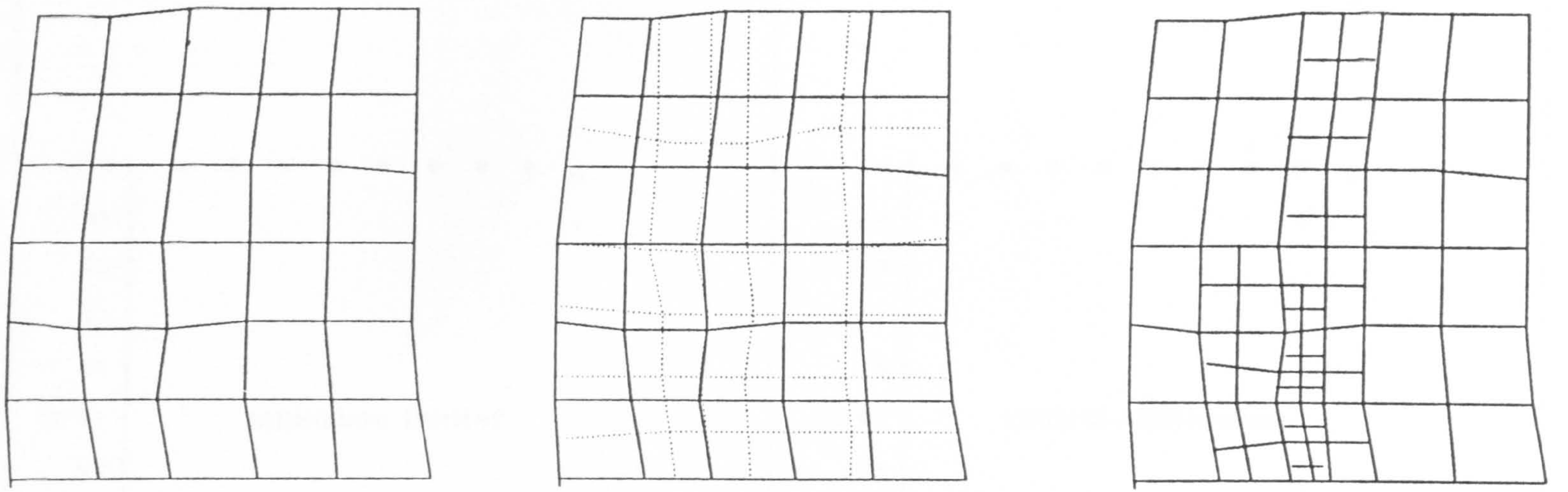

Fig. 6.3 Two types of adaptive grid

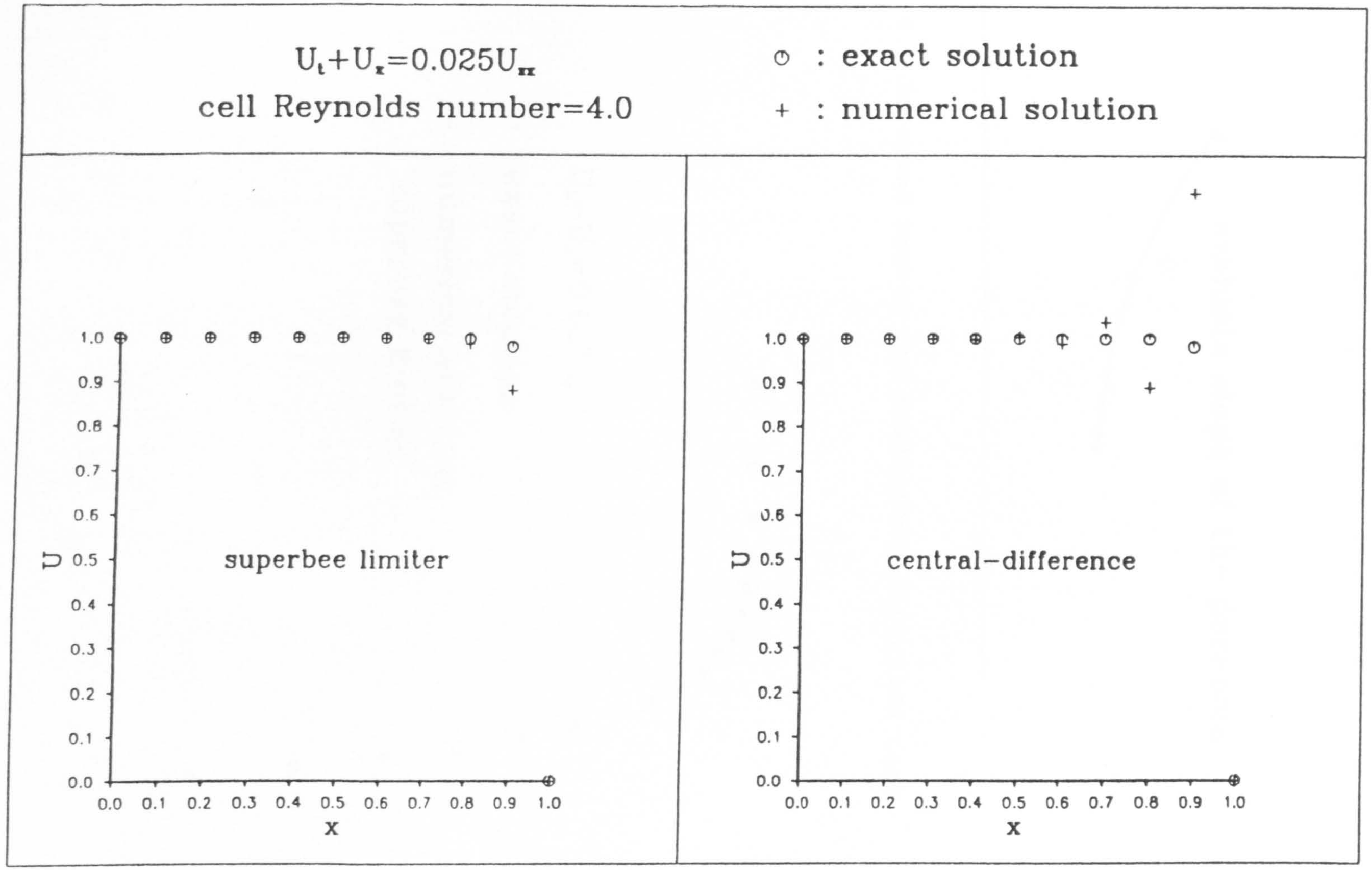

Fig. 6.4 Cell Reynolds number 4 results

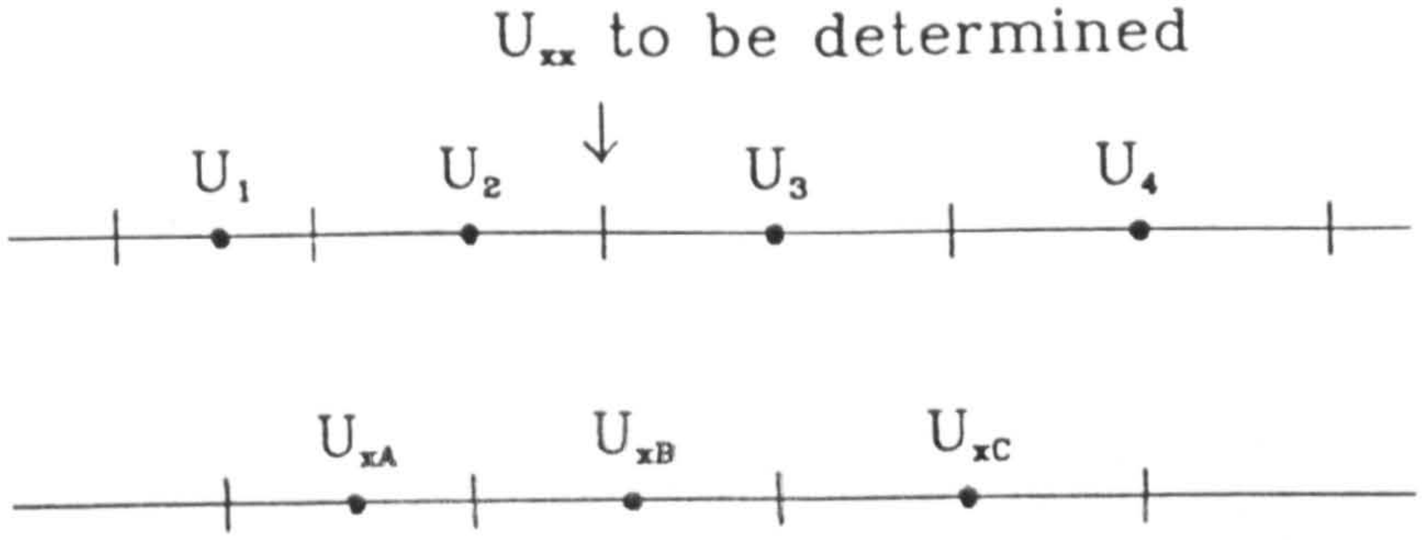

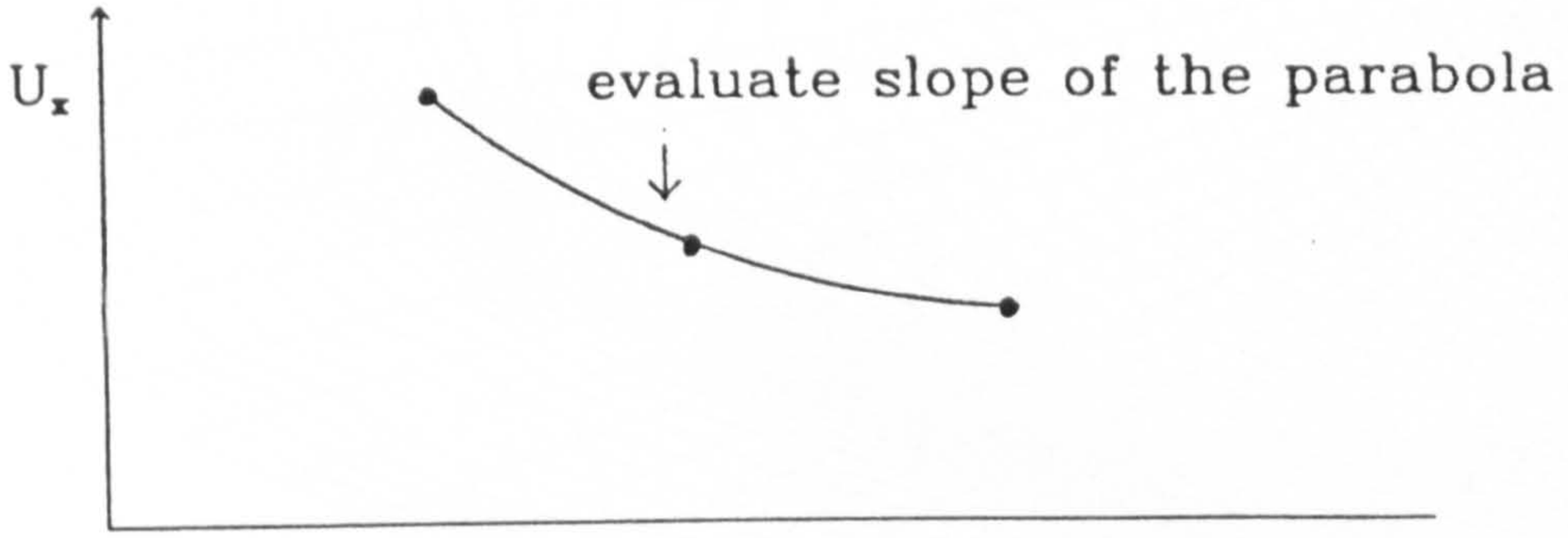

Fig. 6.5 Improved method for evaluating diffusion term

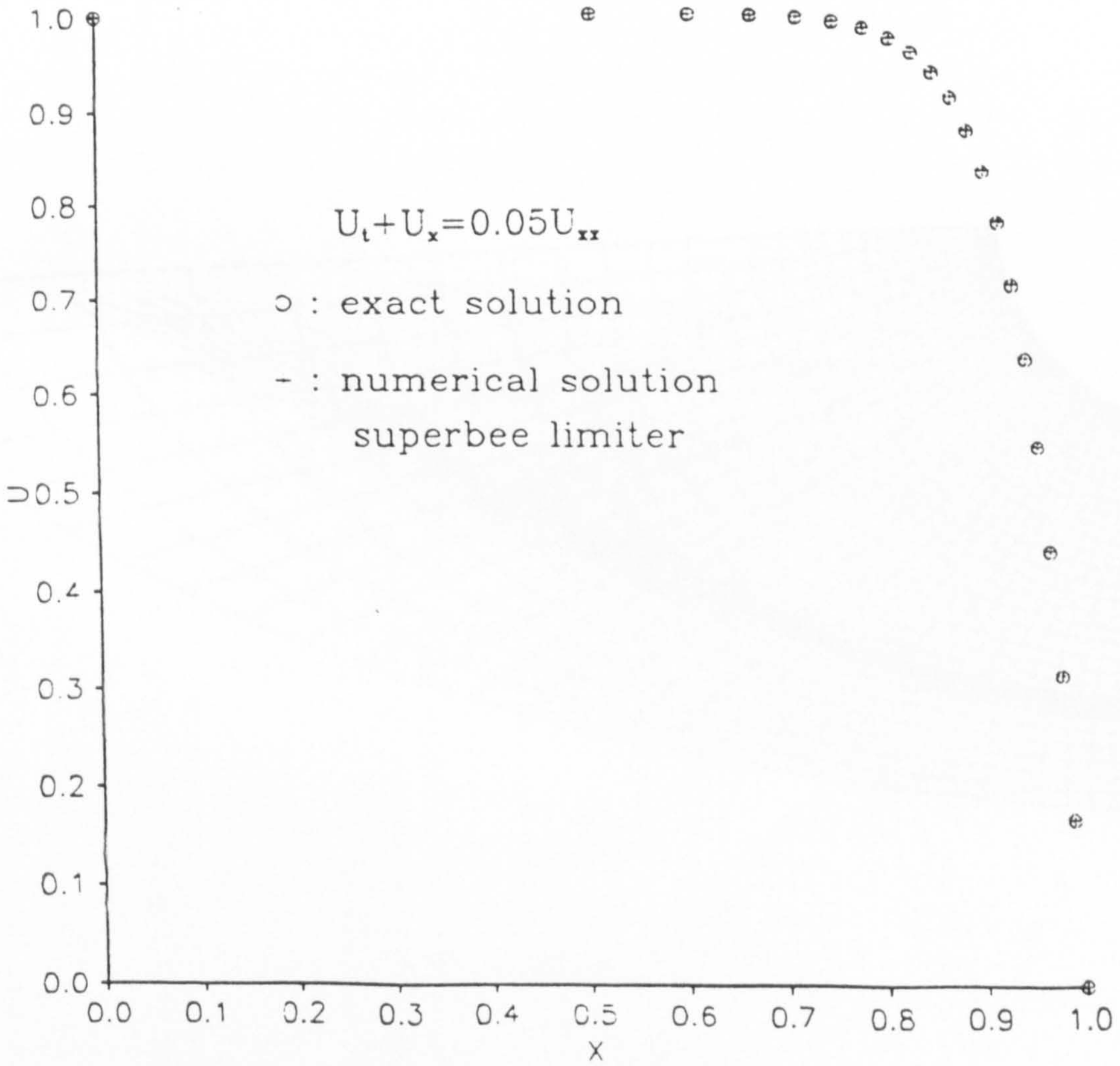

Fig. 6.6 Adaptive grid using Carey and Dinh's weight function

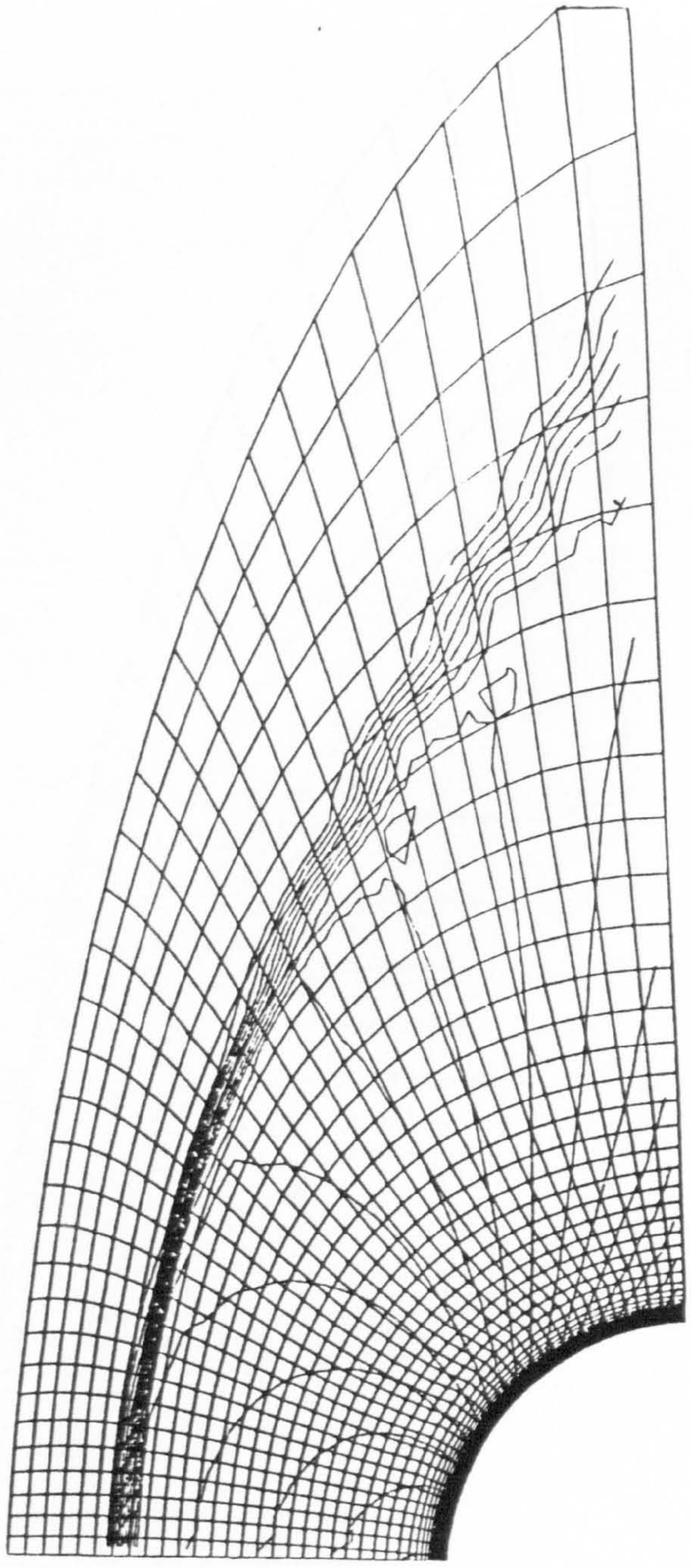

Fig. 6.7 Pressure contours of Mach 2 flow past cylinder

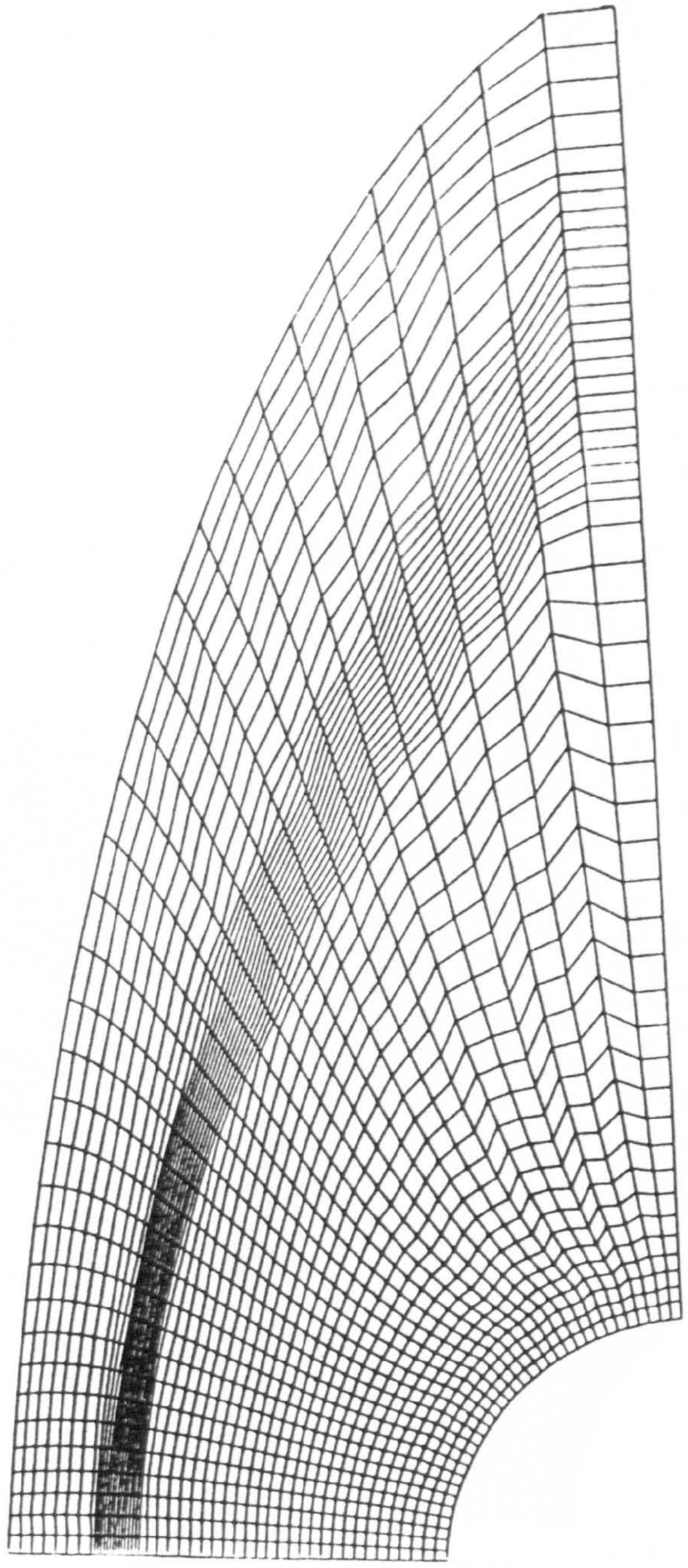

Fig. 6.8 Adaptive grid using unscaled equidistribution law

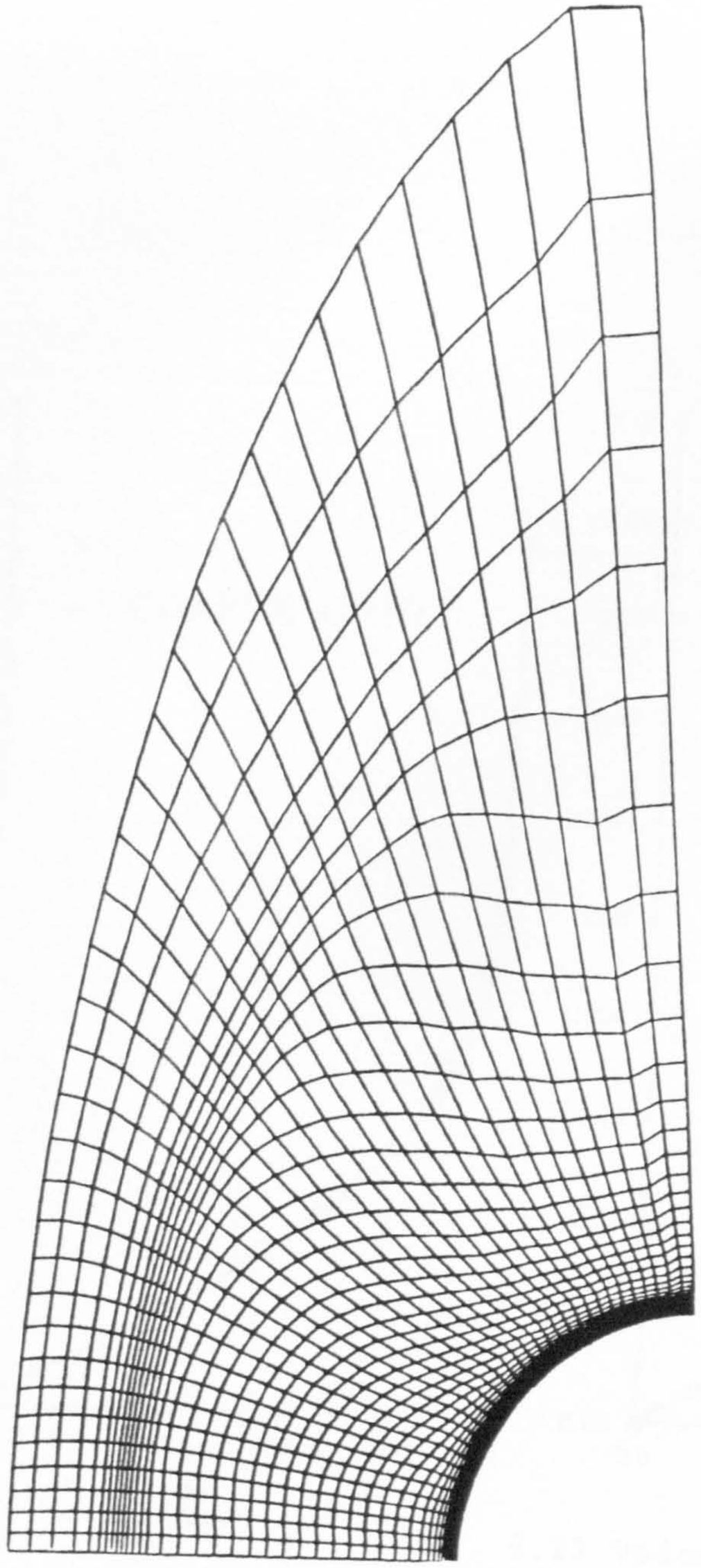

Fig. 6.9 Adaptive grid using scaled equidistribution law

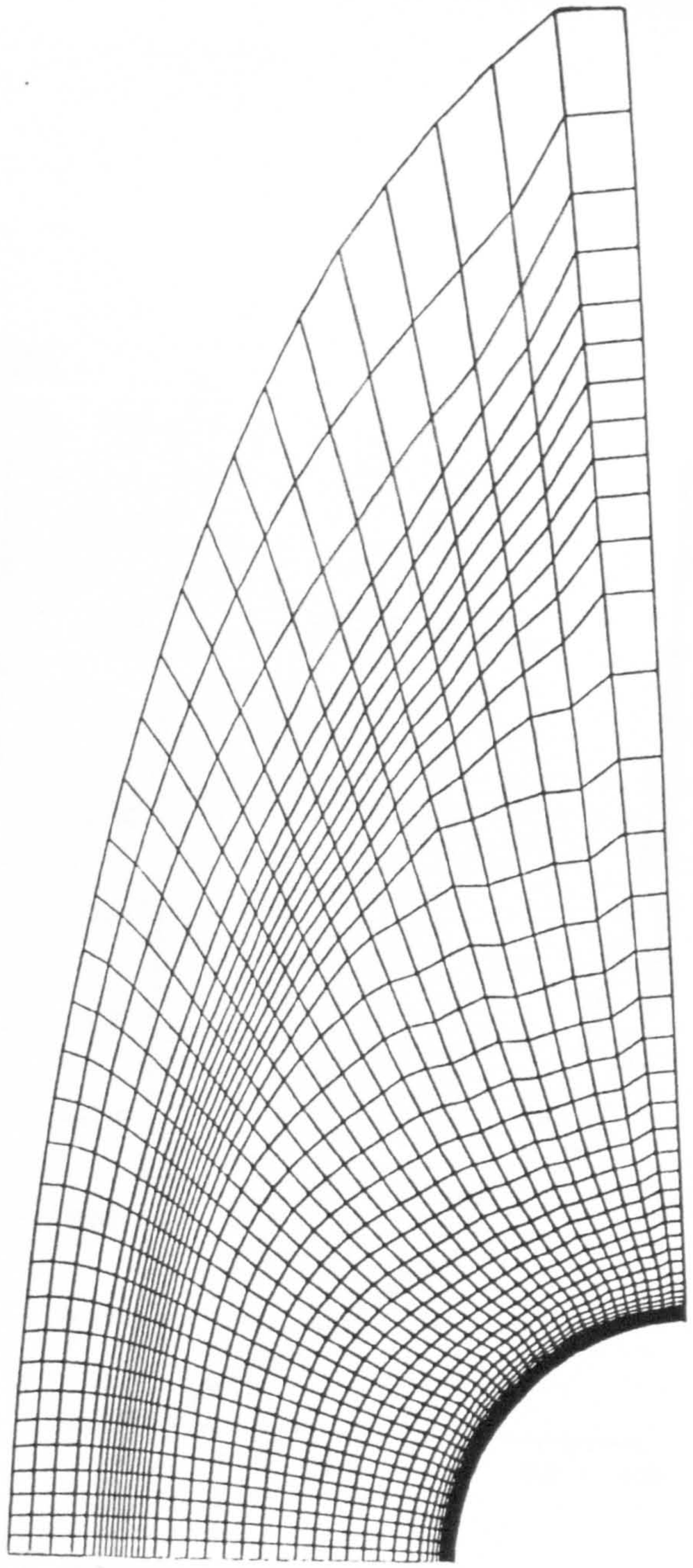

Fig. 6.10 Grid adaptive to pressure gradient based on grid index

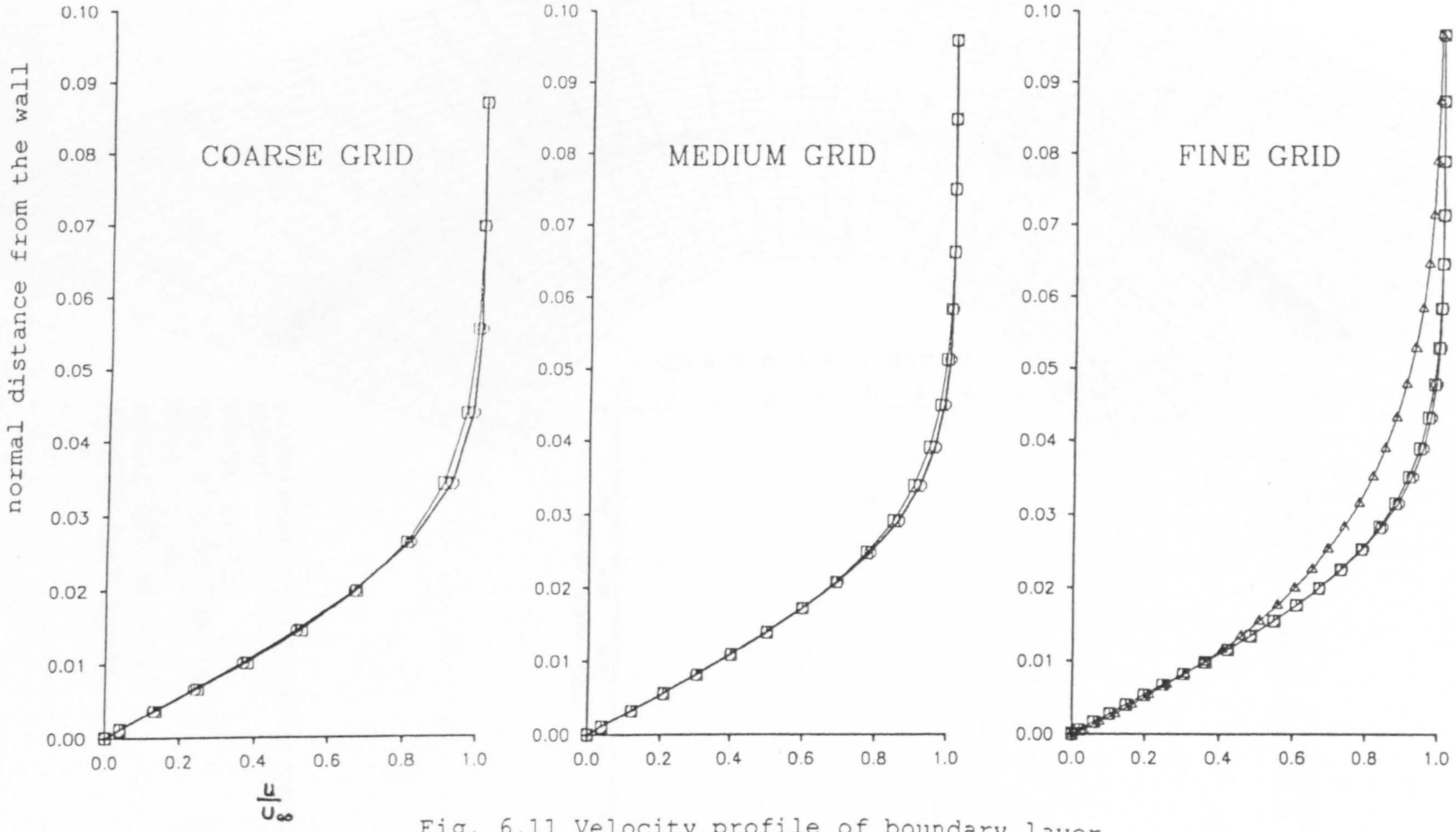

Fig. 6.11 Velocity profile of boundary layer

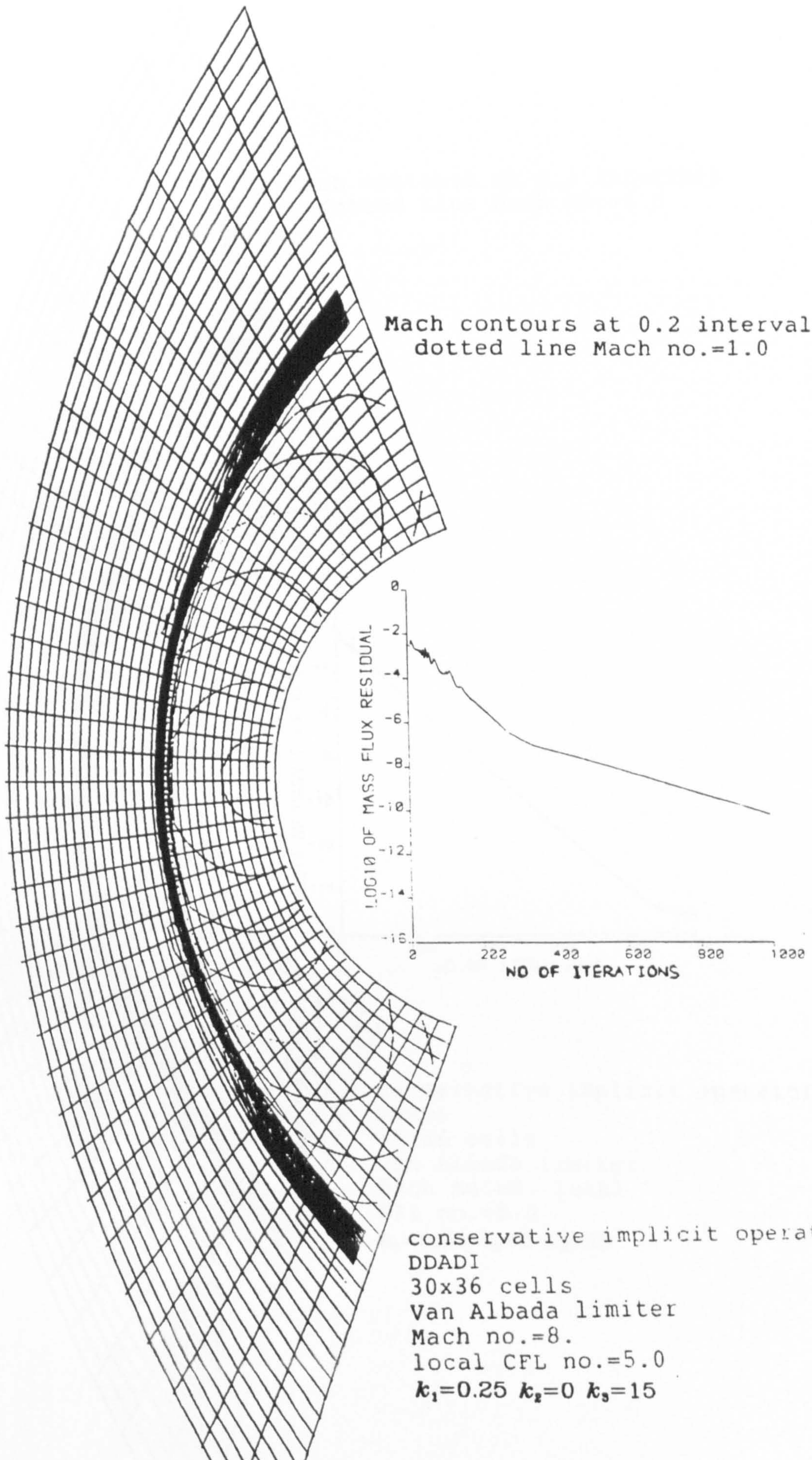

Fig. 6.12 Mach 8 calculation with modified dissipation (A)

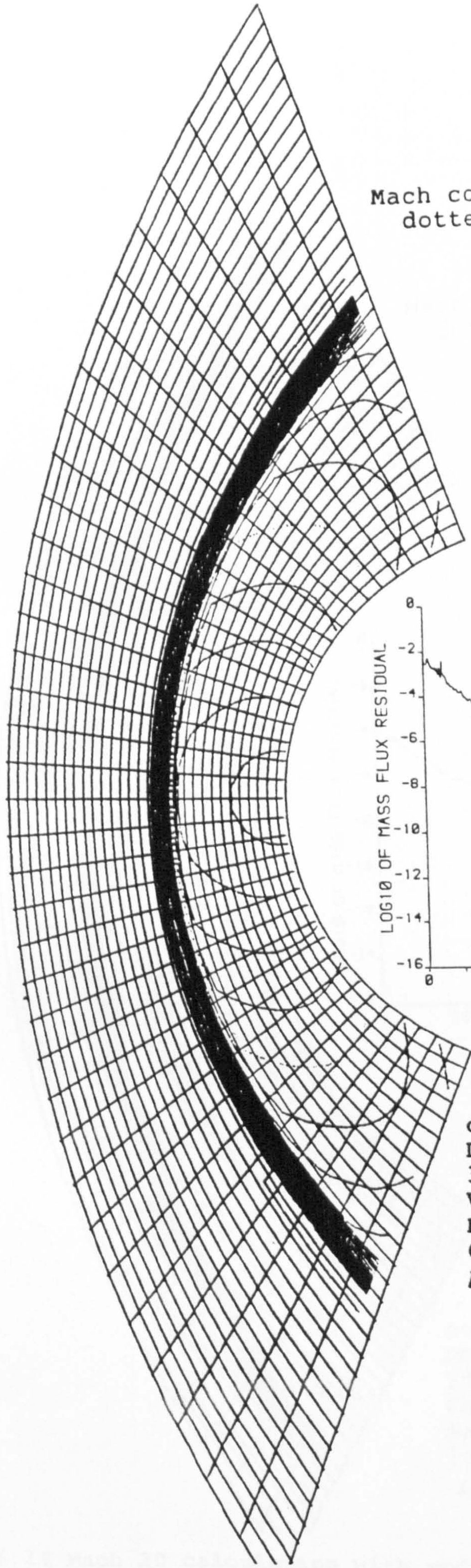

Mach contours at 0.2 intervals
dotted line Mach no.=1.0

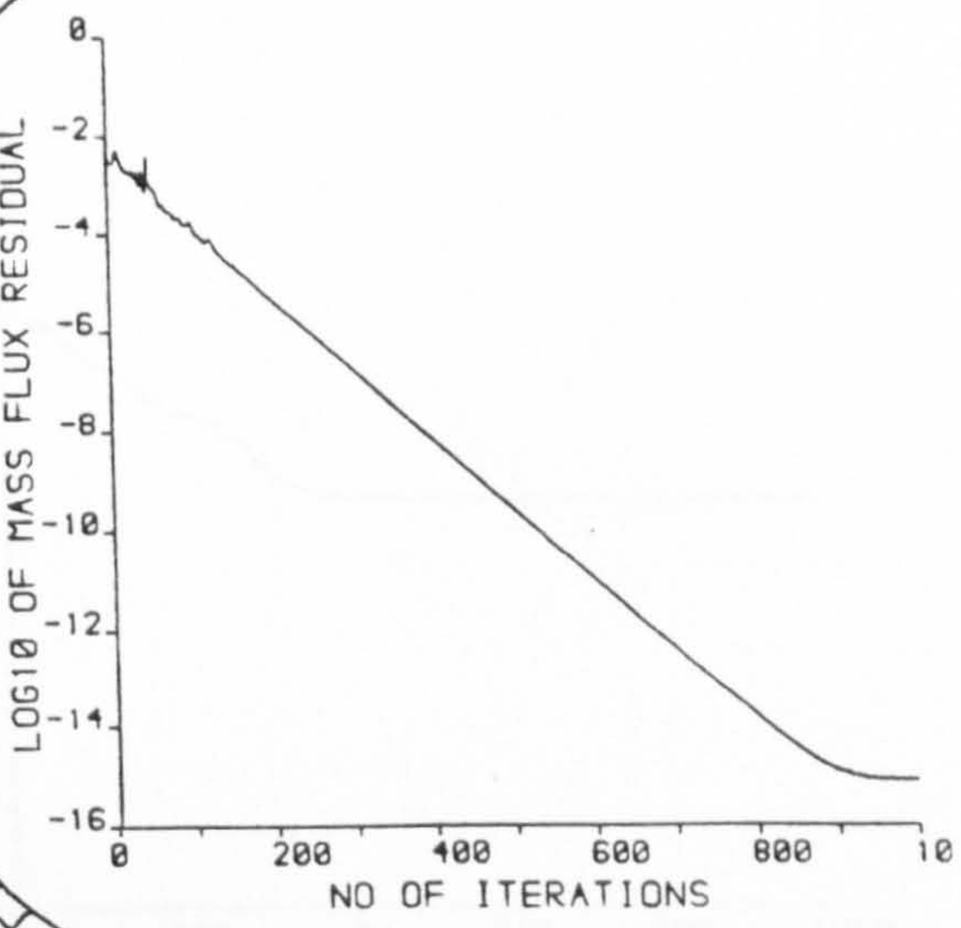

conservative implicit operator
DDADI
30x36 cells
Van Albada limiter
Mach no.=8. local
CFL no.=5.0
k_1=0.25 k_2=5 k_3=15

Fig. 6.13 Mach 8 calculation with modified dissipation (B)

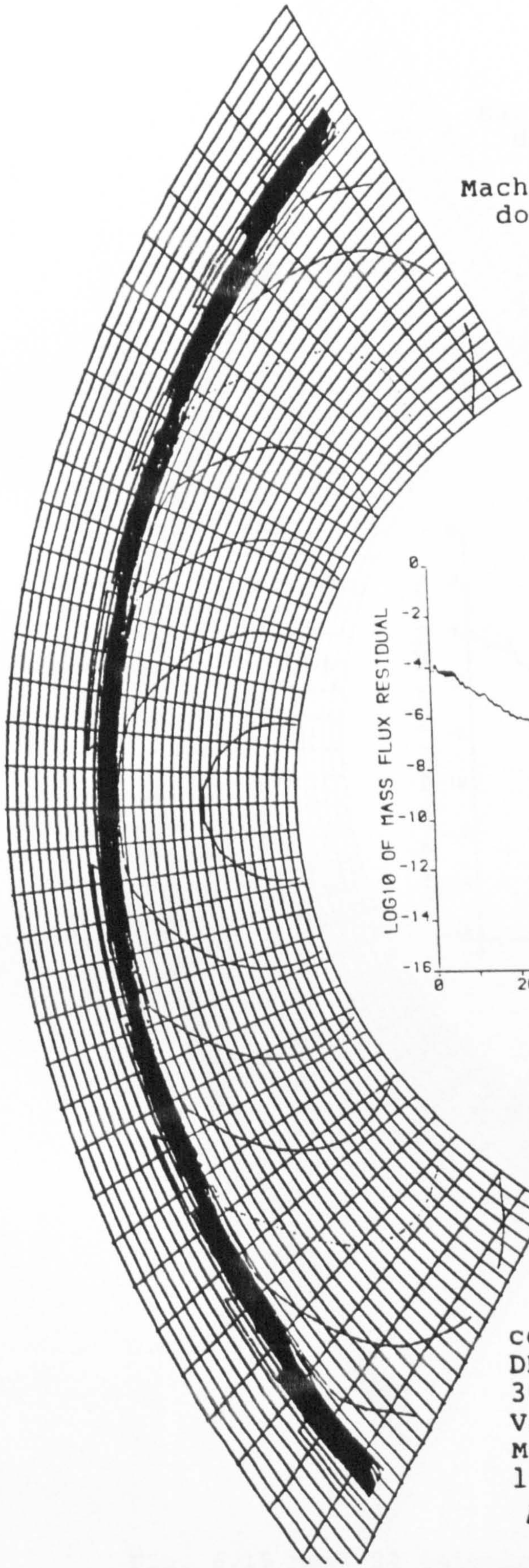

Mach contours at 0.2 intervals
dotted line Mach no.=1.0

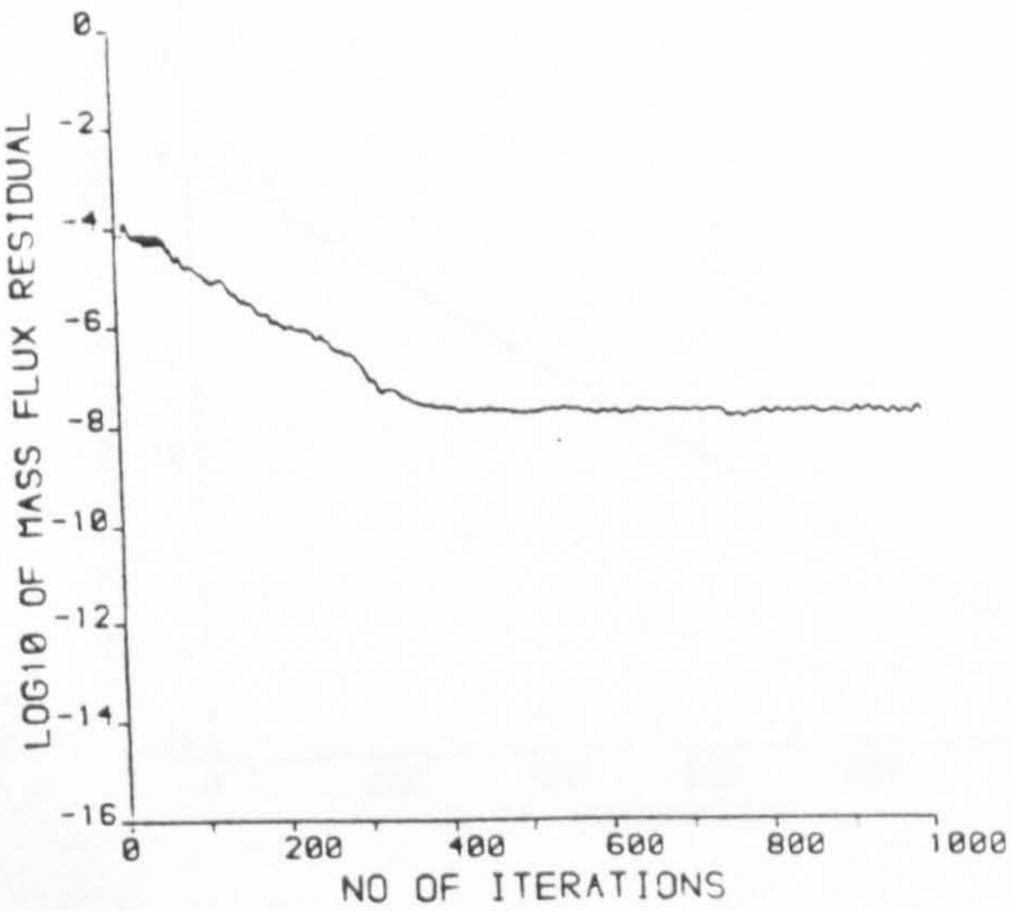

conservative implicit operator
DDADI
30x36 cells
Van Albada limiter
Mach no.=20.
local CFL no.=5.0
k_1=0.25 k_2=0 k_3=15

Fig. 6.14 Mach 20 calculation with modified dissipation (A)

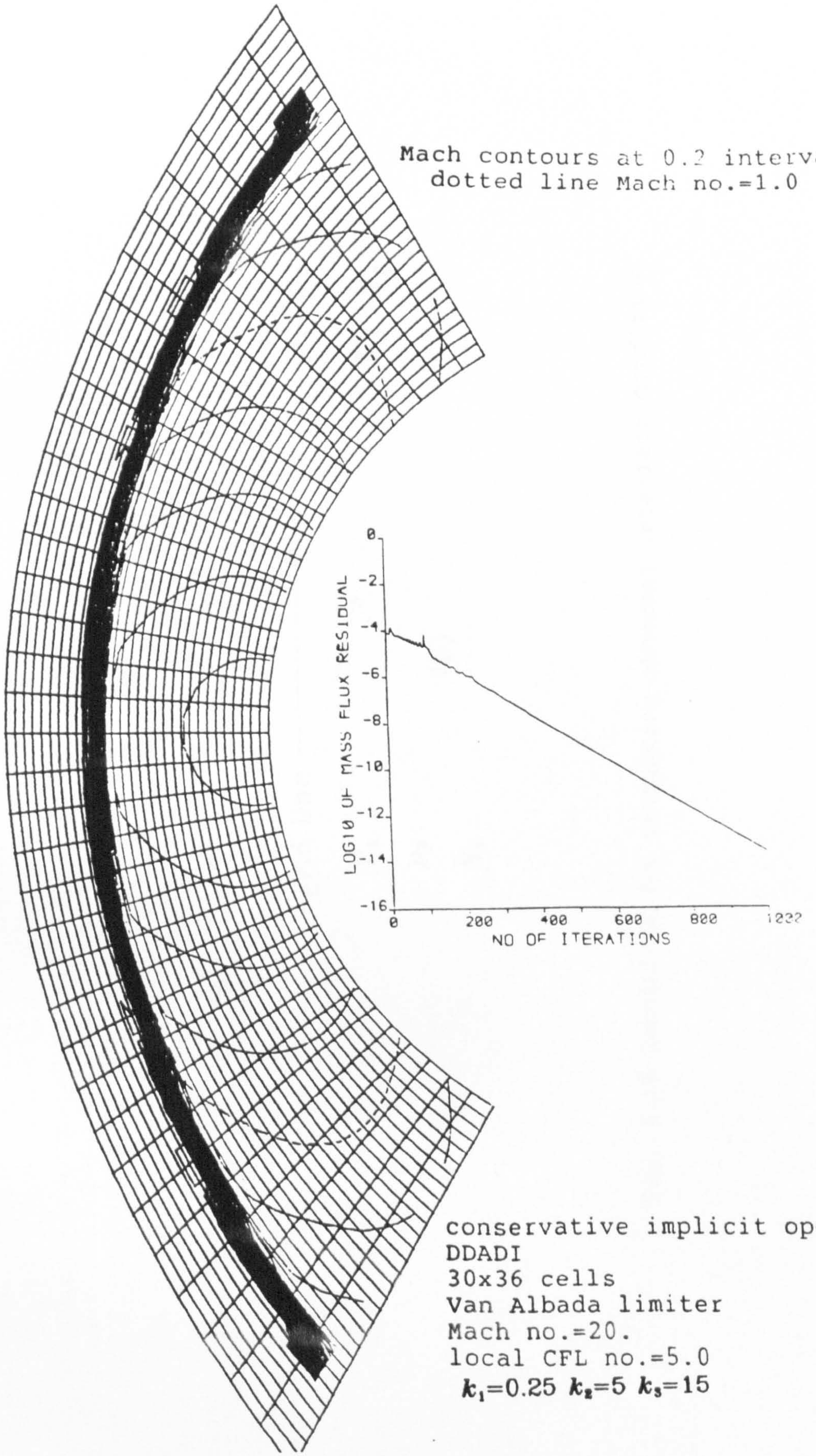

Mach contours at 0.2 intervals
dotted line Mach no.=1.0

conservative implicit operator
DDADI
30x36 cells
Van Albada limiter
Mach no.=20.
local CFL no.=5.0
k_1=0.25 k_2=5 k_3=15

Fig. 6.15 Mach 20 calculation with modified dissipation (B)

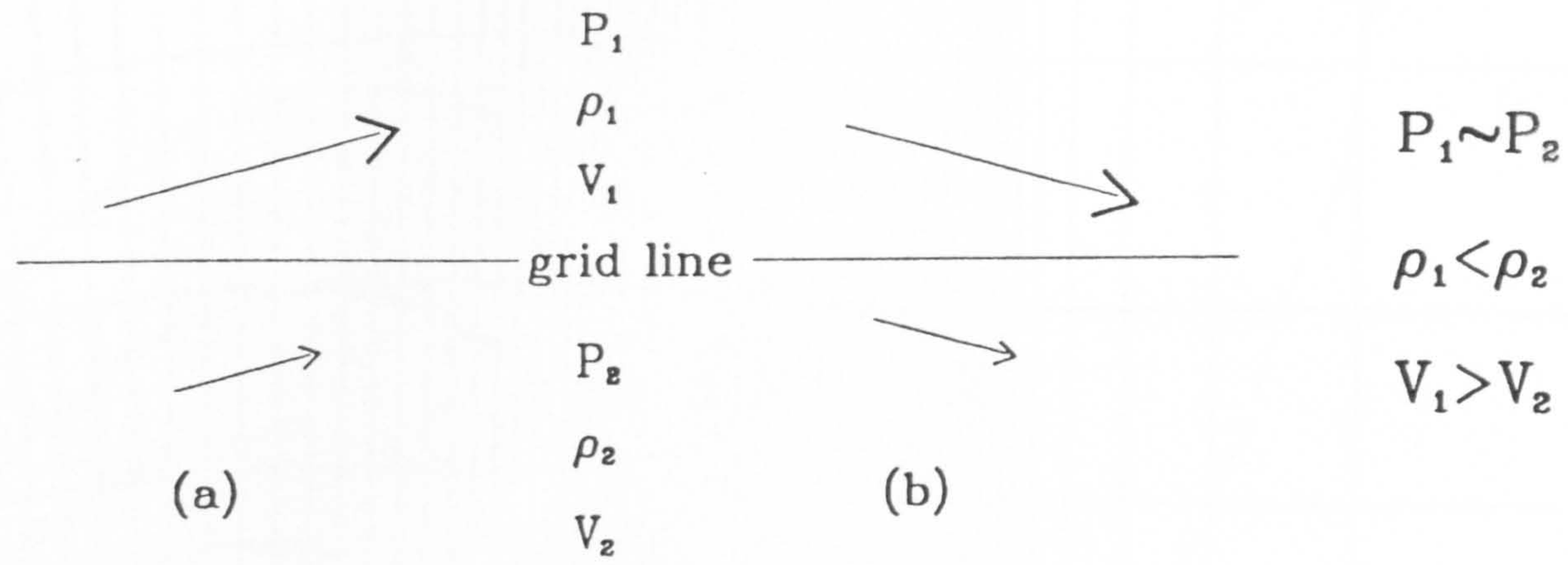

Fig. 6.16 Conditions for generating abnormal interface condition

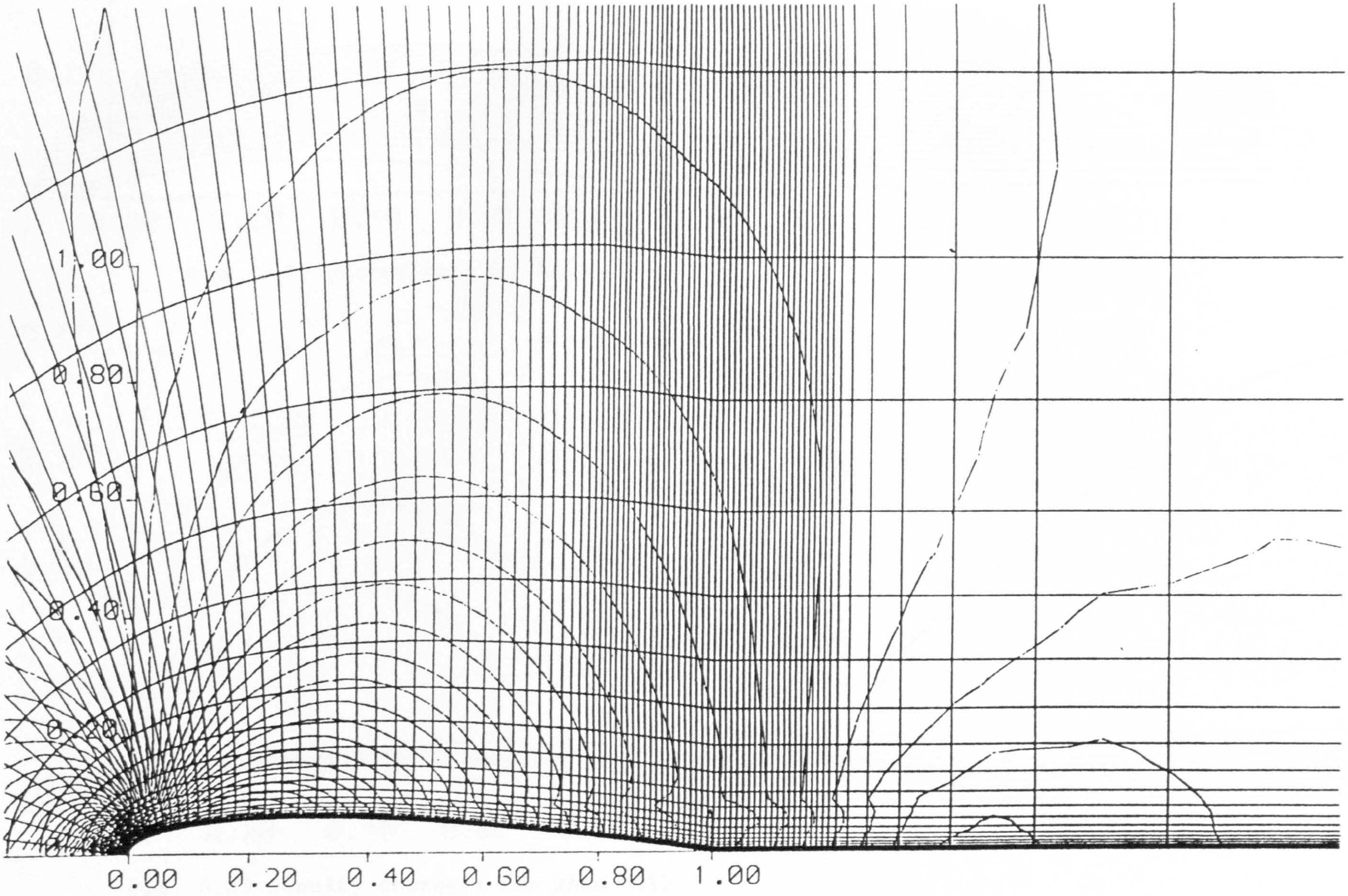

Fig. 6.17 Pressure contours for NACA 0012

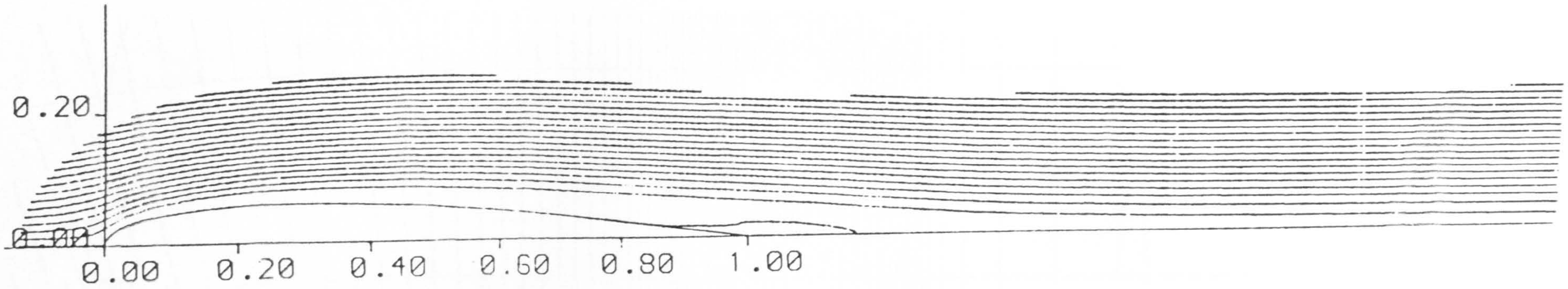

Fig. 6.18 Streamlines for NACA 0012

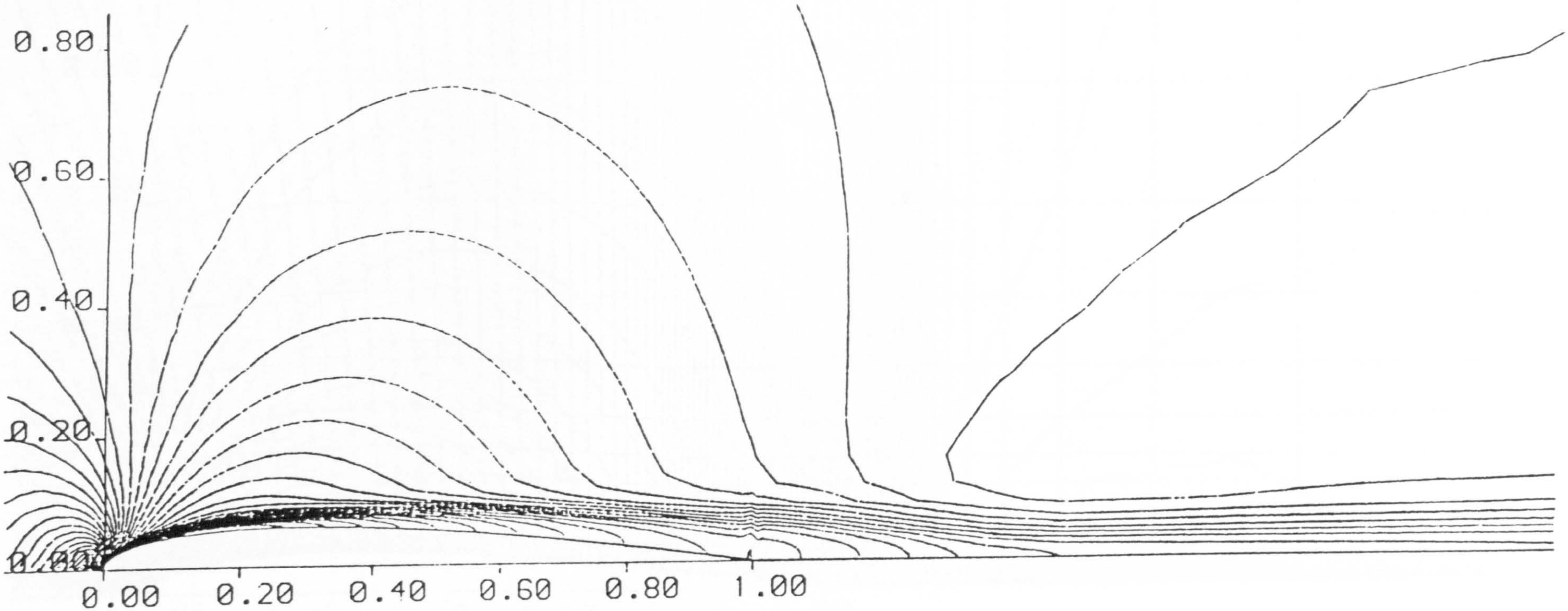

Fig. 6.19 Density contours for NACA 0012

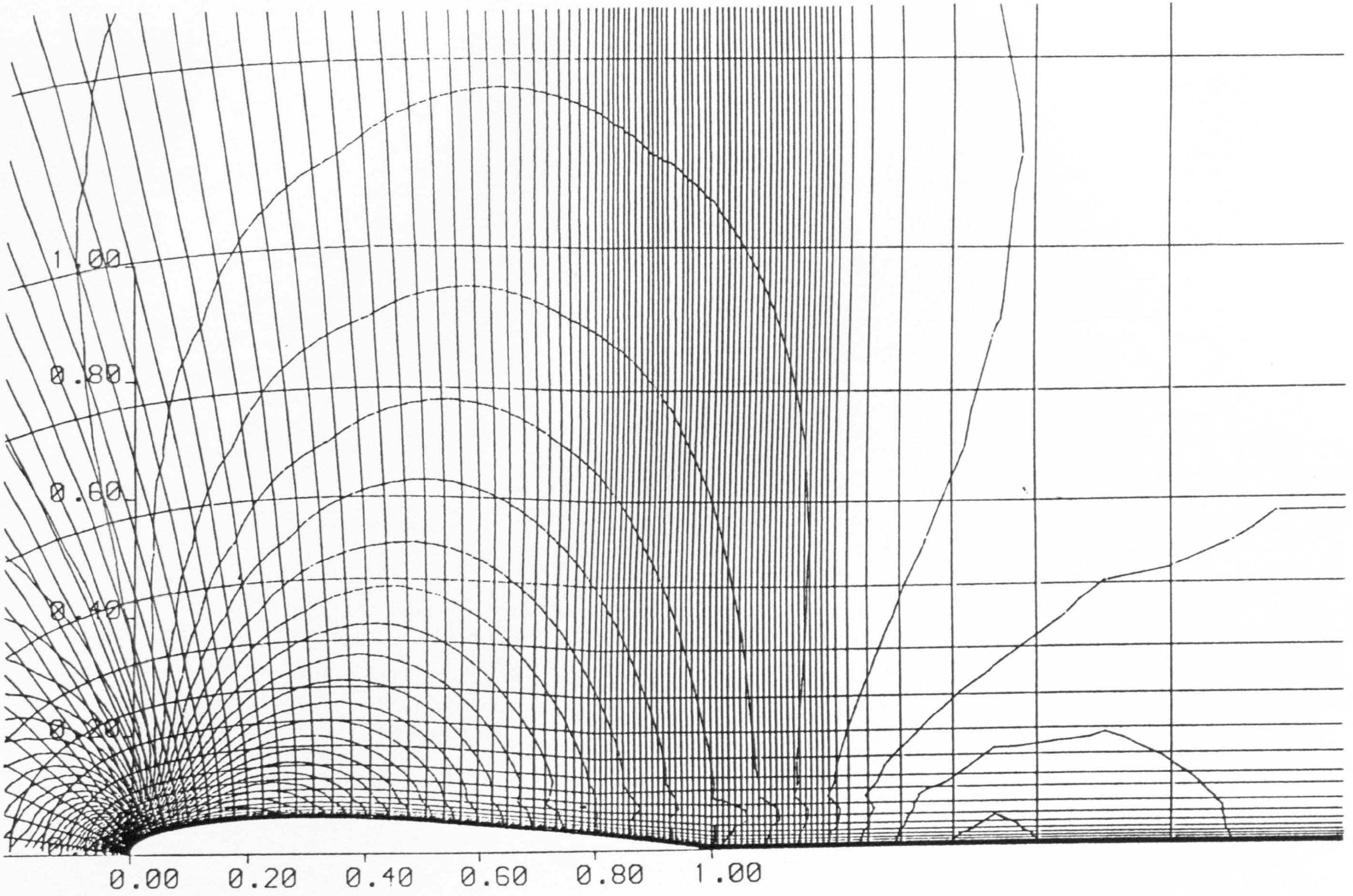

Fig. 6.20 Pressure contours for NACA 0012 with modified grid